On Combustion Instability in Solid Rocket Motors

Thesis by

Sanjeev Malhotra

In Partial Fulfillment of the Requirements
for the Degree of

Doctor of Philosophy

California Institute of Technology
Pasadena, California

2004

(Defended September 4, 2002)

Foreword

This report is the thesis submitted by Sanjeev Malhotra in partial fulfillment of the requirement for the degree of Doctor of Philosophy, March 2004. In addition to myself as chairman, the examining committee consisted of Professors D. S. Cohen (Applied Mathematics), A. Leonard (Aeronautics), and D. Pullin (Aeronautics). G. A. Flandro (University of Tennessee Space Institute) was also a member of the examining committee.

This work was supported partly by the California Institute of Technology and partly by the Caltech Multidisciplinary University Research Initiative under ONR Contract No. N00014-95-1-1338.

F. E. C. Culick

March 2004

On Combustion Instability in Solid Rocket Motors

by

Sanjeev Malhotra

In Partial Fulfillment of the Requirements

for the degree of

Doctor of Philosophy

Abstract

An investigation of combustion instability in solid rocket motors was conducted using perturbation techniques, with particular emphasis placed upon understanding the fluid dynamics of the chamber environment. It was shown that although the phenomena generally manifests itself as oscillations of pressure, with the frequencies measured in tests well predicted by classical acoustic formulas, important aspects of the behavior cannot be explained without due recognition of the two basic processes of fluid dynamics—i.e., the compressing/expanding process and the shearing process.

Thus, a new framework for studying these instabilities that accommodated both linear and nonlinear behavior was developed. The approach differed from previous work in its use of linear stability eigenfunctions—that satisfy the no-slip boundary condition—as a basis for the expansion, with adjoints used to effect a spatial averaging. Among other things, this allowed for the self-consistent inclusion of vortical flow effects.

With respect to the linear behavior, two dominant vorticity-related pathways were shown to exist: one because of sound creating vorticity, and the other, because of that vorticity, in turn, creating more sound. These effects cancel however and thus to leading order no net contribution exists. Though this finding had been reported in an earlier study, restrictive assumptions were introduced. In contrast, we establish that the result is independent of grain geometry and holds for any fluid motion, turbulent or otherwise

A nonlinear coupling to the flame zone owing to vorticity creation was also identified. The term was left unevaluated however, since no satisfactory model of the flame response presently exists. To help circumvent this difficulty, i.e., that much remains to be done on modeling nonlinear processes, the amplitude equations were studied in a general way using perturbation techniques based on ideas of resonance. The advantage of such an approach is that the nonlinear coefficients need not be specified a

priori—only conditions on the linear behavior of the system need to be placed. Closed form results were derived for the limiting periodic behavior when the first mode is unstable and compared against results from numerical integration. Striking agreement was shown.

Contents

List of Figures

List of Tables

List of Symbols

Symbol	: Description
$\mathbf{A}$	: vector potential
c	: sound speed
c_v	: specific heat at constant volume
c_p	: specific heat at constant pressure
$\mathbf{e}_{(\,)}$	: unit vector
$E_m^{\,2}$	: normalization constant $\equiv \frac{1}{2}\int\left(c_m^{\dagger *}c_m + \varphi_m^{\dagger *}\vartheta_m\right)dV$
f	: similarity function in Appendix G; nonlinear coefficient everywhere else
$\mathcal{F}$	: momentum source term
h_i	: metric coefficient
i	: imaginary number
I	: denotes integral
$\mathbf{K}$	: curvature tensor
k	: wave number
$\mathbf{k}$	: wave vector
k_l	: l^{th} axial wave number $\equiv (l\pi R)/L$
k_{ns}	: root of $dJ_n(k_{ns}r)/dr = 0$ at $r = 1$
$\mathcal{K}$	: kinetic energy $\equiv \int \frac{1}{2}\mathbf{u}\cdot\mathbf{u}\,dV$
$\mathcal{K}_\vartheta$	: kinetic energy stored by the longitudinal field $\equiv \int \frac{1}{2}\mathbf{u}_\vartheta\cdot\mathbf{u}_\vartheta\,dV$
$\dot{\mathcal{K}}_{\vartheta\to\mathbf{U}}$	: flow turning integral $\equiv M_b\oint\left(\mathbf{u}_{\vartheta\zeta}\cdot\mathbf{u}_{\omega\zeta}\right)\mathbf{n}\cdot\mathbf{U}dS$
$\dot{\mathcal{K}}_{\vartheta\to\omega}$	: energy flux from longitudinal to transverse $\equiv -\oint\mathbf{A}\cdot\left(\mathbf{n}\times\partial\mathbf{u}_\vartheta/\partial t\right)dS$

$\dot{\mathcal{K}}_{\omega\to\vartheta}$: energy flux from transverse to longitudinal $\equiv -\oint \varphi \mathbf{n}\cdot\partial\mathbf{u}_{\omega}/\partial t\, dS$

L : chamber length

$\mathscr{L}_{(\,)}, \boldsymbol{\mathcal{L}}_{(\,)}$: denotes a linear operator

M_b : injection Mach number

$\mathscr{N}_{(\,)}, \boldsymbol{\mathcal{N}}_{(\,)}$: denotes a nonlinear operator

$\mathbf{n}$: normal coordinate

n^+ : in Appendix E denotes a fast spatial scale

$\tilde{n}$: in Appendix E denotes a slow spatial scale

p : pressure; in Chapter 4 denotes energy

P_m : in Chapter 4 denotes the energy ratio $\equiv p_1^m / p_m$

Pr : Prandtl number $\equiv \left(\mu_s c_p\right)/k$

q : in Chapter 4 denotes phase

$\mathbf{q}$: conductive heat flux vector $\equiv -k\nabla T$

Q : energy source term

Q_m : in Chapter 4 denotes the phase difference $\equiv mq_1 - q_m$

r : radial coordinate; in Chapter 4 denotes a modulation function

R : characteristic length (e.g., the radius for a cylindrical chamber)

Re : Reynolds number; in §5.1 $\equiv \left(u_n^2/k\right)/\nu$

Re_{ω} : Reynolds number associated with shear $\equiv \left(c_o^2/k\right)/\nu_s$ in Chapter 6;
$\equiv \left(\rho_o c_o R\right)/\mu_s$ in Chapters 7-9;

Re_{ϑ} : Reynolds number associated with volumetric expansion $\equiv \left(\frac{4}{3}+\mu_v/\mu_s\right)^{-1}\mathrm{Re}_{\omega}$

s : entropy

S : Strouhal number $\equiv k_{m0}/M_b$

t : time

t_N : in Chapter 4 denotes a slow time scale $\equiv \varepsilon^N t$

t^+ : in Appendix E indicates a normalized time $\equiv kt$

T : temperature

$\mathbf{u}$: velocity

$\mathbf{U}$: mean velocity; in §5.1 indicates the velocity of the plate

$\mathcal{W}$: mass source term

$\mathbf{x}$: spatial coordinates

z : streamwise coordinate

ϕ : damping function; in Chapter 4 denotes a phase shift

ϑ : dilatation

Φ : dissipation function

Greek Symbols

α : growth rate

β : in §5.1 indicates a parameter grouping with units of inverse time $\equiv u_n^2/4\nu$

γ : ratio of specific heats

Γ : fundamental derivative; $=(\gamma+1)/2$ for an ideal gas

δ : measure of the penetration depth

δ_m^j : discrete Dirac-delta function

ε : wave amplitude

ε_{ijk} : permutation tensor

ζ : tangential direction

η : amplitude function; in §5.1 dummy variable of integration

θ : azimuthal coordinate; phase shift

κ : thermal conductivity; principle curvature

μ_s : dynamic viscosity associated with shear

μ_v : dynamic viscosity associated with volumetric expansion

ν : kinematic viscosity; specific volume

ξ : short convective length scale

ρ : density; in §5.1 new variable of integration $\equiv n/\left(2\sqrt{\nu\tau}\right)$;
in Appendix E denotes a modulation function

σ : in Chapter 5 denotes a nonlinear coefficient

$\boldsymbol{\sigma}$: vorticity source strength

τ : shear stress on surface; in §5.1 dummy variable of integration

$\boldsymbol{\tau}$: shear stress on surface

υ, ς : in Appendix C denotes characteristic coordinates

φ : scalar potential

χ : stretching function in Appendix G

$\boldsymbol{\chi}$: in §5.1 indicates a convenient transformation $\equiv u_n \boldsymbol{\omega}_\varsigma - \nu\, \partial \boldsymbol{\omega}_\varsigma / \partial n$

Ψ : steady stream function

ψ : stream function

$\boldsymbol{\Omega}$: steady vorticity

$\boldsymbol{\omega}$: vorticity

Superscripts

$(m, j, k, ...)$: coefficient to be evaluated at index m, index j, etc.

n, r : denotes a function of the ordinary spatial scales

T	: transpose
ε^n	: refers to term of $O\left(\varepsilon^n\right)$
ω	: refers to the transverse field
ϑ	: refers to the longitudinal field
†	: adjoint
*	: complex conjugate

Subscripts

a	: refers to the acoustic field
i	: refers to imaginary part
m	: refers to the mode number
n	: normal direction
r	: refers to real part
s	: in §5.1 indicates the classic Stokes solution; everywhere else refers to the entropy field
U	: refers to the mean flow
ζ	: tangential direction
μ	: refers to term of $O\left(M_b\right)$
ω	: refers to the transverse field
ϑ	: refers to the longitudinal field
$\left(\mathscr{R}\right)$	: resonant terms
$\left(\mathscr{NR}\right)$	: non-resonant terms

Triangular brackets $\langle\ \rangle$ denote time average in Chapters 5 and 8 and the complex valued inner product $\langle \mathbf{x}, \mathbf{y} \rangle \equiv \int \mathbf{y}^{*T} \mathbf{x} dV$ everywhere else.

1. INTRODUCTION

1.1 Brief Overview

During the development of solid rocket motors in the late 1930s and early 1940s, test firings were often marked by erratic behavior. This included unexpected shifts in the mean pressure, structural vibrations and visible changes in the exhaust plume. That these anomalies were somehow the result of *acoustic waves* in the gaseous products of combustion was hypothesized (e.g., Boys and Schofield 1943; Grad 1949) and later established experimentally (e.g., Swanson 1951; Smith and Sprenger 1953) using high-bandwidth pressure transducers. In lieu of a smooth time evolution of chamber pressure, for which the systems were designed, large amplitude pressure oscillations with frequencies close to the natural acoustic resonances of the chamber were observed. Much of the research in the field since has focused on understanding the underlying mechanisms of, and seeking ways to mitigate the effects of, these so-called *combustion instabilities*. While significant progress has been made, the continued manifestation of these generally unwanted[†] pressure oscillations—in *all* types of combustors, from afterburners and ramjets to gas turbines—suggests that much work remains.

1.2 Characteristics and Mechanisms

Combustion instability, despite the terminology, has little to do with unstable combustion[‡]. Instead, it is the result of coupling between chemical processes in the flame zone and unsteady flow processes within the combustion chamber. More specifically, from the point of view of the observer, combustion instability is an unsteady organized fluid motion—with a strong acoustic component—that ultimately is driven by the chemical energy released in some part of the system. Although the precise mechanisms may differ, a fundamental characteristic of this flow transient is that it feeds back and modifies the combustion, giving rise to conditions that are sometimes favorable for this *self-excited* disturbance (i.e., a disturbance that grows without benefit of any external influence) to reach amplitudes of finite value.

To help illustrate how this can occur, suppose for example that the rate of propellant conversion within a solid rocket motor increases because of a fluctuation in pressure or temperature, or, enhanced heat transfer back to the propellant surface owing to turbulent mixing. If the resulting perturbations in mass

---

[†] In the case of pulse combustors, oscillations are desirable since they lead to enhanced rates of heat transfer and/or evaporation (Margolis 1993).

[‡] Even though combustion processes may be *intrinsically* unstable this is *not* the issue, with rare exception, in practical applications.

flow and/or heat release are in *phase* with the initial disturbance, the disturbance grows, and the cycle begins again.

With slight modification, this describes the behavior of a broad class of combustors, for combustion is *always* sensitive to the interplay between chemical kinetics and fluid mechanics. Thus, it is necessary to not only understand the chemical processes from which the energy for driving instabilities is ultimately derived, but also the flow processes that determine the environment within which this energy is released. Our focus here is only on the latter.

1.3 Current Challenges in Understanding

Owing to harsh conditions, detailed measurements of the unsteady flow field within solid rocket motors do not exist. What is known is instead based largely on recordings from typically only a few pressure transducers as well as externally mounted accelerometers and strain gauges. Such data indicate that frequencies observed during instability are remarkably close to the c*lassical* acoustic resonances of the chamber.

That acoustic resonances should be excited is not surprising since nature follows the path of least action. As for *why* classical formulas accurately predict the values observed—the reason is that influences other than the shape and size of the combustor are of higher order in the linear eigenvalue problem that defines these resonances. This is true, for example, of interactions with the mean flow since the Mach number that characterizes this motion is generally small.

Thus, comparison of observed frequencies with those predicted from classical acoustics is not a useful test for any theory. Nonetheless, this agreement has led to the view that to good approximation an irrotational description of the unsteady motion is sufficient to capture the controlling mechanisms. While there is no denying the allure of a simple model, one cannot oversimplify the description.

To consider combustion instabilities solely in terms of perturbations or small departures from classical acoustics overlooks the potential impact of other unsteady flow processes. Although the central role of pressure is not at question here, it is essential to recognize that *two* basic processes of fluid dynamics exist—i.e., the *compressing/expanding* process and the *shearing* process (cf. Wu et al. 1996). Measurements of pressure are a good indicator of the former, but fail to reveal the notable features and importance of the latter.

To shed some light on this issue, consider the Stokes-Helmholtz decomposition, which—owing to its kinematic origins—*always* allows the velocity field to be split into *longitudinal* (i.e., irrotational) and *transverse* (i.e., vortical) waves. These waves kinematically represent the two basic aforementioned

processes of fluid dynamics, and while they may evolve independently within the interior of the domain, more often than not, they are coupled on the boundary.

For example, the alternate compressions and rarefactions of an acoustic wave do not satisfy the no-slip condition; vorticity must therefore be created such that the transverse velocity induced cancels the longitudinal slip on the boundary. Thus, while it may be true that acoustic waves follow their own simple scaling laws, at least in terms of their frequencies, they also give rise to vortical motions.

The validity of neglecting this is certainly open to question, especially within a solid rocket motor, because in such an environment the burning process is localized within a thin zone—on the order of millimeters—near the propellant surface. In other words, *the irrotational description breaks down precisely where the greatest accuracy in modeling the unsteady flow is needed.*

In fact, it has long been realized that something is missing in our understanding of the flow effects responsible for the observed combustion response of propellants. Much experimental data confirms that important differences exist when the incidence of the excited acoustic wave is parallel, rather than perpendicular to, the burning surface; only in the first instance must unsteady vorticity be created.

Such changes in behavior were reported, for example, by Brownlee (1959), who studied two different motor configurations, both of which were subject to combustion instability. For acoustic waves of perpendicular incidence, no effect on the burning rate was observed, even though amplitudes as high as 10% of the chamber pressure were recorded. In contrast, this was not the case for waves of parallel incidence, where much smaller amplitudes were shown to strongly affect the burning rate. To what might these differences be due? The picture has gradually emerged over the years that a variety of unexplained flow phenomena might find their origin in vortical and turbulent flow processes (cf. Price 1992).

Analytical work in this regard has been carried out by Flandro (1995 a, b) who sought a more complete and realistic model of the unsteady motions within cylindrical combustion chambers. Superimposing a small amplitude, purely axial, acoustic disturbance on a description of the mean flow derived earlier by Culick (1966), a solution was sought for the neglected half of the problem. Shown to exist, were waves of vorticity, created on the boundary owing to a kinematic coupling with the acoustic field, and convected deep into the interior of the domain by the incoming flow.

The impact on the combustion processes of such transverse motions becoming *unstable* themselves would likely be significant (cf. Beddini 1998; Lee and Beddini 2000), with effects including—but not limited to—enhanced heat transfer rate back to the propellant surface owing to increased mixing, which as indicated before (e.g., Brownlee 1959), would augment the burning rate. Insofar as combustion

responsiveness is concerned then, acoustically generated vorticity could be the ideal *Trojan* horse. For in the presence of fluid injection, what better way for turbulence to penetrate regions close to the flame zone, than for a turbulent precursor to already exist.

Thus, to understand the environment to which the propellant must respond, the view that motions within the chamber are but small departures from classical acoustics must itself be departed from. In other words, in studying the dynamics of the combustor, it is essential that the interactions between chemical kinetics and the *two* basic fluid processes—i.e., the compressing/expanding process and the shearing process—are recognized and assessed.

1.4 Objectives and Thesis Outline

As the unsteady flow in a combustion chamber is governed by a system of nonlinear partial differential equations, which is difficult to study mathematically as well as computationally expensive to simulate, a useful strategy is to convert this original description of the dynamics into a system of ordinary differential equations[†]. Typically, this is accomplished by expanding the flow variables in a set of basis functions and then spatial averaging over the domain.

Culick (1976) adopted such a strategy to develop a general framework for studying combustion instabilities that accommodated both linear and nonlinear processes. In choosing a basis, direct advantage was taken of the observational result that pressure oscillations during instability closely resemble the *classical acoustic modes* of the chamber, at least in the sense that frequencies measured in tests agree well

---

[†] Even as the problems faced suggest perturbation techniques, numerical methods offer another way of proceeding. Formulations based on modal expansion and spatial averaging are useful when the behavior of disturbances—superimposed on a given, presumed known, mean flow—is sought. To more completely account for all fluid dynamic and chemical processes, as well as their interactions, numerical integration of the complete conservation equations is typically needed. While many challenges remain in this regard, substantial progress has been made over the past five years. The two-dimensional LES simulations of the internal motor flowfield recently carried out by Apte and Yang (2001, 2002), which include computation of the burning propellant, are a notable example.

Despite the allure of a numerical approach however, formulations such as those based on a spatial averaging procedure will likely continue to occupy a central position. Not only do these types of analyses produce relatively inexpensive results, they also yield valuable insight into some of the underlying physical mechanisms responsible for behavior that is observed to be common among different systems. In contrast, numerical simulations provide information essentially on a case-to-case basis. Generalizing these findings to establish *rules of thumb* is not easy owing to the nonlinearity of the processes involved. This drawback is a matter of concern, especially from a controls standpoint where simple models that capture much of the physics are wanted as a starting point.

It follows that the best line of attack would involve using both approaches in parallel, since each has its own virtues.

with predictions based on classical formulas. Thus, it was reasonable to use these modes as a *basis* for expanding the compressing/expanding half of the unsteady flow field.

While application of the resulting framework has been successful over the years in helping understand various aspects of observed behavior (cf. Culick 2000 for the most recent review), difficulties arise because either not all relevant processes are accounted for, or, more often, information is unavailable to model with reasonable accuracy their influence. For example, most earlier efforts assumed the unsteady motions were irrotational in the first approximation; thus, a number of important effects owing to coupling with vortical flow processes were not identified. Flandro (1995 a, b) first recognized and convincingly established this to be true for the linear problem by emphasizing the need to pay close attention to the no-slip boundary condition.

Broadly speaking then, our intent here is to develop a more complete framework for studying energy pathways within combustion chambers, with particular emphasis placed on those that involve the unsteady vorticity field. The remainder of this section summarizes the main objectives and outlines how and where they are addressed in the chapters that follow; note that the achievements of other investigators will only be lightly brushed on below with further elaboration in due course.

In Chapter 2, we begin by constructing a substantial extension of the framework originally developed by Culick (1976). The motivation is to allow new physics to be incorporated in a self-consistent manner as well as to re-express existing physics in a more insightful way. This is accomplished by using linear stability eigenfunctions to expand flow variables and their adjoints to effect a spatial averaging—a common approach in other fields of study.

As such, with respect to the compressing/expanding process, we use the *perturbed* rather than the *unperturbed* modes; more importantly, we also construct a basis in which to expand the vortical half of the flow field[†]. In other words, the linear stability eigenfunctions will satisfy the no-slip boundary condition; moreover, results will be obtained for motors whose grain boundaries can locally be described by a general orthogonal coordinate system.

[†] It is worth noting here that, different *sources* of unsteady vorticity within the chamber may exist. For example, large-scale vortices often arise because of shedding from obstacles (cf. Flandro 1986) or as a consequence of intrinsic instabilities of the mean flow (cf. Casalis et al. 1998). That these vortices often excite acoustic waves is well-known (cf. Flandro and Jacobs 1974), for this is the basic principle active in many wind-driven musical instruments. To assess the importance of this, while desirable, is far too ambitious (at least in the context of this thesis). We focus here only on the unsteady vorticity that must arise for the no-slip condition to be satisfied, by building most notably on the work of Flandro (1995 a, b).

Chapter 3 consists of a simple application of the new framework; in particular, purely *acoustic* motions within a chamber of arbitrary shape, enclosed by a rigid boundary and containing a fluid otherwise at rest, will be investigated. Important features of time-dependent motions within combustion chambers are identified, even though processes that distinguish such chambers from purely acoustical systems are ignored.

Chapter 4 introduces a methodology to solve for the limiting periodic behavior of the amplitude equations. While numerical integration is always possible, results obtained this way are difficult to generalize since the system may evolve differently depending upon the values the linear and nonlinear coefficients assume. Thus, perturbation techniques will be utilized instead; the advantage of doing so is that the nonlinear coefficients need not be specified a priori—only conditions on the linear behavior of the system will need to be placed (e.g., the first mode is unstable while all other modes are stable). This is of great practical value since much work remains to be done on modeling nonlinear processes. The basic idea behind the analysis is that, the long-term behavior of a system of nonlinear ordinary differential equations is determined by its resonance structure. Although this idea is certainly not novel, and dates back to work independently done by Stokes and Poincare, the current effort marks the first application to the field of combustion instability.

Ultimately though, to study combustion instability within solid rocket motors it is necessary to *determine* the coefficients in the amplitude equations. This requires that we solve for the linear stability eigenfunctions. To facilitate such a calculation, we first consider some model problems that allow key elements of the physics to be introduced in a simplified setting. In Chapter 5, we generalize the classic Stokes' problem to include a uniform injection of fluid normal to the boundary; this helps illustrate how the mass flux issuing forth from a burning propellant affects vorticity creation. Then, in Chapter 6, we contrast the behavior of the *acoustic boundary layer*, with and without a uniform injection of fluid through the boundary. Finally, in Chapter 7, we consider the linearized flow field within solid rocket motors, and solve for the acoustic, the vorticity and the thermal eigenfunctions.

Chapter 8 revisits the calculation of linear stability. While Flandro (1995 a, b) first incorporated the effects of vorticity, the applicability of that analysis was limited since the new stability integrals were evaluated *only* for a cylindrical propellant grain under the restrictive assumption that the unsteady vorticity distribution remains laminar—a deficiency corrected in the current effort. Utilizing an energy balance formulation, novel formulae that clearly reflect the interaction between vorticity and sound will be derived, allowing for a substantial clarification—both in terms of the mathematics and the physics involved—of the

mechanisms that allow the former to influence the growth or decay of the latter within solid rockets. Aside from a significantly enhanced physical understanding, what has already been done (Culick 1973; Flandro 1995 a, b) will be improved upon in two key ways: the results obtained will be *independent* of propellant grain geometry; and the derivation of these results will depend largely on kinematics—as such, the conclusions reached will be *independent* of the dynamics and thermodynamics of the medium, and thus applicable for any fluid motion, turbulent or otherwise.

In Chapter 9, we determine the coefficients in the amplitude equations that correspond to three kinds of nonlinear interactions to second order in the wave amplitude: sound-sound, sound-vortical and vortical-vortical. The nonlinear effects of vorticity on combustion instability will then be assessed for some prototypical cases; this is another important contribution of the present effort, since all previous work has been limited to the linear behavior.

Finally, Chapter 10 contains a summary of the key results, as well as suggested directions for future research.

2. GENERAL FRAMEWORK

2.1 Introduction

Culick (1976) developed a general framework for studying combustion instabilities, which accommodated both linear and nonlinear processes[†]. We construct here a substantial extension of that framework.

Historical Overview

Since systems modeled by nonlinear partial differential equations are difficult to study mathematically as well as computationally expensive to simulate, a useful strategy is to convert this original description of the dynamics into a system of ordinary differential equations. With differences mainly in the implementation details, this typically involves expanding the flow variables in a set of basis of functions and then spatial averaging in some way.

Culick (1976) adopted such a strategy to study unsteady motions within combustion chambers. Although justifiable on theoretical grounds, experimental data offered the most compelling evidence. Pressure oscillations during instability closely resemble the *classical acoustic modes* of the chamber, at least in the sense that frequencies measured in tests agree well with predictions based on classical formulas. Thus, it was reasonable to use these modes as a *basis* for expanding the compressing/expanding half of the unsteady flow field.

What made this strategy effective for treating *most*[‡] problems that arise in practice, in a wide class of combustors, is that system specific departures from classical acoustics—at least insofar as the

---

[†] This was necessary since a view founded entirely on linear principles can account for only a small part of what is observed. In *linearly unstable* systems, for example, instabilities that spontaneously emerge from the background noise rarely grow without limit. Instead, such disturbances tend more commonly to some finite limiting motion, typically a periodic limit cycle. Nonlinear processes must act for this to occur. Even if the system is *linearly stable*, not every disturbance need decay. Perturbations of finite amplitude sometimes increase with time—behavior that is also decidedly nonlinear.

‡ Axial-mode instabilities that are triggered by disturbances of finite amplitude often evolve into steep-fronted waves that are sufficiently steep to be more accurately interpreted as weak shock waves (cf. Brownlee 1964; Bloomshield 2000). That an approach based on modal expansion/spatial averaging is only applicable during the steepening process and thus of limited value in such instances has been suggested (cf. Flandro 1985 and Culick 1994 for two different points of view). In contrast, the first nonlinear analysis of combustion instability specifically sought to study the system after shock formation. In particular, by building on the characteristic coordinate perturbation technique (Lighthill 1949; Whitham 1952), Crocco, Sirignano and Mitchell (Sirignano 1964; Sirignano and Crocco 1964; Mitchell, Crocco and Sirignano 1969) modeled a shock wave traveling back and forth in a one-dimensional chamber, reflecting off a planar

compressing/expanding process is concerned—are often small. Thus, even though these departures are inherently related to the damping and driving mechanisms of combustion instabilities, they play essentially a perturbative role in most combustors.

Over the years, application of the resulting framework has been successful in helping understand various aspects of nonlinear behavior (cf. Culick 2000 for the most recent review). With respect to the fluid processes incorporated into the analysis, much effort has been concentrated on sound-sound interactions (i.e., nonlinear acoustics). More recently, the effects of noise within the combustion chamber have also been considered (Burnley 1996; Seywert 2001).

However, test results have shown qualitative changes in the nonlinear behavior of combustion instabilities not explicable with these processes alone. The origin of this behavior does not appear to be associated with combustion dynamics, either.

The Present Framework

Our intent here is to devise a more complete framework for studying pathways of nonlinear energy transfer within combustion chambers, such as those that involve the unsteady vorticity field, or, the mean flow. To this end, we construct a substantial extension of the framework originally developed by Culick (1976); some of the differences are highlighted below.

First, in choosing a basis, Culick (1976) took direct advantage of the observational result that pressure oscillations during instability resemble classical acoustic modes. Accordingly, the unsteady pressure field was expressed as a synthesis of these (normal) modes with unknown time-varying amplitudes. The acoustic velocity was treated in a corresponding manner. In contrast, we adopt the well-established approach of using linear stability eigenfunctions to expand flow variables and their adjoints to effect a spatial averaging. Among other things, this allows us to account for nonlinear energy transfer with the mean flow; previous attempts to incorporate this effect have been unsuccessful (cf. Culick 1997).

Second, both the compressing/expanding process *and* the shearing process are included in our analysis. More specifically, we will obtain an analytical representation of the linear stability eigenfunctions

---

combustion zone at one end and a choked nozzle at the other. Even though their calculations met with partial success in reproducing tests performed on laboratory gas-fueled rockets, an analytical tool of practical value did not result. This was chiefly due to the complexity of the technique and the difficulty in accommodating more than one spatial dimension. Nonetheless, the effort provided valuable insight into some basic issues of nonlinear behavior that remain the focus of much attention; notably, the possible existence of stable limit cycles and the conditions necessary for achieving these end states.

that satisfies the no-slip boundary condition for motors whose grain boundaries can locally be described by a general orthogonal coordinate system, and use this as a basis to study nonlinear combustion instability.

2.2 Equations of Motion

In this section, the equations that govern the flow of *combustion products* in a solid rocket motor are summarized. Only that part of the chamber bounded by the propellant surface, the head-end closure and the nozzle entrance plane is considered; details of the flow through the nozzle itself are significantly more complex and generally omitted.

To simplify the analysis further, other commonly used approximations are adopted. These include approximating the combustion processes by a time-dependent boundary condition at the propellant surface and the combustion products as a fluid with mass-averaged properties (cf. Culick 1975 for further details). The justification for the former is the negligible thickness of the combustion zone compared to other dimensions of the chamber, while experience has shown that the latter is sufficient for capturing the leading order effects of condensed particles within the chamber volume—the most important being a reduction in the speed of sound.

Working with a standard set of non-dimensional variables[†], we have:

Conservation of Mass

$$D\rho/Dt = -\rho\nabla\cdot\mathbf{u} + \mathcal{W} \tag{2.1}$$

Conservation of Momentum

$$\rho\, D\mathbf{u}/Dt = -\nabla p + \mathcal{F} \tag{2.2}$$

Conservation of Energy

$$\rho\, DT/Dt = \gamma\left(\gamma - 1\right)\left(-p\nabla\cdot\mathbf{u} + Q\right) \tag{2.3}$$

Equation of State

$$\gamma\, p = \rho T \tag{2.4}$$

where $D/Dt = \partial/\partial t + \mathbf{u}\cdot\nabla$. Contributions to the source terms $\mathcal{W}$, $\mathcal{F}$ and Q will be made explicit as required.

[†] The equations are written in terms of a standard set of non-dimensional variables:

$$\frac{t}{R/c_o} \to t \quad \frac{\mathbf{x}}{R} \to \mathbf{x} \quad \frac{\mathbf{u}}{c_o} \to \mathbf{u} \quad \frac{p}{\gamma\, p_o} \to p \quad \frac{\rho}{\rho_o} \to \rho \quad \frac{T}{T_o} \to T \quad \frac{c}{c_o} \to c \quad \frac{s}{c_p} \to s$$

$$\frac{R}{\rho_o c_o}\mathcal{W} \to \mathcal{W} \quad \frac{R}{\rho_o c_o^2}\mathcal{F} \to \mathcal{F} \quad \frac{R}{\rho_o c_o^3}Q \to Q$$

Here suffix *o* denotes chamber stagnation properties, *R* is a characteristic length (e.g., the radius for a cylindrical chamber), and c_p is the specific heat at constant pressure.

Although (2.1)–(2.4) are enough to determine the state of the flow, transport equations for some other thermodynamic variables will also prove useful. In particular, we have:

Equation for the Pressure

$$Dp/Dt = -\gamma p \nabla \cdot \mathbf{u} + (\gamma - 1) Q + \gamma^{-1} \mathbb{W} T \tag{2.5}$$

Equation for the Sound Speed

$$Dc/Dt = (\Gamma - 1)\left(-c \nabla \cdot \mathbf{u} + \gamma (\rho c)^{-1} Q \right) \tag{2.6}$$

Equation for the Entropy

$$\rho T \, Ds/Dt = (\gamma - 1)\left(Q - \gamma^{-1} \mathbb{W} T \right) \tag{2.7}$$

where $\Gamma = (\gamma + 1)/2$ for an ideal gas (Γ is often referred to as the fundamental derivative).

Now while pressure is the most common experimental indicator of combustion instability, insofar as the mathematics is concerned, it is not the *most* suitable variable to work with[†]. As such, we choose to formulate the problem here with respect to sound speed instead. This requires that the pressure gradient ∇p in the momentum equation (2.2) be recast,

$$D\mathbf{u}/Dt = -(\Gamma - 1)^{-1} c \nabla c + \rho^{-1} \left(\mathcal{F} + \tfrac{1}{2} (\Gamma - 1)^{-1} \rho T \nabla s \right) \tag{2.8}$$

An important consequence of using the (c, s) thermodynamic framework is that sound-sound interactions will now be captured *entirely* by terms of second order—a result not possible when working with the pressure (cf. Culick 1976; Yang et al. 1987, 1988).

Finally, our choice of coordinate system is justified as follows. Since the flow behavior in the vicinity of the burning propellant is ultimately of concern, to accommodate a variety of grain geometries, vectors are decomposed into normal n and tangential ζ components with respect to the surface in question,

$$\mathbf{a} = (\mathbf{n} \cdot \mathbf{a})\mathbf{n} - \mathbf{n} \times (\mathbf{n} \times \mathbf{a}) \equiv a_n \mathbf{n} + \mathbf{a}_\zeta \tag{2.9}$$

Further details of this coordinate system, including the representation of operators, are provided in Appendix A.

[†] Specifically, pressure does not lead to the greatest number of homogeneous equations; this is to be interpreted in the sense of a perturbation expansion and a flow of information down the hierarchical chain. By way of illustration, it is worthwhile to note that when Fox (1955) considered the problem of the steepening of axial acoustic waves (cf. §C.3 for further details), only a single term in the perturbation expansion of the sound speed was needed within the (c, s) thermodynamic framework.

2.3 Expansion in Mean and Fluctuating Parts

The analysis begins by writing all dependent variables as sums of mean (uppercase) and fluctuating (lowercase) parts:

$$\mathbf{u} = \underbrace{M_b \mathbf{U}(\mathbf{x}) + O\left(M_b^3\right)}_{mean} + \mathbf{u}(\mathbf{x},t), \quad c = \underbrace{1 + O\left(M_b^2\right)}_{mean} + c(\mathbf{x},t), \quad \text{etc.} \tag{2.10}$$

These are measured by the Mach number at the burning surface M_b (which is on the order of $0.001 - 0.01$) and the wave amplitude ε (i.e., $c \sim O(\varepsilon)$, $\mathbf{u} \sim O(\varepsilon), \ldots$), respectively. Perturbation expansions are constructed using these *two* small parameters, which owing to their physical origins, participate differently in the formal procedures. While the details are elaborated upon in due course, some remarks are in order here.

First, *nonlinear behavior* refers to effects higher order in ε and following standard practice only terms at most linear in M_b are retained.

Second, with respect to the mean flow—which is produced by the combustion of fuel and oxidizer—the strategy adopted here (unlike that of a Reynolds averaged approach) is to analyze this motion as though it satisfies its own equations, i.e., is unaffected by the fluctuations. While certain types of behavior can no longer be accomodated[†], the equations are greatly simplified with this commonly used approximation (cf. Culick 1975; Flandro 1995 a, b). What is more, since M_b is small compared to unity, the mean flow is at leading order incompressible (cf. §B.1 for further details). Although this ceases to be true in the aft end of a motor, where the gaseous products of combustion accelerate through the nozzle to supersonic speeds, this part of the chamber is not considered here.

Third, with respect to the fluctuations, it is important to recall that combustion instability has always been identified with the presence of unsteady acoustic motions having well-defined frequencies. From the earliest observations to the present, these frequencies closely match those computed for the classical acoustic modes of a chamber having the same shape as that in question but with no mean flow (i.e., $M_b = 0$) and rigid walls. Thus, despite a combustion chamber containing a non-uniform—and possibly turbulent—motion of chemically reacting species, often present in condensed as well as gaseous phases, exhausting through a choked nozzle, *coherent nearly-classic acoustic waves* exist that behave in good first approximation according to their own simple scaling laws. Of course, it is precisely the departures from classical acoustics that are responsible for combustion instabilities, and in that sense, *this*

[†] For example, unexpected changes in the mean pressure that sometimes accompany oscillations, often called a *DC shift*, can no longer be accommodated. These are usually unacceptable in practice and sometimes even lead to catastrophic failure.

thesis is concerned chiefly with perturbations of a very old problem: *standing/travelling waves in an enclosure*.

Finally, we remark that an important consequence of this point of view, which forms the setting of nearly all investigations of combustion instabilities over the past fifty years (cf. Culick 1994), is that our focus is the behavior of acoustical motions in the *presence* of a mean flow, instead of acoustical motions *generated* by that mean flow. This distinction is important. It is not that the latter does not occur, but rather that experimental observations have established that during combustion instability what emerges from the background (broad-band) noise—which is due in part to turbulent fluctuations, noise emission by combustion processes, and possible other unsteady motions such as flow separations—are *coherent nearly-classic acoustic waves*.

Thus, it is the stability and time evolution of acoustic disturbances *superimposed* on a given, presumed known, mean flow unaffected by the unsteady motions that is our principal concern. Substituting the separation implied by (2.10) into the equations described in the previous section, we have that the unsteady sound speed and velocity evolve according to:

$$\partial c/\partial t + \mathscr{L}_c(...) = \mathscr{N}_c(...) \tag{2.11}$$

$$\partial \mathbf{u}/\partial t + \boldsymbol{\mathscr{L}}_u(...) = \boldsymbol{\mathscr{N}}_u(...) \tag{2.12}$$

and similarly for the unsteady pressure, temperature[†] and entropy:

$$\partial p/\partial t + \mathscr{L}_p(...) = \mathscr{N}_p(...) \tag{2.13}$$

$$\partial T/\partial t + \mathscr{L}_T(...) = \mathscr{N}_T(...) \tag{2.14}$$

$$\partial s/\partial t + \mathscr{L}_s(...) = \mathscr{N}_s(...) \tag{2.15}$$

Note that operators, which are linear $\mathscr{L}_{(\,)}$ and nonlinear $\mathscr{N}_{(\,)}$ in the wave amplitude ε, have been introduced for ease of writing; these are defined in Appendix B.

[†] Contrary to our convention, the *unsteady* temperature is represented by *uppercase* notation.

2.4 Longitudinal and Transverse Waves

Recall that a key motivation of the present effort is to account for unsteady vorticity within the combustion chamber. To this end, we begin with a Stokes-Helmholtz decomposition. This theorem of vector geometry splits the velocity field into *longitudinal* and *transverse* waves[†]:

$$\mathbf{u} = \nabla\varphi + \nabla\times\mathbf{A} \equiv \mathbf{u}_\vartheta + \mathbf{u}_\omega \tag{2.16}$$

The scalar φ and vector $\mathbf{A}$ potential are related to the dilatation $\vartheta = \nabla\cdot\mathbf{u} = \nabla\cdot\mathbf{u}_\vartheta = \nabla^2\varphi$ and the vorticity $\boldsymbol{\omega} = \nabla\times\mathbf{u} = \nabla\times\mathbf{u}_\omega = -\nabla^2\mathbf{A}$, as follows by taking the divergence and curl of (2.16), respectively. Transport equations for ϑ and $\boldsymbol{\omega}$ follow in the same way (i.e., by taking the divergence and the curl of the momentum equation (2.12), respectively),

$$\partial\vartheta/\partial t + \mathscr{L}_\vartheta(...) = \nabla\cdot\mathscr{N}_u(...) \tag{2.17}$$

$$\partial\boldsymbol{\omega}/\partial t + \mathscr{L}_\omega(...) = \nabla\times\mathscr{N}_u(...) \tag{2.18}$$

where by construction $\mathscr{L}_\vartheta(...) = \nabla\cdot\mathscr{L}_u(...)$ and $\mathscr{L}_\omega(...) = \nabla\times\mathscr{L}_u(...)$.

That longitudinal and transverse waves represent kinematically the two basic processes of fluid dynamics—the compressing/expanding process and the shearing process (cf. Wu et al. 1996)—is well known. While transverse (or vorticity) waves are the sole expression of the latter, the compressing/expanding process consists of two different types of longitudinal motions—those that are reversible and those that are not. These are approximately represented by *acoustic* or *sound* waves (denoted $\mathbf{u}_a$) and *thermal* or *entropy* waves (denoted $\mathbf{u}_s$), respectively. Although by no means exact, this decomposition $\mathbf{u}_\vartheta \sim \mathbf{u}_a + \mathbf{u}_s$ suffices for the discussion here, since the entropy generated by sound waves and the sound generated by entropy waves are higher order effects (cf. Chu and Kovasznay 1958). Moreover, we will find that within the chamber volume entropy waves contribute negligibly to $\mathbf{u}_\vartheta$ (cf. Chapters 6 and 7) and thus to good approximation $\mathbf{u}_\vartheta \sim \mathbf{u}_a$.

2.5 Modal Expansion/Spatial Averaging

In this section, we replace the partial differential equations that govern the unsteady flow in a solid rocket motor by a system of ordinary differential equations. This is accomplished by expanding the flow variables in a set of basis functions and then spatial averaging in some way. Since we construct a

---

[†] Note that the identity $\nabla^2\mathbf{u} = \nabla(\nabla\cdot\mathbf{u}) - \nabla\times(\nabla\times\mathbf{u})$ in Fourier space $k^2\hat{\mathbf{u}} = \mathbf{k}(\mathbf{k}\cdot\hat{\mathbf{u}}) - \mathbf{k}\times(\mathbf{k}\times\hat{\mathbf{u}})$ establishes that *dilation* waves oscillate *longitudinal* to—and *vorticity* waves *transverse* to—the direction of the wave vector $\mathbf{k}$; this motivates the naming convection adopted.

substantial extension of the formulation originally developed by Culick (1976), that effort is briefly discussed first.

Culick's Formulation

Because combustion instabilities are, in many respects, closely related to classical acoustic motions, Culick (1976) began with a nonlinear wave equation for the pressure. This was obtained by subtracting the time derivative of (2.13) from (2.17),

$$\nabla^2 p - \partial^2 p / \partial t^2 = h, \quad \mathbf{n} \cdot \nabla p = -f \tag{2.19}$$

The boundary condition set on the gradient of p was found by taking the normal projection of the momentum equation. The source terms h and f are defined below[†].

The basis functions used in the analysis were the solutions of the unperturbed problem, which we denote here by suffix 0:

$$\nabla^2 p_{m0} + k_{m0}^2 p_{m0} = 0, \quad \mathbf{n} \cdot \nabla p_{m0} = 0 \tag{2.20}$$

This follows by setting $h = f = 0$ and $p = p_{m0} e^{-ik_{m0}t}$ in (2.19), where p_{m0} is the unperturbed mode shape for the mth mode and k_{m0} the corresponding wave number. The unsteady pressure field was then expanded as a series with unknown time varying amplitudes η_m

$$p = \sum_{j=1}^{\infty} p_{j0}(\mathbf{x}) \eta_j(t) \tag{2.21}$$

The form of spatial averaging used amounted to comparing the unperturbed problem with the problem to be analyzed. In particular, the difference of (2.19) multiplied by p_{m0} and (2.20) by p was integrated over the domain:

$$-\int p_{m0} \frac{\partial^2 p}{\partial t^2} dV - k_{m0}^2 \int p_{m0}\, p\, dV = \int p_{m0} h dV + \oint p_{m0}\, f\, dS \tag{2.22}$$

Substituting in the modal expansion (2.21), it followed that

$$\ddot{\eta}_m + k_{m0}^2 \eta_m = -\frac{1}{\int p_{m0}^2(\mathbf{x}) dV} \left\{ \int p_{m0} h dV + \oint p_{m0}\, f\, dS \right\} \tag{2.23}$$

where it must be emphasized that h and f contain both linear and nonlinear processes. Note that when evaluating the forcing on the right-hand side of (2.23), the acoustic velocity component

---

[†] $h = -\nabla \cdot \left(\mathscr{L}_u(\ldots) - \nabla p \right) + \partial \left(\mathscr{L}_p(\ldots) - \vartheta \right) / \partial t - \partial \mathscr{N}_p(\ldots) / \partial t + \nabla \cdot \mathscr{N}_u(\ldots)$

$f = \mathbf{n} \cdot \partial \mathbf{u} / \partial t + \mathbf{n} \cdot \left(\mathscr{L}_u(\ldots) - \nabla p \right) - \mathbf{n} \cdot \mathscr{N}_u(\ldots)$

$\mathbf{u}_a = \sum_{j=1}^{\infty} \frac{1}{k_{j0}^2} p_{j0}(\mathbf{x}) \dot{\eta}_j(t)$ was modeled using the leading order in ε projection of the momentum equation onto an irrotational space, i.e., $\partial \mathbf{u}_a / \partial t \sim -\nabla p$.

The Present Framework

Rather than derive a nonlinear wave equation for the pressure, we begin by writing the equations that describe the compressing/expanding process in vector form

$$\frac{\partial}{\partial t}\begin{bmatrix} c \\ \vartheta \end{bmatrix} + \begin{bmatrix} \mathscr{L}_c(...) \\ \mathscr{L}_\vartheta(...) \end{bmatrix} = \begin{bmatrix} \mathscr{N}_c(...) \\ \nabla \cdot \mathscr{N}_u(...) \end{bmatrix} \tag{2.24}$$

where for reasons already stated, we use sound speed as the chief thermodynamic variable[†].

We choose as our basis the linear stability eigenfunctions, the problem statement for which can be obtained, following standard practice, by dropping the nonlinear terms in (2.24) and assuming exponential time dependence (i.e., $c = c_m e^{-ik_m t}$, …),

$$\begin{bmatrix} \mathscr{L}_c(...) \\ \mathscr{L}_\vartheta(...) \end{bmatrix} = ik_m \begin{bmatrix} c_m \\ \vartheta_m \end{bmatrix} \tag{2.25}$$

This can be more succinctly written as

$$\mathscr{L}(\mathbf{f}_m, ...) = ik_m \mathbf{f}_m \tag{2.26}$$

where $\mathbf{f}_m \equiv \begin{bmatrix} c_m & \vartheta_m \end{bmatrix}^T$ and $\mathscr{L}(\mathbf{f}_m, ...) \equiv \begin{bmatrix} \mathscr{L}_c(\mathbf{f}_m, ...) & \mathscr{L}_\vartheta(\mathbf{f}_m, ...) \end{bmatrix}^T$.

In solving (2.26), we obtain not only the desired set of basis functions $\mathbf{f}_m$, but also the wave-amplifying power of the system k_m. Note that to recover from (2.24) the basis functions used by Culick (1976), all damping and driving processes contained in the linear operators need to be dropped. In other words, in contrast with that earlier approach, we expand the acoustic motions here in terms of the *perturbed* rather than the unperturbed modes.

This is not the only difference. Our unsteady flow model will also satisfy the no-slip condition. This requires that we solve (2.26) in concert with the corresponding linearized equation for the vorticity,

$$\mathscr{L}_\omega(...) = ik_m \boldsymbol{\omega}_m \tag{2.27}$$

This is another significant contribution of the work presented here: we construct a basis in which to expand the vortical half of the flow field. The details of solving (2.25) and (2.27) iteratively are provided in Chapter 7.

[†] We could just as easily work in terms of the pressure, in which case our starting point would be

$$\frac{\partial}{\partial t}\begin{bmatrix} p \\ \vartheta \end{bmatrix} + \begin{bmatrix} \mathscr{L}_p(...) \\ \mathscr{L}_\vartheta(...) \end{bmatrix} = \begin{bmatrix} \mathscr{N}_p(...) \\ \nabla \cdot \mathscr{N}_u(...) \end{bmatrix}$$

Regardless of how the eigenfunctions are determined in detail (cf. Chapters 3 and 7), a series expansion of the form

$$c(\mathbf{x},t)=\tfrac{1}{2}\sum_{j=-\infty}^{\infty}c_j(\mathbf{x})\eta_j(t),\quad \vartheta(\mathbf{x},t)=\tfrac{1}{2}\sum_{j=-\infty}^{\infty}\vartheta_j(\mathbf{x})\eta_j(t) \tag{2.28}$$

is considered; negative values of the index denote the complex conjugate. A similar expansion for the vorticity is introduced,

$$\boldsymbol{\omega}(\mathbf{x},t)=\tfrac{1}{2}\sum_{j=-\infty}^{\infty}\boldsymbol{\omega}_j(\mathbf{x})\eta_j(t) \tag{2.29}$$

All that remains is to effect a *spatial averaging* over the domain. Because the eigenfunctions $\mathbf{f}_m$ will in general not form an orthogonal set, it is advantageous to do so by using solutions $\mathbf{f}_m^\dagger$ to the adjoint problem. This is formally defined as (cf. Stakgold 1967)

$$\left\langle \mathscr{L}(\mathbf{f}_m,...),\mathbf{f}_m^\dagger\right\rangle-\left\langle \mathbf{f}_m,\mathscr{L}^\dagger(\mathbf{f}_m^\dagger,...)\right\rangle\equiv\int\nabla\cdot(\ )\,dV \tag{2.30}$$

where $\langle\ \rangle$ is the complex valued inner product $\langle\mathbf{x},\mathbf{y}\rangle\equiv\int\mathbf{y}^{*T}\mathbf{x}dV$. Note that the volume integral on the right-hand side can be expressed solely in terms of the behavior on the boundary by using the divergence theorem. Typically, the boundary conditions for the adjoints are chosen such that this term vanishes identically; for this reason it is convenient to define $\mathbf{f}_m^\dagger$ in terms of the scalar potential, as opposed to the dilatation, i.e., $\mathbf{f}_m^\dagger\equiv\begin{bmatrix}c_m^\dagger & \varphi_m^\dagger\end{bmatrix}^T$ (cf. §C.1 for further details). Accordingly, the eigenfunctions and their adjoints will form a bi-orthogonal set—a very desirable property indeed.

Now introducing the series expansion (2.28) into (2.24) and taking the complex inner product with $\mathbf{f}_m^\dagger$ as previously defined, derives the corresponding amplitude equation for the mth mode:

$$\dot\eta_m+ik_m\eta_m=\tfrac{1}{E_m^2}\left(\int\mathscr{N}_c(...)c_m^{\dagger*}dV-\int\mathscr{N}_u(...)\cdot\nabla\varphi_m^{\dagger*}dV+\oint\varphi_m^{\dagger*}\mathbf{n}\cdot\mathscr{N}_u(...)dS\right) \tag{2.31}$$

where $E_m^2=\tfrac{1}{2}\int\left(c_m^{\dagger*}c_m+\varphi_m^{\dagger*}\vartheta_m\right)dV$. The operators $\mathscr{N}_c(...)$ and $\mathscr{N}_u(...)$ contain c and ϑ as well as the vorticity field $\boldsymbol{\omega}$. These are to be replaced by the series expansions (2.28) and (2.29).

In closing, we note that although our focus is combustion instability within solid rocket motors, the framework developed here is far more general. While no single analysis can hope to accommodate *all* possible instabilities in the different combustors found in operational use, there are nonetheless some features common to *all* combustion systems. Indeed, it has often been emphasized that characteristics shared by combustion systems in many respects dominate the differences—for whatever the system, acoustic waves play a key role in the instability (cf. Culick 1994). Thus, in many respects, their analytical treatment will essentially be the same.

3. NONLINEAR ACOUSTICS

We now investigate purely *acoustic* motions within a chamber of arbitrary shape enclosed by a rigid boundary and containing a fluid otherwise at rest. This simple application of the framework developed in Chapter 2 introduces important features of time-dependent motions within combustion chambers, even though processes that distinguish such chambers from purely acoustical systems are presently ignored.

To begin with, we obtain the bi-orthogonal set of functions used as a basis and a means to effect spatial averaging, by solving the linear stability problem

$$\begin{bmatrix} \mathscr{L}_c\left(c_{m0},\vartheta_{m0}\right) \\ \mathscr{L}_\vartheta\left(c_{m0},\vartheta_{m0}\right) \end{bmatrix} = ik_{m0}\begin{bmatrix} c_{m0} \\ \vartheta_{m0} \end{bmatrix} \tag{3.1}$$

and its adjoint (cf. (2.30)), respectively. This calculation is straightforward since the system (3.1) collapses into a single equation for the mth mode shape c_{m0}:

$$\nabla^2 c_{m0} + k_{m0}^2 c_{m0} = 0, \quad \mathbf{n}\cdot\nabla c_{m0} = 0 \tag{3.2}$$

with all other flow variables expressible in terms of the c_{m0} (cf. §C.1 for further details). Note that the condition $\mathbf{n}\cdot\nabla c_{m0} = 0$ sets the unsteady velocity normal to the boundary to zero and determines the wave numbers k_{m0}.

Next, we evaluate the nonlinear forcing in (2.31). Only terms that describe sound-sound interactions are retained when substituting (B.33) and (B.34) for the nonlinear operators $\mathscr{N}_c\left(...\right)$ and $\mathscr{N}_u\left(...\right)$, respectively. Introducing the modal expansion of the flow field variables as indicated by (2.28) leads eventually to

$$\dot{\eta}_m + ik_{m0}\eta_m = \tfrac{1}{E_m^2}\sum_{j=-\infty}^{\infty}\sum_{k=-\infty}^{\infty} iI^{\vartheta,\vartheta(m,j,k)}\eta_j\eta_k \tag{3.3}$$

where the $I^{\vartheta,\vartheta(m,j,k)}$ are a function of the wave numbers and the mode shapes; the exact relationship is given below†.

To evolve the amplitude equations (3.3) numerically, values for the linear and nonlinear coefficients must be specified. This requires that we solve (3.2) for the c_{m0}. Many well-written books discuss this problem (e.g., Morse and Ingard 1968). Since numerical methods (cf. French et al. 1996) are

---

† In particular, we have

$$I^{\vartheta,\vartheta(m,j,k)} = -\tfrac{1}{8}\left(k_{m0}+k_{j0}+k_{k0}\right)\left(I_1^{\vartheta,\vartheta(m,j,k)} - \left(\Gamma-1\right)^{-1} I_2^{\vartheta,\vartheta(m,j,k)}\right)$$

where $I_1^{\vartheta,\vartheta(m,j,k)} = \int c_{m0}c_{j0}c_{k0}dV$ and $I_2^{\vartheta,\vartheta(m,j,k)} = \left(k_{j0}k_{k0}\right)^{-1}\int c_{m0}\nabla c_{j0}\cdot\nabla c_{k0}dV$.

typically needed for complex shapes, it is useful to consider the simple—yet representative—geometry of a cylindrical propellant grain, for which the c_{m0} can be obtained in closed form:

$$c_{m0}(\mathbf{x}) = J_n(k_{ns} r)\cos(k_l z)\begin{Bmatrix}\cos(n\theta)\\ \sin(n\theta)\end{Bmatrix} \tag{3.4}$$

Here the mth mode is characterized by three indices (l,n,s), with the wave number given by $k_{m0} \equiv \sqrt{k_{ns}^2 + k_l^2}$. The values of $k_l = l\pi R/L$ are proportional to the chamber radius-to-length ratio and the k_{ns} are the roots of the derivative of the Bessel function: $dJ_n(k_{ns}r)/dr\big|_{r=1} = 0$. Only two prototypical cases will be examined in detail: purely axial modes $(l,0,0)$ and so-called[†] purely tangential modes $(0,n,0)$. The corresponding coefficients $I^{\mathcal{G},\mathcal{G}(m,j,k)}$ are evaluated in §C.2. Purely radial modes $(0,0,s)$ are rarely observed experimentally and thus are not considered.

3.1 Axial Modes

First, we consider the case of purely axial modes. That the compressive portion of any such disturbance steepens is well known. Fox (1955), for example, captured this behavior for motions within a closed cylindrical chamber by appealing to the method of characteristics (cf. §C.3 for further details). The close agreement between predictions from that approach and the present method is shown in Figure 3.1.

We now make a few remarks. First, we note that purely axial modes involve the lowest frequencies of oscillation (since the k_{m0} would now be proportional to the chamber radius-to-length ratio, which is small) and thus typically are more lightly damped and therefore easier to excite.

Second, within the mathematical framework introduced here, a necessary condition for such modes to steepen is that the nonlinearities describing sound-sound interactions force the system in a resonant way. That this resonant forcing is a consequence of the wave numbers k_{m0} being integer multiples of the fundamental (i.e., $k_{m0} = mk_{10}$) will be demonstrated in Chapter 4.

Finally, we observe that the modal representation on which our analysis is based is valid only up until shock formation. While the amplitude equations (3.3) may still be evolved beyond that point, the results cease to be meaningful; Figure 3.2 illustrates this clearly.

[†] Note that tangential here is not to be confused with the normal and *tangential* coordinate system introduced earlier.

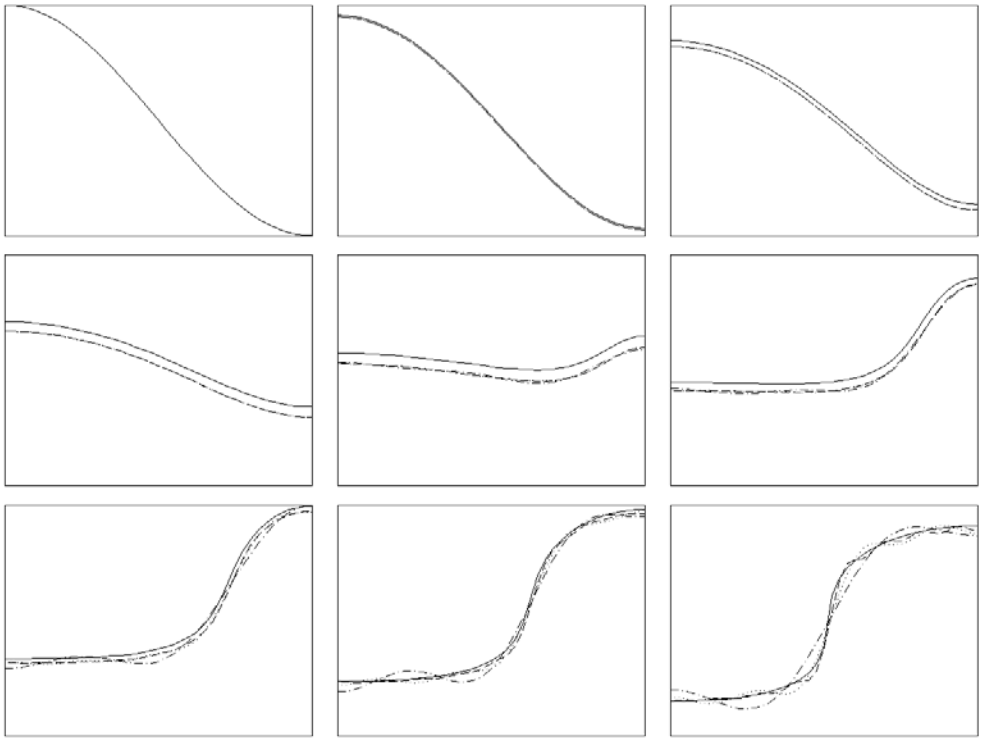

Figure 3.1 Comparison between Fox's solution (solid line) and the modal representation with 4, 8 and 16 modes respectively (dashed lines); the initial condition consists of an $m = 1$ sound wave with $\varepsilon = 0.1$

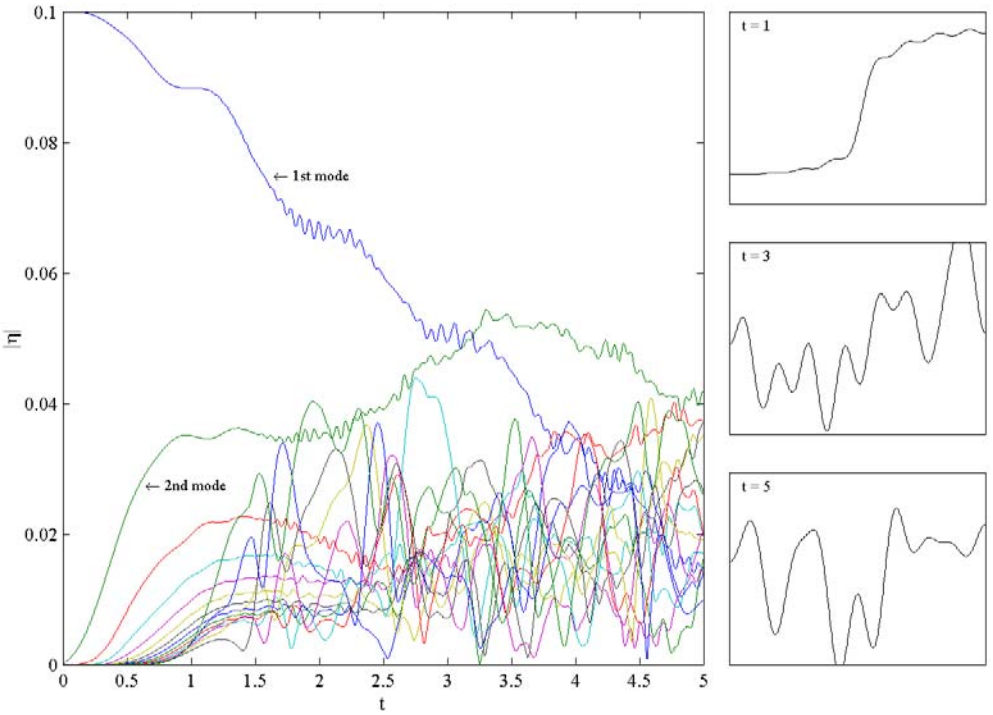

Figure 3.2 *Long* time integration of the amplitude equations with 16 modes retained for the same initial conditions as Figure 3.1; the corresponding waveforms at three representative times are shown on the right—shock formation is seen to occur around $t \sim 1$

The extent to which coupling with other processes, such as combustion, might inhibit the energy cascade to higher and higher wave number remains a subject of some controversy (cf. Flandro 1985 and Culick 1994 for two different points of view). However, it is worthwhile to note that when axial-mode instabilities are triggered, experimental observations often indicate the presence of *steep* wavefronts of pressure. This may suggest that for an initial disturbance of high enough amplitude shock formation is so rapid, that other processes do not have sufficient time to act before the system transitions to another state. The question then becomes whether these processes can unsteepen an already steepend wave. The answer is by no means obvious, since combustion, to use the example given, may respond differently to a shock than to a sinusoidal perturbation. While this matter warrants resolution, further discussion is beyond the scope of the present investigation.

3.2 Tangential Modes

We now turn to the problem of purely tangential modes[†]. Two key differences exist vis-à-vis axial modes of oscillation. First, tangential modes have higher oscillation frequencies and thus are often more heavily damped. For example, this is certainly true with aluminized propellants. The aluminum oxide smoke significantly attenuates higher frequency motions, and under such conditions, only axial modes can typically be driven.

Second, and more important for the discussion here, is that the wave numbers k_{m0} no longer satisfy any resonant triad conditions as, for instance, would be the case if $k_{m0} = mk_{10}$ (we will discuss this point further in Chapter 4). The consequences of this are shown in Figure 3.3. In contrast with purely axial modes (cf. Figs 3.1 and 3.2), sound-sound interactions now result in little energy transfer between modes, much less an actual steepening of the wavefront.

Maslen and Moore (1956) first demonstrated this behavior by working with the partial differential form of the equations, and constructing a uniformly valid solution to higher order in ε using regular perturbations. The physical explanation offered for the absence of steepening was the continuous interruption of this process by the scattering effect of reflection at a curved wall.

[†] $k_{m0} = 1.8412,\ 3.0542,\ 4.2011,\ 5.3176,\ 6.4156,\ 7.5012,\ 8.5778,\ 9.6474, \ldots$

By way of illustration, Figure 3.4 depicts the situation when the k_{m0} have been artificially assigned the value mk_{10}, with the coefficients $I^{\vartheta\vartheta(m,j,k)}$ remaining unchanged. Whether this describes a true steepening (i.e., an energy cascade to higher and higher wave numbers) is not the issue. However, there clearly is now significant energy transfer between modes. This helps establish that the values assumed by the wave numbers rather than the nonlinear coefficients are more critical in determining the behavior of the system. We will explore this idea further in Chapter 4.

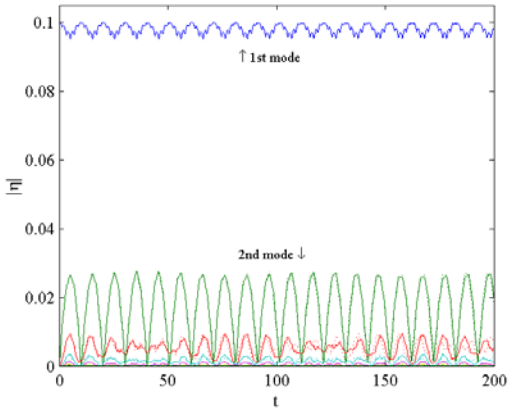

Figure 3.3 Nonlinear behavior for purely tangential modes with the same initial conditions as in Figure 3.1; the results corresponding to a 4 and 16 mode truncation are presented (no discernible difference)

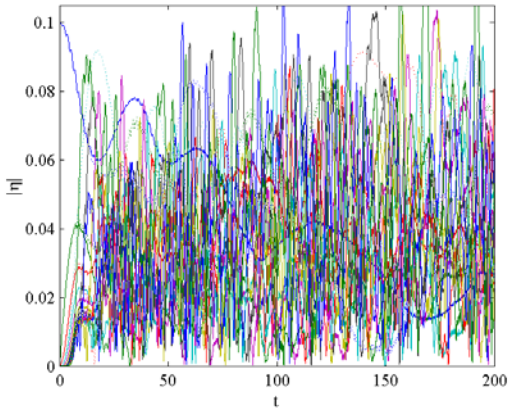

Figure 3.4 The same situation as described in Figure 3.3, except that now $k_{m0} = mk_{10}$

4. RESONANCE STRUCTURE OF THE AMPLITUDE EQUATIONS

4.1 Introduction

An essential part of any analysis based on modal expansion and spatial averaging is solving the resulting amplitude equations. While numerical integration is always possible, results obtained this way are difficult to generalize since the system may evolve differently depending upon the values the linear and nonlinear coefficients assume. Thus, the challenge has been to find a more systematic approach that facilitates broad conclusions being drawn.

Historical Overview

Historically, within the field of combustion instability, this has been accomplished either with analytic solutions or with continuation methods.

Analytic solutions are quite valuable, but only a few have been found thus far and only for problems restricted in important ways. For example, with sound-sound interactions the only nonlinear process taken into account, Awad and Culick (1986) and Yang and Culick (1990) solved for the limiting periodic behavior of purely axial and purely tangential modes, respectively. These solutions were obtained after removing the oscillatory part of the motion from the amplitude equations using the principle of time-averaging[†] and then truncating the system to two-modes. Even though the latter simplification does regrettably introduce errors (cf. Jahnke and Culick 1994; Ananthkrishnan and Culick 2002), insightful conclusions were drawn nonetheless (cf. Culick 1994 for a concise summary).

Studying the system with more than two modes retained is however clearly necessary and previous effort has relied upon continuation methods to achieve this. Well known in other fields, Janhke and Culick (1994) first adopted this numerical approach to investigate nonlinear combustion instabilities by following changes in periodic solutions, usually limit cycles, as one or more parameters were varied. While much more information is obtained this way than from numerical simulations alone, use of a continuation method does *not* resolve the difficulty of determining the behavior over broad ranges of

---

[†] Culick (1976) first applied the technique of *time-averaging* (Krylov and Bogoliubov 1947) to motions in combustion chambers. The relative weakness of the disturbing processes justified this approach as excited modes typically show only small changes in amplitudes and phases during any given cycle of the oscillation. A coupled system of first order equations governing these slowly changing quantities emerged from the analysis, the forcing of which was expressed in terms of weighted integrals of the unaveraged forcing taken over the averaging period. Even though these integrals could only be evaluated in closed form when the unperturbed acoustic wave numbers were integer multiples of the fundamental, time averaging has proven itself a useful tool by greatly reducing the cost of numerical integration (larger time steps are permissible) as well as aiding theoretical work.

parameters. Existing numerical toolsets (Doedal et al. 1991 a, b; Doedal et al. 1997; Doedal et al. 2000) allow only a few parameters to be changed simultaneously, and thus an exhaustive search of the parameter space is simply not possible. As such, most investigations (Jahnke and Culick 1994; Burnley 1996; Isella 2001; Ananthkrishnan and Culick 2002) have focused primarily on the influence of the linear coefficients, as well as, more recently, inputs in models of the combustion response. Although the former are well defined, the latter—except when the flame is assumed to respond quasi-steadily—tend to be *ad*-hoc in nature.

Present Effort

Unfortunately, this is part of a larger problem, for with the exception of sound-sound interactions, much work remains to be done on modeling nonlinear processes. Thus, without a good basis for assigning values to the nonlinear coefficients, one should consider them as parameters. While the resulting system cannot (practically speaking) be studied computationally, even with continuation methods, perturbation techniques can be utilized since then the nonlinear coefficients need not be specified a priori—only conditions on the linear behavior of the system need to be placed (e.g., the first mode is unstable while all other modes are stable).

The basic idea behind such an analysis is that, the long-term behavior of a system of nonlinear ordinary differential equations is determined by its resonance structure. Although this idea is certainly not novel, and dates back to work independently done by Stokes and Poincare, the current effort marks the first application to the field of combustion instability. Essentially, the amplitude equations can be viewed as describing the motions of a set of nonlinearly coupled oscillators (cf. Culick 1994 for further discussion), with the small terms on the right-hand sides as terms forcing the linear oscillators represented by the left-hand sides. In general, the response of such a system is of the same order as the forcing, *except* when any of the forcing terms has the same period as one of the oscillators. These resonances lead to an enhanced response which may after a long time change the amplitude of the oscillators at first order, even though the interaction itself is second order or higher. The examples worked out in Chapter 3 certainly illustrate this behavior.

By using ideas of resonance, we will show how to derive perturbation results for any desired number of modes, and in the process identity those nonlinear coefficients that have the greatest impact on

the system. We begin by expanding the forcing in (2.31) to include the nonlinearity expected to *naturally occur*† to second and third order in the wave amplitude ε,

$$\dot{\eta}_m + ik_m\eta_m = \frac{1}{E_m^2}\left(\begin{array}{c}\displaystyle\sum_{j,k}\left(f_r^{\varepsilon\varepsilon(m,j,k)} + i\,f_i^{\varepsilon\varepsilon(m,j,k)}\right)\eta_j\,\eta_k + \\ \displaystyle+\sum_{j,k,l}\left(f_r^{\varepsilon\varepsilon\varepsilon(m,j,k,l)} + i\,f_i^{\varepsilon\varepsilon\varepsilon(m,j,k,l)}\right)\eta_j\,\eta_k\,\eta_l\end{array}\right) \tag{4.1}$$

where

$$\sum_{j,k} = \sum_{j=-\infty}^{\infty}\sum_{k=-\infty}^{\infty} \tag{4.2}$$

While we are not concerned here with the physical origin of the terms, it is worthwhile to point out that sound-sound interactions, as shown in Chapter 3, contribute to $f_i^{\varepsilon\varepsilon(m,j,k)}$; similarly, other effects, such as interactions with the unsteady vorticity field, will add to, or subtract from, the coefficients.

Turning now to the analysis of (4.1), we first consider the case when the k_m are real (cf. §4.2), and then study the behavior when the k_m have an imaginary component as well (cf. §4.3). The basic difference is that for the latter, modes also grow or decay exponentially in the linear limit rather than just oscillate harmonically.

4.2 Real Wave Numbers

With other techniques exist, we construct here a perturbation solution of (4.1) in terms of a hierarchy of successively slower time scales: $t_0 = t,\quad t_1 = \varepsilon t,\quad t_2 = \varepsilon^2 t, ...,\quad t_N = \varepsilon^N t$ (cf. Kevorkian and Cole 1996).

We begin by assuming a solution of the form

$$\eta_m(t;\varepsilon) = \varepsilon\left(\eta_{m0}(t_0,t_1,...) + \varepsilon\eta_{m1}(t_0,t_1,...) + \varepsilon^2\eta_{m2}(t_0,t_1,...) + ...\right) \tag{4.3}$$

and then compute

$$\frac{d\eta_m}{dt} = \varepsilon\frac{\partial\eta_{m0}}{\partial t_0} + \varepsilon^2\left(\frac{\partial\eta_{m1}}{\partial t_0} + \frac{\partial\eta_{m0}}{\partial t_1}\right) + \varepsilon^3\left(\frac{\partial\eta_{m2}}{\partial t_0} + \frac{\partial\eta_{m1}}{\partial t_1} + \frac{\partial\eta_{m0}}{\partial t_2}\right) + ... \tag{4.4}$$

using the chain rule.

Next, we substitute (4.3) and (4.4) into (4.1) to obtain the following differential equations for the various terms in the expansion of η_m to $O(\varepsilon^3)$:

$$\frac{\partial\eta_{m0}}{\partial t_0} + ik_m\eta_{m0} = 0 \tag{4.5}$$

† By this it is meant terms that arise as the products of flow variables, giving rise to, for example, interactions between the sound, thermal and vorticity fields.

$$\frac{\partial \eta_{m1}}{\partial t_0} + ik_m \eta_{m1} + \frac{\partial \eta_{m0}}{\partial t_1} = \frac{1}{E_m^2} \sum_{j,k} \begin{pmatrix} f_r^{\varepsilon\varepsilon(m,j,k)} + \\ +i\, f_i^{\varepsilon\varepsilon(m,j,k)} \end{pmatrix} \eta_{j0}\, \eta_{k0} \tag{4.6}$$

$$\frac{\partial \eta_{m2}}{\partial t_0} + ik_m \eta_{m2} + \frac{\partial \eta_{m1}}{\partial t_1} + \frac{\partial \eta_{m0}}{\partial t_2} = \frac{1}{E_m^2} \begin{pmatrix} \sum_{j,k} \left(f_r^{\varepsilon\varepsilon(m,j,k)} + i\, f_i^{\varepsilon\varepsilon(m,j,k)} \right) \left(\eta_{j0}\, \eta_{k1} + \eta_{k0} \eta_{j1} \right) + \\ + \sum_{j,k,l} \left(f_r^{\varepsilon\varepsilon\varepsilon(m,j,k,l)} + i\, f_i^{\varepsilon\varepsilon\varepsilon(m,j,k,l)} \right) \eta_{j0}\, \eta_{k0}\, \eta_{l0} \end{pmatrix} \tag{4.7}$$

Terms of $O(\varepsilon)$

The solution of (4.5) is

$$\eta_{m0} = r_{m0}(t_1, ...) e^{-i\left(k_m t_0 + \phi_{m0}(t_1, ...)\right)} \tag{4.8}$$

where at this stage of the analysis $r_{m0}(t_1, ...)$ and $\phi_{m0}(t_1, ...)$ are undetermined functions, which may depend on the slower time scales $t_1,\ t_2, ...$ but not on t_0. *Determining these functions is our chief interest here* and this is accomplished by suppressing resonant terms at higher order.

To help motivate this key idea, let us assume for the moment that $\partial \eta_{m0} / \partial t_1 = 0$. We can then immediately solve (4.6) for η_{m1}:

$$\eta_{m1} = \frac{i}{E_m^2} \sum_{j,k} \frac{1}{k_j + k_k - k_m} \begin{pmatrix} f_r^{\varepsilon\varepsilon(m,j,k)} + \\ +i\, f_i^{\varepsilon\varepsilon(m,j,k)} \end{pmatrix} r_{j0}\, r_{k0}\, e^{-i\left(\left(k_j + k_k\right) t_0 + \phi_{j0} + \phi_{k0}\right)} + r_{m1} e^{-i\left(k_m t_0 + \phi_{m1}\right)} \tag{4.9}$$

In examining this result, the basic principle to bear in mind is that a perturbation expansion is valid only if higher order contributions are *higher order*. Terms in the sum that satisfy the corresponding resonant triad condition $k_j + k_k - k_m \le O(\varepsilon)$ violate this principle, as the denominator would then be $O(\varepsilon)$ or less, and thus the contribution to η_{m1} would be $O(\eta_{m0})$.

To avoid such inconsistent behavior, the forcing of (4.6) should be partitioned into terms, which are resonant $(\mathscr{R})$, and terms, which are not $(\mathscr{NR})$:

$$\sum_{j,k} \quad = \sum_{\substack{j,k \\ k_j + k_k \sim k_m}} + \sum_{\substack{j,k \\ k_j + k_k \not\sim k_m}} \equiv \sum_{\substack{j,k \\ (\mathscr{R})}} + \sum_{\substack{j,k \\ (\mathscr{NR})}} \tag{4.10}$$

Resonant terms effect a response larger than themselves and need to be suppressed. The procedure for doing so is straightforward. Rather than assume that $\partial \eta_{m0} / \partial t_1 = 0$, we instead set $\partial \eta_{m0} / \partial t_1$ equal to these terms; after substituting in (4.8), we have

$$\frac{\partial r_{m0}}{\partial t_1} - i r_{m0} \frac{\partial \phi_{m0}}{\partial t_1} = \frac{1}{E_m^2} \sum_{\substack{j,k \\ (\mathscr{R})}} \begin{pmatrix} f_r^{\varepsilon\varepsilon(m,j,k)} + \\ +i\, f_i^{\varepsilon\varepsilon(m,j,k)} \end{pmatrix} r_{j0}\, r_{k0}\, e^{i\left(\phi_{m0} - \phi_{j0} - \phi_{k0}\right)} \tag{4.11}$$

The real and imaginary parts of (4.11) give evolution equations for r_{m0} and ϕ_{m0}, respectively. While one typically has to resort to a numerical solution, it has at least been established that significant

energy transfer between modes is *possible* only when at least some resonant triad conditions are satisfied. This accounts for basic differences observed in Chapter 3 between purely axial and purely tangential modes, as well as the dramatic change in the behavior of the latter when the wave numbers were artificially forced to be integer multiples of the fundamental (cf. Figs 3.3 and 3.4).

Resonance Conditions Unsatisfied

Now we consider what happens if *no* resonant triad conditions are satisfied. This, for example, is the case for purely tangential modes (cf. §3.2). Since we are justified in setting $\partial\eta_{m0}/\partial t_1 = 0$, the result for η_{m1} given by (4.9) is indeed valid. To complete the solution, it remains to determine the behavior of the unknown amplitudes $r_{m0}(t_2,t_3,...)$ and $r_{m1}(t_1,t_2,...)$ and phases $\phi_{m0}(t_2,t_3,...)$ and $\phi_{m1}(t_1,t_2,...)$. To this end, the equations governing the $O(\varepsilon^2)$ behavior need to be appealed to.

Recall, the basic idea is that resonant forcing terms must be suppressed. Consider those terms in (4.7) that arise owing to the interaction between the zeroth and first order solutions. Insofar as the forced part of η_{j1} is concerned, the form of the dependence on the t_0 scale that results from the product with η_{k0} is $e^{-i(k_j+k_k+k_l)t_0}$, with summation occurring over all three indices. This same combination also arises from the cubic nonlinearity. This suggests that even in the absence of *any* triad conditions $k_j + k_k - k_m = O(\varepsilon)$ being satisfied, resonance occurs owing to *self-interaction*, i.e., when for instance $j = -k$ and $l = m$.

To avoid this it is necessary to let

$$\frac{\partial\eta_{m1}}{\partial t_1} = 0, \quad \frac{\partial\eta_{m0}}{\partial t_2} = \tfrac{2}{E_m^2}\eta_{m0}\sum_j\left(\sigma_r^{(m,j)} + i\sigma_i^{(m,j)}\right)r_{j0}^2 \tag{4.12}$$

where the coefficients $\sigma_r^{(m,j)}$ and $\sigma_i^{(m,j)}$ follow from (4.6) and are defined below†. The first equation simply indicates that $r_{m1} = r_{m1}(t_2,t_3,...)$ and $\phi_{m1} = \phi_{m1}(t_2,t_3,...)$. Introducing the solution for η_{m0} from (4.8), we can expand the second equation to obtain

$$\frac{\partial r_{m0}}{\partial t_2} - ir_{m0}\frac{\partial\phi_{m0}}{\partial t_2} = \tfrac{2}{E_m^2}r_{m0}\sum_j\left(\sigma_r^{(m,j)} + i\sigma_i^{(m,j)}\right)r_{j0}^2 \tag{4.13}$$

---

† $\sigma_r^{(m,j)} = -\sum_k \frac{1}{E_k^2}\left(\frac{1}{k_m-k_j-k_k}\begin{pmatrix} f_r^{\varepsilon\varepsilon(m,j,k)} f_i^{\varepsilon\varepsilon(k,m,-j)} + \\ + f_i^{\varepsilon\varepsilon(m,j,k)} f_r^{\varepsilon\varepsilon(k,m,-j)}\end{pmatrix} - \frac{1}{k_k}\begin{pmatrix} f_r^{\varepsilon\varepsilon(m,m,k)} f_i^{\varepsilon\varepsilon(k,j,-j)} + \\ + f_i^{\varepsilon\varepsilon(m,m,k)} f_r^{\varepsilon\varepsilon(k,j,-j)}\end{pmatrix}\right) + f_r^{\varepsilon\varepsilon\varepsilon(m,m,j,-j)}$

$\sigma_i^{(m,j)} = \sum_k \frac{1}{E_k^2}\left(\frac{1}{k_m-k_j-k_k}\begin{pmatrix} f_r^{\varepsilon\varepsilon(m,j,k)} f_r^{\varepsilon\varepsilon(k,m,-j)} - \\ - f_i^{\varepsilon\varepsilon(m,j,k)} f_i^{\varepsilon\varepsilon(k,m,-j)}\end{pmatrix} - \frac{1}{k_k}\begin{pmatrix} f_r^{\varepsilon\varepsilon(m,m,k)} f_r^{\varepsilon\varepsilon(k,j,-j)} - \\ - f_i^{\varepsilon\varepsilon(m,m,k)} f_i^{\varepsilon\varepsilon(k,j,-j)}\end{pmatrix}\right) + f_i^{\varepsilon\varepsilon\varepsilon(m,m,j,-j)}$

The real and imaginary parts of (4.13) give evolution equations for r_{m0} and ϕ_{m0}, respectively. As before, a numerical solution typically has to be resorted to.

However, an important simplification does occur when all the $\sigma_r^{(m,j)}$ vanish. This, for example, would be the case if either $f_r^{\varepsilon\varepsilon(m,j,k)}$ or $f_i^{\varepsilon\varepsilon(m,j,k)}$ are identically zero, and assuming a third order nonlinearity, if $f_r^{\varepsilon\varepsilon\varepsilon(m,m,j,-j)}$ are zero as well. We digress to point out that for the sound-sound interactions studied in Chapter 3, $\sigma_r^{(m,j)}=0$ since no contribution to the $f_r^{\varepsilon\varepsilon(m,j,k)}$ coefficients arose. Had the problem been alternatively formulated with pressure, as opposed to sound speed, as the primary thermodynamic variable, third order effects would have been entirely captured by $f_i^{\varepsilon\varepsilon\varepsilon(m,j,k,l)}$, and so similarly $\sigma_r^{(m,j)}=0$. Returning to (4.13), under these conditions a closed form solution exists; in particular, since the real part of the forcing would be zero, $\partial r_{m0}/\partial t_2 = 0$ from which it follows that $r_{m0} = r_{m0}(t_3, t_4, \ldots)$. Integrating what remains of (4.13) is straightforward,

$$\phi_{m0} = \phi_{m0}(t_2, t_3, \ldots) = -\frac{2}{E_m^2}\left(\sum_j \sigma_i^{(m,j)} r_{j0}^2\right) t_2 + \phi_{m0}(t_3, t_4, \ldots) \tag{4.14}$$

Were the analysis to stop here $r_{m0} = r_{m0}(t_3, t_4, \ldots)$ and $\phi_{m0}(t_3, t_4, \ldots)$ would be assumed constant and chosen to satisfy the initial conditions. The leading order solution $\eta_{m0} = r_{m0} e^{-i(k_m t_0 + \phi_{m0})}$ would then simply consist of an $O(\varepsilon^2)$ perturbation to the wave number k_m given by (4.14), with this shift in frequency a function of: the initial amplitudes; the unperturbed wave numbers; and the nonlinear coefficients. Such a solution clearly exhibits the behavior observed in Figure 3.3, where no sustained energy transfer between modes was seen to occur; Figure 4.1 compares the analytic solution given above with numerical integration of (4.1) for a similar example.

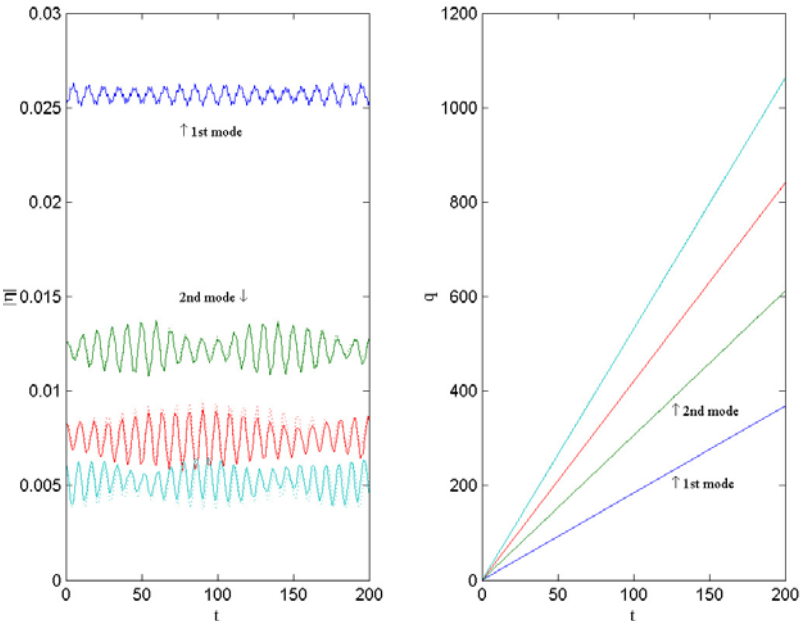

Figure 4.1 Comparison between the closed form analytic solution (dashed line) and numerical integration (solid line) for the case of 4 purely tangential modes; the initial conditions are $\eta_m = \varepsilon/m$ where $\varepsilon = 0.025$; the angle q is defined by $\eta_m = |\eta_m| e^{-iq_m}$

4.3 Complex Wave Numbers

In the previous section, we showed that when the wave numbers are real, for certain types of nonlinearity (e.g., sound-sound interactions), resonant triad conditions if not satisfied initially remain forever unsatisfied. However, for the sorts of problems of interest here, the wave numbers will in general be complex and of the form $k_m = k_{m0} + M_b k_{m\mu}$, where M_b is the injection Mach number and $k_{m\mu} \equiv -\theta_{m\mu} + i\alpha_{m\mu}$ is the perturbation to the unperturbed wave number k_{m0} (cf. Chapters 7 and 8 for further details). When this is the case, the amplitude equations (4.1) evolve in a decidedly different manner.

Figure 4.2 illustrates this clearly with a typical example when the first mode is linearly unstable and all other modes are stable. This is a case of practical interest since energy released by combustion processes often causes the first mode to be unstable, while dissipative mechanisms tend to stabilize the higher modes.

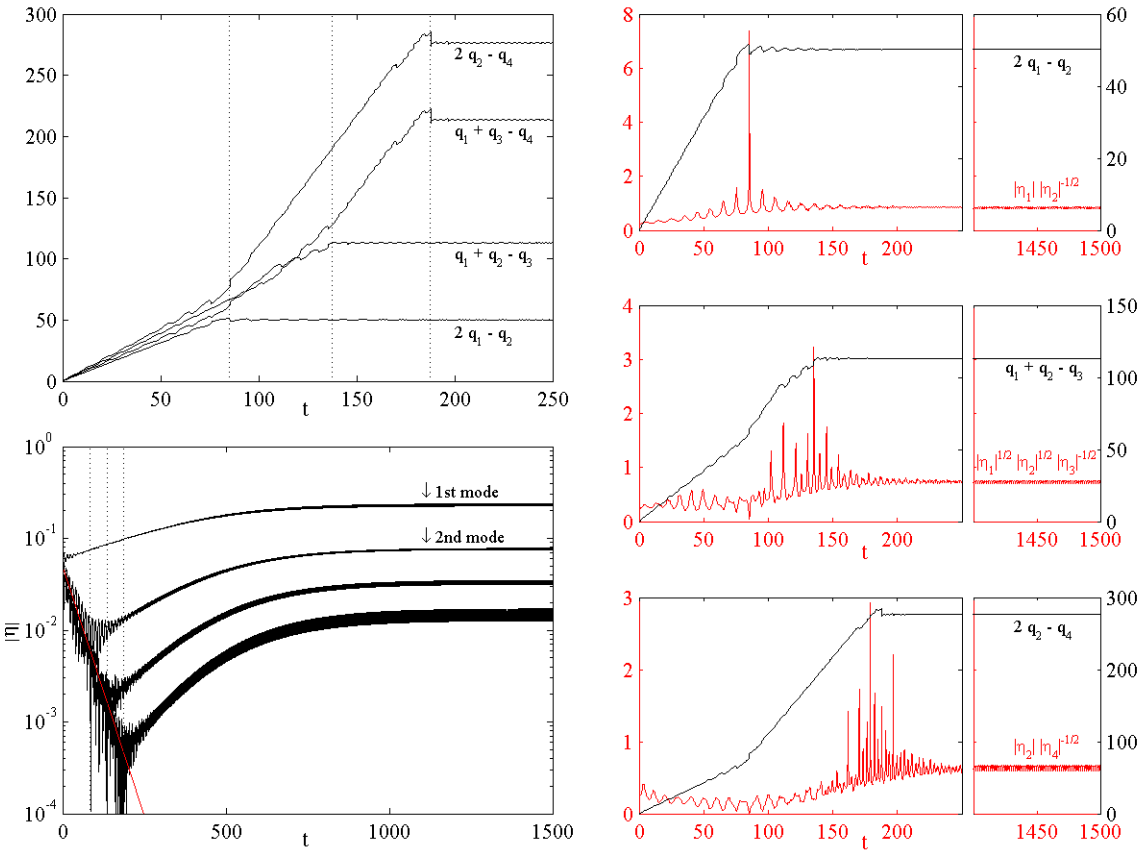

Figure 4.2 Time evolution of the first four tangential modes when $M_b k_{1\mu} = 0.003i$ and $M_b k_{m\mu} = -0.025i$ for all other modes; the initial disturbance values are the same $\eta_{1\to4} = \varepsilon = 0.05$

What is to be observed (cf. the sequence of images on the right of Figure 4.2) is that now even if *no* resonant triad conditions are initially satisfied, this ceases to be true as the system evolves. In other words, the phases (cf. (4.15) for a precise definition) lock, and on a time scale short in comparison with that which measures the energy transfer between modes[†]. More surprising perhaps is that the corresponding ratios of the absolute values of the amplitudes exhibit the exact same behavior and tend to lock almost in sync.

Our objective here is to explain this behavior mathematically as well as derive formulae that predict the limiting state. To do so, it is more effective to recast the system (4.1) in terms of the energy p_m and phase q_m (cf. Kevorkian and Cole 1996):

$$p_m \equiv \tfrac{E_m^2}{2}\left|\eta_m\right|^2, \quad q_m \equiv \tan^{-1}\left(-\eta_m^{(i)}\big/\eta_m^{(r)}\right) \tag{4.15}$$

where $\eta_m = \frac{1}{E_m}\sqrt{2p_m}\,e^{-iq_m}$ and as before negative indices denote the complex conjugate.

Evolution equations for p_m:

$$\dot{p}_m = 2k_m^{(i)}p_m + \sum_{j,k}\tfrac{2\sqrt{2}}{E_m E_j E_k}\sqrt{p_m p_j p_k}\begin{pmatrix} f_r^{\varepsilon\varepsilon(m,j,k)}\cos\left(q_m - q_j - q_k\right) - \\ - f_i^{\varepsilon\varepsilon(m,j,k)}\sin\left(q_m - q_j - q_k\right)\end{pmatrix} \tag{4.16}$$

and q_m:

$$\dot{q}_m = k_m^{(r)} - \sum_{j,k}\tfrac{\sqrt{2}}{E_m E_j E_k}\frac{\sqrt{p_j p_k}}{\sqrt{p_m}}\begin{pmatrix} f_r^{\varepsilon\varepsilon(m,j,k)}\sin\left(q_m - q_j - q_k\right) + \\ + f_i^{\varepsilon\varepsilon(m,j,k)}\cos\left(q_m - q_j - q_k\right)\end{pmatrix} \tag{4.17}$$

can be derived by differentiating (4.15) with respect to time, and substituting (4.1) where appropriate. Note that only second order nonlinearities have been retained.

A few remarks are now in order. First, a more general definition of a resonant triad condition than that given in §4.2 is $q_j + q_k - q_m \sim$ constant. Only when this *phase locking* occurs can a significant amount of energy be transferred between modes. Second, for the cases of interest here, this energy transfer ultimately leads to a stable periodic limit cycle and the phases must then be integral multiples of the fundamental. To capture this long time behavior it is sufficient to consider the resonance structure of the equations. This can be obtained simply by replacing the summation over k with that contribution which arises when $k = m - j$.

Now we use the (p_m, q_m) framework as a starting point to understand the behavior depicted in Figure 4.2. Recall that we are considering a case where only the first mode is unstable; other scenarios can

---

[†] In studying a *two-mode approximation* for tangential modes using the set of amplitude equations derived earlier by Culick (1976), Burnley (1996) also observed that phases lock on a short time scale (no comment was made on the amplitudes); no explanation of this phenomenon was given.

also be considered, but we aim here only to illustrate the basic procedure. We begin by introducing a new set of variables:

$$P_m \equiv p_1^m \big/ p_m\,, \quad Q_m \equiv m q_1 - q_m \tag{4.18}$$

Differentiating (4.18) and making the necessary substitutions, derives evolution equation equations for P_m and Q_m. In particular, we have

$$\begin{aligned}\frac{\dot{P}_m}{2P_m} = \left(m k_1^{(i)} - k_m^{(i)}\right) + m\sum_j \frac{\sqrt{2}}{E_1 E_j E_{1-j}} \frac{\sqrt{P_1}}{\sqrt{P_j P_{1-j}}} \left(\begin{array}{l} f_r^{\varepsilon\varepsilon(1,j,1-j)} \cos\left(Q_1 - Q_j - Q_{1-j}\right) + \\ + f_i^{\varepsilon\varepsilon(1,j,1-j)} \sin\left(Q_1 - Q_j - Q_{1-j}\right) \end{array} \right) - \\ - \sum_j \frac{\sqrt{2}}{E_m E_j E_{m-j}} \frac{\sqrt{P_m}}{\sqrt{P_j P_{m-j}}} \left(\begin{array}{l} f_r^{\varepsilon\varepsilon(m,j,m-j)} \cos\left(Q_m - Q_j - Q_{m-j}\right) + \\ + f_i^{\varepsilon\varepsilon(m,j,m-j)} \sin\left(Q_m - Q_j - Q_{m-j}\right) \end{array} \right)\end{aligned} \tag{4.19}$$

and

$$\begin{aligned}\dot{Q}_m = \left(m k_1^{(r)} - k_m^{(r)}\right) + m\sum_j \frac{\sqrt{2}}{E_1 E_j E_{1-j}} \frac{\sqrt{P_1}}{\sqrt{P_j P_{1-j}}} \left(\begin{array}{l} f_r^{\varepsilon\varepsilon(1,j,1-j)} \sin\left(Q_1 - Q_j - Q_{1-j}\right) - \\ - f_i^{\varepsilon\varepsilon(1,j,1-j)} \cos\left(Q_1 - Q_j - Q_{1-j}\right) \end{array} \right) - \\ - \sum_j \frac{\sqrt{2}}{E_m E_j E_{m-j}} \frac{\sqrt{P_m}}{\sqrt{P_j P_{m-j}}} \left(\begin{array}{l} f_r^{\varepsilon\varepsilon(m,j,m-j)} \sin\left(Q_m - Q_j - Q_{m-j}\right) - \\ - f_i^{\varepsilon\varepsilon(m,j,m-j)} \cos\left(Q_m - Q_j - Q_{m-j}\right) \end{array} \right)\end{aligned} \tag{4.20}$$

If *no* resonance conditions are satisfied initially, i.e., $m k_1^{(r)} - k_m^{(r)} \neq 0$, what (4.19) and (4.20) suggest is that at the outset the Q_m should grow linearly and the P_m exponentially. Growth as opposed to decay of all the P_m follows provided that $k_m^{(i)} < m k_1^{(i)}$, which certainly is true if the first mode is unstable and the rest of the modes are stable, although we need not be so restrictive.

Now consider the equation for $\dot{Q}_2$:

$$\begin{aligned}\dot{Q}_2 = \left(2k_1^{(r)} - k_2^{(r)}\right) + 2\sum_j \frac{\sqrt{2}}{E_1 E_j E_{1-j}} \frac{\sqrt{P_1}}{\sqrt{P_j P_{1-j}}} \left(\begin{array}{l} f_r^{\varepsilon\varepsilon(1,j,1-j)} \sin\left(Q_1 - Q_j - Q_{1-j}\right) - \\ - f_i^{\varepsilon\varepsilon(1,j,1-j)} \cos\left(Q_1 - Q_j - Q_{1-j}\right) \end{array} \right) - \\ - \sum_j \frac{\sqrt{2}}{E_2 E_j E_{2-j}} \frac{\sqrt{P_2}}{\sqrt{P_j P_{2-j}}} \left(\begin{array}{l} f_r^{\varepsilon\varepsilon(2,j,2-j)} \sin\left(Q_2 - Q_j - Q_{2-j}\right) - \\ - f_i^{\varepsilon\varepsilon(2,j,2-j)} \cos\left(Q_2 - Q_j - Q_{2-j}\right) \end{array} \right)\end{aligned} \tag{4.21}$$

The key here is to identify the dominant nonlinear term. Consider the first sum. Because the P_m grow exponentially to begin with, the ratio $\sqrt{P_1}\big/\sqrt{P_j P_{1-j}} = 1\big/\sqrt{P_j P_{1-j}}$ gets progressively smaller over time for all j; hence, no terms in this sum are of concern. Now consider the second sum. Since the numerator of the ratio $\sqrt{P_2}\big/\sqrt{P_j P_{2-j}}$ is the same for all terms (and grows exponentially), we need only identify the term with the smallest denominator. Clearly, this occurs when $j = 1$, since then $\sqrt{P_j P_{2-j}} = P_1 = 1$. Thus, to leading order

$$\dot{Q}_2 \sim \left(2k_1^{(r)} - k_2^{(r)}\right) - \frac{\sqrt{2}}{E_2 E_1 E_1} \sqrt{P_2} \left(f_r^{\varepsilon\varepsilon(2,1,1)} \sin Q_2 - f_i^{\varepsilon\varepsilon(2,1,1)} \cos Q_2 \right) \tag{4.22}$$

Since Q_2 grows linearly initially, the expression in parenthesis in the second term will oscillate about zero. Consequently, because P_2 grows exponentially, there comes a time when the two terms balance and thus $\dot{Q}_2 \sim 0$. If this is a stable limit point, Q_2 remains constant thereafter; however, this can only occur if P_2 has also become constant. Therefore, we need also consider the equation for $\dot{P}_2$ and identify the dominant nonlinear term. Since the amplitude ratios in the two sums are the same for both equations, we have

$$\frac{\dot{P}_2}{2P_2} \sim \left(2k_1^{(i)} - k_2^{(i)}\right) - \frac{\sqrt{2}}{E_2 E_1 E_1}\sqrt{P_2}\left(f_r^{\varepsilon\varepsilon(2,1,1)}\cos Q_2 + f_i^{\varepsilon\varepsilon(2,1,1)}\sin Q_2\right) \tag{4.23}$$

Essentially then, the pair (4.22) and (4.23) define the approach to the first resonance, after which the respective left-hand sides are zero and the limiting values of Q_2 and P_2 can be obtained:

$$\tan Q_2 \sim \frac{f_i^{\varepsilon\varepsilon(2,1,1)} + \frac{K_2^{(r)}}{K_2^{(i)}} f_r^{\varepsilon\varepsilon(2,1,1)}}{f_r^{\varepsilon\varepsilon(2,1,1)} - \frac{K_2^{(r)}}{K_2^{(i)}} f_i^{\varepsilon\varepsilon(2,1,1)}} \tag{4.24}$$

and

$$\sqrt{P_2} \sim \frac{1}{\frac{\sqrt{2}}{E_2 E_1 E_1}}\left|\frac{K_2^{(r)}}{f_r^{\varepsilon\varepsilon(2,1,1)}\sin Q_2 - f_i^{\varepsilon\varepsilon(2,1,1)}\cos Q_2}\right| = \frac{1}{\frac{\sqrt{2}}{E_2 E_1 E_1}}\left|\frac{K_2^{(i)}}{f_r^{\varepsilon\varepsilon(2,1,1)}\cos Q_2 + f_i^{\varepsilon\varepsilon(2,1,1)}\sin Q_2}\right| \tag{4.25}$$

where $K_2^{(\ldots)} = 2k_1^{(\ldots)} - k_2^{(\ldots)}$.

Note that when the first mode is unstable, the resonance conditions are successively satisfied, first Q_2, then Q_3, etc. Although we offer no formal proof of this statement, that this is so can be seen from Figure 4.2 (which recall is a typical example) as well as the structure of the equations. Reasoning similar to that used to obtain the limiting values of Q_2 and P_2 can be applied to find Q_3, P_3, Q_4 and P_4 (as well as higher modes). The behavior of each successive resonance depends on the behavior of the previous ones and Table 4.1 identifies the additional linear and nonlinear coefficients on which there is a functional dependence. Since the rest of the calculations involve more algebra, we refer to Appendix D for details.

Q_2 (4.24), P_2 (4.25)	$K_2^{(r)}$ $K_2^{(i)}$ $f_r^{\varepsilon\varepsilon(2,1,1)}$ $f_i^{\varepsilon\varepsilon(2,1,1)}$
Q_3 (D.4), P_3 (D.5)	$K_3^{(r)}$ $K_3^{(i)}$ $f_r^{\varepsilon\varepsilon(3,2,1)}$ $f_i^{\varepsilon\varepsilon(3,2,1)}$
Q_4 (D.8), P_4 (D.9)	$K_4^{(r)}$ $K_4^{(i)}$ $f_r^{\varepsilon\varepsilon(4,2,2)}$ $f_i^{\varepsilon\varepsilon(4,2,2)}$ $f_r^{\varepsilon\varepsilon(4,3,1)}$ $f_i^{\varepsilon\varepsilon(4,3,1)}$

Table 4.1 Linear and nonlinear coefficients on which the resonances have a functional dependence

Given that we are considering here the case of first mode instability, it is enough to retain only four modes in the truncation to capture the correct qualitative behavior (cf. Ananthkrishnan et al. 2002). However, all the necessary reasoning has been explained to extend the algorithm to include more modes. Since the ratios $P_m = p_1^m / p_m$ and differences in phase $Q_m \equiv mq_1 - q_m$ are all known, all that remains is to determine the amplitude of p_1. Starting from (4.16) with $k = m - j$ and substituting in for $\sqrt{p_2} = p_1^2 / \sqrt{P_2}$, etc., a polynomial equation for the limit of p_1 is easily derived,

$$\begin{aligned}
&\left\{2k_1^{(i)}\right\} + \left\{\frac{\sqrt{2}}{E_1 E_2 E_1}\frac{4}{\sqrt{P_2}}\left(f_r^{\varepsilon\varepsilon(1,2,-1)}\cos Q_2 - f_i^{\varepsilon\varepsilon(1,2,-1)}\sin Q_2\right)\right\} p_1 + \\
&+\left\{\frac{\sqrt{2}}{E_1 E_3 E_2}\frac{4}{\sqrt{P_2 P_3}}\left(f_r^{\varepsilon\varepsilon(1,3,-2)}\cos\left(Q_3 - Q_2\right) - f_i^{\varepsilon\varepsilon(1,3,-2)}\sin\left(Q_3 - Q_2\right)\right)\right\} p_1^2 + \\
&+\left\{\frac{\sqrt{2}}{E_1 E_4 E_3}\frac{4}{\sqrt{P_3 P_4}}\left(f_r^{\varepsilon\varepsilon(1,4,-3)}\cos\left(Q_4 - Q_3\right) - f_i^{\varepsilon\varepsilon(1,4,-3)}\sin\left(Q_4 - Q_3\right)\right)\right\} p_1^3 + \ldots = 0
\end{aligned} \tag{4.26}$$

Figure 4.3 compares the limiting values predicted analytically using the preceding formulas, with those calculated numerically for the situation described in Figure 4.2. Figure 4.4 compares the above results with the behavior computed using the continuation method encoded in AUTO 2000. The agreement is quite remarkable, and the analytic results of considerable practical value, especially since the nonlinear coefficients did not have to be specified a priori.

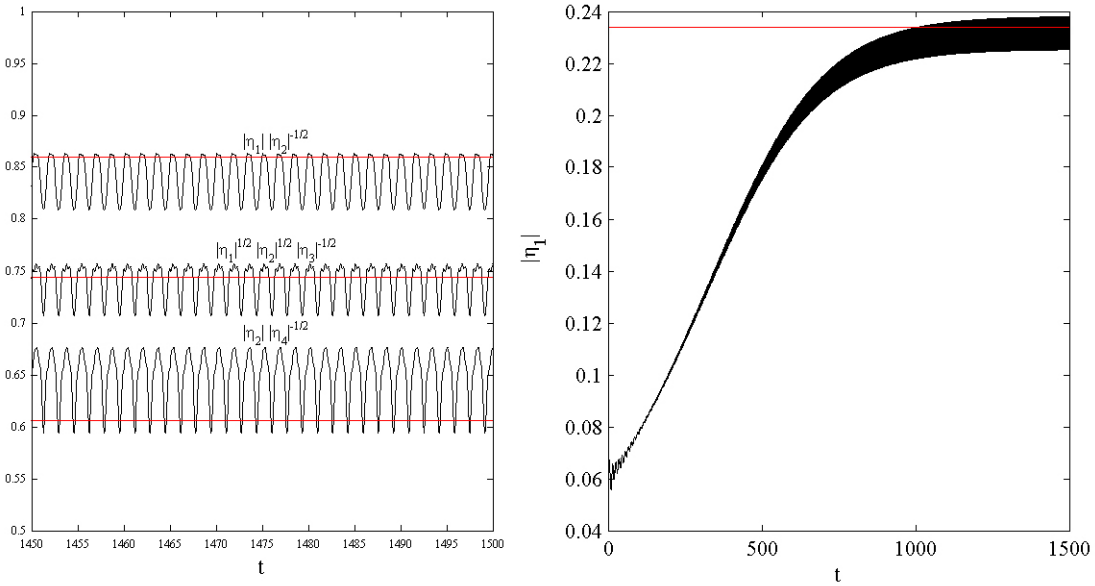

Figure 4.3 Comparison between the result shown in Figure 4.2 (black curves) and the analytic approximation for the limiting values (red lines)

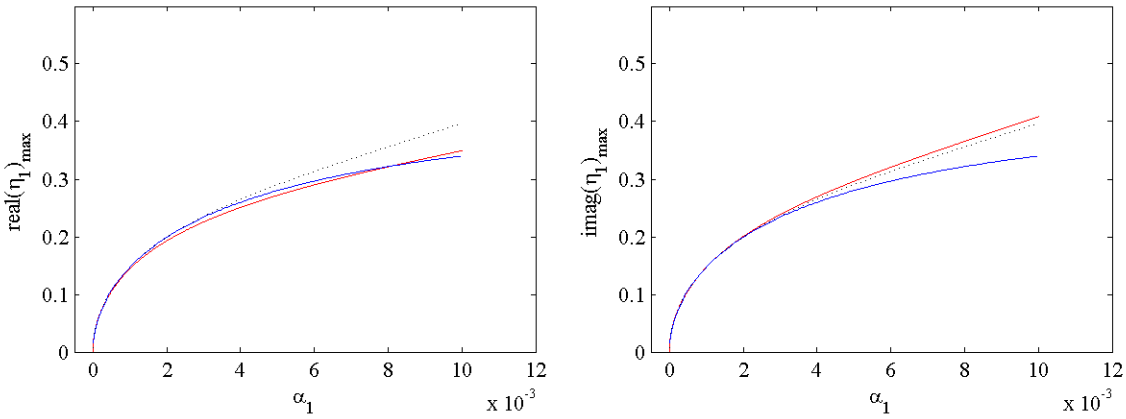

Figure 4.4 Tangential mode instability, 4 mode approximation with $M_b \alpha_{2\mu \to 4\mu} = -0.025$, and $\theta_n = 0$; red curve (AUTO 2000) corresponds to the original amplitude equations; black (dashed) curve (AUTO 2000) coincides with the behavior given by the resonance structure; and the blue curve corresponds to the simple analytic approximation

Finally, we remark that the same techniques used here to derive analytic results for the limiting behavior when the first mode is unstable, can also be applied to treat other problems, such as, for example, when the second mode is unstable. The algebra then becomes slightly more complicated, since more modes need to be retained in the truncation to capture the correct qualitative behavior; however, this is not a serious obstacle, especially if software capable of symbolic manipulation is used (e.g., Mathematica). Even if additional closed form solutions are not derived however, the viewpoint presented here would help in the identification of the nonlinear coefficients that most significantly impact system behavior, which itself would be an important development given that much work remains to be done on modeling nonlinear processes.

5. VORTICITY CREATION

To use our general framework to study combustion instability within solid rocket motors it is necessary to determine the coefficients in the amplitude equations. In part, this requires that we solve for the linearized vorticity field. Our concern here is to facilitate such a calculation, by illustrating how the mass flux issuing forth from a burning propellant affects vorticity creation. To this end, we generalize the classic Stokes' problem (i.e., the incompressible, viscous flow established by an infinite flat plate moving parallel to itself) to include a uniform *injection of fluid* normal to the boundary.

5.1 A Generalization of Stokes' Problem

Exact Solution

We obtain here the exact solution of our model problem. For reasons of symmetry, the flow only depends on the coordinate n and time t. Thus, the momentum equation—in dimensional form—reduces to

$$\mathbf{n}\times\frac{\partial\mathbf{u}_\zeta}{\partial t}+u_n\boldsymbol{\omega}_\zeta=\nu\frac{\partial\boldsymbol{\omega}_\zeta}{\partial n} \tag{5.1}$$

where $\boldsymbol{\omega}_\zeta=\mathbf{n}\times\partial\mathbf{u}_\zeta/\partial n$ is the vorticity, ν is the kinematic viscosity and $\mathbf{n}$ is the unit normal vector pointing into the fluid domain. By virtue of mass conservation $\partial u_n/\partial n=0,$ the normal velocity u_n everywhere equals its value at the plate; since uniform injection is assumed, u_n is taken to be constant and positive.

Although we can solve (5.1) for $\mathbf{u}_\zeta,$ more insight into vorticity creation comes from applying this equation to the boundary and enforcing the no-slip condition $\mathbf{u}_\zeta(0,t)=\mathbf{U}_\zeta(t)$ (note that contrary to our earlier convention, $\mathbf{U}_\zeta$ here is the velocity of the plate and *not* the steady part of $\mathbf{u}_\zeta$),

$$\boldsymbol{\sigma}_\zeta\equiv u_n\boldsymbol{\omega}_\zeta-\nu\frac{\partial\boldsymbol{\omega}_\zeta}{\partial n}=-\mathbf{n}\times\frac{d\,\mathbf{U}_\zeta}{dt} \tag{5.2}$$

This derives the so-called *vorticity source strength* $\boldsymbol{\sigma}_\zeta$, which establishes the physical sources of boundary vorticity (i.e., $\boldsymbol{\sigma}_\zeta=-\mathbf{n}\times d\,\mathbf{U}_\zeta/dt$) as well as the transport mechanisms responsible for sending this vorticity into the domain (i.e., $\boldsymbol{\sigma}_\zeta=u_n\boldsymbol{\omega}_\zeta-\nu\,\partial\boldsymbol{\omega}_\zeta/\partial n$). Lighthill (1963) first† introduced this quantity in studying vorticity creation from a *solid* boundary. The basic difference that results from a continuous

† Since then, much research on this subject has taken place (cf. Wu and Wu 1996 for a thorough review of the literature).

injection of fluid through (or from) the boundary is that, *convection competes*[†] *with viscous diffusion, and both mechanisms transport boundary vorticity into the domain*.

Before discussing the consequences of this, we take the curl of (5.1)

$$\frac{\partial \boldsymbol{\omega}_\zeta}{\partial t} + u_n \frac{\partial \boldsymbol{\omega}_\zeta}{\partial n} = \nu \frac{\partial^2 \boldsymbol{\omega}_\zeta}{\partial n^2} \tag{5.3}$$

and solve for the vorticity field, assuming the fluid and boundary are initially at rest with an arbitrary source of vorticity $\boldsymbol{\sigma}_\zeta$ imposed thereafter (i.e., $\boldsymbol{\sigma}_\zeta(t) = 0$ for $t < 0$). As standard methods suffice[‡], only the result is quoted here:

$$\boldsymbol{\omega}_\zeta(n,t) = \frac{1}{u_n}\left(\boldsymbol{\chi}(n,t) + \int_0^\infty e^{-\frac{u_n}{\nu}\eta} \frac{\partial \boldsymbol{\chi}}{\partial \eta}(n+\eta,t)\, d\eta\right) \tag{5.4}$$

where

$$\boldsymbol{\chi}(n,t) = \frac{n}{2\sqrt{\pi\nu}} \int_0^t \frac{\boldsymbol{\sigma}_\zeta(t-\tau)}{\tau^{3/2}} \exp\left(-\frac{(n-u_n\tau)^2}{4\nu\tau}\right) d\tau \tag{5.5}$$

Inviscid Limit

To help establish how introducing another mechanism for transporting boundary vorticity affects vorticity creation, we now pose the following question: Does our solution behave differently when $\nu \to 0$ and when $\nu = 0$?

Consider first the *inviscid limit* (i.e., $\nu \to 0$). The asymptotic expansion of the first term in the solution of $\boldsymbol{\omega}_\zeta$ can be obtained by appealing to Laplace's Method[¶] (cf. Bleistein and Handelsman 1975), while the second term vanishes identically. It follows that

---

[†] That the amount of vorticity sent into the domain is independent of how it is sent can be seen by integrating the curl of (5.1) over the domain and then introducing (5.2) to obtain

$$\frac{d}{dt}\int_0^\infty \boldsymbol{\omega}_\zeta dn = \boldsymbol{\sigma}_\zeta\left(= -\mathbf{n} \times d\,\mathbf{U}_\zeta / dt\right)$$

This also establishes that $\boldsymbol{\sigma}_\zeta$ is indeed a measure of vorticity creation.

[‡] For example, the problem can be solved using Laplace transforms. In doing so, it is easier to introduce $\boldsymbol{\chi} \equiv u_n \boldsymbol{\omega}_\zeta - \nu\, \partial \boldsymbol{\omega}_\zeta / \partial n$ as the dependent variable (note that (5.5) gives the inverse of this relationship), since even though a linear equation of the same form as $\boldsymbol{\omega}_\zeta$ must be satisfied, the boundary condition $\boldsymbol{\chi}(0,t) = \boldsymbol{\sigma}_\zeta(t)$ is much simpler.

[¶] $\lim_{\varepsilon \to 0} I(\varepsilon) = \int_a^b e^{-p(\tau)/\varepsilon} q(\tau)\, d\tau \sim e^{-p(\tau_0)/\varepsilon} q(\tau_0) \left(2\pi\varepsilon / p''(\tau_0)\right)^{1/2}$

where τ_0 is the absolute minimum of $p(\tau)$; for (5.5), clearly $\tau_0 = n/u_n$.

$$\lim_{\nu\to 0}\boldsymbol{\omega}_\zeta(n,t)=\frac{1}{u_n}\boldsymbol{\sigma}_\zeta\left(t-\frac{1}{u_n}n\right) \tag{5.6}$$

Remarkably, this same result is found for a *strictly inviscid fluid* (i.e., $\nu=0$), where

$$\partial\boldsymbol{\omega}_\zeta/\partial t+u_n\,\partial\boldsymbol{\omega}_\zeta/\partial n=0,\quad u_n\boldsymbol{\omega}_\zeta(0,t)=\boldsymbol{\sigma}_\zeta(t) \tag{5.7}$$

Why is this uniformity in convergence significant? When a small parameter such as ν multiplies derivatives of highest order, setting that parameter equal to zero reduces the order of the governing equation and typically causes some boundary conditions to be given up (cf. Lagerstrom 1964). This is certainly true for a solid boundary, where a pure sliding motion exists when $\nu=0$ (if $\nu\neq 0$, vorticity diffuses into the domain and induces on the boundary a velocity that satisfies the no-slip condition). In stark contrast, as demonstrated above, with fluid injection one can get around the viscous origin of the no-slip condition to simply retain it in a mathematical analysis of inviscid flow[†]. This special behavior is a consequence of having introduced *another* mechanism for transporting boundary vorticity into the domain—convection.

When is Convection the Controlling Transport Mechanism?

While our analysis in subsequent chapters does *not* assume that the fluid is inviscid, flows where the transport of boundary vorticity is controlled by convective rather than diffusive mechanisms will be of interest.

To determine the condition for this to be so, we first substitute (5.5) in (5.4) and carry out the required integration,

$$\boldsymbol{\omega}_\zeta(0,t)=\frac{1}{\sqrt{\pi\nu}}\int_0^t\frac{\boldsymbol{\sigma}_\zeta(t-\tau)}{\tau^{1/2}}e^{-\beta\tau}d\tau-\sqrt{\beta/\nu}\int_0^t\boldsymbol{\sigma}_\zeta(t-\tau)\operatorname{erfc}\left(\sqrt{\beta\tau}\right)d\tau \tag{5.8}$$

Now if $\boldsymbol{\sigma}_\zeta$ is not singular, we can asymptotically expand this exact result for large $\beta\equiv u_n^2/4\nu$. It then follows from (5.2) that the convective and diffusive contributions of $\boldsymbol{\sigma}_\zeta$ are given by

$$u_n\boldsymbol{\omega}_\zeta(0,t)\sim\boldsymbol{\sigma}_\zeta(t)-\frac{1}{4}\frac{1}{\beta}\boldsymbol{\sigma}'_\zeta(t)+\frac{1}{8}\frac{1}{\beta^2}\boldsymbol{\sigma}''_\zeta(t)+\ldots \tag{5.9}$$

[†] This fact can also be shown by working with the velocity and so we are justified in inferring from (5.6) that the no-slip condition is satisfied. Note that the tangent component of $\mathbf{u}$ can be obtained by integrating the vorticity distribution (5.4),

$$\mathbf{u}_\zeta=\tfrac{1}{2}\left(\int_0^t\mathbf{U}'_\zeta(t-\tau)\operatorname{erfc}\left(\tfrac{n-u_n\tau}{2\sqrt{\nu\tau}}\right)d\tau+e^{\frac{u_n}{\nu}n}\int_0^t\mathbf{U}'_\zeta(t-\tau)\operatorname{erfc}\left(\tfrac{n+u_n\tau}{2\sqrt{\nu\tau}}\right)d\tau\right)$$

Once again, the Euler limit, i.e., $\lim_{\nu\to 0}\mathbf{u}_\zeta(n,t)=\mathbf{U}_\zeta(t-n/u_n)$, converges uniformly to the solution for an Euler flow. It must be emphasized that whether such a result applies for flows more complex than those considered in the thesis remains an open question.

and

$$\nu\frac{\partial\boldsymbol{\omega}_\zeta(0,t)}{\partial n}\sim-\frac{1}{4}\frac{1}{\beta}\boldsymbol{\sigma}'_\zeta(t)+\frac{1}{8}\frac{1}{\beta^2}\boldsymbol{\sigma}''_\zeta(t)+\ldots \tag{5.10}$$

respectively. Taking the ratio of these results, we find

$$\frac{u_n\boldsymbol{\omega}_\zeta(0,t)}{\nu\,\partial\boldsymbol{\omega}_\zeta(0,t)/\partial n}\sim\frac{\beta}{O(\partial/\partial t)} \tag{5.11}$$

where $O(\partial/\partial t)^{-1}$ is a characteristic time scale of $\boldsymbol{\sigma}_\zeta$ (e.g., the period of oscillation for an oscillating plate).

Thus, the transport of boundary vorticity is controlled by convective rather than diffusive mechanisms when $\beta/O(\partial/\partial t)$ is large. We assess the consequences of this for the flow as a whole in §5.2.

5.2 An Oscillating Plate

Thus far, the discussion has been for a general in-plane motion of the plate. We now consider the specific case of a harmonic oscillation, i.e., $\mathbf{U}_\zeta(t)=Ue^{ikt}\boldsymbol{\zeta}_1$. Our objective here is to compare the magnitude of boundary vorticity generated and the depth to which this vorticity penetrates the flow, with and without a uniform injection of fluid through the boundary.

Since only the limiting periodic behavior (i.e., $t\to\infty$) is wanted for our comparison, seeking a solution of the form $\boldsymbol{\omega}_\zeta(n,t)=\omega_\zeta(0,0)e^{i(kt-\lambda n)}\boldsymbol{\zeta}_2$ is simpler than using (5.4). The complex constants $\omega_\zeta(0,0)$ and λ are determined by substituting into (5.2) and (5.3), respectively.

For the case of fluid injection, we are interested in the behavior when the transport of boundary vorticity is controlled by convective rather than diffusive mechanisms. Recall from (5.11) that this is so when $\beta/O(\partial/\partial t)$ is large; thus we effect a perturbation of our exact solution† for large

$$\frac{\beta}{O(\partial/\partial t)}\sim\mathrm{Re}\equiv\frac{u_n^2/k}{\nu} \tag{5.12}$$

Taking the real part of the solution and retaining terms up to $O(\mathrm{Re}^{-1})$ yields

$$\frac{\boldsymbol{\omega}_\zeta(n,t)}{(k/u_n)U}\sim-e^{-n/\delta}\sin\left(k\left(t-n/u_n\right)-1/\mathrm{Re}\right)\boldsymbol{\zeta}_2 \tag{5.13}$$

where $\delta\equiv(u_n/k)\mathrm{Re}$ is a good measure of the penetration depth, since the vorticity wave decays exponentially with n.

---

† The exact solution is

$$\frac{\omega_\zeta(0,0)}{(k/u_n)U}=\frac{2i}{1+\sqrt{1+i(4/\mathrm{Re})}}\sim\left(1-\frac{3}{2}\frac{1}{\mathrm{Re}^2}+\frac{79}{8}\frac{1}{\mathrm{Re}^4}\ldots\right)e^{i\left(\frac{\pi}{2}-\frac{1}{\mathrm{Re}}+\frac{10}{3}\frac{1}{\mathrm{Re}^3}+\ldots\right)}$$

$$\frac{\lambda}{(k/u_n)}=i\frac{\mathrm{Re}}{2}\left(1-\sqrt{1+i(4/\mathrm{Re})}\right)\sim\left(1-\frac{2}{\mathrm{Re}^2}+\ldots\right)-i\frac{1}{\mathrm{Re}}\left(1-\frac{5}{\mathrm{Re}^2}+\ldots\right)$$

By a similar calculation, the classic result for a solid boundary (denoted here by suffix c) can also be obtained:

$$\frac{\boldsymbol{\omega}_{c\zeta}(n,t)}{\sqrt{2}U/\delta_c} = e^{-n/\delta_c}\cos\left(kt - n/\delta_c + \pi/4\right)\boldsymbol{\zeta}_2 \tag{5.14}$$

Here $\delta_c = (2\nu/k)^{1/2}$.

Both solutions are depicted in Figure 5.1. *From the ratio of penetration depth*

$$\delta/\delta_c \sim \tfrac{1}{\sqrt{2}}\,\mathrm{Re}^{3/2} \tag{5.15}$$

vorticity is seen to propagate significantly further into the domain when fluid is injected through the boundary. However, the magnitude of this vorticity is notably reduced

$$\left|\boldsymbol{\omega}_{\zeta}(0,t)\right| \Big/ \left|\boldsymbol{\omega}_{c\zeta}(0,t)\right| \sim \mathrm{Re}^{-1/2} \tag{5.16}$$

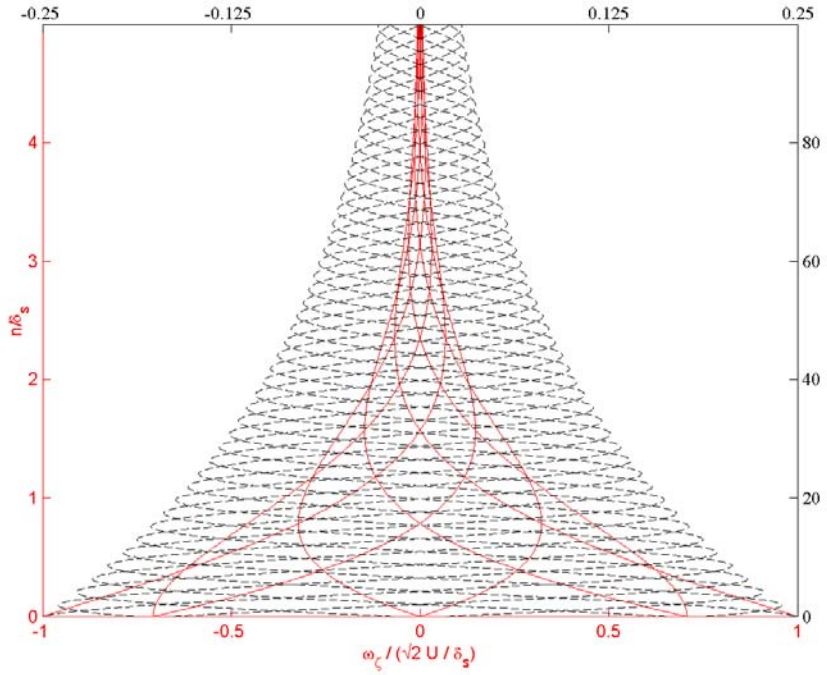

Figure 5.1 Comparison between the classic Stokes solution (red) for an oscillating plate and the generalized case (black) when fluid is injected through the boundary at 8 equally spaced times for $\mathrm{Re} = 16$; *all* axes are normalized with respect to the classic Stokes parameters

Another important consequence of fluid injection worth pointing out is that, less work is done by the plate against frictional stresses during each cycle. That this is so follows since

$$\left\langle \boldsymbol{\tau}\cdot\mathbf{u}_{\zeta}\right\rangle \Big/ \left\langle \boldsymbol{\tau}_c\cdot\mathbf{u}_{c\zeta}\right\rangle \sim \delta_c/\delta \sim \sqrt{2}\,\mathrm{Re}^{-3/2} \tag{5.17}$$

where $\boldsymbol{\tau} = \mu\boldsymbol{\omega}\times\mathbf{n}$ is the shear stress on the boundary and $\langle\ \rangle$ denotes the time average.

5.3 Some Final Remarks

We note here that while an exact solution was found for the simple model problem considered, flows that are more complex require the application of either numerical or perturbation techniques. Our concern is with the latter and the insight gained in the present chapter can be used to guide the selection process.

Typically, a small parameter multiplying the highest order derivative suggests the application of singular perturbation techniques (Lagerstrom 1988). However, for a boundary with fluid injection, another transport mechanism is introduced that achieves the same end as the physics that derivatives of highest order describe. As such, a reduction in the order of the equation does not imply a sacrifice of the boundary conditions. This is reflected in the convergence of the Euler limit to the solution for a strictly Euler flow; in other words, the inviscid approximation now *adheres* to the boundary. The mathematics, in part, is divorced from the physics, as the solution does not concern itself with how events on the boundary ultimately came to pass.

However, viscous diffusion still plays a role; through its slow, but cumulative action, vorticity that flows into the domain is damped. Such behavior, is reminiscent—at least for the case of the oscillating plate—of the gradual decay of periodic solutions first calculated by the astronomer Lindstedt (cf. Kevorkian and Cole 1996), and suggests the possible effectiveness of the method of multiple scales. The applicability of this technique to the generalization of Stokes' second problem is illustrated in Appendix E.

6. ACOUSTIC BOUNDARY LAYER

In Chapter 5, we established that fluid injected through (or from) a boundary fundamentally changes the vorticity creation process, as convection now competes with viscous diffusion, and both mechanisms transport boundary vorticity into the domain. Before investigating how this affects the linearized vorticity field within solid rocket motors (cf. Chapter 7), it is instructive to contrast the behavior of the *acoustic boundary layer*, with and without a uniform injection of fluid through the boundary. While this problem is only a slight generalization of Stokes' oscillating plate considered in §5.2 (at least in terms of the vorticity field), key elements of the physics can again be introduced in a simplified setting.

6.1 Equations of Motion

We use here the conservation equations introduced in Chapter 2; however, the linear operators are much simplified since the mean flow now just describes a uniform injection of fluid through the boundary (i.e., $\mathbf{U} = \mathbf{n}$ with $\mathbf{n}$ being the unit normal vector pointing into the fluid domain). Writing out the momentum equation $\partial \mathbf{u}/\partial t + \mathscr{L}_u(...) = 0$ then, we have

$$\bar{D}\mathbf{u}/Dt = -\nabla\left(p - \mathrm{Re}_\vartheta^{-1}\vartheta\right) - \mathrm{Re}_\omega^{-1}\nabla\times\boldsymbol{\omega} \tag{6.1}$$

where $\bar{D}/Dt = \partial/\partial t + M_b\,\partial/\partial n$, M_b is the injection Mach number and Re_ω is defined below (cf. (6.5)). The no-injection limit is recovered by setting $M_b = 0$.

To proceed, we partition the flow into longitudinal and transverse waves, which as previously noted, are given kinematic expression in the dilatation and the vorticity. Transport equations for ϑ and $\boldsymbol{\omega}$ follow naturally from the divergence and curl of (6.1), respectively. A direct partition of the momentum equation into irrotational and solenoidal spaces can also be effected owing to the simplicity of the convective term. In particular, we have

$$\bar{D}\mathbf{u}_\vartheta/Dt = -\nabla\left(p - \mathrm{Re}_\vartheta^{-1}\vartheta\right) \tag{6.2}$$

and

$$\bar{D}\mathbf{u}_\omega/Dt = -\mathrm{Re}_\omega^{-1}\nabla\times\boldsymbol{\omega} \tag{6.3}$$

The vorticity transport equation (or (6.3) for that matter) is sufficient to solve for the shearing process. When treating the compressing/expanding process, a useful strategy is to combine the equation for the pressure $\partial p/\partial t + \mathscr{L}_p(...) = 0$, the temperature $\partial T/\partial t + \mathscr{L}_T(...) = 0$, the entropy $\partial s/\partial t + \mathscr{L}_s(...) = 0$ and the dilation $\partial\vartheta/\partial t + \nabla\cdot\mathscr{L}_u(...) = 0$ to obtain the following coupled system (cf. Morse and Ingard 1968):

$$\left(\frac{\bar{D}^2}{Dt^2} - \frac{1}{\mathrm{Re}_\vartheta}\frac{\bar{D}}{Dt}\nabla^2\right)(\gamma p - T) = \nabla^2 p, \quad \frac{\bar{D}s}{Dt} = \frac{\bar{D}}{Dt}\left(T - (\gamma-1)p\right) = \frac{1}{\mathrm{Pr}\,\mathrm{Re}_\omega}\nabla^2 T \tag{6.4}$$

where[†]

$$\mathrm{Re}_\omega \equiv \frac{\rho_o c_o^2/k}{\mu_s}, \quad \mathrm{Re}_\vartheta \equiv \left(\tfrac{4}{3}+\mu_v/\mu_s\right)^{-1}\mathrm{Re}_\omega, \quad \mathrm{Pr} \equiv \frac{\mu_s c_p}{\kappa} \tag{6.5}$$

6.2 Waves

6.2.1 Acoustic Wave

Our objective here is to understand the similarities and differences in how and why a *plane* acoustic wave oriented tangent to the boundary, i.e.,

$$p \sim \cos\zeta_1 e^{it} \tag{6.6}$$

gives rise to vorticity and thermal waves, with and without a uniform injection of fluid through the boundary. To this end, we focus more on the ratio of various characteristic parameters rather than the mathematical solution itself, which is given in Appendix F.

6.2.2 Vorticity Wave

First, we seek to understand how sound generates vorticity by appealing to the vorticity source strength $\boldsymbol{\sigma}_\zeta$. Applying the tangent component of the momentum equation to the boundary and enforcing the no-slip condition, we have

$$\boldsymbol{\sigma}_\zeta \equiv M_b\boldsymbol{\omega}_\zeta - \frac{1}{\mathrm{Re}_\omega}\frac{\partial\boldsymbol{\omega}_\zeta}{\partial n} = -\mathbf{n}\times\nabla\left(p + M_b u_n - \mathrm{Re}_\vartheta^{-1}\vartheta\right) \tag{6.7}$$

Recall that this establishes the physical sources of boundary vorticity as well as the transport mechanisms responsible for sending this vorticity into the domain (cf. §5.1).

With or without fluid injection, the dominant physical source here is the gradient of pressure tangent to the boundary; the other terms are much smaller in comparison. This gradient gives rise to a longitudinal motion of fluid that does *not* satisfy the no-slip condition. Vorticity must therefore be created such that on the boundary an equal and opposite fluid motion is induced.

This can be seen most clearly when $M_b = 0$, since substituting the tangent component of (6.2) into (6.7) gives

$$\boldsymbol{\sigma}_\zeta = \mathbf{n}\times\partial\mathbf{u}_\vartheta/\partial t \tag{6.8}$$

which essentially defines a Stokes problem (cf. Chapter 5). Thus, *sound creates vorticity by making it appear as if the boundary oscillates parallel to itself.*

[†] Since the problem here has no characteristic length scale, the reference length R is chosen to be $R = c_o/k$ where k is the frequency of the acoustic wave. Note also that μ_s and μ_v are the dynamic viscosities for the shearing and the compressing/expanding process, respectively; c_p is the specific heat at constant pressure; and κ is the thermal conductivity.

As for how this vorticity is transported into the domain, when $M_b \neq 0,$ convection *competes* with viscous diffusion to achieve this end. The relative efficacy with which these two mechanisms act depends upon the values assumed by the parameters M_b and Re_ω. We can establish this as well as some important scales of the problem by considering the vorticity transport equation†

$$\frac{\partial \boldsymbol{\omega}_\zeta}{\partial t} + M_b \frac{\partial \boldsymbol{\omega}_\zeta}{\partial n} \sim \frac{1}{\mathrm{Re}_\omega} \frac{\partial^2 \boldsymbol{\omega}_\zeta}{\partial n^2} \tag{6.9}$$

Now if convection dominates, the terms on the left-hand side can be equated and it follows that $\partial/\partial n \sim O\left(M_b^{-1}\right)$. This is valid however only if the diffusive contribution is higher order. That $\left(M_b^2 \,\mathrm{Re}_\omega\right)^{-1}$ must be small for this to be so can be seen by estimating the magnitude of the viscous term using $\partial/\partial n \sim O\left(M_b^{-1}\right)$. Note that this same condition was derived in an alternative way for the Stokes problem (cf. (5.12)); the appearance of the injection Mach number M_b here is simply an artifact of having normalized velocities by the sound speed. The other limiting case is when the transport of vorticity is controlled by diffusive mechanisms—the simplest manifestation of which is when $M_b = 0$. For this case, we have by equating the first and third terms that $\partial/\partial n \sim O\left(\mathrm{Re}_\omega^{1/2}\right)$.

As standard methods suffice in solving (6.9) for a source of vorticity given by $\boldsymbol{\sigma}_\zeta \sim -\mathbf{n}\times\nabla p,$ only the results are discussed here. From the ratio of penetration depth

$$\delta_{injection}/\delta \sim \tfrac{1}{\sqrt{2}}\left(M_b^2 \,\mathrm{Re}_\omega\right)^{3/2} \tag{6.10}$$

vorticity is seen to propagate significantly further into the domain when fluid is injected through the boundary. However, the magnitude of this vorticity is notably reduced

$$\left|\boldsymbol{\omega}_\zeta(0,t)\right|_{injection} \Big/ \left|\boldsymbol{\omega}_\zeta(0,t)\right| \sim \left(M_b^2 \,\mathrm{Re}_\omega\right)^{-1/2} \tag{6.11}$$

Not surprisingly, the same behavior was found for Stokes' oscillating plate (cf. (5.15) and (5.16), respectively).

Once the vorticity field is known, there are several ways to obtain the induced velocity. For example, one can first solve the Poisson equation $\nabla^2 \mathbf{A} = -\boldsymbol{\omega}$ and then take the curl of the vector potential $\mathbf{A}$ (since $\mathbf{u}_\omega \equiv \nabla \times \mathbf{A}$). This yields, in part, an unsteady component of flow in the normal direction $u_{\omega n}$ — a new feature of the present example (vis-à-vis Stokes' oscillating plate). When $M_b = 0,$ the amplitude ratio of the resulting flow pattern is $\left|u_{\omega n}/u_{\omega\zeta}\right| \sim \mathrm{Re}_\omega^{-1/2}$. In contrast, when $M_b \neq 0$ and convective rather than diffusive mechanisms dominate, we have $\left|u_{\omega n}/u_{\omega\zeta}\right| \sim M_b$. Since $u_{\omega\zeta}$ is of the same order of magnitude for both cases by virtue of the no-slip condition, it follows that

† Note that for the viscous and heat conduction terms, gradients in the normal direction dominate; in this context then the Laplacian is approximated by $\nabla^2 \sim \partial^2/\partial n^2$.

$$\left|u_{\omega n}(0,\zeta,t)\right|_{injection} \Big/ \left|u_{\omega n}(0,\zeta,t)\right| \sim \left(M_b^2\,\mathrm{Re}_\omega\right)^{1/2} \tag{6.12}$$

That $u_{\omega n}$ plays a more prominent role when $M_b \neq 0$ can be attributed to the diminished importance of viscous processes. Although $u_{\omega n}$ is but a small correction of $u_{\omega\zeta}$ — with or without fluid injection—this component of velocity is quite important, especially since $u_{\omega n} \neq 0$ on the boundary. The physical significance of this is elaborated upon below.

Having established how sound generates vorticity, we now consider whether this vorticity generates additional sound. To this end, we examine the case when $M_b = 0$ by way of illustration. With the boundary assumed perfectly rigid, fluctuations of velocity normal to the boundary must be suppressed. Introducing the *no-through* condition into (6.1) and substituting the normal projection of (6.3), we have

$$\frac{\partial}{\partial n}\left(p - \mathrm{Re}_\vartheta^{-1}\,\vartheta\right) = \mathbf{n}\cdot\frac{\partial \mathbf{u}_\omega}{\partial t} \tag{6.13}$$

Now for an irrotational flow, the right-hand side of (6.13) vanishes identically; this is not the case, however, when the flow is made to satisfy the no-slip condition as demonstrated above. Accordingly, this result indicates how vorticity, once created, feeds back and modifies the pressure distribution. More specifically, (6.13) conveys that *vorticity creates additional sound by making it appear as if the boundary oscillates normal to itself.* Thus, despite the absence of any physical motion, sound is generated aerodynamically through an action similar to that of a speaker (cf. Lighthill 1952 for the earliest discussion of this idea).

6.2.3 Thermal Wave

Following Morse and Ingard (1968), we solve for the thermal wave by considering the thermal effect on the pressure as higher order. Thus, the pressure is treated as a known forcing in the *heat* equation (i.e., the equation on the right of (6.4)), suggesting an ansatz of the form

$$T = T_s + (\gamma - 1)\,p \tag{6.14}$$

Here T_s is the departure from purely isentropic flow, which is driven in part by the need to avoid a *slip* in temperature on the boundary. Substituting (6.14) into the equation on the right of (6.4), we have

$$\frac{\partial T_s}{\partial t} + M_b\frac{\partial T_s}{\partial n} \sim \frac{1}{\mathrm{Pr}\,\mathrm{Re}_\omega}\frac{\partial^2 T_s}{\partial n^2} \tag{6.15}$$

Since this has a formal resemblance to the vorticity transport equation (6.9), it follows that the thermal and the vorticity wave share many features in common.

Our principal interest here is the induced thermal velocity $\mathbf{u}_s$. We can solve for this by starting with the continuity equation, appropriately recast, $\bar{D}p/Dt + \vartheta = \bar{D}s/Dt$ and partitioning the dilatation into

leading order contributions owing to acoustic and entropy waves, i.e., $\vartheta \sim \vartheta_a + \vartheta_s$. It follows that $\vartheta_s = \nabla^2 \varphi_s \sim \bar{D}s/Dt = \left(\mathrm{Pr}\,\mathrm{Re}_\omega\right)^{-1} \nabla^2 T_s$, which gives

$$\mathbf{u}_s = \nabla \varphi_s \sim \frac{1}{\mathrm{Pr}\,\mathrm{Re}_\omega} \nabla T_s \tag{6.16}$$

Physically, this describes a flow of fluid up the temperature gradient, i.e., from regions of cold to regions of hot[†]. While the tangential component of this motion is negligible—scaling as $O\left(\mathrm{Re}_\omega^{-1}\right)$—this is not necessarily true for the normal component. Using the estimates for $\partial/\partial n$ (cf. the discussion following (6.9)), when $M_b = 0$, we have $u_{sn} \sim O\left(\left(\mathrm{Pr}\,\mathrm{Re}_\omega\right)^{-1/2}\right) O\left(T_s\right)$ and $\left|u_{sn}/u_{\omega n}\right| \sim \mathrm{Pr}^{-1/2} \left|T_s\right|$. In contrast, when $M_b \neq 0$, $u_{sn} \sim O\left(\left(M_b^2\,\mathrm{Re}_\omega\right)^{-1} \left(M_b/\mathrm{Pr}\right)\right) O\left(T_s\right)$ and $\left|u_{sn}/u_{\omega n}\right| \sim \mathrm{Pr}^{-1} \left(M_b^2\,\mathrm{Re}_\omega\right)^{-1} \left|T_s\right|$.

Thus, in analogy with the vorticity wave, the thermal wave cancels out the effect of temperature fluctuations on the boundary at the *expense* of a contribution to u_n. The essential point to be observed however is that the thermal velocity no longer plays an important role when fluid is injected through the boundary, since we assume $\left(M_b^2\,\mathrm{Re}_\omega\right)^{-1}$ to be small. This departs from the behavior for the classic case, where the flow induced in the normal direction by both the vorticity and entropy wave is of comparable magnitude. In other words, while $u_{\omega n}$ becomes more significant owing to fluid injection (cf. (6.12)), the opposite is true for u_{sn},

$$\left|u_{sn}\left(0,\zeta,t\right)\right|_{injection} \Big/ \left|u_{sn}\left(0,\zeta,t\right)\right| \sim \mathrm{Pr}^{-1/2} \left(M_b^2\,\mathrm{Re}_\omega\right)^{-1/2} \tag{6.17}$$

[†] Although perhaps counter-intuitive, this is required by conservation of mass. Entropy diffusion predicts that a local temperature maximum is not sustained over time, and thus from the equation of state, the density must be simultaneously increasing—fluid must flow toward the temperature maximum for this to be so (cf. Morse and Ingard 1968).

7. LINEAR STABILITY EIGENFUNCTIONS

Having discussed the physics of a few model problems in previous chapters, we now consider the linearized flow field within solid rocket motors and solve for the acoustic, the vorticity and the thermal eigenfunctions.

7.1 Acoustic Eigenfunctions

Even though our general framework of combustion instability is formulated using sound-speed, we solve for the acoustic eigenfunctions in terms of the pressure to be consistent with earlier analyses (e.g., Culick 1973, 1975; Flandro 1995 a, b). No increase in labor results since to the order of approximation in M_b considered, these thermodynamic variables are proportional to one another, i.e., $p \sim (\Gamma - 1)^{-1} c$.

Thus in lieu of (2.25), we have as our starting point

$$\begin{bmatrix} \mathcal{L}_p(...) \\ \mathcal{L}_\vartheta(...) \end{bmatrix} = ik_m \begin{bmatrix} p_m \\ \vartheta_m \end{bmatrix} \tag{7.1}$$

While exact solutions can only be found under very restrictive conditions, such as those considered in Chapter 3, we can still proceed analytically by capitalizing upon the *smallness* of the injection Mach number M_b (which typically is on the order of $0.001-0.01$). Terms indicating an interaction with the mean flow are scaled by this parameter and so the linear operators $\mathcal{L}_p(...)$ and $\mathcal{L}_\vartheta(...)$ can be written as

$$\mathcal{L}_p(...) = \mathcal{L}_{p0}(...) + M_b \mathcal{L}_{p\mu}(...) + ..., \quad \mathcal{L}_\vartheta(...) = \mathcal{L}_{\vartheta 0}(...) + M_b \mathcal{L}_{\vartheta\mu}(...) + ... \tag{7.2}$$

where $\mathcal{L}_{p0}(p, \vartheta) \equiv \vartheta$ and $\mathcal{L}_{\vartheta 0}(p, \vartheta) \equiv \nabla^2 p$; the other operators are defined in §G.1.

Now in solving (7.1), a regular perturbation expansion

$$\begin{aligned} k_m &= k_{m0} + M_b k_{m\mu} + ... \\ p_m &= p_{m0} + M_b p_{m\mu} + ... \\ \vartheta_m &= \vartheta_{m0} + M_b \vartheta_{m\mu} + ... \end{aligned} \tag{7.3}$$

suffices. This can be justified on mathematical grounds; however, the most compelling evidence is experimental: frequencies observed during instability are remarkably close to the classical acoustic resonances of the chamber.

Substituting the above expansions in (7.1) recovers to leading order

$$\begin{bmatrix} \mathcal{L}_{p0}(p_{m0}, \vartheta_{m0}) \\ \mathcal{L}_{\vartheta 0}(p_{m0}, \vartheta_{m0}) \end{bmatrix} = ik_{m0} \begin{bmatrix} p_{m0} \\ \vartheta_{m0} \end{bmatrix} \tag{7.4}$$

the behavior of classic acoustics, which has already been discussed in Chapter 3. Here we are chiefly concerned with solving for the $O(M_b)$ perturbations, which are governed by

$$\begin{bmatrix} \mathscr{L}_{p0}\left(p_{m\mu},\vartheta_{m\mu}\right) \\ \mathscr{L}_{\vartheta 0}\left(p_{m\mu},\vartheta_{m\mu}\right) \end{bmatrix} + \begin{bmatrix} \mathscr{L}_{p\mu}\left(\mathbf{U},p_{m0},\mathbf{u}_{m0}\right) \\ \mathscr{L}_{\vartheta\mu}\left(\mathbf{U},p_{m0},\mathbf{u}_{m0}\right) \end{bmatrix} = ik_{m0}\begin{bmatrix} p_{m\mu} \\ \vartheta_{m\mu} \end{bmatrix} + ik_{m\mu}\begin{bmatrix} p_{m0} \\ \vartheta_{m0} \end{bmatrix} \tag{7.5}$$

To this end, we first take the inner product $\langle \mathbf{x},\mathbf{y}\rangle \equiv \int \mathbf{y}^{*T}\mathbf{x}dV$ of (7.5) with $\mathbf{f}_{j0}^{\dagger} = \begin{bmatrix} p_{j0}^{\dagger} & \varphi_{j0}^{\dagger} \end{bmatrix}^T$ to obtain (cf. §G.2 for details)

$$\begin{aligned} &i\left(k_{m0}-k_{j0}\right)\int\left(p_{j0}^{\dagger *}p_{m\mu}+\varphi_{j0}^{\dagger *}\vartheta_{m\mu}\right)dV + ik_{m\mu}2E_{m0}^2\delta_m^j = \\ &= ik_{m0}\oint\varphi_{j0}^{\dagger *}\mathbf{n}\cdot\left(\mathbf{u}_{m\vartheta\mu}+M_b^{-1}\mathbf{u}_{m\omega 0}\right)dS - \int\mathscr{L}_{u\mu}\left(\mathbf{U},p_{m0},\mathbf{u}_{m0}\right)\cdot\nabla\varphi_{j0}^{\dagger *}dV + \int\mathscr{L}_{p\mu}\left(\mathbf{U},p_{m0},\mathbf{u}_{m0}\right)p_{j0}^{\dagger *}dV \end{aligned} \tag{7.6}$$

where $E_{m0}^2 = \frac{1}{2}\int\left(p_{m0}^{\dagger *}p_{m0}+\varphi_{m0}^{\dagger *}\vartheta_{m0}\right)dV$ and δ_m^j is the discrete Dirac-delta function.

A few remarks are needed before proceeding. First, recall that the normal component of the acoustic velocity at the boundary is assumed to satisfy the no-through condition in the first approximation. However, an $O(M_b)$ response exists owing to the flame zone, which is denoted here by $\mathbf{n}\cdot\mathbf{u}_{m\vartheta\mu}$; this term appears in the first integral on the right-hand side of (7.6). As for $\mathbf{n}\cdot\mathbf{u}_{m\omega 0}$ (which we will show scales as $O(M_b)$), this is the normal component of the vortical velocity induced at the boundary.

Second, once the *leading order solution* is known, the unknowns in (7.5) and (7.6) are the perturbations to the wave numbers (i.e., $k_{m\mu}$) and the corrections to the mode shapes (i.e., $p_{m\mu}$ and $\vartheta_{m\mu}$). *Leading order solution* here refers however not only to the solution for the leading order acoustic field, but also the leading order vorticity and thermal fields as well. The simplest way to demonstrate why this must be the case is to note that $\mathscr{L}_{\vartheta\mu}\left(\mathbf{U},p,\mathbf{u},...\right) = \nabla\cdot\left(\mathbf{u}\cdot\nabla\mathbf{U}+\mathbf{U}\cdot\nabla\mathbf{u}\right)+...$ To evaluate this term, for example, all contributions to $\mathbf{u}$ must be known, not just those that come from acoustics. The details of solving for the vorticity and thermal fields are discussed in §7.2 and §7.3, respectively.

Returning to (7.6), when $j = m$ the first term on the left-hand side vanishes identically, yielding a formula for $k_{m\mu}$:

$$ik_{m\mu} = -\alpha_{m\mu} - i\theta_{m\mu} = \frac{1}{2E_{m0}^2}\left(\begin{array}{c} ik_{m0}\oint\varphi_{m0}^{\dagger *}\mathbf{n}\cdot\left(\mathbf{u}_{m\vartheta\mu}+M_b^{-1}\mathbf{u}_{m\omega 0}\right)dS - \int\mathscr{L}_{u\mu}\left(\mathbf{U},p_{m0},\mathbf{u}_{m0}\right)\cdot\nabla\varphi_{m0}^{\dagger *}dV + \\ +\int\mathscr{L}_{p\mu}\left(\mathbf{U},p_{m0},\mathbf{u}_{m0}\right)p_{m0}^{\dagger *}dV \end{array}\right) \tag{7.7}$$

Culick (1975) obtained a similar result by starting with a perturbed equation for the pressure, except that *no* vortical terms appeared on the right-hand side as the unsteady motions in that analysis were assumed irrotational in the first approximation. Flandro (1995 a, b) restored the *missing* terms and provided a model to evaluate them for a simple geometry and under somewhat restrictive conditions. We discuss this further in Chapter 8.

When $j \neq m$ the second term on the left-hand side of (7.6) vanishes identically, yielding an expression involving the unknown perturbations to the mode-shapes. By considering a series expansion of $p_{m\mu}$ and $\vartheta_{m\mu}$ in terms of the leading order mode shapes,

$$p_{m\mu} = \sum_{\substack{k=1,\\ k\neq m}}^{\infty} \alpha^{p}_{mk\mu}\, p_{k0}, \quad \vartheta_{m\mu} = \sum_{\substack{k=1,\\ k\neq m}}^{\infty} \alpha^{\vartheta}_{mk\mu}\, \vartheta_{k0} \tag{7.8}$$

we can use this expression to help determine the coefficients. Further details of this procedure are provided in §G.3. However, the essential point is that the approach introduced here allows us to solve not only for $k_{m\mu}$ but also for $p_{m\mu}$ and $\vartheta_{m\mu}$.

7.2 Vorticity Eigenfunctions

7.2.1 Historical Overview

A simplification often introduced when describing the flow field within solid rocket motors is to restrict consideration to a cylindrical propellant grain. Doing so and thus able to draw an analogy to a duct with porous wall, Culick (1966) solved for the *steady* streamlines.

Most existing unsteady solutions have been constructed by perturbing this steady flow field in one way or another. For example, Varapaev and Yagodkin (1969) first considered the question of stability, with more extensive development of the theory by Casalis et al. (1998) and Griffond et al. (2000, 2001). These recent additions sought in part a basic understanding of the *parietal* or *surface vortex shedding* phenomena, which has been identified as a possible source of instability in the ARIANE 5 booster and involves large pressure oscillations being driven by so-called *crawling* vortices (Lupoglazoff and Vuillot 1992, 1996, 1998).

Since combustion instability is however generally characterized by excited acoustic modes, Flandro (1995 a, b) following a somewhat different approach and bypassed questions regarding the stability of the steady flow to focus instead on better understanding the mechanisms and energy pathways that govern the growth or decay of the unsteady flow. Superimposing a purely axial acoustic disturbance upon Culick's (1966) earlier solution, Flandro asked and answered the important question: *what is missing*? Critical of the simplification of allowing oscillatory *slip flow* on propellant surfaces, a more complete and realistic model of the unsteady motions within combustion chambers was developed, by solving for the shearing half of the problem using perturbation methods. Shown to exist were waves of coherent *acoustically-generated* vorticity, created on the boundary owing to a kinematic coupling with the acoustic field and convected deep into the interior by the mass flux issuing forth from the burning propellant. Using

details of this solution, the effect of vorticity on system stability was then established, a more in-depth discussion of which is deferred to Chapter 8.

Since that time a number of different investigations (e.g., Majdalani et al. 1998; Zhao et al. 2000; Garcia-Shafer et al. 2001) have dealt with the same problem with slight differences in emphasis. The solutions obtained all collapse to the order of approximation considered, and compare well with both experiments earlier carried out by Brown et al. (1986) and cold-flow numerical simulations performed by Roh (Majdalani and Roh 2000).

The Present Effort

The goal here is to extend the range of unsteady *laminar* flow models, which seek to describe the chamber dynamics of potentially unstable solid rocket motors, by solving for the vorticity field using the method of multiple scales[†]. An important consequence of this approach is that a clear demarcation can be made between information required for stability computations, which involve integrations over the domain, and information required for determining the detailed structure within the domain. It turns out, that insofar as the former is concerned, surprisingly little is needed. This allows for a considerable generalization of stability results to propellants whose grain boundaries can locally be described by a general orthogonal coordinate system; this is realized by introducing a coordinate system based on normal and tangential coordinates. This is a significant contribution since previous results were limited to the vorticity field that accompanies a purely axial acoustic wave within a cylindrical chamber.

7.2.2 Calculation

We now solve for the vorticity eigenfunctions to leading order. This means simply that we obtain here the linearized vorticity field that induces on the boundary a fluid motion equal and opposite that which accompanies the *leading order* acoustic field.

Vorticity Source Strength

We begin by deriving the vorticity source strength $\boldsymbol{\sigma}_{\zeta}$, i.e., the basic measure of the vorticity creation process (cf. §5.1). Applying the tangent component of the linearized momentum equation to the boundary and enforcing the no-slip condition, we have

---

[†] Although Flandro (1995 a, b) recognized that multiple scales existed, the perturbation machinery needed to benefit more fully from this observation was not introduced. Both Zhao et al. (2000) and Garcia-Shafer et al. (2001), motivated by Flandro's earlier work, corrected for this *deficiency*, but once again, only a cylindrical propellant grain subject to axial-mode instability was considered.

$$\boldsymbol{\sigma}_\zeta \equiv \left(\mathbf{n}\cdot M_b\mathbf{U}\right)\boldsymbol{\omega}_\zeta - \frac{1}{\mathrm{Re}_\omega}\frac{\partial \boldsymbol{\omega}_\zeta}{\partial n} = -\begin{pmatrix} \mathbf{n}\times\nabla\left(p + M_b\mathbf{U}\cdot\mathbf{u} - \mathrm{Re}_\vartheta^{-1}\,\vartheta\right) + \\ +\left(\mathbf{n}\cdot\mathbf{u}\right)M_b\boldsymbol{\Omega}_\zeta + \mathrm{Re}_\omega^{-1}\,\mathbf{K}\cdot\boldsymbol{\omega}_\zeta \end{pmatrix} \tag{7.9}$$

Recall that this establishes the physical sources of boundary vorticity as well as the transport mechanisms responsible for sending this vorticity into the domain.

The gradient of pressure tangent to the grain boundary is the dominant physical source here as the other terms are at least two orders of magnitude in M_b smaller by comparison[†]; hence $\boldsymbol{\sigma}_\zeta \sim -\mathbf{n}\times\nabla p$. The boundary vorticity that results is not only *diffused* but also *convected* into the domain by the mass flux issuing forth from the burning propellant. However, when $\left(M_b^2\,\mathrm{Re}_\omega\right)^{-1}$ is small, convection is the controlling mechanism (this was demonstrated for the acoustic boundary layer in §6.2 and will be justified further below); since this is true of typical motor systems (cf. Table 7.1), it follows that $\boldsymbol{\sigma}_\zeta \sim \left(\mathbf{n}\cdot M_b\mathbf{U}\right)\boldsymbol{\omega}_\zeta$.

Now equating the two expressions for $\boldsymbol{\sigma}_\zeta$, there results an *a-priori* estimate for the vorticity on the boundary:

$$\boldsymbol{\omega}_\zeta\big|_{boundary} \sim -\left(\mathbf{n}\cdot M_b\mathbf{U}\right)^{-1}\mathbf{n}\times\nabla p \tag{7.10}$$

since p is known to *leading order* from classic acoustics. This is a result of great importance, with the reasons why becoming clear in due course.

An estimate for how normal derivatives of the vorticity field scale can also be obtained, by deriving another expression for the vorticity on the boundary and comparing it to (7.10). To this end, we expand the tangent component of $\boldsymbol{\omega} \equiv \nabla\times\mathbf{u}_\omega$ and retain only the dominant contribution[‡], which gives $\boldsymbol{\omega}_\zeta \sim \mathbf{n}\times\partial\mathbf{u}_{\omega\zeta}/\partial n$. It follows by virtue of the no-slip condition $\mathbf{u}_{\omega\zeta} = -\mathbf{u}_{\vartheta\zeta}$ and the result $\mathbf{u}_{\vartheta\zeta} \sim O\left(\nabla_\zeta p\right)$ from classical acoustics that

$$\boldsymbol{\omega}_\zeta\big|_{boundary} \sim \mathbf{n}\times\partial\mathbf{u}_{\omega\zeta}/\partial n \sim O\left(\partial/\partial n\right)O\left(\nabla_\zeta p\right) \tag{7.11}$$

Comparing (7.10) and (7.11) then implies

$$\partial/\partial n \sim O\left(1/M_b\right) \tag{7.12}$$

which provides a scaling estimate for normal derivatives of the vorticity field. It should be emphasized that (7.10) and (7.12) were derived for $\left(M_b^2\,\mathrm{Re}_\omega\right)^{-1}$ small, and thus do not apply when $M_b = 0$.

[†] Since the velocity fluctuation u_n at the burning surface is proportional to the injection Mach number, both $\mathbf{n}\times\nabla\left(M_b\mathbf{U}\cdot\mathbf{u}\right) = \mathbf{n}\times\nabla\left(M_bU_nu_n\right)$ and $\left(\mathbf{n}\cdot\mathbf{u}\right)M_b\boldsymbol{\Omega}_\zeta$ are $O\left(M_b^2\right)$. Terms scaled by the inverse of the Reynolds number contribute even less.

[‡] The exact result is $\boldsymbol{\omega}_\zeta \equiv \mathbf{n}\times\partial\mathbf{u}_{\omega\zeta}/\partial n - \mathbf{n}\times\left(\nabla u_{\omega n} + \mathbf{K}\cdot\mathbf{u}_{\omega\zeta}\right)$.

	$L\,(m)$	$R\,(m)$	M_b	Re_ω	k $1L/1T$	δ	S	$M_b/(k\delta)$
Small Research Motor (Culick and Yang 1992)	0.60	0.025	1.7^{-3}	3.32^{6}	1.31^{-1}	0.951	77.0	0.0137
					1.84	0.005	1083.1	0.1920
Tactical Rocket (typical geometry)	2.03	0.102	3.1^{-3}	1.33^{7}	1.58^{-1}	15.9	50.9	0.0012
					1.84	0.117	593.9	0.0144
Cold Flow Experiment (Shaeffer and Brown 1992)	1.73	0.051	3.3^{-3}	2.71^{6}	9.26^{-2}	11.4	28.1	0.0031
					1.84	0.029	557.9	0.0623
Space Shuttle SRM	35.1	0.70	2.3^{-3}	9.25^{7}	6.27^{-2}	287	27.2	0.0001
					1.84	0.332	800.5	0.0038

Table 7.1 Physical parameters for typical motors systems (cf. Flandro 1995 b)

Motivating the Method of Multiple Scales

While a regular perturbation expansion sufficed when solving for the acoustic eigenfunctions, such an approach is not applicable here since qualitatively different behavior is observed when $M_b = 0$ and when M_b is small.

Let us elaborate on this point further. When $M_b = 0,$ vorticity creation is controlled entirely by viscous processes and singular perturbation techniques apply. This involves constructing an outer solution, which is asymptotically matched to an inner solution valid near the boundary where viscous effects are taken into account. Because this invariably couples the behavior on the boundary, with that in the interior, a priori estimation of the former is unrealizable. In contrast, when $M_b \neq 0,$ diffusion competes with convection and *both* mechanisms transport boundary vorticity into the domain.

While this argues against the application of either regular or singular perturbation techniques (cf. Chapter 5), it remains to motivate the *method of multiple scales.* Two key ideas are needed in this regard. First, for the cases of interest here, boundary vorticity penetrates substantially further into the domain since convection is the controlling transport mechanism. Second, this vorticity wave propagates with the mean flow, while sound waves propagate at the *speed of sound*. Given then that both waves coexist spatially and

exhibit the same temporal dependence, a convective length scale that reflects the disparity in distance traveled per unit time can be introduced.

To better understand this latter point as well as to motivate the functional form of such a scale, consider the vorticity transport equation

$$\partial\boldsymbol{\omega}/\partial t + M_b \nabla \times \left(\boldsymbol{\omega} \times \mathbf{U} + \boldsymbol{\Omega} \times \mathbf{u}\right) = \mathrm{Re}_{\omega}^{-1} \nabla^2 \boldsymbol{\omega} \tag{7.13}$$

Since normal derivatives of the vorticity field scale as $\partial/\partial n \sim O\left(1/M_b\right)$, it is not difficult to see that the term which balances $\partial \boldsymbol{\omega}_{\zeta}/\partial t$ is $M_b U_n \, \partial \boldsymbol{\omega}_{\zeta}/\partial n$. By comparison, the dominant viscous term is $\mathrm{Re}_{\omega}^{-1} \partial^2 \boldsymbol{\omega}_{\zeta}/\partial n^2 \sim O\left(\left(M_b^2 \, \mathrm{Re}_{\omega}\right)^{-1}\right) O\left(\boldsymbol{\omega}_{\zeta}\right)$; since our analysis assumes that $\left(M_b^2 \, \mathrm{Re}_{\omega}\right)^{-1}$ is small, viscous diffusion no longer plays a key role in the transport of vorticity. However, it does still act to dissipate vorticity; we will return to this later. Thus to leading order (7.13) reduces to a description of a wave convected along a *characteristic* path,

$$\partial \boldsymbol{\omega}_{\zeta}/\partial t + M_b U_n \, \partial \boldsymbol{\omega}_{\zeta}/\partial n \sim 0 \tag{7.14}$$

By virtue of the arguments advanced then, we define ξ such that in the first approximation $t - \xi$ is a *characteristic* along which vorticity waves are convected into the interior. It follows from (7.14) that

$$\partial \xi/\partial n = \left(M_b U_n\right)^{-1} \tag{7.15}$$

While ξ can be found by integration, it is sufficient for the analysis here to know that by a suitable choice of integration limits ξ vanishes on the chamber boundary.

Flandro (1995 b) first recognized the mathematical value of ξ and used it, in particular, to determine the dominant viscous term. However, the physical origin of the scale was left unmotivated and the perturbation machinery needed to benefit more fully from its existence was not introduced. Instead, the analysis relied on heuristic arguments to make simplifications where needed.

In contrast, we explicitly formulate the problem here using the method of multiple-scales. As such, normal derivatives now transform as

$$\frac{\partial}{\partial n} = \frac{\partial \xi}{\partial n}\frac{\partial}{\partial \xi} + \frac{\partial}{\partial n} = \frac{1}{M_b U_n}\frac{\partial}{\partial \xi} + \frac{\partial}{\partial n} \tag{7.16}$$

It should be emphasized that in carrying out the solution ξ and n are treated as independent variables; the *dimension,* in other words, is temporarily increased.

Now a *two-scale* expansion for $\boldsymbol{\omega}_{\zeta}$ of the form $\boldsymbol{\omega}_{\zeta} \sim \boldsymbol{\omega}_{\zeta 0}\left(\mathbf{x}, \xi, t\right) + M_b \boldsymbol{\omega}_{\zeta 1}\left(\mathbf{x}, \xi, t\right) + \ldots$ is sought. Substituting this in (7.13) and using (7.16), we find that $\boldsymbol{\omega}_{\zeta 0}$ is governed by a first order wave equation in ξ,

$$\partial \boldsymbol{\omega}_{\zeta 0}\left(\mathbf{x}, \xi, t\right)/\partial t + \partial \boldsymbol{\omega}_{\zeta 0}\left(\mathbf{x}, \xi, t\right)/\partial \xi = 0 \tag{7.17}$$

where the solution

$$\boldsymbol{\omega}_{\zeta 0}\left(\mathbf{x},\xi,t\right)=\boldsymbol{\omega}_{\zeta 0}^{n}\left(\mathbf{x}\right)e^{-ik_{m0}\left(t-\xi\right)} \tag{7.18}$$

is expressed in terms of an unknown function $\boldsymbol{\omega}_{\zeta 0}^{n}\left(\mathbf{x}\right)$ of the *original* spatial scales.

Note that the behavior of $\boldsymbol{\omega}_{\zeta 0}^{n}\left(\mathbf{x}\right)$ follows from suppressing secular terms at higher order. We make a few remarks in this regard. First, it is here that viscous processes enter into the analysis in a significant way in causing the vorticity wave to decay. Second, closed form solutions of $\boldsymbol{\omega}_{\zeta 0}^{n}\left(\mathbf{x}\right)$ are generally too difficult to construct, except for simple geometries, such as a cylindrical propellant grain. Last, and perhaps of greatest consequence, is that integrals which determine the effects of vorticity on the acoustic field can be evaluated *without* detailed knowledge of $\boldsymbol{\omega}_{\zeta 0}^{n}\left(\mathbf{x}\right)$. That this is so will be shown in §7.2.3. Only the behavior on the boundary is needed and this can be obtained from (7.10). Substituting in (7.18) and the leading order solution for the pressure field, i.e., $p\sim p_0=p_{m0}\left(\mathbf{x}\right)e^{-ik_{m0}t}$, we have[†]

$$\boldsymbol{\omega}_{\zeta 0}^{n}\Big|_{boundary}=-\left(\mathbf{n}\cdot M_b\mathbf{U}\right)^{-1}\mathbf{n}\times\nabla p_{m0} \tag{7.19}$$

Solving for $\boldsymbol{\omega}_{\zeta 0}^{n}\left(\mathbf{x}\right)$ may still be important though and we discuss this further in §7.2.4.

Completing the Description of the Vorticity Field

We now seek to complete the description of the vorticity field by solving for the vector potential $\mathbf{A}$ and the induced velocity $\mathbf{u}_{\omega}$.

First, we solve the Poisson equation $\nabla^2\mathbf{A}=-\boldsymbol{\omega}$ for $\mathbf{A}_{\zeta}$. This calculation is straightforward since derivatives with respect to ξ dominate in the first approximation, i.e., $\nabla^2\sim\left(M_b^2U_n^2\right)^{-1}\partial^2/\partial\xi^2+O\left(M_b^{-1}\right)$. Thus the tangent component becomes $\left(M_b^2U_n^2\right)^{-1}\partial^2\mathbf{A}_{\zeta 0}/\partial\xi^2=-\boldsymbol{\omega}_{\zeta 0}$, and on using (7.18), this can be integrated immediately to

$$\mathbf{A}_{\zeta 0}\left(\mathbf{x},\xi,t\right)=\left(M_bU_n/k_{m0}\right)^2\,\boldsymbol{\omega}_{\zeta 0}\left(\mathbf{x},\xi,t\right) \tag{7.20}$$

Having tacitly fixed the gauge of $\mathbf{A}$ by requiring that $\nabla\cdot\mathbf{A}=0$, this condition can be used to find A_{n0}. While we refrain from doing so here since this component of the vector potential is not required for subsequent calculations, we note that for any vector $\mathbf{f}$ that satisfies $\nabla\cdot\mathbf{f}=\partial f_n/\partial n-\kappa f_n+\nabla_{\zeta}\cdot\mathbf{f}_{\zeta}=0$ and has a functional dependence on ξ similar to that of the vorticity, simple scaling arguments show that $f_n\sim O\left(M_b/k_{m0}\right)O\left(\nabla_{\zeta}\cdot\mathbf{f}_{\zeta}\right)$. For example, this is not only true of A_{n0} but also the normal component of the vorticity.

[†] Note that although the vorticity field corresponding to each of the acoustic modes is needed, we omit the suffix m to simplify the notation.

It remains to determine $\mathbf{u}_{\omega}$, which follows simply from expanding $\nabla \times \mathbf{A}$ [†]:

$$\mathbf{u}_{\omega\zeta 0}\left(\mathbf{x},\xi,t\right) = i\left(M_b/k_{m0}\right)U_n\,\mathbf{n}\times\boldsymbol{\omega}_{\zeta 0}\left(\mathbf{x},\xi,t\right) \tag{7.21}$$

$$u_{\omega n0}\left(\mathbf{x},\xi,t\right) = \left(M_b/k_{m0}\right)^2\left(\mathbf{n}\times\nabla_{\zeta}\right)\cdot\left(U_n^2\,\boldsymbol{\omega}_{\zeta 0}\left(\mathbf{x},\xi,t\right)\right) \tag{7.22}$$

This completes the description of the vorticity field.

In summary, we have obtained the leading order solution for the vortical half of the unsteady flow field by using the method of multiple scales. This solution has been expressed in terms of the normal velocity of the steady flow U_n and $\boldsymbol{\omega}_{\zeta 0}\left(\mathbf{x},\xi,t\right)$ (and thus the unknown function $\boldsymbol{\omega}^n_{\zeta 0}\left(\mathbf{x}\right)$ of the original spatial scales). Later, it will prove useful to also have an expression for $\mathbf{n}\times\partial\mathbf{A}_0/\partial t$ in terms of $\mathbf{u}_{\omega\zeta 0}$. From (7.20) and (7.21), it follows that

$$\mathbf{n}\times\partial\mathbf{A}_0/\partial t = -M_bU_n\,\mathbf{u}_{\omega\zeta 0} = M_bU_n\,\mathbf{u}_{\vartheta\zeta 0} \tag{7.23}$$

Lastly, we examine the behavior of the induced velocity on the boundary by substituting (7.18) for $\boldsymbol{\omega}_{\zeta 0}\left(\mathbf{x},\xi,t\right)$ and (7.19) for $\boldsymbol{\omega}^n_{\zeta 0}\left(\mathbf{x}\right)$. Consider the tangent component first. From (7.21), we have $\mathbf{u}_{\omega\zeta 0} = \left(i/k_{m0}\right)\nabla_{\zeta}p_0$. Given that the solution for the scalar potential is $\varphi_{a0} = -\left(i/k_{m0}\right)p_0$ (cf. (C.2)) it follows that the no-slip condition is indeed satisfied, i.e., $\mathbf{u}_{a\zeta 0} + \mathbf{u}_{\omega\zeta 0} = 0$ (that the tangent velocity induced by the thermal wave is negligible will be shown in §7.3). Now consider the normal component. From (7.22), we have $u_{\omega n0} = -M_bk_{m0}^{-2}\nabla_{\zeta}\cdot\left(U_n\nabla_{\zeta}p_0\right)$. The physical significance of this not vanishing on the grain boundary is succinctly summed up by the latter part of the statement: sound generates vorticity, which in turn, *generates more sound*. We elaborate upon this further in Chapter 8.

7.2.3 Evaluating Stability Integrals

We now show that volume stability integrals involving the vorticity field can be evaluated *without* detailed knowledge of $\boldsymbol{\omega}^n_{\zeta 0}\left(\mathbf{x}\right)$. These integrals, whether describing linear or nonlinear effects, are of the form $I = \int f\left(\mathbf{x}\right)e^{ik_{m0}\xi}dV$. Because the integrand here consists of some unknown function $f\left(\mathbf{x}\right)$ of $\boldsymbol{\omega}^n_{\zeta 0}\left(\mathbf{x}\right)$ which changes *slowly* in comparison with the exponential term that *rapidly* oscillates about zero (with characteristic frequency $S = k_{m0}/M_b$), cancellations occur when integrating over the domain. Thus,

---

[†] Expanding $\nabla\times\mathbf{A}$ in our chosen coordinate system, we obtain

$$u_{\omega n} = \left(\mathbf{n}\times\nabla_{\zeta}\right)\cdot\mathbf{A}_{\zeta},\quad \mathbf{u}_{\omega\zeta} = \frac{\partial}{\partial n}\left(\mathbf{n}\times\mathbf{A}_{\zeta}\right) - \mathbf{n}\times\left(\nabla_{\zeta}A_n + \mathbf{K}\cdot\mathbf{A}_{\zeta}\right)$$

Both expressions here are exact. Consider $u_{\omega n}$ first. As only tangential derivatives arise, no further simplification of the expression is possible. The result (7.22) may be obtained by substituting for $\mathbf{A}_{\zeta 0}$ from (7.20). Now consider $\mathbf{u}_{\omega\zeta}$. Since $\partial/\partial n \sim O\left(1/M_b\right)$ clearly the term involving the normal derivative dominates, i.e., $\mathbf{u}_{\omega\zeta} \sim \partial\left(\mathbf{n}\times\mathbf{A}_{\zeta}\right)/\partial n$. Introducing then the expression for $\mathbf{A}_{\zeta 0}$ given by (7.20), and noting that to leading order $\partial/\partial n = \left(M_bU_n\right)^{-1}\partial/\partial\xi$, we obtain (7.21).

it is entirely plausible that the principal contribution arises solely from the value the integrand assumes on the boundary.

Flandro (1995 a, b) made a similar observation, but only after *first* solving for the detailed vorticity distribution within a cylindrical chamber and using this solution to evaluate integrals. No formal asymptotic result was ever derived. Thus, a clear elucidation of precisely what information was actually needed did not result. In contrast, we clearly differentiate here between the information required to evaluate integrals and that required for detailed knowledge of the vorticity field within the chamber.

Writing out the differential volume element in I for a coordinate system given by $\mathbf{x} = (n, \zeta_1, \zeta_2)$ with corresponding metric coefficients $(1, h_1, h_2)$, we have

$$I = \int f(\mathbf{x}) e^{ik_{m0}\xi} dV = \int f(\mathbf{x}) e^{ik_{m0}\xi} h_1 h_2 \, d\zeta_1 \, d\zeta_2 \, dn \tag{7.24}$$

Now integrating by parts *within* the multi-scale framework[†] one obtains

$$I \sim -i \frac{M_b}{k_{m0}} \oint U_n f(\mathbf{x}) d\mathbf{S} + i \frac{M_b}{k_{m0}} \int e^{ik_{m0}\xi} U_n \frac{\partial \left(f(\mathbf{x}) h_1 h_2 \right)}{\partial n} dn d\zeta_1 d\zeta_2 \tag{7.25}$$

Integrating the second term by parts again, we find that its contribution is $O\left(\left(M_b / k_{m0} \right)^2 \right)$. Thus to leading order, we have

$$I = \int f(\mathbf{x}) e^{ik_{m0}\xi} dV \sim -i \frac{M_b}{k_{m0}} \oint U_n f(\mathbf{x}) d\mathbf{S} \tag{7.26}$$

This is a result of great practical importance: volume stability integrals that describe the energy flux to and from the vorticity field collapse to integration over burning surfaces and in so doing introduce a factor of M_b / k_{m0}. Thus, as earlier claimed, detailed knowledge of $\boldsymbol{\omega}^n_{\zeta 0}(\mathbf{x})$ is *not necessary* to evaluate stability integrals, only the behavior of $\boldsymbol{\omega}^n_{\zeta 0}(\mathbf{x})$ on the boundary is needed (cf. (7.19)).

An important consequence is that now stability integrals can be evaluated under far more general conditions than previously possible; more specifically, reasonably complex grain geometries can now be accommodated provided they can be locally described by a general orthogonal coordinate system. In contrast, Flandro's analysis (1995 a, b) was limited to the case of axial mode instability in a cylindrical chamber; however, our work does build upon many of his ideas insofar as the vorticity field is concerned.

Finally, it must be emphasized that the asymptotic result (7.26) holds only if the flow remains laminar, for only then are cancellations certain to occur. To minimize the impact of this, we will recast the integrals that need evaluation using *standard vector identities*, such that only the surface integrals will contribute when the flow is laminar. Such a step is important because even if the vortical flow transitions

---

[†] During intermediary steps, the fast and slow scales are treated as independent variables.

downstream of the surface, the behavior at the burning surface is in large measure constrained by kinematics. Equation (7.26) then will only be utilized to show that the remaining volume integrals make a negligible contribution when the flow is laminar; whether these integrals contribute when the flow is turbulent is something that would need to be assessed.

7.2.4 Detailed Structure

Even though stability integrals can be evaluated *without* detailed knowledge of the vorticity field, the caveat here is that vorticity can affect combustion instabilities in more than one way. For example, the highly oscillatory structure of (acoustically-generated) vorticity waves, which on the one hand is responsible for the *collapse* of volume integrations, on the other hand increases the likelihood that these waves become *unstable* themselves.

If this transition occurs near the boundary (where such vorticity is created) the impact on the combustion processes would likely be significant, with effects including—but not limited to—enhancing the heat transfer rate back to the burning propellant owing to increased mixing. In other words, insofar as combustion responsiveness is concerned, acoustically generated vorticity could be the ideal *Trojan* horse. What better way for turbulence to penetrate regions close to the flame zone, than for a turbulent precursor to already exist, especially given the nature of an injection driven flow[†]. This idea was first introduced by Beddini (1998), with some preliminary results presented by Lee and Beddini (2000).

Before the stability of the vorticity field can be assessed however, *detailed* knowledge of the laminar behavior is necessary. As previously noted, closed form results are typically only possible for simple geometries. In §G.4, we take up this problem for one such case—that of a cylindrical chamber. Flandro (1995 a, b) and others have studied this problem when only a purely axial acoustic motion exists. In contrast, our calculation captures the behavior for a general acoustic motion.

7.3 Thermal Eigenfunctions

We now solve for the thermal eigenfunctions to leading order. For the case of a classic acoustic boundary layer, the normal component of the thermal velocity is equal in magnitude to that induced by the vorticity (cf. §6.2.3). Here we establish whether this is also true when a flow through the boundary exists.

[†] Much in the same way that boundary layers are blown off, for random motions to penetrate regions close to the surface, considerable kinetic energy would be required.

As demonstrated in Chapter 6, in solving for the thermal motion, a useful tactic is to combine the equation for the pressure $\partial p/\partial t + \mathscr{L}_p(...) = 0,$ the temperature $\partial T/\partial t + \mathscr{L}_T(...) = 0$ and the entropy $\partial s/\partial t + \mathscr{L}_s(...) = 0,$ to obtain

$$\bar{D}s/Dt = \bar{D}\left(T - (\gamma - 1)p\right)/Dt = (\gamma - 1)Q \tag{7.27}$$

where $\bar{D}/Dt = \partial/\partial t + M_b \mathbf{U}\cdot\nabla$ and $Q = \left((\gamma-1)\,\mathrm{Pr}\,\mathrm{Re}_\omega\right)^{-1}\nabla^2 T + \mathrm{Re}_\omega^{-1}\Phi$. Examination of (7.27), suggests the following ansatz

$$T = T_s + (\gamma - 1)p \tag{7.28}$$

where the first term is the thermal fluctuation associated with the *entropy* of the fluid (we also have from (7.27) that $s \sim T_s$), in the absence of variations of which, the temperature would follow the pressure in an isentropic manner, as reflected by the second term.

Substituting (7.28) in (7.27) gives

$$\frac{\bar{D}s}{Dt} = \frac{\bar{D}T_s}{Dt} \sim \frac{1}{\mathrm{Pr}\,\mathrm{Re}_\omega}\nabla^2 T_s \tag{7.29}$$

Note that some higher order physical effects have been omitted from the right-hand side. In particular, the flow of heat that accompanies the alternate compressions and rarefactions of the sound wave and the irreversible loss of kinetic energy[‡] (i.e., dissipation).

To solve (7.29) for T_s, the method of multiple scales is again justified since we need to resolve waves that propagate at vastly different rates, i.e., the speed of sound versus the mean flow. Thermal fluctuations associated with the entropy of the fluid clearly fall into the latter class.

As with the vorticity then, a *two-scale* expansion for $T_s \sim T_{s0}(\mathbf{x},\xi,t) + M_b T_{s1}(\mathbf{x},\xi,t) + ...$ is sought, where in accordance with the method, normal derivatives now transform as in (7.16). It is easily shown, upon introducing (7.16) into (7.29), that the leading term of the expansion $T_{s0}(\mathbf{x},\xi,t)$ is governed by a first order wave equation in ξ, i.e., $\partial T_{s0}(\mathbf{x},\xi,t)/\partial t + \partial T_{s0}(\mathbf{x},\xi,t)/\partial\xi = 0,$ with solution

$$T_{s0}(\mathbf{x},\xi,t) = T_{s0}^n(\mathbf{x})e^{-ik_{m0}(t-\xi)} \tag{7.30}$$

As before (cf. §7.2) suppression of secular terms at higher order determines the unknown function $T_{s0}^n(\mathbf{x})$ of the *original* spatial scales.

However, the corresponding thermal velocity $\mathbf{u}_{s0}$ can be determined simply from the functional form of T_{s0}. Starting with the continuity equation, appropriately recast $\bar{D}p/Dt + \vartheta = \bar{D}s/Dt$, a leading order partition of the dilatation into contributions owing to acoustic and entropy waves, i.e., $\vartheta_0 = \vartheta_{a0} + \vartheta_{s0}$,

---

[‡] Although the magnitude of the unsteady vorticity in some sense is considered *large*, a negligible amount of heat is generated owing to viscous dissipation, the dominant term of which is $\Phi \sim M_b \boldsymbol{\Omega}\cdot\boldsymbol{\omega}$.

is simple to effect. In particular, we have $\vartheta_{s0} = \bar{D}s_0 / Dt$. It then follows from (7.29) that $\vartheta_{s0} = \nabla^2 \varphi_{s0} = \left(\mathrm{Pr}\,\mathrm{Re}_\omega\right)^{-1} \nabla^2 T_{s0}$, and so

$$\mathbf{u}_{s0} = \nabla \varphi_{s0} = \frac{1}{\mathrm{Pr}\,\mathrm{Re}_\omega} \nabla T_{s0} \tag{7.31}$$

The tangential component of this motion is negligible—scaling as $O\left(\mathrm{Re}_\omega^{-1}\right)$. The motion in the normal direction is given by

$$u_{sn0} = i\,\mathrm{Pr}^{-1} k_{m0} M_b \left(M_b^2\,\mathrm{Re}_\omega\right)^{-1} \frac{1}{U_n} T_{s0} \tag{7.32}$$

where T_{s0} is defined by (7.30). Recall in our analysis that $\left(M_b^2\,\mathrm{Re}_\omega\right)^{-1}$ is assumed small. Thus, in contrast with the classical acoustic boundary layer, flow through the boundary reduces the importance of the thermal velocity in a solid rocket motor.

8. LINEAR STABILITY

8.1 Introduction

Much effort has been devoted to improving predictions of linear stability, since solid rocket motors deemed stable during design often exhibit large amplitude pressure oscillations during qualification testing[†].

Following the ideas of an *energy balance* pioneered by Kirchoff, the first stability results appeared in the 1960s (McClure et al. 1960; Cantrell and Hart 1964; Hart and McClure 1965). A different algorithm based on a *perturbed eigenvalue problem* for the pressure was later introduced by Culick (1970, 1973 and 1975). It yielded results consistent[‡] with earlier work and has since formed the cornerstone of the Standard Stability Prediction Program (Lovine et al. 1976; Nickerson et al. 1983), generally referred to by its acronym SSPP, now currently in use.

Both schools of thought adopted the widely accepted point of view that combustion instability stems from perturbations to the classical acoustic resonances of the chamber, with stability represented as an additive set of *stability integrals*. Difficulties arise because either not all relevant processes are accounted for, or, more often, information is unavailable to model with reasonable accuracy their influence. A number of investigations have focused on interactions between the acoustic field and combustion, condensed species, the nozzle, etc. (cf. Culick and Yang 1992 for a thorough review).

However, one serious omission of these earlier efforts followed from the assumption that the unsteady motions are irrotational in the first approximation. Thus, the original set of stability integrals did not include a number of important effects owing to coupling with vortical flow processes. Flandro (1995 a, b) first recognized and convincingly established this to be true by emphasizing the need to pay close attention to the no-slip boundary condition.

[†] Although instabilities can be triggered in linearly stable systems by disturbances of sufficiently large amplitude, we refer here to situations where motors are in fact linearly unstable, despite predictions to the contrary.

[‡] To avoid the loss of acoustic energy within the volume being compensated by the gain of energy for the mean flow, a correct representation of the former, as noted by Culick (1975), is required. This change needs to be made in some early work based on an energy balance approach to yield entirely self-consistent results.

A Brief History of Flow Turning

In retrospect, a correction accounting for the energy loss due to vorticity generation was incorporated into the acoustic instability algorithm much earlier. However, from the time of inclusion in the mid 1970s up until only recently, it was not recognized as such.

To help clarify how the flow field established by a burning surface couples to acoustic motions tangent to the grain boundary, Culick (1973) developed a one-dimensional formulation of the rocket motor stability problem. What resulted was a novel damping effect—christened flow turning—that was attributed to gas particles produced in the flame zone having to turn in order to acquire the motion of the acoustic flow.

An inviscid, multidimensional treatment of the same problem (Culick 1975) that did not explicitly account for vortical flow effects recovered no such result, however. The one-dimensional stability integral was then *patched* on and argued to give reasonable approximation to a process believed otherwise too complicated to model. While not an unusual strategy, much debate followed regarding its merits.

An oft-cited reason for the absence of *flow turning* in Culick's multidimensional formulation was the omission of processes of viscous decay near the flame zone (cf. Culick and Yang 1992). Experimental investigations even sought to measure this effect directly (Magiawala et al. 1979); although certainly important, no definitive answers were forthcoming. Partial resolution of this issue was only recently provided by Flandro (1995 a, b).

For any rocket motor chamber that supports pressure oscillations tangent to the grain boundary, a purely acoustic representation of the unsteady flow field fails to satisfy the no-slip condition. Critical of this, Flandro found both an inviscid (1995 a) and a viscous (1995 b) solution for the unsteady vorticity field within a cylindrical chamber. This was accomplished by superimposing a purely *axial* acoustic disturbance on a steady flow established by a uniform injection from the boundary, and solving for the other half the problem.

Then *restoring all rotational terms* that were dropped in the earlier analysis (Culick 1975), and evaluating these new stability integrals using the *laminar* models for the unsteady vorticity field obtained, Flandro first identified a term that yielded—in both cases—a damping effect indistinguishable from the flow turning loss. This was a significant finding.

What Flandro (1995 a, b) essentially showed was that the no-slip condition is key to flow turning *naturally* reappearing in a multidimensional treatment of the stability problem. This, in fact, is why Culick's (1973) original one-dimensional formulation first captured the flow turning effect. Although not a

requirement of the mathematical protocol, the unsteady motions in that analysis were forced to enter normal to the propellant boundary; the no-slip condition was for all practical purposes imposed.

Had this been Flandro's only result, use of an irrotational description *might* have been entirely justified, at least insofar as questions of linear stability, for even though such a description of the fluid dynamics is not rich enough to satisfy the no-slip condition, effective modeling (Culick 1973) at first glance circumvents that inherent limitation.

Another Finding: Radial Pumping.

However, another important result of Flandro's analysis (1995 a, b) was a destabilizing *radial pumping* mechanism[†] shown to exist on the chamber boundary, owing to the normal component of velocity induced by vorticity being non-zero there.

This effect has also led to much debate. Apart from its physical origin being somewhat unclear—questions for instance arose as to whether a new source of mass needed to be found within the combustion zone—for the particular configuration considered, i.e., a cylindrical propellant grain subject to axial mode instability, *a key mathematical observation was that the energy gained because of this radial pumping compensated the loss due to flow turning.*

In other words, to the order of approximation considered, no *net* contribution existed owing to the effects of vorticity. A physical explanation of this rather surprising result was not offered. *Was this merely a fortuitous finding or rather a deeper reflection of the underlying physics*?

The Present Effort

We aim to address this question here. We do so, in part, by deriving novel formulae that clearly reflect the interaction between vorticity and sound, allowing for a substantial clarification—both in terms of the mathematics and the physics involved—of the mechanisms that allow the former to influence the growth or decay of the latter within solid rockets. Aside from a significantly enhanced physical understanding, what has already been done (Culick 1973; Flandro 1995 a, b) is improved upon in two key ways.

First, the results obtained are *independent* of propellant grain geometry. The importance of this can hardly be overestimated. Flandro's analysis (1995 a, b) relied heavily on the assumption of a cylindrical chamber with only the case of a purely axial acoustic wave examined; the setting considered by

---

[†] Culick (1973) first demonstrated the existence of such a mechanism in the context of an acoustic boundary layer over an *impermeable* surface. While it was hypothesized that this periodic radial pumping may affect the losses/gains at a permeable surface, this process was inadvertently overlooked in later work.

Culick (1973) was even simpler. Second, the derivation of these results depends largely on kinematics. In other words, the conclusions reached are *independent* of the dynamics and thermodynamics of the medium, and thus applicable for any fluid motion, turbulent or otherwise.

8.2 Problem Formulation

As noted earlier, linear stability can be formulated either by using an acoustic energy balance or as a perturbed eigenvalue problem. Formulas for the latter approach were derived in §7.1. From these the perturbations to the wave numbers $k_{m\mu}$ and thus the growth rates $\alpha_{m\mu}$ and the shifts in frequency $\theta_{m\mu}$ can be obtained (as well as the corrections to the acoustic mode shapes). In contrast, an acoustic energy balance only determines the growth rates. However, working with the energy of the disturbance results in an improved understanding of the physical mechanisms involved. Thus, we first formulate linear stability along these lines and then evaluate the relevant formulas from §7.1 in §H.1.

Now whether acoustic waves grow or decay can be determined by evaluating the time rate-of-change of the potential $\mathcal{P} \equiv \int \frac{1}{2} p^2 \, dV$ and kinetic $\mathcal{K}_\vartheta \equiv \int \frac{1}{2} \mathbf{u}_\vartheta \cdot \mathbf{u}_\vartheta \, dV$ energy they carry. In doing so, some care is required since two different time scales exist: one associated with the frequency of the oscillation and the other with processes of modulation, i.e., damping and driving. The energy transfer affecting the latter takes place slowly, and to leading order, the shape of the wave remains unchanged during any given cycle (cf. Morse and Ingard 1968). Thus only the time average behavior is typically needed, which is denoted here by $\langle ... \rangle$. It follows that

$$\alpha_{m\mu} = \frac{1}{2\langle \mathcal{P} + \mathcal{K}_\vartheta \rangle} \left\langle \dot{\mathcal{P}} + \dot{\mathcal{K}}_\vartheta \right\rangle \tag{8.1}$$

Note that we are justified in calling this an *acoustic* energy balance even though $\mathcal{K}_\vartheta$ is the kinetic energy of the unsteady *longitudinal motions* and thus includes contributions from *both* acoustic and entropy waves, since as shown in §7.3 the velocity induced by the latter is negligible.

Potential Energy

The equation for $\dot{\mathcal{P}} = \int p \, \partial p / \partial t \, dV$ is obtained by substituting from (2.13) for $\partial p / \partial t$ and retaining only terms linear in ε; this gives $\dot{\mathcal{P}} = -\int \mathcal{L}_p (...) \, p \, dV$. Now replacing $\mathcal{L}_p (...)$ by (B.30) and applying some vector identities, we have after omitting effects owing to the condensed phase (cf. Culick and Yang 1992 for the more general result) that

$$\dot{\mathcal{P}} = -M_b \oint \tfrac{1}{2} p^2 \, \mathbf{n} \cdot \mathbf{U} \, dS - \int p \vartheta \, dV + (\gamma - 1) \int p Q \, dV \tag{8.2}$$

We choose here not to focus on the physical mechanisms involved, except to note that the last term, which involves the energy source Q, describes Rayleigh's Criterion, and shows that unsteady heat addition may encourage oscillations (cf. Culick 1994 for a more detailed discussion of this important mechanism).

Kinetic Energy

In deriving an equation for $\dot{\mathcal{K}}_\vartheta = \int \mathbf{u}_\vartheta \cdot \partial \mathbf{u}_\vartheta / \partial t \, dV$, it is more convenient[†] to first rewrite this as $\dot{\mathcal{K}}_\vartheta = \oint \varphi \mathbf{n} \cdot \partial \mathbf{u}_\vartheta / \partial t \, dS - \int \varphi \, \partial \vartheta / \partial t \, dV$. Now substituting from (2.17) for $\partial \vartheta / \partial t$ and retaining only terms linear in ε, we have after using the momentum equation evaluated on the boundary that

$$\dot{\mathcal{K}}_\vartheta = -\oint \varphi \, \mathbf{n} \cdot \partial \mathbf{u}_\omega / \partial t \, dS - \int \mathcal{L}_u (...) \cdot \mathbf{u}_\vartheta \, dV \tag{8.3}$$

Much of the focus here will be on studying $\dot{\mathcal{K}}_\vartheta$ since it is here that the effects of vorticity arise; for example, the first term contains the normal component of the vortical velocity.

8.3 Energy Transfer between the Longitudinal and Transverse Fields

To help understand how energy is transferred between the longitudinal and transverse fields, we start with the kinetic energy of the unsteady velocity field, i.e., $\mathcal{K} \equiv \int \tfrac{1}{2} \mathbf{u} \cdot \mathbf{u} \, dV$, and introduce the Stokes-Helmholtz decomposition $\mathbf{u} = \nabla \varphi + \nabla \times \mathbf{A} \equiv \mathbf{u}_\vartheta + \mathbf{u}_\omega$. It follows that $\mathcal{K} = \mathcal{K}_\vartheta + \mathcal{K}_{\vartheta \leftrightarrow \omega} + \mathcal{K}_\omega$, where $\mathcal{K}_\vartheta \equiv \int \tfrac{1}{2} \mathbf{u}_\vartheta \cdot \mathbf{u}_\vartheta \, dV$ and $\mathcal{K}_\omega \equiv \int \tfrac{1}{2} \mathbf{u}_\omega \cdot \mathbf{u}_\omega \, dV$ give the kinetic energy of the longitudinal and transverse fields, respectively. That the energy flux between the two is described by the time rate-of-change of $\mathcal{K}_{\vartheta \leftrightarrow \omega} \equiv \int \mathbf{u}_\vartheta \cdot \mathbf{u}_\omega \, dV$ seems plausible and will indeed be shown. It is useful to write this as $\dot{\mathcal{K}}_{\vartheta \leftrightarrow \omega} = \dot{\mathcal{K}}_{\vartheta \to \omega} - \dot{\mathcal{K}}_{\omega \to \vartheta}$, where

$$\dot{\mathcal{K}}_{\vartheta \to \omega} \equiv \int \mathbf{u}_\omega \cdot \partial \mathbf{u}_\vartheta / \partial t \, dV, \quad \dot{\mathcal{K}}_{\omega \to \vartheta} \equiv -\int \mathbf{u}_\vartheta \cdot \partial \mathbf{u}_\omega / \partial t \, dV \tag{8.4}$$

In this section, we investigate $\dot{\mathcal{K}}_{\vartheta \to \omega}$ and $\dot{\mathcal{K}}_{\omega \to \vartheta}$ in detail. To elucidate more clearly the physical mechanisms, we use as the backdrop for part of the discussion the classic acoustic boundary layer; this is a useful setting since exact relationships can be derived. We are justified in doing so, since the fluxes in question follow from a Stokes-Helmholtz decomposition of $\mathbf{u}$ and thus are not unique to a solid rocket motor. We will show that $\dot{\mathcal{K}}_{\vartheta \to \omega}$ occurs because of sound generating vorticity and $\dot{\mathcal{K}}_{\omega \to \vartheta}$ because of that vorticity in turn generating sound.

[†] In contrast with earlier work (e.g., Cantrell and Hart 1964), the unsteady flow is *not* assumed irrotational here. Thus, to obtain an expression for $\partial \mathbf{u}_\vartheta / \partial t$, the momentum equation $\partial \mathbf{u} / \partial t + \mathcal{L}_u (...) = 0$ would need to be projected onto a curl-free space. Although possible, this step requires a Stoke-Helmholtz decomposition of the operator $\mathcal{L}_u (...)$, which is generally cumbersome. Instead, we can use a simple identity $\int \nabla \alpha \cdot \mathbf{a} \, dV = \oint \alpha \mathbf{n} \cdot \mathbf{a} \, dS - \int \alpha \nabla \cdot \mathbf{a} \, dV$ to obtain the more convenient formula given by (8.3).

8.3.1 Sound Generating Vorticity

To establish the mechanism of $\dot{\mathcal{K}}_{\vartheta\to\omega}$, we first express this flux as a surface integral

$$\dot{\mathcal{K}}_{\vartheta\to\omega} \equiv \int \mathbf{u}_\omega \cdot \partial\mathbf{u}_\vartheta/\partial t \, dV = -\oint \mathbf{A}\cdot\left(\mathbf{n}\times\partial\mathbf{u}_\vartheta/\partial t\right) dS \tag{8.5}$$

and then relate $\mathbf{n}\times\partial\mathbf{u}_\vartheta/\partial t$ to the creation of vorticity. The basic idea is that *longitudinal waves create transverse waves by making it appear as if the boundary oscillates parallel to itself*. Stated another way: to satisfy the no-slip condition, vorticity must be created such that on the boundary a fluid motion equal and opposite $\mathbf{n}\times\partial\mathbf{u}_\vartheta/\partial t$ is induced.

This is most clearly seen for the classic acoustic boundary layer—recall from (6.8) that $\boldsymbol{\sigma}_\zeta = \mathbf{n}\times\partial\mathbf{u}_\vartheta/\partial t$, which essentially defines a Stokes problem. A similar results holds, albeit only approximately, for a solid rocket motor, where to leading order $\partial\mathbf{u}_\vartheta/\partial t \sim -\nabla p$. Since the gradient of pressure tangent to the grain boundary is the dominant physical source of boundary vorticity (cf. §7.2), i.e., $\boldsymbol{\sigma}_\zeta \sim -\mathbf{n}\times\nabla p$, it follows that $\boldsymbol{\sigma}_\zeta \sim \mathbf{n}\times\partial\mathbf{u}_\vartheta/\partial t$. Substituting in (8.5), we have

$$\dot{\mathcal{K}}_{\vartheta\to\omega} \sim -\oint \mathbf{A}\cdot\boldsymbol{\sigma}_\zeta \, dS \tag{8.6}$$

This demonstrates conclusively that $\dot{\mathcal{K}}_{\vartheta\to\omega}$ is intimately related to the creation of vorticity given that the vorticity source strength $\boldsymbol{\sigma}_\zeta$ is most basic measure of this process.

Having established the mechanism of $\dot{\mathcal{K}}_{\vartheta\to\omega}$, we now consider how this flux relates to $\dot{\mathcal{K}}_\vartheta$. Even though the expression for $\dot{\mathcal{K}}_{\vartheta\to\omega}$ is the same for both the classic acoustic boundary layer and a solid rocket motor, what differs is the transport mechanism by which boundary vorticity enters the domain: viscous diffusion in one instance, and convection by the mass flux issuing forth from a burning propellant, in the other. This difference will be reflected in how $\dot{\mathcal{K}}_{\vartheta\to\omega}$ relates to $\dot{\mathcal{K}}_\vartheta$.

For the classic acoustic boundary layer, it can be show that (cf. §H.2 for details)

$$\dot{\mathcal{K}}_\vartheta = \ldots - \dot{\mathcal{K}}_{\vartheta\to\omega} + \ldots \quad \text{with } \dot{\mathcal{K}}_{\vartheta\to\omega} \geq 0 \tag{8.7}$$

This clearly indicates that when a longitudinal wave excites a transverse wave through coupling on the boundary, it loses energy in the process.

Insofar as a solid rocket motor is concerned, while $\dot{\mathcal{K}}_{\vartheta\to\omega}$ does not directly appear in the equation for $\dot{\mathcal{K}}_\vartheta$, in §8.5 a mathematical connection will be shown to exist between this flux and Culick's *flow turning* (1973).

8.3.2 Vorticity Generating Sound

To establish the mechanism of $\dot{\mathcal{K}}_{\omega\to\vartheta}$, we first express this flux as a surface integral

$$\dot{\mathcal{K}}_{\omega\to\vartheta} \equiv -\int \mathbf{u}_\vartheta \cdot \partial\mathbf{u}_\omega/\partial t \, dV = -\oint \varphi\mathbf{n}\cdot\partial\mathbf{u}_\omega/\partial t \, dS \tag{8.8}$$

and then relate $\mathbf{n}\cdot\partial\mathbf{u}_\omega/\partial t$ to the creation of sound. The basic idea is that *transverse waves create longitudinal waves by making it appear as if the boundary oscillates normal to itself.*

Once again, this is most clearly seen for the classic acoustic boundary layer. Recall from (6.13) that $\partial\left(p-\mathrm{Re}_\vartheta^{-1}\vartheta\right)\big/\partial n=\mathbf{n}\cdot\partial\mathbf{u}_\omega/\partial t$, which indicates that sound is generated aerodynamically through an action similar to that of a speaker despite the absence of any physical motion (cf. Lighthill 1952 for the earliest discussion of this idea).

While (8.8) helps identify the mechanism of $\dot{\mathcal{K}}_{\omega\to\vartheta}$, to evaluate this flux (which is necessary since it is the first term in the expression for $\dot{\mathcal{K}}_\vartheta$ as given by (8.3)) it is useful to first rewrite it as

$$\dot{\mathcal{K}}_{\omega\to\vartheta}=-\oint\mathbf{u}_\vartheta\cdot\left(\mathbf{n}\times\partial\mathbf{A}/\partial t\right)dS \tag{8.9}$$

Now recall from (7.23) that for a solid rocket motor $\mathbf{n}\times\partial\mathbf{A}/\partial t\sim-\left(\mathbf{n}\cdot M_b\mathbf{U}\right)\mathbf{u}_{\omega\zeta}$. Substituting this result in (8.9), we obtain

$$\dot{\mathcal{K}}_{\omega\to\vartheta}\sim M_b\oint\left(\mathbf{u}_{\vartheta\zeta}\cdot\mathbf{u}_{\omega\zeta}\right)\mathbf{n}\cdot\mathbf{U}\,dS\geq 0 \tag{8.10}$$

where the sign of the integrand is simply a consequence of the no-slip condition $\mathbf{u}_{\omega\zeta}=-\mathbf{u}_{\vartheta\zeta}$. Since $\dot{\mathcal{K}}_{\omega\to\vartheta}\geq 0$ and $\dot{\mathcal{K}}_\vartheta=\dot{\mathcal{K}}_{\omega\to\vartheta}+\ldots$ from (8.3), it follows that this mechanism is destabilizing (i.e., it amplifies rather than attenuates instabilities). Stated another way: the sound created by vorticity constructively interferes with the sound responsible for creating that vorticity.

There are a few remarks to be made on the generality of our estimate for $\dot{\mathcal{K}}_{\omega\to\vartheta}$. First, it must be emphasized that *only* the behavior on the boundary was needed to arrive at (8.10). Let us elaborate on this point further. The essential step was to use (7.23). Recall that in obtaining this result only two key elements of the physics were used, specifically the scaling derived from the no-slip condition and that vorticity created on the boundary is chiefly convected into the domain by the mean flow at a rate, which is $O\left(M_b\right)$ smaller than that at which sound waves propagate. Because these key elements are likely unaffected by any probable *downstream* transition to turbulence, this bodes well for the generality of (8.10). Second, with respect to more complex geometries, the result can be applied to any propellant grain that can be locally described by a general orthogonal coordinate system.

Lastly, we observe that $\dot{\mathcal{K}}_{\omega\to\vartheta}$ is essentially Flandro's (1995 a, b) controversial *radial pumping* correction. However, the calculation in that analysis was only valid for the special case of axial mode instability in a cylindrical chamber, with no clear elucidation of the physics involved. In contrast, not only has a far more general estimate been obtained here, but also a deeper understanding of the mechanism has been achieved.

8.4 Kinetic Energy of the Longitudinal Field

We now turn to the evaluation of $\dot{\mathcal{K}}_{\vartheta}$. Substituting (B.29) for $\mathcal{L}_u(...)$ in (8.3), we find

$$\dot{\mathcal{K}}_{\vartheta} = \dot{\mathcal{K}}_{\omega\to\vartheta} - \dot{\mathcal{K}}_{\vartheta\leftrightarrow\mathbf{U}} - \oint p\mathbf{n}\cdot\mathbf{u}_{\vartheta}\,dS + \int p\,\vartheta\,dV + \int \mathcal{F}\cdot\mathbf{u}_{\vartheta}\,dV \tag{8.11}$$

The first term on the right is the rate of energy transfer from the transverse field; this flux has already been evaluated in §8.3, with the result given by (8.10). The second term describes the interactions with the mean flow; these will be discussed in detail below. The integrand in the third term indicates the classical linear *pressure coupling* with the flame zone[†] (cf. Culick and Yang 1992) and the fourth term reflects the effect of pressure within the interior. An integral of identical form but opposite sign appears in the equation (8.2) for $\dot{\mathcal{P}}$ and so this is simply the well-known mechanism for the *reversible* energy exchange between potential and kinetic. Finally, the last term involves the momentum source $\mathcal{F}$, and while other contributions may exist, those due to viscous effects are negligible[‡].

Interactions with the Mean Flow

We now consider the interactions with the mean flow $\dot{\mathcal{K}}_{\vartheta\leftrightarrow\mathbf{U}}$. Following Flandro (1995 a, b) these can be expressed as

$$\dot{\mathcal{K}}_{\vartheta\leftrightarrow\mathbf{U}} = M_b\int \mathbf{u}_{\vartheta}\cdot\left(\nabla\left(\mathbf{U}\cdot\mathbf{u}\right) + \boldsymbol{\omega}\times\mathbf{U} + \boldsymbol{\Omega}\times\mathbf{u}\right)dV \tag{8.12}$$

To use this as the starting for our calculation however complicates the analysis unnecessarily. For example, not only is detailed knowledge of the unsteady vorticity field needed to evaluate some of the terms but also the physical mechanisms are unclear.

In contrast, we proceed here by first recasting (8.12) using standard vector identities (cf. §H.3 for further details)

$$\dot{\mathcal{K}}_{\vartheta\leftrightarrow\mathbf{U}} = M_b\left(\begin{array}{c}\oint\left(\tfrac{1}{2}\mathbf{u}_{\vartheta}\cdot\mathbf{u}_{\vartheta}\right)\mathbf{n}\cdot\mathbf{U}dS + \oint\left(\mathbf{u}_{\vartheta\zeta}\cdot\mathbf{u}_{\omega\zeta}\right)\mathbf{n}\cdot\mathbf{U}dS + \int\mathbf{u}_{\vartheta}\cdot\nabla\mathbf{U}\cdot\mathbf{u}_{\vartheta}\,dV \\ +\int\mathbf{u}_{\omega}\cdot\mathbf{f}\left(\mathbf{u}_{\vartheta},\mathbf{U}\right)dV\end{array}\right) \tag{8.13}$$

[†] The reacting surface is commonly represented by an effective admittance—future emphasis needs to be placed on assessing the sensitivity of the combustion processes to a rotational flow environment.

[‡] Those terms that describe viscous effects are

$$\int\mathcal{F}\cdot\mathbf{u}_{\vartheta}\,dV = \mathrm{Re}_{\omega}^{-1}\oint\mathbf{u}_{\vartheta}\cdot\left(\boldsymbol{\omega}\times\mathbf{n}\right)dS + \mathrm{Re}_{\vartheta}^{-1}\oint\vartheta\,\mathbf{n}\cdot\mathbf{u}_{\vartheta}\,dS - \mathrm{Re}_{\vartheta}^{-1}\int\vartheta^2\,dV$$

With respect to the first integral, since longitudinal motions slip, effecting a scrubbing of the surface, the work done by the shearing stresses $\boldsymbol{\tau} = \mathrm{Re}_{\omega}^{-1}\boldsymbol{\omega}\times\mathbf{n}$ is no longer zero. To estimate the contribution, recall from (7.10) that $\boldsymbol{\omega}_{\zeta}\sim O\left(M_b^{-1}\right)$ and so $\mathrm{Re}_{\omega}^{-1}\oint\mathbf{u}_{\vartheta}\cdot\left(\boldsymbol{\omega}\times\mathbf{n}\right)dS\sim O\left(\left(M_b^2\,\mathrm{Re}_{\omega}\right)^{-1}\right)O\left(M_b\right)$. Thus, this flux is not generally significant since $\left(M_b^2\,\mathrm{Re}_{\omega}\right)^{-1}$ is small for the cases of interest here (cf. Table 7.1). The second and third terms contribute even less.

where $\mathbf{f}\left(\mathbf{u}_\vartheta,\mathbf{U}\right)\equiv\mathbf{u}_\vartheta\cdot\nabla\mathbf{U}+\nabla\mathbf{U}\cdot\mathbf{u}_\vartheta-\boldsymbol{\Omega}\times\mathbf{u}_\vartheta$. While (8.12) and (8.13) are formally equivalent, the latter representation of $\dot{\mathcal{K}}_{\vartheta\leftrightarrow\mathbf{U}}$ offers significant advantages from both a mathematical and a physical point of view. The reasons for this will become clear in due course.

First, let us consider the terms in (8.13) that an irrotational analysis (e.g., Cantrell and Hart 1964; Culick 1975) would recover. We choose here not to focus on the physical mechanisms involved and simply note that using the leading order solution for the acoustic field, it can be shown that (cf. §H.4 for further details)

$$\left\langle \oint\left(\tfrac{1}{2}\mathbf{u}_\vartheta\cdot\mathbf{u}_\vartheta\right)\mathbf{n}\cdot\mathbf{U}dS+\int\mathbf{u}_\vartheta\cdot\nabla\mathbf{U}\cdot\mathbf{u}_\vartheta dV\right\rangle\sim\left\langle \oint\tfrac{1}{2}p^2\mathbf{n}\cdot\mathbf{U}dS\right\rangle\leq 0 \tag{8.14}$$

Next, we consider the vortical terms in (8.13). With respect to the volume integral, this can be collapsed to integration over burning surfaces by applying the earlier asymptotic result (7.26); because of the factor of M_b/k_{m0} that is introduced, the contribution of this integral is $O\left(M_b^2\right)$ and thus negligible. However, it must be emphasized that this *only* applies if the flow remains laminar. To account for the effect of turbulence in estimating this term requires additional modeling—a proposition that is beyond the scope of the present investigation.

What remains in (8.13) is a stabilizing flux of energy *from* the longitudinal motions *to* the mean flow,

$$\dot{\mathcal{K}}_{\vartheta\rightarrow\mathbf{U}}\equiv M_b\oint\left(\mathbf{u}_{\vartheta\zeta}\cdot\mathbf{u}_{\omega\zeta}\right)\mathbf{n}\cdot\mathbf{U}dS\geq 0 \tag{8.15}$$

Unlike with the volume integral discussed above, it must be emphasized that the *only* condition required for an evaluation is *no-slip* $\mathbf{u}_{\omega\zeta}=-\mathbf{u}_{\vartheta\zeta}$ (this also accounts for the sign of the integrand). This constraint is purely kinematic, and thus valid for *any* motion whatsoever, turbulent or otherwise. Moreover, since only vector identities were used to obtain (8.13), it follows that the result is not limited to any particular geometry. In §8.5, we discuss the physics of $\dot{\mathcal{K}}_{\vartheta\rightarrow\mathbf{U}}$ as well as the different manifestations of this flux recovered in earlier analyses (Culick 1973; Flandro 1995 a, b).

Summary

Let us summarize our findings for $\dot{\mathcal{K}}_\vartheta$; our primary concern recall was to understand the effects of vorticity. Combining (8.11), (8.13) and (8.15) we have that to leading order these are given by

$$\dot{\mathcal{K}}_\vartheta\sim\dot{\mathcal{K}}_{\omega\rightarrow\vartheta}-\dot{\mathcal{K}}_{\vartheta\rightarrow\mathbf{U}}+\ldots \tag{8.16}$$

where we reiterate that only *if* the flow is turbulent might the last integral in (8.13) contribute.

What is striking to observe now is that $\dot{\mathcal{K}}_{\vartheta\to\mathbf{U}} \sim \dot{\mathcal{K}}_{\omega\to\vartheta}$ (cf. (8.10) and (8.15)). Thus, to the order of approximation considered, no *net* contribution exists owing to the effects of vorticity and so (8.16) reduces to

$$\left\langle \dot{\mathcal{K}}_{\vartheta} \right\rangle \sim \left\langle -\oint p\mathbf{n}\cdot\mathbf{u}_{\vartheta}\, dS - M_b \oint \tfrac{1}{2} p^2 \mathbf{n}\cdot\mathbf{U} dS + \int p\,\vartheta\, dV \right\rangle \tag{8.17}$$

While this completes the mathematical part of the discussion, much remains in terms of the physics.

8.5 Physical Interpretation

It seems somewhat remarkable that, to the order of approximation considered, no *net* contribution exists to the stability (or instability) of the acoustic field owing to the effects of vorticity. This, as shown in the previous section, is a consequence of $\dot{\mathcal{K}}_{\vartheta\to\mathbf{U}} \sim \dot{\mathcal{K}}_{\omega\to\vartheta}$. We aim to address here whether this is merely a fortuitous finding or rather a deeper reflection of the underlying physics.

8.5.1 Revisiting Flow Turning

We begin by establishing that $\dot{\mathcal{K}}_{\vartheta\to\mathbf{U}} \equiv M_b \oint \left(\mathbf{u}_{\vartheta\zeta}\cdot\mathbf{u}_{\omega\zeta}\right)\mathbf{n}\cdot\mathbf{U} dS$ is the multidimensional analog of Culick's *flow turning* (1973). Enforcing the no-slip condition $\mathbf{u}_{\omega\zeta} = -\mathbf{u}_{\vartheta\zeta}$ and substituting the leading order solution of the longitudinal field, i.e., $\mathbf{u}_{\vartheta\zeta} \sim -\left(i/k_{m0}\right)\nabla_{\zeta} p$, we find

$$\dot{\mathcal{K}}_{\vartheta\to\mathbf{U}} \sim -\left(M_b / k_{m0}^2\right) \oint \left|\nabla_{\zeta} p\right|^2 \mathbf{n}\cdot\mathbf{U} dS \tag{8.18}$$

This recovers the one-dimensional stability result Culick first derived, if one replaces the tangential gradient in pressure by the derivative in the axial direction. Not only does this validate Culick's original *patching* procedure, but also it clearly establishes that vortical flow effects are key to flow turning *naturally* reappearing in a multidimensional analysis.

Flandro (1995 a, b) reached the same conclusion by evaluating $M_b \int \mathbf{u}_{\vartheta}\cdot\left(\boldsymbol{\omega}\times\mathbf{U}\right) dV$. However, this required *detailed* knowledge of the unsteady vorticity distribution within the chamber, which insofar as practical application is concerned, is a serious limitation for the following reasons. First, the unsteady vorticity distribution can be obtained analytically only for very simple geometries. Second, and perhaps more important, the laminar solution in all likelihood will not remain a valid description; the very nature of the vorticity field makes it an ideal candidate to become unstable itself.

Thus, despite Flandro having recovered *flow turning*, what remained unanswered was the dependence of such a recovery on the level of approximation introduced. In other words, it had not been resolved whether an energy gain, for example, was a plausible outcome instead under more realistic flow conditions, or, if upon integration over the domain, a loss *always* results—as suggested by Culick's analysis

To address this issue, as well as to accommodate more complex grain geometries, for which previous analyses provide little guidance, appeal to numerical simulations seemed inevitable. Fortunately, however, such a tack, which has its own host of associated difficulties, is unnecessary if the transformation from (8.12) to (8.13) is first effected. Recall that what resulted from recasting the interactions with the mean flow with the help of vector identities was $\dot{\mathcal{K}}_{\mathcal{G}\to\mathbf{U}} \equiv M_b \oint \left(\mathbf{u}_{\mathcal{G}\zeta} \cdot \mathbf{u}_{\omega\zeta}\right)\mathbf{n}\cdot\mathbf{U}dS$.

What must be stressed here is that this new surface integral, now correctly identified as flow turning, requires only the statement of no-slip condition for its evaluation. The merit of such advancement is that not only are more complex grain geometries just as easily accommodated, but also any concerns regarding the influence of turbulence, at least insofar as this interaction is concerned, are completely laid to rest[†]. Enormous practical advantage is thereby offered over the volume integral that Flandro (1995 a, b) asserted was the multidimensional analog of this important damping effect first discovered by Culick (1973).

The Mechanism of Flow Turning

Apart from being simple, mathematically rigorous, and dependent only upon kinematics for its derivation, the new definition of flow turning introduced here, plays an equally important role in enhancing our understanding of the physical mechanism involved.

For all the insight offered by Flandro's analysis (1995 a, b), Culick's (1973) original interpretation remained unquestioned: flow turning was still attributed to gas particles produced in the flame zone having to turn in order to acquire the motion of the acoustic flow. Even though this is not incorrect from a certain point of view, a much sharper picture emerges by relating *flow turning* to the *creation of vorticity*.

While Flandro certainly recognized the importance of satisfying the no-slip condition, and underscored the central role played by vorticity in this important damping effect, *no* connection with vorticity creation was ever established. The point is best made by noting that the term Flandro identified as flow turning involved integration over the *volume* of the domain, whereas vorticity is *only*[‡] created on the boundary for the problem considered.

[†] Note that if the flow becomes turbulent, the last term in (8.13), i.e., $M_b \int \mathbf{u}_\omega \cdot \mathbf{f}\left(\mathbf{u}_\mathcal{G}, \mathbf{U}\right) dV$, may contribute. However, regarding the terms retained, the steps leading to (8.15) are independent of whether the flow is laminar or turbulent.

[‡] Vorticity is also generated in the flame zone, but this was not part of the model considered by Flandro (1995 a, b).

In contrast, by using our new definition, it can be shown that (cf. §H.5 for details)

$$\left\langle \dot{\mathcal{K}}_{\mathcal{G}\to\mathbf{U}} \right\rangle \sim -\oint \left\langle \mathbf{A}\cdot\boldsymbol{\sigma}_{\zeta} \right\rangle dS \tag{8.19}$$

This clearly establishes that *flow turning is intimately related to the creation of vorticity* given that the vorticity source strength $\boldsymbol{\sigma}_{\zeta}$ is the most basic measure of this process. This also allows us to place flow turning in the larger context of energy pathways between the longitudinal and transverse fields, since recall from (8.6) that $\dot{\mathcal{K}}_{\mathcal{G}\to\omega} \sim -\oint \mathbf{A}\cdot\boldsymbol{\sigma}_{\zeta}\, dS$ and therefore

$$\left\langle \dot{\mathcal{K}}_{\mathcal{G}\to\mathbf{U}} \right\rangle \sim \left\langle \dot{\mathcal{K}}_{\mathcal{G}\to\omega} \right\rangle \tag{8.20}$$

8.5.2 On the Net Contribution of Vorticity

As noted earlier, Flandro (1995 a, b) reported (for the simple case considered) that the gain owing to *radial pumping* compensated the loss due to *flow turning*. The reasons why however were never explained, largely because a clear understanding of the physical mechanisms did not exist.

That is why (8.20) is so important, for it establishes that flow turning describes one pathway, i.e., the *flow* of energy from the longitudinal to the transverse field owing to the creation of vorticity. The controversial *radial-pumping* effect was already shown in §8.3.2 to describe the complementary flux, i.e., the *flow* of energy from the transverse to the longitudinal field. Thus, a very elegant physical picture, supported by quite simple mathematical formulae, emerges: *sound generates vorticity, which in turn, generates more sound*; *Culick's flow turning and Flandro's radial pumping describe, respectively, the two halves of this process*.

Having now understood the mechanisms, the conclusion reached basically establishes that: *the rate of energy loss experienced by the sound field in generating vorticity is compensated by the rate of energy gain owing to generation of more sound by that vorticity*. More succinctly stated, the energy flux between the longitudinal and transverse fields is—to leading order—*reversible*. What is important to realize is that this finding $\dot{\mathcal{K}}_{\mathcal{G}\to\mathbf{U}} \sim \dot{\mathcal{K}}_{\omega\to\mathcal{G}}$ *is* a reflection of the underlying physics of the problem. With fluid injected through the boundary, convection as opposed to viscous diffusion becomes the dominant mechanism for transporting (acoustically-generated) boundary vorticity into the domain. The manner in which this vorticity creates sound, moreover, via the *appearance* of an oscillating boundary—essentially mimicking the action of a speaker—is already effectively inviscid in nature. As such, it is not an unforeseen consequence that, since dissipative effects no longer substantially enter into either of the creation mechanisms, *the means for making the kinetic energy unrecoverable no longer exists.*

8.6 Implications for SSPP

Summing together (8.2) and (8.16), we find

$$\left\langle \dot{\mathcal{P}} + \dot{\mathcal{K}}_{\vartheta} \right\rangle = 2\alpha_{m\mu} \left\langle \mathcal{P} + \mathcal{K}_{\vartheta} \right\rangle \sim \left\langle -\oint p\mathbf{n}\cdot\mathbf{u}_{\vartheta}\, dS - M_b \oint p^2 \mathbf{n}\cdot\mathbf{U} dS + (\gamma - 1)\int pQdV \right\rangle \tag{8.21}$$

A few final remarks are useful in closing. Aside from a greatly enhanced physical understanding—which helps explain the mathematical observations—the current effort improves on what has been done (Culick 1973; Flandro 1995 a, b) in two key ways: the results obtained are *independent* of grain geometry; and the derivation of these results depends largely on kinematics. Accordingly, the conclusions reached can be applied to reasonably complex grain geometries, *irrespective* of whether the motion is turbulent or not.

The conclusions, in other words, support but also *significantly extend* the findings of an earlier study by Flandro (1995 a, b), in which the importance of incorporating vortical flow effects in the acoustic instability algorithm was first demonstrated. What limited the applicability of that analysis, however, is that the new stability integrals were evaluated *only* for a cylindrical propellant grain under the quite restrictive assumption that the unsteady vorticity distribution remains laminar. On a practical level then much has been gained with the present advancement.

Of course, the ultimate test of any theory is based on comparison with experiment. The Standard Stability Prediction Program (Lovine et al. 1976, Nickerson et al. 1983) has often failed to give satisfactory results with *flow turning* patched on (cf. Flandro 1995 a, b). In other words, stability trends were more accurately predicted without this *correction*. The present effort provides insight for this observation obtained from practitioners in the field.

Specifically, the reason is not that *flow turning* does not exist, at least not in the modified sense introduced here, but rather that the complementary process, i.e., the transfer of energy from the transverse to the longitudinal field, needs also to be accounted for. This energy pathway is recovered only when vortical flow effects are taken into account. Owing to the energy flux between longitudinal and transverse fields being reversible in the first approximation, there is no net contribution.

9. NONLINEAR BEHAVIOR

Basis functions for expanding the longitudinal (i.e., acoustic and thermal) and transverse (i.e., vortical) parts of the unsteady flow field were derived in Chapter 7. These functions were then utilized in Chapter 8 to re-examine the calculation of linear stability, with emphasis placed on understanding the effects of vorticity. Now we turn to the nonlinear behavior and consider three kinds of nonlinear interactions to second order in the wave amplitude: sound-sound, sound-vortical and vortical-vortical.

9.1 Energy Balance Considerations

We begin by motivating why effects of vorticity might play an important role. For that purpose, the energy balance, first introduced in Chapter 8, is extended to accommodate nonlinear terms. Recall that an improved physical understanding of some underlying mechanisms resulted by formulating linear stability along such lines. In particular, Culick's (1973) *flow turning* and Flandro's (1995 a, b) *radial pumping* were shown to represent the energy flux from the longitudinal to the transverse field and vice-versa, respectively. Given this earlier success, it is reasonable to expect that valuable insight into the nonlinear behavior can also be gained.

Recall from §8.2 that the time rate of change of kinetic energy stored by the longitudinal motions is given by $\dot{\mathcal{K}}_\vartheta = \oint \varphi \mathbf{n} \cdot \partial \mathbf{u}_\vartheta / \partial t \, dS - \int \varphi \, \partial \vartheta / \partial t \, dV$. Substituting from (2.17) for $\partial \vartheta / \partial t$, we find

$$\dot{\mathcal{K}}_\vartheta = -\oint \varphi \mathbf{n} \cdot \frac{\partial \mathbf{u}_\omega}{\partial t} dS - \int \mathcal{L}_u (...) \cdot \mathbf{u}_\vartheta \, dV + \int \mathcal{N}_u (...) \cdot \mathbf{u}_\vartheta \, dV \tag{9.1}$$

where the third term represents the nonlinear effects; of these, our concern is the energy flux to and from the transverse field. This can be studied by setting $\mathcal{N}_u (...) = -\mathbf{u} \cdot \nabla \mathbf{u}$. Using standard vector identities, we have

$$\int \mathcal{N}_u (...) \cdot \mathbf{u}_\vartheta \, dV = \begin{pmatrix} -\oint (\mathbf{u}_\vartheta \cdot \mathbf{u}_\omega) \mathbf{n} \cdot \mathbf{u} \, dS + \int (\mathbf{u}_\vartheta \cdot \mathbf{u}_\omega) \vartheta \, dV - \\ -\int \mathbf{u}_\vartheta \cdot (\nabla \mathbf{u}_\vartheta) \cdot \mathbf{u}_\vartheta \, dV + \int \mathbf{u}_\omega \cdot (\nabla \mathbf{u}_\vartheta) \cdot \mathbf{u}_\omega \, dV + ... \end{pmatrix} \tag{9.2}$$

While the physics of all the terms here may be elaborated upon†, we focus on the surface integral (for reasons that become clear in due course). This can be rewritten as

$$\oint (\mathbf{u}_\vartheta \cdot \mathbf{u}_\omega) \mathbf{n} \cdot \mathbf{u} dS \sim \oint (\mathbf{u}_{\vartheta\zeta} \cdot \mathbf{u}_{\omega\zeta}) \mathbf{n} \cdot \mathbf{u} dS = -\oint |\mathbf{u}_{\vartheta\zeta}|^2 \mathbf{n} \cdot \mathbf{u} dS \tag{9.3}$$

since: the contribution from $u_{\vartheta n} u_{\omega n}$ is $O(\varepsilon^2 M_b^2)$ and thus negligible; and $\mathbf{u}_{\vartheta\zeta} = -\mathbf{u}_{\omega\zeta}$ by virtue of the no-slip condition.

---

† For example, the third and fourth terms describe the flux of energy that results when longitudinal velocity gradients stretch or compress the *local* streamtubes corresponding to the longitudinal and the transverse fields, respectively.

We now make two key observations. First, a striking similarity exists between (9.3) and the new, more robust, definition of *flow turning* $\dot{\mathcal{K}}_{\vartheta\to\mathbf{U}} \equiv M_b \oint \left(\mathbf{u}_{\vartheta\zeta}\cdot\mathbf{u}_{\omega\zeta}\right)\mathbf{n}\cdot\mathbf{U}dS$ introduced in §8.4. Thus, by analogy, the flux here can be interpreted as a nonlinear energy transfer owing to vorticity creation, for just as the mean flow convects unsteady vorticity into the domain, so does the unsteady flow. Second, since unsteady combustion processes help determine the behavior of $\mathbf{n}\cdot\mathbf{u}$ (which is not constrained to be inwardly pointing), this flux indicates a *natural*—vis-à-vis velocity coupling perhaps (cf. Price 1992)—nonlinear interaction with the flame zone that can be either stabilizing or destabilizing.

This clearly establishes the importance of accounting for vortical flow effects, absent which, only the third term in (9.2) remains. The difficulty in using an energy balance to do so however is that, energy transfer *between* individual modes cannot be resolved (that this may not be a serious limitation has been suggested by Flandro 1985). To capture this coupling what is required in some respects is a projection of $\mathbf{N}_u(...)$ not on $\mathbf{u}_\vartheta$, but rather on each of the modes from which this motion may be synthesized. With this, we return to the framework developed in Chapter 2.

9.2 Nonlinear Interactions

For the purposes of our discussion here, the nonlinearities in the amplitude equations

$$\dot{\eta}_m + ik_m\eta_m = \tfrac{1}{E_m^2}\left(\int \mathcal{N}_c(...)c_m^{\dagger *}dV - \int \mathcal{N}_u(...)\cdot\nabla\varphi_m^{\dagger *}dV + \oint \varphi_m^{\dagger *}\mathbf{n}\cdot\mathcal{N}_u(...)dS\right) \tag{9.4}$$

for our general framework of combustion instability, can be written as

$$\dot{\eta}_m + ik_m\eta_m = \tfrac{1}{E_m^2}\left(I^{\vartheta\vartheta} + I^{\vartheta\omega} + I^{\omega\omega} + I^{\mathcal{B}} + ...\right) \tag{9.5}$$

where $I^{\mathcal{B}} = \oint \varphi_m^{\dagger *}\mathbf{n}\cdot\mathbf{N}_u(...)dS$ is a boundary term, which will be elaborated upon shortly, and $I^{\vartheta\vartheta}$, $I^{\vartheta\omega}$ and $I^{\omega\omega}$ are the sound-sound, the sound-vortical and the vortical-vortical interactions, respectively. Substituting (B.33) and (B.34) for the nonlinear operators $\mathcal{N}_c(...)$ and $\mathcal{N}_u(...)$, and omitting from consideration non-isentropic effects[†], we find

$$I^{\vartheta\vartheta} = -\int(\mathbf{u}_\vartheta\cdot\nabla c)c_m^{\dagger *}dV - (\Gamma-1)\int c\vartheta c_m^{\dagger *}dV + \int\nabla\left(\tfrac{1}{2}\tfrac{1}{\Gamma-1}c^2 + \tfrac{1}{2}\mathbf{u}_\vartheta\cdot\mathbf{u}_\vartheta\right)\cdot\nabla\varphi_m^{\dagger *}dV \tag{9.6}$$

$$I^{\vartheta\omega} = -\int(\mathbf{u}_\omega\cdot\nabla c)c_m^{\dagger *}dV + \int(\mathbf{u}_\vartheta\cdot\nabla\mathbf{u}_\omega + \mathbf{u}_\omega\cdot\nabla\mathbf{u}_\vartheta)\cdot\nabla\varphi_m^{\dagger *}dV \tag{9.7}$$

$$I^{\omega\omega} = \int(\mathbf{u}_\omega\cdot\nabla\mathbf{u}_\omega)\cdot\nabla\varphi_m^{\dagger *}dV \tag{9.8}$$

Note that the nonlinearities these terms give rise to were studied in a general way in Chapter 4, starting with a system of the form

---

[†] As with the linear problem, contributions owing to viscous effects are negligible. Thus, it is sufficient to set $\mathbf{N}_u(...) = -\mathbf{u}\cdot\nabla\mathbf{u} - \frac{1}{\Gamma-1}c\nabla c$ and $N_c(...) = -\mathbf{u}\cdot\nabla c - (\Gamma-1)c\vartheta$.

$$\dot{\eta}_m + ik_m\eta_m = \tfrac{1}{E_m^2}\sum_{j,k}\Big(f_r^{\varepsilon\varepsilon(m,j,k)} + i\, f_i^{\varepsilon\varepsilon(m,j,k)}\Big)\eta_j\,\eta_k \tag{9.9}$$

Essentially, our goal here is to now determine the nonlinear coefficients.

Sound-Sound Interactions

Consider first the sound-sound interactions $I^{\vartheta\vartheta}$. Using some vector identities to recast (9.6), we have

$$\begin{aligned} I^{\vartheta\vartheta} = &-\int\left(\mathbf{u}_\vartheta\cdot\nabla c\right)c_m^{\dagger *}dV - \left(\Gamma-1\right)\int c\,\vartheta\, c_m^{\dagger *}dV - \int\left(\tfrac{1}{2}\tfrac{1}{\Gamma-1}c^2 + \tfrac{1}{2}\mathbf{u}_\vartheta\cdot\mathbf{u}_\vartheta\right)\vartheta_m^{\dagger *}dV + \\ &+\oint\left(\tfrac{1}{2}\tfrac{1}{\Gamma-1}c^2 + \tfrac{1}{2}\mathbf{u}_\vartheta\cdot\mathbf{u}_\vartheta\right)\mathbf{n}\cdot\nabla\varphi_m^{\dagger *}\,dS \end{aligned} \tag{9.10}$$

In evaluating (9.10), we could use the perturbed eigenfunctions obtained in Chapter 7; this would yield an $O\left(\varepsilon^2 M_b\right)$ correction to the leading order expression found in Chapter 3, that describes a nonlinear energy flux with the mean flow. However, we refrain from doing so since the new terms involve parameters such as the flame response for which no satisfactory model presently exists. Thus, for the purposes of our discussion here, we take (cf. Chapter 3)

$$I^{\vartheta\vartheta(m,j,k)} = -\tfrac{1}{8}\left(k_{m0}+k_{j0}+k_{k0}\right)\left(I_1^{\vartheta\vartheta(m,j,k)} - \left(\Gamma-1\right)^{-1} I_2^{\vartheta\vartheta(m,j,k)}\right) \tag{9.11}$$

where

$$\begin{aligned} I_1^{\vartheta\vartheta(m,j,k)} &= \int c_{m0}\,c_{j0}\,c_{k0}\,dV \\ I_2^{\vartheta\vartheta(m,j,k)} &= \left(k_{j0}k_{k0}\right)^{-1}\int c_{m0}\nabla c_{j0}\cdot\nabla c_{k0}\,dV \end{aligned} \tag{9.12}$$

Sound-Vortical Interactions

Consider next the sound-vortical interactions $I^{\vartheta\omega}$. Using some vector identities to recast (9.7), we have

$$\begin{aligned} I^{\vartheta\omega} = &\oint\left(\mathbf{u}_\omega\cdot\nabla\varphi_m^{\dagger *}\right)\mathbf{n}\cdot\mathbf{u}_\vartheta\,dS + \oint\left(\mathbf{n}\times\mathbf{A}\right)\cdot\left(\nabla\times\left(\mathbf{u}_\vartheta\times\nabla\varphi_m^{\dagger *}\right) - \vartheta_m^{\dagger *}\mathbf{u}_\vartheta - c_m^{\dagger *}\nabla c\right)dS + \\ &+\int\mathbf{A}\cdot\nabla\times\left(\nabla\times\left(\mathbf{u}_\vartheta\times\nabla\varphi_m^{\dagger *}\right) - \vartheta_m^{\dagger *}\mathbf{u}_\vartheta - c_m^{\dagger *}\nabla c\right)dV \end{aligned} \tag{9.13}$$

We can evaluate the volume integral here by applying the earlier asymptotic result (7.26), which collapses volume integrations to integration over burning surfaces; because of the factor of M_b/k_{m0} that is introduced in the process, it follows that the contribution of this term is negligible since the vector potential **A** also scales as M_b/k_{m0} (cf. (7.20). That this finding *only* applies if the flow remains laminar must be emphasized; to account for the effect of turbulence, additional modeling is required.

With respect to the surface integrals in (9.13), the first one simplifies to $\oint\left(\mathbf{u}_\omega\cdot\nabla\varphi_m^{\dagger *}\right)\mathbf{n}\cdot\mathbf{u}_\vartheta\,dS \sim -\oint\left(\mathbf{u}_{\vartheta\zeta}\cdot\nabla_\zeta\varphi_m^{\dagger *}\right)\mathbf{n}\cdot\mathbf{u}_\vartheta\,dS$ by using the no-slip condition and retaining terms at

most linear in M_b. To evaluate the second integral, a series expansion for $\mathbf{n}\times\mathbf{A}$ on the boundary is needed. This follows from (2.29) and (7.23). In particular

$$\mathbf{n}\times\mathbf{A}(\mathbf{x},t)=\tfrac{1}{2}\sum_{j=-\infty}^{\infty}\left(\mathbf{n}\times\mathbf{A}_{j\zeta}(\mathbf{x})\right)\eta_j(t)\sim\tfrac{i}{2}M_bU_n\sum_{j=-\infty}^{\infty}\left(\frac{1}{k_{j0}}\nabla_\zeta\varphi_j\right)\eta_j \tag{9.14}$$

Now after a tedious, but straightforward calculation, we have

$$I^{\vartheta\omega}\sim-\tfrac{1}{8(\Gamma-1)}M_b\sum_{j,k}\begin{pmatrix}\left(\frac{k_{j0}+k_{m0}}{k_{k0}}+\frac{k_{k0}+k_{m0}}{k_{j0}}\right)I_1^{\vartheta\omega(m,j,k)}+k_{m0}\left(\frac{k_{k0}}{k_{j0}}I_2^{\vartheta\omega(m,j,k)}+\frac{k_{j0}}{k_{k0}}I_2^{\vartheta\omega(m,k,j)}\right)\\ -(\Gamma-1)\left(I_3^{\vartheta\omega(m,j,k)}+I_3^{\vartheta\omega(m,k,j)}\right)\end{pmatrix}\eta_j\eta_k \tag{9.15}$$

where

$$I_1^{\vartheta\omega(m,j,k)}\equiv\frac{1}{k_{j0}k_{k0}}\oint U_nc_{m0}\nabla_\zeta c_{j0}\cdot\nabla_\zeta c_{k0}\,dS$$

$$I_2^{\vartheta\omega(m,j,k)}\equiv\frac{1}{k_{j0}k_{k0}^2k_{m0}^2}\oint U_n\nabla_\zeta c_{j0}\cdot\nabla\times\left(\nabla c_{k0}\times\nabla c_{m0}\right)dS \tag{9.16}$$

$$I_3^{\vartheta\omega(m,j,k)}\equiv\frac{1}{k_{j0}k_{m0}}\oint\left(\nabla_\zeta c_{m0}\cdot\nabla_\zeta c_{j0}\right)\mathbf{n}\cdot\nabla\varphi_{k\mu}\,dS$$

Vortical-Vortical Interactions

Consider now the vortical-vortical interactions $I^{\omega\omega}$. Using some vector identities to recast (9.8), we have

$$I^{\omega\omega}=\oint(\mathbf{n}\times\mathbf{A})\cdot\nabla\left(\mathbf{u}_\omega\cdot\nabla\varphi_m^{\dagger*}\right)dS-\int\mathbf{u}_\omega\cdot\nabla\left(\nabla\varphi_m^{\dagger*}\right)\cdot\mathbf{u}_\omega\,dV \tag{9.17}$$

That the surface integral here can also be expressed as $\oint\left(\mathbf{u}_\omega\cdot\nabla\varphi_m^{\dagger*}\right)\mathbf{n}\cdot\mathbf{u}_\omega dS$ is worth noting, since by combining this expression with the first term in (9.13), we obtain $\oint\left(\mathbf{u}_\omega\cdot\nabla\varphi_m^{\dagger*}\right)\mathbf{n}\cdot\mathbf{u}dS$. This can be interpreted as the *modal projection* of the nonlinear flow turning analog $\oint\left(\mathbf{u}_\omega\cdot\mathbf{u}_\vartheta\right)\mathbf{n}\cdot\mathbf{u}dS\sim-\oint\left|\mathbf{u}_{\vartheta\zeta}\right|^2\mathbf{n}\cdot\mathbf{u}dS$ identified in §9.1. Returning now to the form of the surface integral introduced in (9.17), by using the no-slip condition and retaining terms at most linear in M_b, we have

$$\oint(\mathbf{n}\times\mathbf{A})\cdot\nabla\left(\mathbf{u}_\omega\cdot\nabla\varphi_m^{\dagger*}\right)dS\sim-\oint(\mathbf{n}\times\mathbf{A})\cdot\nabla\left(\mathbf{u}_{\vartheta\zeta}\cdot\nabla_\zeta\varphi_m^{\dagger*}\right)dS \tag{9.18}$$

Recall that a series expansion for $\mathbf{n}\times\mathbf{A}$ is given by (9.14).

Insofar as the volume integral in (9.17) is concerned, it describes a transfer of energy owing to a stretching/compressing of the local unsteady vortical streamtube. Expanding the integrand, we have

$$\begin{aligned}\mathbf{u}_\omega\cdot\nabla\mathbf{f}\cdot\mathbf{u}_\omega=&\left(u_{\omega n}\frac{\partial f_n}{\partial n}+\mathbf{u}_{\omega\zeta}\cdot\nabla_\zeta f_n+\mathbf{u}_{\omega\zeta}\cdot\mathbf{K}\cdot\mathbf{f}_\zeta\right)u_{\omega n}+\\&+u_{\omega n}\frac{\partial\mathbf{f}_\zeta}{\partial n}\cdot\mathbf{u}_{\omega\zeta}-f_n\mathbf{u}_{\omega\zeta}\cdot\mathbf{K}\cdot\mathbf{u}_{\omega\zeta}+\mathbf{u}_{\omega\zeta}\cdot\nabla_\zeta\mathbf{f}_\zeta\cdot\mathbf{u}_{\omega\zeta}\end{aligned} \tag{9.19}$$

where $\mathbf{f} = \nabla\varphi_m^{\dagger *}$. Now by applying the earlier asymptotic result (7.26), integration of these terms over the volume of the domain can be collapsed to integration over burning surfaces; because of the factor of M_b/k_{m0} that is introduced in the process, any term in (9.19) that is $O(M_b)$ on the boundary or less makes a negligible contribution. Thus, we find

$$\int \mathbf{u}_\omega \cdot \nabla\left(\nabla\varphi_m^{\dagger *}\right)\cdot \mathbf{u}_\omega \, dV \sim \int \mathbf{u}_{\omega\zeta} \cdot \nabla_\zeta\left(\nabla_\zeta \varphi_m^{\dagger *}\right)\cdot \mathbf{u}_{\omega\zeta}\, dV \tag{9.20}$$

That this simplification *only* applies if the flow remains laminar must be emphasized. To account for the effect of turbulence in estimating $\int \mathbf{u}_\omega \cdot \nabla\left(\nabla\varphi_m^{\dagger *}\right)\cdot \mathbf{u}_\omega \, dV$ requires additional modeling.

Combining (9.18) and (9.20), it follows that (9.17) reduces to

$$I^{\omega\omega} \sim -\oint (\mathbf{n}\times\mathbf{A})\cdot\nabla\left(\mathbf{u}_{\vartheta\zeta}\cdot\nabla_\zeta\varphi_m^{\dagger *}\right)dS - \int \mathbf{u}_{\omega\zeta}\cdot\nabla_\zeta\left(\nabla_\zeta\varphi_m^{\dagger *}\right)\cdot\mathbf{u}_{\omega\zeta}\, dV \tag{9.21}$$

We evaluate this expression in §I.3. The result is

$$I^{\omega\omega} \sim \tfrac{1}{8(\Gamma-1)} M_b \sum_{j,k}\left(k_{m0}\left(\tfrac{k_{k0}}{k_{j0}} I_1^{\omega\omega(m,j,k)} + \tfrac{k_{j0}}{k_{k0}} I_1^{\omega\omega(m,k,j)}\right) - \tfrac{2k_{m0}}{k_{j0}+k_{k0}} I_2^{\omega\omega(m,j,k)}\right)\eta_j\eta_k \tag{9.22}$$

where

$$I_1^{\omega\omega(m,j,k)} \equiv \frac{1}{k_{j0}k_{k0}^2k_{m0}^2}\oint U_n \nabla_\zeta c_{j0}\cdot\nabla\left(\nabla_\zeta c_{k0}\cdot\nabla_\zeta c_{m0}\right)dS$$

$$I_2^{\omega\omega(m,j,k)} \equiv \begin{cases} 0, \text{ if } j=-k \\ \dfrac{1}{k_{j0}k_{k0}k_{m0}^2}\oint U_n\nabla_\zeta c_{j0}\cdot\nabla_\zeta\left(\nabla_\zeta c_{m0}\right)\cdot\nabla_\zeta c_{k0}\, dS \end{cases} \tag{9.23}$$

Boundary Terms

Finally, we consider the boundary term $I^{\mathcal{B}} = \oint \varphi_m^{\dagger *}\,\mathbf{n}\cdot\mathbf{N}_u(...)\,dS$. Substituting (B.34) for $\mathbf{N}_u(...)$, we have

$$\mathbf{n}\cdot\mathbf{N}_u(...) = -u_n\frac{\partial u_n}{\partial n} - \tfrac{1}{\Gamma-1}c\frac{\partial c}{\partial n} + ... \tag{9.24}$$

since terms involving the tangent component of velocity vanish due to the no-slip condition.

Note that we can obtain an expression for $\partial c/\partial n$ by using the normal projection of the linearized momentum equation on the boundary[†]. In particular, we have

$$\tfrac{1}{\Gamma-1}\frac{\partial c}{\partial n} = -\frac{\partial u_n}{\partial t} - M_b\frac{\partial(U_n u_n)}{\partial n} + ... \sim -\frac{\partial u_n}{\partial t} - M_b U_n\frac{\partial u_n}{\partial n} + ... \tag{9.25}$$

where the term neglected in the approximation on the far right is proportional to the square of the injection Mach number.

[†] This is valid since c would in any case be replaced by a series expansion in terms of the linear stability eigenfunctions.

Now substituting (9.25) into (9.24) and splitting the velocity using a Stokes-Helmholtz decomposition, we have

$$\begin{aligned}\mathbf{n}\cdot\mathbf{N}_u\left(...\right) \sim & -u_{\vartheta n}\frac{\partial u_{\vartheta n}}{\partial n}-u_{\vartheta n}\frac{\partial u_{\omega n}}{\partial n}-u_{\omega n}\frac{\partial u_{\vartheta n}}{\partial n}-u_{\omega n}\frac{\partial u_{\omega n}}{\partial n}+\\ & +c\left(\frac{\partial u_{\omega n}}{\partial t}+M_b U_n\frac{\partial u_{\omega n}}{\partial n}\right)+c\left(\frac{\partial u_{\vartheta n}}{\partial t}+M_b U_n\frac{\partial u_{\vartheta n}}{\partial n}\right)+...\end{aligned} \tag{9.26}$$

The advantage of using (9.26) to evaluate $I^{\mathcal{B}}$ is that contributions owing to sound-sound and sound-vortical interactions are clear.

We derive an alternative expression for $\mathbf{n}\cdot\mathbf{N}_u\left(...\right)$ however and sacrifice clarity for conciseness. We begin by noting that on the boundary[†]

$$\partial u_n/\partial n=\vartheta+\kappa u_n \tag{9.27}$$

By combining (9.24), (9.25) and (9.27), it follows that

$$\mathbf{n}\cdot\mathbf{N}_u\left(...\right)\sim-\vartheta u_n+c\left(\frac{\partial u_n}{\partial t}+M_b U_n\vartheta\right)+... \tag{9.28}$$

Now using (9.28) and following the same procedure as before, we have

$$I^{\mathcal{B}}\sim-\tfrac{1}{8}M_b\sum_{j,k}\left(\begin{array}{c}\left(1+\frac{1}{(\Gamma-1)}\frac{k_{k0}}{k_{j0}}\right)k_{k0}I_1^{\mathcal{B}(m,j,k)}+\left(1+\frac{1}{(\Gamma-1)}\frac{k_{j0}}{k_{k0}}\right)k_{j0}I_1^{\mathcal{B}(m,k,j)}-\\ -\frac{k_{j0}+k_{k0}}{k_{m0}}I_2^{\mathcal{B}(m,j,k)}+\left(\left(\Gamma-1\right)+\frac{k_{k0}}{k_{j0}}\right)\frac{k_{j0}}{k_{m0}}I_3^{\mathcal{B}(m,k,j)}+\left(\left(\Gamma-1\right)+\frac{k_{j0}}{k_{k0}}\right)\frac{k_{k0}}{k_{m0}}I_3^{\mathcal{B}(m,j,k)}\end{array}\right)\eta_j\eta_k \tag{9.29}$$

where,

$$\begin{aligned}I_1^{\mathcal{B}(m,j,k)}&\equiv\frac{1}{k_{j0}k_{k0}k_{m0}}\oint U_n\nabla_\zeta c_{j0}\cdot\nabla_\zeta\left(c_{k0}c_{m0}\right)dS\\ I_2^{\mathcal{B}(m,j,k)}&\equiv\oint U_n c_{m0}c_{j0}c_{k0}\,dS,\quad I_3^{\mathcal{B}(m,j,k)}\equiv\oint c_{m0}c_{j0}\mathbf{n}\cdot\nabla\varphi_{k\mu}dS\end{aligned} \tag{9.30}$$

[†] We begin with the Stokes-Helmholtz decomposition $\mathbf{u}=\mathbf{u}_\vartheta+\mathbf{u}_\omega$. Now since $\mathbf{u}_\omega$ is divergence free, i.e., $\nabla\cdot\mathbf{u}_\omega=\partial u_{\omega n}/\partial n-\kappa u_{\omega n}+\nabla_\zeta\cdot\mathbf{u}_{\omega\zeta}=0,$ it follows by using the no-slip condition $\mathbf{u}_{\omega\zeta}=-\mathbf{u}_{\vartheta\zeta}=-\nabla_\zeta\varphi$ that on the boundary

$$\frac{\partial u_n}{\partial n}=\frac{\partial u_{\vartheta n}}{\partial n}+\frac{\partial u_{\omega n}}{\partial n}=\frac{\partial^2\varphi}{\partial n^2}+\frac{\partial u_{\omega n}}{\partial n}=\frac{\partial^2\varphi}{\partial n^2}-\nabla_\zeta\cdot\mathbf{u}_{\omega\zeta}+\kappa u_{\omega n}=\frac{\partial^2\varphi}{\partial n^2}+\nabla_\zeta^2\varphi+\kappa u_{\omega n}$$

This can be more succinctly written as $\partial u_n/\partial n=\vartheta+\kappa u_n$ since $\vartheta=\nabla^2\varphi=\partial^2\varphi/\partial n^2-\kappa\,\partial\varphi/\partial n+\nabla_\zeta^2\varphi.$

A Final Remark

Having evaluated all the nonlinear forcing terms, we observe that all but two of the integrals that comprise $I^{\vartheta\omega}$, $I^{\omega\omega}$ and $I^{\mathcal{B}}$ are real (cf. (9.16), (9.23) and (9.30), respectively). Thus, these effects only contribute to the $f_r^{\varepsilon\varepsilon(m,j,k)}$ coefficient in (9.9); sound-sound interactions, in contrast, only contribute to the $f_i^{\varepsilon\varepsilon(m,j,k)}$ coefficient.

The integrals that are the exceptions, i.e., $I_3^{\vartheta\omega(m,j,k)} = \left(k_{j0}k_{m0}\right)^{-1}\oint\left(\nabla_\zeta c_{m0}\cdot\nabla_\zeta c_{j0}\right)\mathbf{n}\cdot\nabla\varphi_{k\mu}\,dS$ and $I_3^{\mathcal{B}(m,j,k)} \equiv \oint c_{m0}c_{j0}\mathbf{n}\cdot\nabla\varphi_{k\mu}\,dS$, involve the flame response, which typically has both a real and an imaginary component; the real component will contribute to $f_r^{\varepsilon\varepsilon(m,j,k)}$ and the imaginary component will contribute to $f_i^{\varepsilon\varepsilon(m,j,k)}$.

9.3 Some Results

Figures 9.1and 9.2 contrast the behavior of purely axial and purely tangential modes, with and without the effects of vorticity included (results for the integrals are given in Appendix I). Although little difference can be observed, vorticity may still play an important role in the nonlinear behavior, since those coefficients that required the flame response as input (i.e., $I_3^{\vartheta\omega(m,j,k)}$ and $I_3^{\mathcal{B}(m,j,k)}$) were left unevaluated.

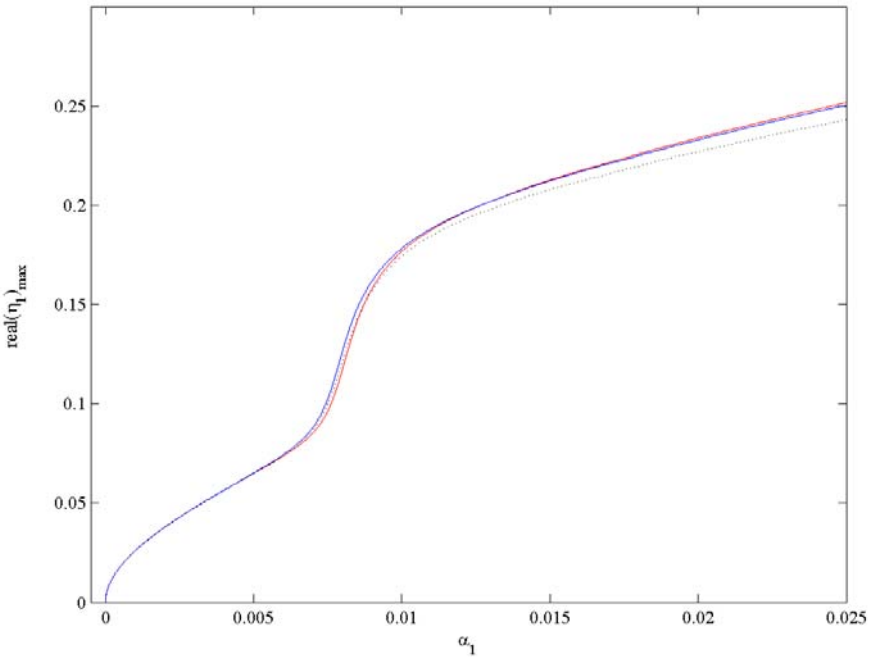

Figure 9.1 Axial mode instability, 4 mode approximation with $M_b\alpha_{2\mu\to4\mu} = -0.025$, and $\theta_n = 0$; red curve (AUTO 2000) corresponds to the inclusion of sound-sound, sound-vortical, vortical-vortical and boundary interactions; blue curve (AUTO 2000) corresponds to the inclusion of sound-sound, sound-vortical and vortical-vortical interactions; black (dashed) curve (AUTO 2000) coincides with the behavior solely owing to the sound-sound interaction

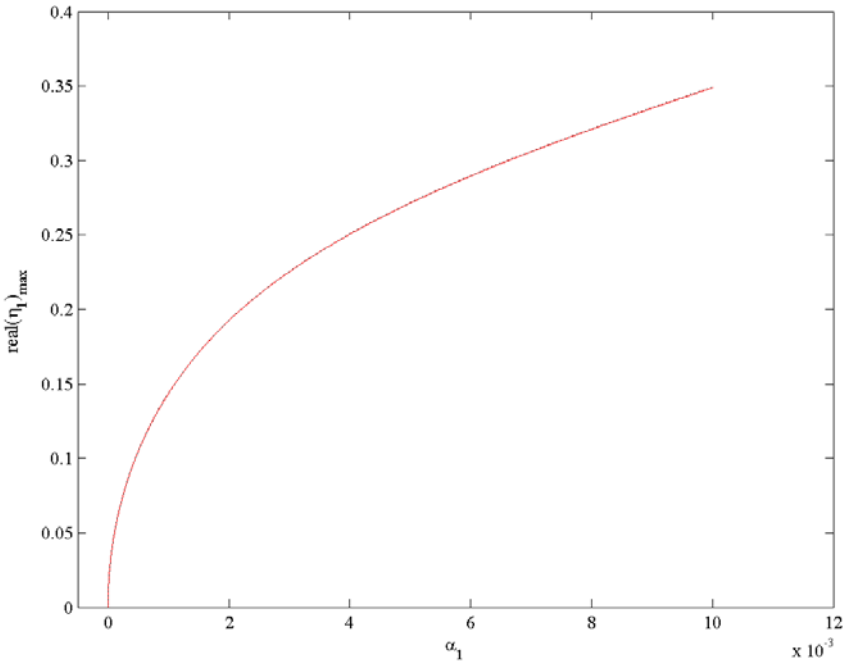

Figure 9.2 Tangential mode instability, 4 mode approximation with $M_b \alpha_{2\mu \to 4\mu} = -0.025$, and $\theta_n = 0$; red curve (AUTO 2000) corresponds to the inclusion of sound-sound, sound-vortical, vortical-vortical and boundary interactions; black (dashed) curve (AUTO 2000) coincides with the behavior solely owing to the sound-sound interaction

10. Final Remarks

The problem of combustion instability in solid rocket motors has been studied in the present effort with a focus on the *two* basic fluid dynamic processes—i.e., the compressing/expanding process and the shearing process. The main contributions/conclusions can be summarized as follows.

In Chapter 2, we constructed a general framework for studying combustion instabilities that accommodates both linear and nonlinear processes. This was a substantial extension of Culick's (1976) original analysis, accomplished by using linear stability eigenfunctions—that satisfied the no-slip boundary condition—to expand flow variables and their adjoints to effect a spatial averaging.

The resulting amplitude equations were then studied in Chapter 4 using perturbation techniques based on ideas of resonance. Closed form results were derived for the limiting periodic behavior when the first mode is unstable and compared against results from numerical integration. The agreement was quite remarkable and demonstrated the merit of the approach, especially since the nonlinear coefficients did not have to be specified a priori. The same methodology can also be applied to treat other problems, such as, for example, when the second mode is unstable. Even if additional closed form solutions are not obtained however, the approach introduced helps identify the nonlinear coefficients that most significantly impact system behavior. This is an important development given that much work remains to be done on modeling nonlinear processes.

Ultimately though, to study combustion instability within solid rocket motor, it was necessary to *determine* the coefficients in the amplitude equations. This required solving for the linear stability eigenfunctions. To facilitate such a calculation, some model problems that allowed key elements of the physics to be introduced in a simplified setting were first considered. In Chapter 5, for example, the classic Stokes' problem was generalized to include a uniform injection of fluid normal to the boundary; this helped illustrate how the mass flux issuing forth from a burning propellant affects vorticity creation.

In particular, it was shown that with fluid injection, convection competes with viscous diffusion, and both mechanisms transport boundary vorticity into the domain. The consequences of this for the flow as a whole were significant. Most striking was that the Euler (inviscid) limit converged uniformly to the solution for a strictly Euler (inviscid) flow. It was found, in other words, that one can sometimes get around the viscous origin of the no-slip condition to simply retain it in a mathematical analysis of inviscid flow. This result notwithstanding, the analysis in subsequent chapters did not assume that the fluid was inviscid; however, flows where the transport of boundary vorticity was controlled by convective rather than

diffusive mechanisms were of interest. Under such conditions, vorticity was shown to propagate significantly further into the domain; the magnitude of this vorticity was however notably reduced.

Then, in Chapter 6, we contrasted the behavior of the *acoustic boundary layer*, with and without a uniform injection of fluid through the boundary; this problem was only a slight generalization of the oscillating Stokes' flow. The new feature exhibited was an unsteady component of flow in the normal direction—a consequence of the vorticity and the thermal wave canceling out velocity and temperature fluctuations on the boundary, respectively. In the absence of fluid injection, both contributions were of comparable magnitude. In contrast, with fluid injection and convective rather than diffusive mechanisms dominating, the normal component of the vortical velocity was more significant, with the opposite being true for the thermal velocity.

The linearized flow field within solid rocket motors was next considered in Chapter 7. Solutions were obtained for the acoustic, the thermal and the vorticity eigenfunctions, with the method of multiple scales used to solve for the latter. An important consequence of this approach—vis-à-vis Flandro's earlier analysis (1995 a, b)—was the clear demarcation between information required to evaluate stability integrals that determine the effects of vorticity, and information required for determining the detailed structure of the vorticity field within the chamber. It turned out, that insofar as the former was concerned, only the behavior on the boundary was needed; more specifically, an asymptotic result was derived, which showed that volume integrations collapse to integration over burning surfaces.

Linear stability was then revisited in Chapter 8. Flandro (1995 a, b) had previously shown that for a cylindrical propellant grain subject to axial mode instability, no net contribution exists owing to the effects of vorticity, since energy gained because of radial pumping compensates the loss due to flow turning. A physical explanation of this surprising result was never offered. To ascertain whether this was merely fortuitous, novel formulae that clearly reflect the interaction between vorticity and sound were derived. What emerged was a very elegant physical picture. Sound generates vorticity, which in turn, generates more sound; Culick's flow turning and Flandro's radial pumping where shown to describe, respectively, the two halves of this process. That these two effects cancel then basically establishes that: the rate of energy loss experienced by the sound field in generating vorticity is compensated by the rate of energy gain owing to generation of more sound by that vorticity. More succinctly stated, the energy flux between the longitudinal and transverse fields is—to leading order—reversible.

It is important to realize that this finding is a reflection of the underlying physics. With fluid injected through the boundary, convection as opposed to viscous diffusion becomes the dominant

mechanism for transporting (acoustically-generated) boundary vorticity into the domain. The manner in which this vorticity creates sound, moreover, via the appearance of an oscillating boundary—essentially mimicking the action of a speaker—is already effectively inviscid in nature. As such, it is not an unforeseen consequence that, since dissipative effects no longer substantially enter into either of the creation mechanisms, the means for making the kinetic energy unrecoverable no longer exists.

Aside from a greatly enhanced physical understanding then—which helps explain the mathematical observations—the current effort improved on what has been done (Culick 1973; Flandro 1995 a, b) in two key ways: the linear stability results obtained were *independent* of grain geometry; and the derivation of these results depended largely on kinematics. Accordingly, the conclusions reached can be applied to reasonably complex grain geometries, *irrespective* of whether the motion is turbulent or not. The conclusions, in other words, support but also *significantly extend* the findings of an earlier study by Flandro (1995 a, b), in which the importance of incorporating vortical flow effects in the acoustic instability algorithm was first demonstrated.

Finally, Chapter 9 examined the nonlinear effects of vorticity. We first extended the energy balance introduced in Chapter 8 to accommodate nonlinear terms; shown to exist, was a flow-turning analog that provided a natural nonlinear coupling with the flame zone—a key feature not present in earlier analyses. Motivated by this finding, we then returned to the amplitude equations and determined the coefficients that model sound-sound, sound-vortical and vortical-vortical interactions. While simulation of some prototypical cases revealed qualitatively similar behavior with and without the effects of vorticity included, no definitive conclusions could be drawn, since those coefficients describing nonlinear interactions with the vorticity field that required the flame response as input were left unevaluated. Building the requisite models to correct for this omission would be an important area of future research.

A. Normal-Tangential Coordinate System

To accommodate a variety of grain geometries, we use a general orthogonal coordinate system cast in terms of normal n and tangential ζ components. In such a system, vectors can be uniquely written as

$$\mathbf{c} = c_n \mathbf{n} + \mathbf{c}_\zeta \tag{A.1}$$

where

$$c_n = \mathbf{n}\cdot\mathbf{c}, \quad \mathbf{c}_\zeta = -\mathbf{n}\times(\mathbf{n}\times\mathbf{c}) \tag{A.2}$$

which follows by setting $\mathbf{a}=\mathbf{b}=\mathbf{n}$ in the identity $(\mathbf{a}\cdot\mathbf{b})\mathbf{c} = (\mathbf{a}\cdot\mathbf{c})\mathbf{b} - \mathbf{a}\times(\mathbf{b}\times\mathbf{c})$.

Differential operators can also be similarly decomposed; this can be shown in a number of different ways. We choose here to follow the work of Tai (1992), who introduced the following concise representation

$$\nabla \circ \mathbf{f} = \sum_i \frac{\mathbf{e}_i}{h_i} \circ \frac{\partial \mathbf{f}}{\partial v_i} \tag{A.3}$$

Here $\circ$ is some kind of useful tensor product, $\mathbf{e}_i$ denotes a unit vector, v_i is the variable in that direction and h_i the corresponding shape factor. For simplicity, we take $\mathbf{e}_1 = \mathbf{n}$. To ensure that the coordinate system is orthogonal, we must have $h_1 = 1$,

$$\frac{\partial \mathbf{e}_j}{\partial v_i} = \frac{1}{h_j}\frac{\partial h_i}{\partial v_j}\mathbf{e}_i \text{ when } i \neq j \text{ and } \frac{\partial \mathbf{e}_i}{\partial v_i} = -\left(\frac{1}{h_j}\frac{\partial h_i}{\partial v_j}\mathbf{e}_j + \frac{1}{h_k}\frac{\partial h_i}{\partial v_k}\mathbf{e}_k\right) \tag{A.4}$$

(cf. Tai 1992 for further details).

We now introduce the tangent operator ∇_ζ; this is to be interpreted in the same way as (A.3),

$$\nabla_\zeta \circ \mathbf{f} = \sum_{i=2,3} \frac{\mathbf{e}_i}{h_i} \circ \frac{\partial \mathbf{f}}{\partial v_i} \tag{A.5}$$

except that only tangent derivatives arise.

Curvature

Before proceeding, we note that the curvature tensor is formally defined as $\mathbf{K} \equiv -\nabla_\zeta \mathbf{n}$, the trace of which gives the first (or principle) curvature

$$\kappa \equiv -(\nabla_\zeta \cdot \mathbf{n}) = -\left(\frac{\mathbf{e}_2}{h_2}\cdot\frac{\partial \mathbf{n}}{\partial v_2} + \frac{\mathbf{e}_3}{h_3}\cdot\frac{\partial \mathbf{n}}{\partial v_3}\right) = -\left(\frac{1}{h_2}\frac{\partial h_2}{\partial n} + \frac{1}{h_3}\frac{\partial h_3}{\partial n}\right) \tag{A.6}$$

Gradient

Using (A.3) and (A.5), the gradient of a scalar can be written as

$$\nabla f = \sum_i \frac{\mathbf{e}_i}{h_i}\frac{\partial f}{\partial v_i} = \mathbf{n}\frac{\partial f}{\partial n} + \nabla_\zeta f \tag{A.7}$$

Divergence

Consider now the divergence of a vector:

$$\nabla \cdot \mathbf{f} = \sum_i \frac{\mathbf{e}_i}{h_i} \cdot \frac{\partial \mathbf{f}}{\partial v_i} = \sum_{i,j} \frac{\mathbf{e}_i}{h_i} \cdot \frac{\partial \left(f_j \mathbf{e}_j \right)}{\partial v_i} \tag{A.8}$$

This can be written out as

$$\nabla \cdot \mathbf{f} = \frac{\mathbf{e}_1}{h_1} \cdot \left(\frac{\partial \left(f_1 \mathbf{e}_1 \right)}{\partial v_1} + \frac{\partial \left(f_2 \mathbf{e}_2 \right)}{\partial v_1} + \frac{\partial \left(f_3 \mathbf{e}_3 \right)}{\partial v_1} \right) + \frac{\mathbf{e}_2}{h_2} \cdot \frac{\partial \left(f_1 \mathbf{e}_1 \right)}{\partial v_2} + \frac{\mathbf{e}_3}{h_3} \cdot \frac{\partial \left(f_1 \mathbf{e}_1 \right)}{\partial v_3} + \nabla_\zeta \cdot \mathbf{f}_\zeta \tag{A.9}$$

where $\nabla_\zeta \cdot \mathbf{f}_\zeta$ is to be interpreted in the same way as (A.8), except that only tangent derivatives and components arise (i.e., the dummy indices i and j start from 2). The other terms can be more concisely expressed as $\partial f_n / \partial n - \kappa f_n$; this can be shown using (A.4) and (A.6). Thus, we have

$$\nabla \cdot \mathbf{f} = \frac{\partial f_n}{\partial n} - \kappa f_n + \nabla_\zeta \cdot \mathbf{f}_\zeta \tag{A.10}$$

Curl

Lastly, we consider the curl of a vector:

$$\nabla \times \mathbf{f} = \sum_i \frac{\mathbf{e}_i}{h_i} \times \frac{\partial \mathbf{f}}{\partial v_i} \tag{A.11}$$

This can be written out as

$$\nabla \times \mathbf{f} = \sum_i \frac{\mathbf{e}_i}{h_i} \times \frac{\partial \mathbf{f}}{\partial v_i} = \sum_{i,j} \frac{\mathbf{e}_i}{h_i} \times \frac{\partial \left(f_j \mathbf{e}_j \right)}{\partial v_i} = \sum_{i,j} \frac{1}{h_i} \frac{\partial f_j}{\partial v_i} \varepsilon_{ijk} \mathbf{e}_k + \sum_i f_i \frac{\mathbf{e}_i}{h_i} \times \frac{\partial \mathbf{e}_i}{\partial v_i} \tag{A.12}$$

where ε_{ijk} is the permutation tensor. Expanding further, we have

$$\nabla \times \mathbf{f} = \frac{1}{h_2 h_3} \left(\frac{\partial \left(h_3 f_3 \right)}{\partial v_2} - \frac{\partial \left(h_2 f_2 \right)}{\partial v_3} \right) \mathbf{u}_1 + \left(\frac{1}{h_3} \frac{\partial f_1}{\partial v_3} - \frac{\partial f_3}{\partial v_1} - \frac{f_3}{h_3} \frac{\partial h_3}{\partial v_1} \right) \mathbf{u}_2 + \left(\frac{\partial f_2}{\partial v_1} - \frac{1}{h_2} \frac{\partial f_1}{\partial v_2} + \frac{f_2}{h_2} \frac{\partial h_2}{\partial v_1} \right) \mathbf{u}_3 \tag{A.13}$$

That this may be far more concisely expressed as

$$\left(\nabla \times \mathbf{f} \right)_n = \left(\mathbf{n} \times \nabla_\zeta \right) \cdot \mathbf{f}_\zeta, \quad \left(\nabla \times \mathbf{f} \right)_\zeta = \frac{\partial}{\partial n} \left(\mathbf{n} \times \mathbf{f}_\zeta \right) - \mathbf{n} \times \left(\nabla_\zeta f_n + \mathbf{K} \cdot \mathbf{f}_\zeta \right) \tag{A.14}$$

is a simple exercise of algebraic manipulation.

B. Governing Equations

B.1 The dimensional equations that govern the flow of *combustion products* in a solid rocket motor are

Conservation of Mass

$$D\rho/Dt = -\rho\nabla\cdot\mathbf{u} + \mathbb{W} \tag{B.1}$$

Conservation of Momentum

$$\rho\, D\mathbf{u}/Dt = -\nabla p + \mathcal{F} \tag{B.2}$$

Equation for the Pressure[†]

$$Dp/Dt = -\gamma\, p\nabla\cdot\mathbf{u} + (\gamma-1)Q + \rho^{-1} p\,\mathbb{W} \tag{B.3}$$

Equation of State

$$p = \rho\mathcal{R}T \tag{B.4}$$

where $D/Dt = \partial/\partial t + \mathbf{u}\cdot\nabla$ and contributions to the mass $\mathbb{W}$, momentum $\mathcal{F}$ and energy Q *source* terms will be made explicit as required.

Now we introduce a standard set of dimensionless variables that fit the needs of the general combustion instability problem:

$$\frac{t}{R/c_o}\to t \quad \frac{\mathbf{x}}{R}\to\mathbf{x} \quad \frac{\mathbf{u}}{c_o}\to\mathbf{u} \quad \frac{p}{\gamma p_o}\to p \quad \frac{\rho}{\rho_o}\to\rho \quad \frac{T}{T_o}\to T \quad \frac{c}{c_o}\to c \quad \frac{s}{c_p}\to s$$
$$\frac{R}{\rho_o c_o}\mathbb{W}\to\mathbb{W} \quad \frac{R}{\rho_o c_o^2}\mathcal{F}\to\mathcal{F} \quad \frac{R}{\rho_o c_o^3}Q\to Q \tag{B.5}$$

Here suffix *o* denotes chamber stagnation properties, R is a characteristic length (e.g., the radius for a cylindrical chamber), and c_p is the specific heat at constant pressure. Note that to help emphasize the central role of compressibility in the unsteady field, velocities are referenced to the speed of sound and time is made dimensionless by introducing the acoustic time scale R/c_o.

Substituting (B.5) into (B.1)—(B.3), we have

Conservation of Mass

$$D\rho/Dt = -\rho\nabla\cdot\mathbf{u} + \mathbb{W} \tag{B.6}$$

Conservation of Momentum

$$\rho\, D\mathbf{u}/Dt = -\nabla p + \mathcal{F} \tag{B.7}$$

Equation for the Pressure

$$Dp/Dt = -\gamma\, p\nabla\cdot\mathbf{u} + (\gamma-1)Q + \gamma^{-1}\mathbb{W}T \tag{B.8}$$

[†] This can be derived by differentiating (2.4) and substituting (2.1) and the energy equation (i.e., $\rho c_v\, DT/Dt = -p\nabla\cdot\mathbf{u} + Q$) where appropriate.

While these equations can be solved using some sort of numerical analysis, to proceed analytically, we begin by writing all dependent variables as sums of mean $(\overline{x})$ and fluctuating (x') parts

$$\mathbf{u} = \overline{\mathbf{u}}(\mathbf{x}) + \mathbf{u}'(\mathbf{x},t), \quad \rho = \overline{\rho}(\mathbf{x}) + \rho'(\mathbf{x},t), \quad p = \overline{p}(\mathbf{x}) + p'(\mathbf{x},t), \quad \text{etc.} \tag{B.9}$$

where the latter are taken to be all of the same order in the wave amplitude ε (i.e., $\mathbf{u}' \sim O(\varepsilon)$, $\rho' \sim O(\varepsilon)$, ...). The rationale for such an approach is discussed in §2.3. It is sufficient here to note that the mean flow is assumed to satisfy its own equations, i.e., is unaffected by the fluctuations. This gives

Equations for the Mean Flow

$$\nabla\cdot(\overline{\rho}\overline{\mathbf{u}}) = \overline{\mathscr{W}}, \quad \overline{\mathbf{u}}\cdot\nabla\overline{\mathbf{u}} = -\tfrac{1}{\overline{\rho}}\nabla\overline{p} + \tfrac{1}{\overline{\rho}}\overline{\mathscr{F}}, \quad \overline{\mathbf{u}}\cdot\nabla\overline{p} = -\gamma\overline{p}\nabla\cdot\overline{\mathbf{u}} + (\gamma-1)\overline{Q} + \gamma^{-1}\overline{\mathscr{W}}\,\overline{T} \tag{B.10}$$

Equations for the Fluctuations

$$\partial\rho'/\partial t + \nabla\cdot(\overline{\rho}\mathbf{u}' + \rho'\overline{\mathbf{u}}) = -\nabla\cdot(\rho'\mathbf{u}') + \mathscr{W}' \tag{B.11}$$

$$\partial\mathbf{u}'/\partial t + \overline{\mathbf{u}}\cdot\nabla\mathbf{u}' + \mathbf{u}'\cdot\nabla\overline{\mathbf{u}} + \mathbf{u}'\cdot\nabla\mathbf{u}' = -\tfrac{1}{\overline{\rho}+\rho'}\nabla p' + \tfrac{\rho'}{\overline{\rho}(\overline{\rho}+\rho')}\nabla\overline{p} + \tfrac{1}{\overline{\rho}+\rho'}\mathscr{F}' - \tfrac{\rho'}{\overline{\rho}(\overline{\rho}+\rho')}\overline{\mathscr{F}} \tag{B.12}$$

$$\begin{aligned}\partial p'/\partial t + \overline{\mathbf{u}}\cdot\nabla p' + \mathbf{u}'\cdot\nabla\overline{p} + \mathbf{u}'\cdot\nabla p' = {} & -\gamma\overline{p}\nabla\cdot\mathbf{u}' - \gamma p'\nabla\cdot\overline{\mathbf{u}} - \gamma p'\nabla\cdot\mathbf{u}' + (\gamma-1)Q' + \\ & + \gamma^{-1}\left(\overline{\mathscr{W}}\,T' + \mathscr{W}'\overline{T} + \mathscr{W}'T'\right)\end{aligned} \tag{B.13}$$

which can be more succinctly written as

$$\partial\rho'/\partial t + \mathscr{L}_\rho(...) = \mathscr{N}_\rho(...) \tag{B.14}$$

$$\partial\mathbf{u}'/\partial t + \mathscr{L}_u(...) = \mathscr{N}_u(...) \tag{B.15}$$

$$\partial p'/\partial t + \mathscr{L}_p(...) = \mathscr{N}_p(...) \tag{B.16}$$

by introducing operators, which are linear $\mathscr{L}_{(\,)}$ and nonlinear $\mathscr{N}_{(\,)}$ in the wave amplitude ε. Note that it is these unsteady equations (which can also be cast in terms of the entropy and sound speed) that our analysis is principally concerned with.

It remains to establish how we evaluate the mean flow in the above operators. Setting the source terms to zero for simplicity, it follows from (B.10) that

$$\nabla\cdot(\overline{\rho}\overline{\mathbf{u}}) = 0, \quad \overline{\mathbf{u}}\cdot\nabla\overline{\mathbf{u}} = -\tfrac{1}{\overline{\rho}}\nabla\overline{p}, \quad \overline{\mathbf{u}}\cdot\nabla\overline{p} = -\gamma\overline{p}\nabla\cdot\overline{\mathbf{u}} \tag{B.17}$$

Now before discussing the case of a solid rocket motor, we consider some model problems examined in the thesis, for which the mean flow has a simple description. For example, Chapter 3 considers the problem of *purely* acoustic motions within a chamber of arbitrary shape enclosed by a rigid boundary and containing a fluid otherwise at *rest*. In this instance, we have

$$\overline{\mathbf{u}} = 0, \quad \overline{\rho} = 1, \quad \overline{p} = 1/\gamma \tag{B.18}$$

In Chapter 6, we consider the acoustic boundary layer, with and without a uniform injection of fluid through the boundary. For the latter, the mean flow is given by (B.18), and for the former, we have

$$\bar{\mathbf{u}} = M_b \mathbf{n}, \quad \bar{\rho} = 1, \quad \bar{p} = 1/\gamma \tag{B.19}$$

Here $\mathbf{n}$ is the unit normal vector pointing into the fluid domain and M_b is the injection Mach number.

That (B.19) is not a small M_b expansion must be emphasized; $\bar{\mathbf{u}} = M_b \mathbf{n}$ is simply the exact description of a uniform injection of fluid through the boundary. This example serves to underscore that we are concerned with studying acoustical motions in the presence of a mean flow versus acoustical motions generated by that mean flow (cf. §2.3 for further discussion of this point).

Returning to the case of a solid rocket motor, to avoid confusion, we first rescale the variables

$$\tilde{\mathbf{u}} = M_b^{-1} \bar{\mathbf{u}}, \quad \tilde{\rho} = \bar{\rho}, \quad \tilde{p} = \bar{p} \tag{B.20}$$

so that the velocity is now referenced to the *injection velocity* and not the speed of sound. This gives

$$\nabla \cdot \left(\tilde{\rho} \tilde{\mathbf{u}} \right) = 0, \quad \tilde{\mathbf{u}} \cdot \nabla \tilde{\mathbf{u}} = -\frac{1}{\tilde{\rho} M_b^2} \nabla \tilde{p}, \quad \tilde{\mathbf{u}} \cdot \nabla \tilde{p} = -\gamma \tilde{p} \nabla \cdot \tilde{\mathbf{u}} \tag{B.21}$$

Now if we put

$$\tilde{\mathbf{u}} = \mathbf{U}_0 + M_b^2 \mathbf{U}_1 + M_b^4 \mathbf{U}_2 + ..., \quad \tilde{\nu} = \tilde{\rho}^{-1} = 1 + M_b^2 \mathrm{N}_1 + M_b^4 \mathrm{N}_2 + ..., \quad \tilde{p} = 1/\gamma + M_b^2 P_1 + M_b^4 P_2 + ... \tag{B.22}$$

and substitute these expansions into (B.21), we recover at leading order the incompressible Euler equations:

$$\nabla \cdot \mathbf{U}_0 = 0, \quad \mathbf{U}_0 \cdot \nabla \mathbf{U}_0 = -\nabla P_1 \tag{B.23}$$

with P_1 the incompressible pressure. This (along with the appropriate boundary conditions) defines the base state for our analysis. While complex geometries invariably require numerical integration, a closed form solution does exist for the case of a cylindrical propellant grain; further details are given in §G.3.

In analyzing the unsteady flow, only terms at most linear in M_b are retained. Therefore, when substituting in for the mean velocity, only the first term in the expansion is needed, i.e., $\bar{\mathbf{u}} = M_b \mathbf{U} + ...$ (the suffix 0 is dropped for simplicity); similarly, the mean thermodynamic state is approximately uniform, i.e., $\bar{p} = 1/\gamma + ...$, etc.

Making these changes in the momentum equation (B.12) for example, and omitting the primes on the unsteady flow components, we have

$$\partial \mathbf{u} / \partial t + M_b \left(\mathbf{U} \cdot \nabla \mathbf{u} + \mathbf{u} \cdot \nabla \mathbf{U} \right) + \mathbf{u} \cdot \nabla \mathbf{u} = -\nabla p + \tfrac{\rho}{1+\rho} \nabla p + \mathcal{F} - \tfrac{\rho}{1+\rho} \mathcal{F} \tag{B.24}$$

which recall can be more succinctly written as

$$\partial \mathbf{u} / \partial t + \mathcal{L}_u (...) = \mathcal{N}_u (...) \tag{B.25}$$

with

$$\mathcal{L}_u (...) = M_b \left(\mathbf{U} \cdot \nabla \mathbf{u} + \mathbf{u} \cdot \nabla \mathbf{U} \right) + \nabla p - \mathcal{F}_{linear} \tag{B.26}$$

and

$$\mathcal{N}_u(...) = -\mathbf{u}\cdot\nabla\mathbf{u} + \tfrac{\rho}{1+\rho}\nabla p + \left(\mathcal{F}_{nonlinear} - \tfrac{\rho}{1+\rho}\mathcal{F}\right) \tag{B.27}$$

Following the same procedure, the other unsteady equations can be simplified; the corresponding operators are given in §B.2.

B.2 *Operator Definitions*

Linear Operators

$$\mathcal{L}_c(...) = M_b\mathbf{U}\cdot\nabla c - (\Gamma-1)(-\nabla\cdot\mathbf{u} + \gamma Q_{linear}) \tag{B.28}$$

$$\mathcal{L}_u(...) = M_b\left(\nabla(\mathbf{U}\cdot\mathbf{u}) + \boldsymbol{\omega}\times\mathbf{U} + \boldsymbol{\Omega}\times\mathbf{u}\right) + (\Gamma-1)^{-1}\nabla c - \mathcal{F}_{linear} - \tfrac{1}{2}(\Gamma-1)^{-1}\nabla s \tag{B.29}$$

$$\mathcal{L}_p(...) = M_b\mathbf{U}\cdot\nabla p + \nabla\cdot\mathbf{u} - (\gamma-1)Q_{linear} - \gamma^{-1}\mathcal{W}_{linear} \tag{B.30}$$

$$\mathcal{L}_T(...) = M_b\mathbf{U}\cdot\nabla T + (\gamma-1)\nabla\cdot\mathbf{u} - \gamma(\gamma-1)Q_{linear} \tag{B.31}$$

$$\mathcal{L}_s(...) = M_b\mathbf{U}\cdot\nabla s - (\gamma-1)\left(Q_{linear} - \gamma^{-1}\mathcal{W}_{linear}\right) \tag{B.32}$$

Nonlinear Operators

$$\mathcal{N}_c(...) = -\mathbf{u}\cdot\nabla c + (\Gamma-1)\left(-c\nabla\cdot\mathbf{u} + \gamma Q_{nonlinear} - \gamma\tfrac{\rho+c+\rho c}{1+\rho+c+\rho c}Q\right) \tag{B.33}$$

$$\mathcal{N}_u(...) = -\nabla\left(\tfrac{1}{2}\mathbf{u}\cdot\mathbf{u}\right) - \boldsymbol{\omega}\times\mathbf{u} - (\Gamma-1)^{-1}c\nabla c + \left(\mathcal{F}_{nonlinear} - \tfrac{\rho}{1+\rho}\mathcal{F} + \tfrac{1}{2}(\Gamma-1)^{-1}T\nabla s\right) \tag{B.34}$$

$$\mathcal{N}_p(...) = -\mathbf{u}\cdot\nabla p - \gamma p\nabla\cdot\mathbf{u} + (\gamma-1)Q_{nonlinear} + \gamma^{-1}\mathcal{W}_{nonlinear} + \gamma^{-1}\mathcal{W}T \tag{B.35}$$

$$\mathcal{N}_T(...) = -\mathbf{u}\cdot\nabla T + \gamma(\gamma-1)\left(-\tfrac{1}{\gamma}\tfrac{\gamma p-\rho}{1+\rho}\nabla\cdot\mathbf{u} + Q_{nonlinear} - \tfrac{\rho}{1+\rho}Q\right) \tag{B.36}$$

$$\mathcal{N}_s(...) = -\mathbf{u}\cdot\nabla s + (\gamma-1)\left(Q_{nonlinear} - \tfrac{\rho+T+\rho T}{1+\rho+T+\rho T}Q - \gamma^{-1}\mathcal{W}_{nonlinear} + \gamma^{-1}\tfrac{\rho}{1+\rho}\mathcal{W}\right) \tag{B.37}$$

Note that if we neglect the effect of condensed particles, and retain only viscous and heat conduction contributions, the source terms reduce to

$$\mathcal{W} = 0, \quad \mathcal{F} = \mathrm{Re}_\omega^{-1}\nabla\times\boldsymbol{\omega} - \mathrm{Re}_\vartheta^{-1}\nabla\vartheta, \quad Q = \left((\gamma-1)\,\mathrm{Pr}\,\mathrm{Re}_\omega\right)^{-1}\nabla^2 T + \mathrm{Re}_\omega^{-1}\Phi \tag{B.38}$$

C. Calculations for Chapter 3

C.1 Writing out the linear stability problem

$$\begin{bmatrix} \mathscr{L}_c\left(c_{m0},\vartheta_{m0}\right) \\ \mathscr{L}_\vartheta\left(c_{m0},\vartheta_{m0}\right) \end{bmatrix} = \begin{bmatrix} 0 & \left(\Gamma-1\right) \\ \left(\Gamma-1\right)^{-1}\nabla^2 & 0 \end{bmatrix}\begin{bmatrix} c_{m0} \\ \vartheta_{m0} \end{bmatrix} = ik_{m0}\begin{bmatrix} c_{m0} \\ \vartheta_{m0} \end{bmatrix} \tag{C.1}$$

we have

$$\varphi_{m0} = -i\left(k_{m0}\left(\Gamma-1\right)\right)^{-1}c_{m0}, \quad \vartheta_{m0} = ik_{m0}\left(\Gamma-1\right)^{-1}c_{m0} \tag{C.2}$$

This expresses the acoustic velocity field in terms of the c_{m0}.

Adjoint Problem

Recall that the adjoint problem is formally defined as (cf. Stakgold 1967)

$$\left\langle \mathscr{L}\left(\mathbf{f}_m,...\right),\mathbf{f}_m^\dagger\right\rangle - \left\langle \mathbf{f}_m,\mathscr{L}^\dagger\left(\mathbf{f}_m^\dagger,...\right)\right\rangle \equiv \int \nabla\cdot(\ )\,dV \tag{C.3}$$

with $\langle\ \rangle$ the complex valued inner product $\langle \mathbf{x},\mathbf{y}\rangle \equiv \int \mathbf{y}^{*T}\mathbf{x}\,dV$. Using (C.1) and the vector identity $\alpha\nabla^2\beta - \beta\nabla^2\alpha = \nabla\cdot\left(\alpha\nabla\beta - \beta\nabla\alpha\right)$, we have

$$\left\langle \mathscr{L}\left(\mathbf{f}_{m0}\right),\mathbf{f}_{m0}^\dagger\right\rangle - \left\langle \mathbf{f}_{m0},\mathscr{L}^\dagger\left(\mathbf{f}_{m0}^\dagger\right)\right\rangle = \left(\Gamma-1\right)^{-1}\oint\left(\varphi_{m0}^{\dagger *}\mathbf{n}\cdot\nabla c_{m0} - c_{m0}\,\mathbf{n}\cdot\nabla\varphi_{m0}^{\dagger *}\right)dS \tag{C.4}$$

where $\mathbf{f}_{m0}^\dagger \equiv \begin{bmatrix} c_{m0}^\dagger & \varphi_{m0}^\dagger \end{bmatrix}^T$ and

$$\mathscr{L}^\dagger\left(\mathbf{f}_{m0}^\dagger\right) \equiv \begin{bmatrix} 0 & \left(\Gamma-1\right)^{-1}\nabla^2 \\ \left(\Gamma-1\right) & 0 \end{bmatrix}\begin{bmatrix} c_{m0}^\dagger \\ \varphi_{m0}^\dagger \end{bmatrix} \tag{C.5}$$

Since hardwall boundary conditions are assumed for both the acoustic field and its adjoint, the right-hand side of (C.4) vanishes, leaving $\left\langle \mathscr{L}\left(\mathbf{f}_{m0}\right),\mathbf{f}_{m0}^\dagger\right\rangle = \left\langle \mathbf{f}_{m0},\mathscr{L}^\dagger\left(\mathbf{f}_{m0}^\dagger\right)\right\rangle$. Accordingly, the eigenfunction problem for the adjoint operator is given by $\mathscr{L}^\dagger\left(\mathbf{f}_{m0}^\dagger\right) = -ik_{m0}^*\mathbf{f}_{m0}^\dagger$, which can be written out as follows

$$\varphi_{m0}^\dagger = ik_{m0}^{-1}\left(\Gamma-1\right)c_{m0}^\dagger, \quad \vartheta_{m0}^\dagger = \nabla^2\varphi_{m0}^\dagger = -ik_{m0}\left(\Gamma-1\right)c_{m0}^\dagger \tag{C.6}$$

after noting that the eigenvalues are real (i.e., $k_{m0}^* = k_{m0}$).

Now by combining the equations of (C.6), it can be shown that $\nabla^2 c_{m0}^\dagger = -k_{m0}^2\,c_{m0}^\dagger$ and so $c_{m0}^\dagger = c_{m0}$. This completes the expression of the adjoint field in terms of the c_{m0}.

C.2 Here we give results for the nonlinear coefficients that describe sound-sound interactions.

Axial Modes

$$I_1^{\vartheta,\vartheta(m,j,k)} = \tfrac{E_1^2}{2}\left(\delta_{|m|}^{|j-k|} + \delta_{|m|}^{|j+k|}\right), \quad I_2^{\vartheta,\vartheta(m,j,k)} = \tfrac{E_1^2}{2}\left(\delta_{|m|}^{|j-k|} - \delta_{|m|}^{|j+k|}\right) \tag{C.7}$$

Tangential Modes

$$I_1^{\vartheta\vartheta(m,j,k)} = \tfrac{\pi}{2} c_1^{\vartheta\vartheta(m,j,k)} \left(\delta_{|m|}^{|j-k|} + \delta_{|m|}^{|j+k|} \right)$$

$$I_2^{\vartheta\vartheta(m,j,k)} = \tfrac{\pi}{2} \left(\left(c_{2\alpha}^{\vartheta\vartheta(m,j,k)} + c_{2\beta}^{\vartheta\vartheta(m,j,k)} \right) \delta_{|m|}^{|j-k|} + \left(c_{2\alpha}^{\vartheta\vartheta(m,j,k)} - c_{2\beta}^{\vartheta\vartheta(m,j,k)} \right) \delta_{|m|}^{|j+k|} \right) \tag{C.8}$$

The integrals $c_1^{\vartheta\vartheta(m,j,k)}$, $c_{2\alpha}^{\vartheta\vartheta(m,j,k)}$ and $c_{2\beta}^{\vartheta\vartheta(m,j,k)}$:

$$c_1^{\vartheta\vartheta(m,j,k)} = \int_0^1 r J_m\left(k_{m0} r\right) J_j\left(k_{j0} r\right) J_k\left(k_{k0} r\right) dr \tag{C.9}$$

$$c_{2\alpha}^{\vartheta\vartheta(m,j,k)} = \left(k_{j0} k_{k0}\right)^{-1} \int_{r=0}^1 r J_m\left(k_{m0} r\right) \left(d\, J_j\left(k_{j0} r\right) / dr \right) \left(d\, J_k\left(k_{k0} r\right) / dr \right) dr \tag{C.10}$$

$$c_{2\beta}^{\vartheta\vartheta(m,j,k)} = \left(j / k_{j0} \right) \left(k / k_{k0} \right) \left(\int_{r=0}^1 r^{-1} J_m\left(k_{m0} r\right) J_j\left(k_{j0} r\right) J_k\left(k_{k0} r\right) dr \right) \tag{C.11}$$

must be evaluated numerically.

C.3 By appealing to the method of characteristics, Fox (1955) described the steepening behavior of purely axial acoustic motions within a cylindrical chamber, enclosed by a rigid boundary and containing a fluid otherwise at rest. We briefly review that solution here.

The starting point for the analysis is a coupled system of nonlinear equations for the sound speed $c = c(z,t)$ and the acoustic velocity $\mathbf{u}_\vartheta = \mathbf{u}_a = u_{az}(z,t)\mathbf{e}_z$, found by taking the axial component of (2.11) and (2.12) for a flow assumed adiabatic,

$$\frac{\partial c}{\partial t} + u_{az} \frac{\partial c}{\partial z} = -(\Gamma - 1)(1+c) \frac{\partial u_{az}}{\partial z}, \quad \frac{\partial u_{az}}{\partial t} + u_{az} \frac{\partial u_{az}}{\partial z} = -\frac{1}{\Gamma - 1}(1+c) \frac{\partial c}{\partial z} \tag{C.12}$$

The essential point to be observed is that by introducing *characteristic coordinates* (ς, υ) defined by

$$\frac{\partial z}{\partial \varsigma} = \left(1 + c + u_{az}\right) \frac{\partial t}{\partial \varsigma}, \quad \frac{\partial z}{\partial \upsilon} = -\left(1 + c - u_{az}\right) \frac{\partial t}{\partial \upsilon} \tag{C.13}$$

the original nonlinear system (C.12) can be transformed† into a linear one

$$\frac{\partial}{\partial \varsigma}\left(u_{az} + \frac{1}{\Gamma - 1} c \right) = 0, \quad \frac{\partial}{\partial \upsilon}\left(u_{az} - \frac{1}{\Gamma - 1} c \right) = 0 \tag{C.14}$$

---

† Using (C.13) it can be shown that space and time derivatives transform as

$$\frac{\partial}{\partial z} = \frac{1}{2(1+c)(\partial t/\partial \varsigma)} \frac{\partial}{\partial \varsigma} - \frac{1}{2(1+c)(\partial t/\partial \upsilon)} \frac{\partial}{\partial \upsilon}, \quad \frac{\partial}{\partial t} = \frac{\left(1 + c - u_{az}\right)}{2(1+c)(\partial t/\partial \varsigma)} \frac{\partial}{\partial \varsigma} + \frac{\left(1 + c + u_{az}\right)}{2(1+c)(\partial t/\partial \upsilon)} \frac{\partial}{\partial \upsilon}$$

Substituting into (C.12) and taking linear combinations of the results derives (C.14).

Thus, when considered as functions of (ς,υ), both u_{az} and c can be solved for *exactly*

$$u_{az}(\varsigma,\upsilon)=r(\upsilon)+l(\varsigma),\quad c(\varsigma,\upsilon)=(\Gamma-1)\big(r(\upsilon)-l(\varsigma)\big) \tag{C.15}$$

where r and l are determined by satisfying the initial conditions. Even though more complex behavior can be accommodated, consideration is restricted here to the case of a sound wave that initially coincides with an *axial acoustic mode*:

$$u_{az}(z,0)=0,\quad c(z,0)=\varepsilon\cos(k_l\, z) \tag{C.16}$$

with k_l the acoustic wave number and ε the small parameter that characterizes the wave amplitude. If we choose, for simplicity, the parameterization of the initial line $t=0$ as $z=\varsigma=\upsilon$, it then follows from (C.15) and (C.16) that

$$l(\varsigma)=-\frac{\varepsilon}{2}\frac{1}{\Gamma-1}\cos(k_l\varsigma),\quad r(\upsilon)=\frac{\varepsilon}{2}\frac{1}{\Gamma-1}\cos(k_l\upsilon) \tag{C.17}$$

Upon substituting this result back into (C.15) and using some trigonometric identities, we have

$$u_{az}(\varsigma,\upsilon)=\frac{\varepsilon}{\Gamma-1}\sin\left(k_l\frac{\varsigma+\upsilon}{2}\right)\sin\left(k_l\frac{\varsigma-\upsilon}{2}\right),\quad c(\varsigma,\upsilon)=\varepsilon\cos\left(k_l\frac{\varsigma+\upsilon}{2}\right)\cos\left(k_l\frac{\varsigma-\upsilon}{2}\right) \tag{C.18}$$

which recall is the exact solution.

The perturbation comes in determining the characteristic directions from (C.13). Consider an expansion for space and time of the form

$$z(\varsigma,\upsilon)\sim z_0(\varsigma,\upsilon)+\varepsilon z_1(\varsigma,\upsilon)+...,\quad t(\varsigma,\upsilon)\sim t_0(\varsigma,\upsilon)+\varepsilon t_1(\varsigma,\upsilon)+... \tag{C.19}$$

To satisfy the parameterization of the line $t=0$ introduced, the first approximations are given by

$$z_0(\varsigma,\upsilon)=\frac{\varsigma+\upsilon}{2},\quad t_0(\varsigma,\upsilon)=\frac{\varsigma-\upsilon}{2} \tag{C.20}$$

Introducing this result into (C.18) recovers—not surprisingly—the behavior of classic acoustics

$$u_{az}(\varsigma,\upsilon)\sim\frac{\varepsilon}{\Gamma-1}\sin(k_l z_0)\sin(k_l t_0),\quad c(\varsigma,\upsilon)\sim\varepsilon\cos(k_l z_0)\cos(k_l t_0) \tag{C.21}$$

absent any nonlinear interaction.

Steepening effects first manifest themselves in the $O(\varepsilon)$ corrections to the characteristic directions. Substituting (C.19) into (C.13), we have

$$\frac{\partial(z_1-t_1)}{\partial\varsigma}=(c+u_{az})\frac{\partial t_0}{\partial\varsigma},\quad \frac{\partial(z_1+t_1)}{\partial\upsilon}=-(c-u_{az})\frac{\partial t_0}{\partial\upsilon} \tag{C.22}$$

with solution

$$\begin{aligned} z_1(\varsigma,\upsilon)&=\frac{1}{8}\frac{\Gamma}{\Gamma-1}(\upsilon-\varsigma)\big(\cos(k_l\varsigma)-\cos(k_l\upsilon)\big)\\ t_1(\varsigma,\upsilon)&=\frac{1}{8}\frac{\Gamma}{\Gamma-1}(\upsilon-\varsigma)\big(\cos(k_l\varsigma)+\cos(k_l\upsilon)\big)+\frac{1}{4k_l}\frac{\Gamma-2}{\Gamma-1}\big(\sin(k_l\upsilon)-\sin(k_l\varsigma)\big)\end{aligned} \tag{C.23}$$

Even though the calculation is easily extended to $O(\varepsilon^2)$, the result here suffices. The algorithm for determining the behavior at a given point in (z,t) space involves numerically inverting (C.19) to find the corresponding values for the characteristic coordinates (ς,υ); the acoustic velocity and the sound speed then follow from (C.18).

D. Calculations for Chapter 4

We consider first the equation for Q_3:

$$\begin{aligned}\dot{Q}_3 = K_3^{(r)} + 3\sum_j \frac{\sqrt{2}}{E_1 E_j E_{1-j}} \frac{\sqrt{P_1}}{\sqrt{P_j P_{1-j}}} \left(\begin{array}{l} f_r^{\varepsilon\varepsilon(1,j,1-j)} \sin\left(Q_1 - Q_j - Q_{1-j}\right) - \\ - f_i^{\varepsilon\varepsilon(1,j,1-j)} \cos\left(Q_1 - Q_j - Q_{1-j}\right) \end{array} \right) - \\ - \sum_j \frac{\sqrt{2}}{E_3 E_j E_{3-j}} \frac{\sqrt{P_3}}{\sqrt{P_j P_{3-j}}} \left(\begin{array}{l} f_r^{\varepsilon\varepsilon(3,j,3-j)} \sin\left(Q_3 - Q_j - Q_{3-j}\right) - \\ - f_i^{\varepsilon\varepsilon(3,j,3-j)} \cos\left(Q_3 - Q_j - Q_{3-j}\right) \end{array} \right)\end{aligned} \tag{D.1}$$

where $K_3^{(\ldots)} = 3k_1^{(\ldots)} - k_3^{(\ldots)}$ and identify the dominant nonlinear term using arguments similar to those introduced in §4.3,

$$\dot{Q}_3 \sim K_3^{(r)} - 2\frac{\sqrt{2}}{E_3 E_2 E_1} \frac{\sqrt{P_3}}{\sqrt{P_2}} \left(f_r^{\varepsilon\varepsilon(3,2,1)} \sin\left(Q_3 - Q_2\right) - f_i^{\varepsilon\varepsilon(3,2,1)} \cos\left(Q_3 - Q_2\right) \right) \tag{D.2}$$

Since $Q_3 - Q_2$ grows linearly to begin with (there will be a change in slope after the first resonance condition is satisfied owing to the fact that Q_2 has reached its limit point) and P_3 grows exponentially, there comes a time when the two terms balance and $\dot{Q}_3 \sim 0$. For this to be a stable limit point, P_3 as governed by

$$\frac{\dot{P}_3}{2P_3} \sim K_3^{(i)} - 2\frac{\sqrt{2}}{E_3 E_2 E_1} \frac{\sqrt{P_3}}{\sqrt{P_2}} \left(f_r^{\varepsilon\varepsilon(3,2,1)} \cos\left(Q_3 - Q_2\right) + f_i^{\varepsilon\varepsilon(3,2,1)} \sin\left(Q_3 - Q_2\right) \right) \tag{D.3}$$

must also have reached its limit point. Solving (D.2) and (D.3) for these limiting values, we have

$$\tan\left(Q_3 - Q_2\right) \sim \frac{F_3^{(i)} + \frac{K_3^{(r)}}{K_3^{(i)}} F_3^{(r)}}{F_3^{(r)} - \frac{K_3^{(r)}}{K_3^{(i)}} F_3^{(i)}} \tag{D.4}$$

$$\frac{\sqrt{P_3}}{\sqrt{P_2}} \sim \left| \frac{K_3^{(r)}}{F_3^{(r)} \sin\left(Q_3 - Q_2\right) - F_3^{(i)} \cos\left(Q_3 - Q_2\right)} \right| = \left| \frac{K_3^{(i)}}{F_3^{(i)} \sin\left(Q_3 - Q_2\right) + F_3^{(r)} \cos\left(Q_3 - Q_2\right)} \right| \tag{D.5}$$

where $F_3^{(r)} = \frac{2\sqrt{2}}{E_3 E_2 E_1} f_r^{\varepsilon\varepsilon(3,2,1)}$ and $F_3^{(i)} = \frac{2\sqrt{2}}{E_3 E_2 E_1} f_i^{\varepsilon\varepsilon(3,2,1)}$. This defines the behavior after the second resonance condition has been satisfied.

Now consider the dominant terms in the equations for Q_4:

$$\begin{aligned}\dot{Q}_4 \sim K_4^{(r)} - \frac{\sqrt{2}}{E_4 E_2 E_2} \frac{\sqrt{P_4}}{P_2} \left(f_r^{\varepsilon\varepsilon(4,2,2)} \sin\left(Q_4 - 2Q_2\right) - f_i^{\varepsilon\varepsilon(4,2,2)} \cos\left(Q_4 - 2Q_2\right) \right) - \\ - 2\frac{\sqrt{2}}{E_4 E_3 E_1} \frac{\sqrt{P_4}}{\sqrt{P_3}} \left(f_r^{\varepsilon\varepsilon(4,3,1)} \sin\left(Q_4 - Q_3\right) - f_i^{\varepsilon\varepsilon(4,3,1)} \cos\left(Q_4 - Q_3\right) \right)\end{aligned} \tag{D.6}$$

and P_4:

$$\frac{\dot{P}_4}{2P_4} \sim K_4^{(i)} - \frac{\sqrt{2}}{E_4 E_2 E_2}\frac{\sqrt{P_4}}{P_2}\left(f_r^{\varepsilon\varepsilon(4,2,2)} \cos\left(Q_4 - 2Q_2\right) + f_i^{\varepsilon\varepsilon(4,2,2)} \sin\left(Q_4 - 2Q_2\right)\right) - \\ -2\frac{\sqrt{2}}{E_4 E_3 E_1}\frac{\sqrt{P_4}}{\sqrt{P_3}}\left(f_r^{\varepsilon\varepsilon(4,3,1)} \cos\left(Q_4 - Q_3\right) + f_i^{\varepsilon\varepsilon(4,3,1)} \sin\left(Q_4 - Q_3\right)\right) \tag{D.7}$$

where $K_4^{(\ldots)} = 4k_1^{(\ldots)} - k_4^{(\ldots)}$. This defines the approach to the third resonance, after which the respective left-hand sides are zero and the limiting values of Q_4 and P_4 can be obtained:

$$\tan Q_4 \sim \frac{F_4^{(i)} + \frac{K_4^{(r)}}{K_4^{(i)}} F_4^{(r)}}{F_4^{(r)} - \frac{K_4^{(r)}}{K_4^{(i)}} F_4^{(i)}} \tag{D.8}$$

$$\sqrt{P_4} \sim \left| \frac{K_4^{(r)}}{F_4^{(r)} \sin Q_4 - F_4^{(i)} \cos Q_4} \right| = \left| \frac{K_4^{(i)}}{F_4^{(i)} \sin Q_4 + F_4^{(r)} \cos Q_4} \right| \tag{D.9}$$

where $F_4^{(r)}$ and $F_4^{(i)}$ given by

$$F_4^{(r)} = \frac{\sqrt{2}}{E_4 E_2 E_2}\frac{1}{P_2}\left(f_r^{\varepsilon\varepsilon(4,2,2)} \cos 2Q_2 - f_i^{\varepsilon\varepsilon(4,2,2)} \sin 2Q_2\right) + \frac{\sqrt{2}}{E_4 E_3 E_1}\frac{2}{\sqrt{P_3}}\left(f_r^{\varepsilon\varepsilon(4,3,1)} \cos Q_3 - f_i^{\varepsilon\varepsilon(4,3,1)} \sin Q_3\right) \\ F_4^{(i)} = \frac{\sqrt{2}}{E_4 E_2 E_2}\frac{1}{P_2}\left(f_r^{\varepsilon\varepsilon(4,2,2)} \sin 2Q_2 + f_i^{\varepsilon\varepsilon(4,2,2)} \cos 2Q_2\right) + \frac{\sqrt{2}}{E_4 E_3 E_1}\frac{2}{\sqrt{P_3}}\left(f_r^{\varepsilon\varepsilon(4,3,1)} \sin Q_3 + f_i^{\varepsilon\varepsilon(4,3,1)} \cos Q_3\right) \tag{D.10}$$

E. The Method of Multiple Scales: A Simple Example

We use here the *method of multiple scales* to compute the vorticity field established by Stokes' oscillating plate generalized to include a uniform injection of fluid normal to the boundary. Recall from (5.2)–(5.3) that

$$\frac{\partial \boldsymbol{\omega}_\zeta}{\partial t} + u_n \frac{\partial \boldsymbol{\omega}_\zeta}{\partial n} = \nu \frac{\partial^2 \boldsymbol{\omega}_\zeta}{\partial n^2}, \quad u_n \boldsymbol{\omega}_\zeta - \nu \frac{\partial \boldsymbol{\omega}_\zeta}{\partial n} = \boldsymbol{\sigma}_\zeta \quad \text{at} \quad n = 0 \tag{E.1}$$

where the vorticity source strength $\boldsymbol{\sigma}_\zeta$ is now taken to be a harmonic function.

In solving (E.1), the essential idea is that coexisting spatial scales of different order control the physics; a fast scale

$$n^+ = \frac{k}{u_n}\left(1 + \sum_{m=2}^{M} \frac{\alpha_m}{\mathrm{Re}^m} + O\left(\frac{1}{\mathrm{Re}^{M+1}}\right)\right) n \tag{E.2}$$

describes the oscillatory behavior, where the α_m are constants independent of Re to be determined, and a slow scale

$$\tilde{n} = \frac{k}{u_n}\frac{1}{\mathrm{Re}} n \tag{E.3}$$

describes the cumulative effect of viscous decay. Since these scales are separated by $O\left(\mathrm{Re}^{-1}\right)$, this suggests the mathematical approximation of treating them as independent variables during the solution process. Thus, the chain rule gives

$$\frac{\partial}{\partial n} = \frac{k}{u_n}\left(\left(1 + \sum_{m=2}^{M} \frac{\alpha_m}{\mathrm{Re}^m} + \ldots\right)\frac{\partial}{\partial n^+} + \frac{1}{\mathrm{Re}}\frac{\partial}{\partial \tilde{n}}\right) \tag{E.4}$$

$$\frac{\partial^2}{\partial n^2} = \frac{k^2}{u_n^2}\left(\left(1 + \sum_{m=2}^{M} \frac{\alpha_m}{\mathrm{Re}^m} + \ldots\right)^2 \frac{\partial^2}{\partial n^{+2}} + \frac{2}{\mathrm{Re}}\left(1 + \sum_{m=2}^{M} \frac{\alpha_m}{\mathrm{Re}^m} + \ldots\right)\frac{\partial^2}{\partial n^+ \partial \tilde{n}} + \frac{1}{\mathrm{Re}^2}\frac{\partial^2}{\partial \tilde{n}^2}\right) \tag{E.5}$$

Introducing this transformation into (E.1), we find

$$\begin{gathered} \frac{\partial \boldsymbol{\omega}_\zeta}{\partial t^+} + \frac{\partial \boldsymbol{\omega}_\zeta}{\partial n^+} = \frac{1}{\mathrm{Re}}\left(\frac{\partial^2 \boldsymbol{\omega}_\zeta}{\partial n^{+2}} - \frac{\partial \boldsymbol{\omega}_\zeta}{\partial \tilde{n}}\right) + \frac{1}{\mathrm{Re}^2}\left(2\frac{\partial^2 \boldsymbol{\omega}_\zeta}{\partial n^+ \partial \tilde{n}} - \alpha_2 \frac{\partial \boldsymbol{\omega}_\zeta}{\partial n^+}\right) + \ldots \\ \boldsymbol{\omega}_\zeta = \frac{1}{u_n}\boldsymbol{\sigma}_\zeta + \frac{1}{\mathrm{Re}}\frac{\partial \boldsymbol{\omega}_\zeta}{\partial n^+} + \frac{1}{\mathrm{Re}^2}\frac{\partial \boldsymbol{\omega}_\zeta}{\partial \tilde{n}} + \ldots \quad \text{at} \quad n^+, \tilde{n} = 0 \end{gathered} \tag{E.6}$$

where $t^+ = kt,$ with k the frequency of oscillation.

Now a *two-scale* expansion for $\boldsymbol{\omega}_\zeta$ of the form

$$\boldsymbol{\omega}_\zeta(n,t) = \boldsymbol{\omega}_\zeta\left(n^+, \tilde{n}, t^+; \mathrm{Re}\right) \sim \boldsymbol{\omega}_{\zeta 0}\left(n^+, \tilde{n}, t^+\right) + \frac{1}{\mathrm{Re}}\boldsymbol{\omega}_{\zeta 1}\left(n^+, \tilde{n}, t^+\right) + \ldots \tag{E.7}$$

is sought. Substituting into (E.6), we have that $\boldsymbol{\omega}_{\zeta 0}\left(n^+, \tilde{n}, t^+\right)$ is governed by a first-order wave equation in the fast scale n^+,

$$\frac{\partial \boldsymbol{\omega}_{\zeta 0}}{\partial t^+}+\frac{\partial \boldsymbol{\omega}_{\zeta 0}}{\partial n^+}=0,\quad \boldsymbol{\omega}_{\zeta 0}\left(0,0,t^+\right)=\frac{1}{u_n}\boldsymbol{\sigma}_\zeta\left(t^+\right) \tag{E.8}$$

with solution

$$\boldsymbol{\omega}_{\zeta 0}\left(n^+,\tilde{n},t^+\right)=\frac{1}{u_n}\rho_0\left(\tilde{n}\right)\boldsymbol{\sigma}_\zeta\left(t^+-n^+ +\theta_0\left(\tilde{n}\right)\right) \tag{E.9}$$

where $\rho_0\left(0\right)=1$ and $\theta_0\left(0\right)=0$ to satisfy the boundary condition. It must be emphasized that $\rho_0\left(\tilde{n}\right)$ and $\theta_0\left(\tilde{n}\right)$ are no longer *constants of integration* but functions of the slow scale $\tilde{n}$ determined by suppressing *secular* terms at higher order.

This leads us to the next term of the expansion (E.7), which is also governed by a first-order wave equation in the fast scale n^+,

$$\frac{\partial \boldsymbol{\omega}_{\zeta 1}}{\partial t^+}+\frac{\partial \boldsymbol{\omega}_{\zeta 1}}{\partial n^+}=\frac{\partial^2 \boldsymbol{\omega}_{\zeta 0}}{\partial n^{+2}}-\frac{\partial \boldsymbol{\omega}_{\zeta 0}}{\partial \tilde{n}},\quad \boldsymbol{\omega}_{\zeta 1}\left(0,0,t^+\right)=\frac{\partial \boldsymbol{\omega}_{\zeta 0}}{\partial n^+}\left(0,0,t^+\right) \tag{E.10}$$

except the equation is now forced. Using (E.9) to evaluate the right-hand side and noting that since $\boldsymbol{\sigma}_\zeta$ is assumed harmonic $\boldsymbol{\sigma}_\zeta''\left(t^+\right)=-\boldsymbol{\sigma}_\zeta\left(t^+\right)$, we have

$$\frac{\partial \boldsymbol{\omega}_{\zeta 1}}{\partial t^+}+\frac{\partial \boldsymbol{\omega}_{\zeta 1}}{\partial n^+}=-\frac{1}{u_n}\left(\frac{d\rho_0}{d\tilde{n}}+\rho_0\right)\boldsymbol{\sigma}_\zeta\left(t^+-n^+ +\theta_0\right)-\frac{1}{u_n}\left(\rho_0\frac{d\theta_0}{d\tilde{n}}\right)\boldsymbol{\sigma}_\zeta'\left(t^+-n^+ +\theta_0\right) \tag{E.11}$$

That both forcing terms here are *secular* follows because they are homogenous solutions of the operator on the left-hand side. If no mechanism existed to suppress them, the perturbation to the leading order solution would grow without bound—behavior not reflected by the physics of the problem. To avoid this, we set

$$\frac{d\rho_0}{d\tilde{n}}+\rho_0=0,\quad \frac{d\theta_0}{d\tilde{n}}=0 \tag{E.12}$$

Taking account of the boundary conditions, we have $\rho_0\left(\tilde{n}\right)=e^{-\tilde{n}}$ and $\theta_0\left(\tilde{n}\right)=0$. This determines $\boldsymbol{\omega}_\zeta$ to $O\left(1\right)$.

Now we proceed further and extend the results to $O\left(\mathrm{Re}^{-1}\right)$. Because no forcing terms remain in (E.11), $\boldsymbol{\omega}_{\zeta 1}$ is driven entirely by the boundary, consideration of which, gives

$$\boldsymbol{\omega}_{\zeta 1}\left(n^+,\tilde{n},t^+\right)=-\frac{1}{u_n}\rho_1\left(\tilde{n}\right)\boldsymbol{\sigma}_\zeta'\left(t^+-n^+ +\theta_1\left(\tilde{n}\right)\right) \tag{E.13}$$

where $\rho_1\left(0\right)=1$ and $\theta_1\left(0\right)=0$. Once again the unknown functions $\rho_1\left(\tilde{n}\right)$ and $\theta_1\left(\tilde{n}\right)$ of the slow spatial scale are determined by suppressing secular terms at higher order,

$$\frac{\partial \boldsymbol{\omega}_{\zeta 2}}{\partial t^+}+\frac{\partial \boldsymbol{\omega}_{\zeta 2}}{\partial n^+}=\frac{\partial^2 \boldsymbol{\omega}_{\zeta 1}}{\partial n^{+2}}-\frac{\partial \boldsymbol{\omega}_{\zeta 1}}{\partial \tilde{n}}+2\frac{\partial^2 \boldsymbol{\omega}_{\zeta 0}}{\partial n^+\partial \tilde{n}}-\alpha_2\frac{\partial \boldsymbol{\omega}_{\zeta 0}}{\partial n^+} \tag{E.14}$$

Without carrying out the details, we can use the results calculated so far to evaluate the right-hand side. All terms are found to be secular and we suppress them by setting

$$\frac{d\rho_1}{d\tilde{n}} + \rho_1 = 0, \quad \frac{d\theta_1}{d\tilde{n}} = 0, \quad \left(2 + \alpha_2\right)\rho_0 = 0 \tag{E.15}$$

Thus $\alpha_2 = -2,$ and taking account of the boundary conditions, we have $\rho_1\left(\tilde{n}\right) = e^{-\tilde{n}}$ and $\theta_1\left(\tilde{n}\right) = 0$. This determines $\boldsymbol{\omega}_\zeta$ to $O\left(\mathrm{Re}^{-1}\right)$.

To summarize, the first two terms in the multiple scale solution of the vorticity field, established by Stokes' oscillating plate with fluid injected through the boundary, are

$$\boldsymbol{\omega}_\zeta\left(n,t\right) \sim \frac{1}{u_n} e^{-\tilde{n}} \left(\boldsymbol{\sigma}_\zeta\left(t^+ - n^+\right) - \frac{1}{\mathrm{Re}} \boldsymbol{\sigma}'_\zeta\left(t^+ - n^+\right) \right) \tag{E.16}$$

This recovers the perturbation expansion of the exact solution given in §5.2 (cf. (5.13) specifically) if we set $\boldsymbol{\sigma}_\zeta\left(t^+\right) = -kU \sin t^+ \boldsymbol{\zeta}_2$.

F. Results for Chapter 6

Table F.1 Summary of the results for the vortical and thermal waves generated within an acoustic boundary layer, with and without a uniform injection of fluid through the boundary

Without Injection $M_b = 0$	**With Injection** $M_b \neq 0$
$\delta = \left(2/\mathrm{Re}_\omega\right)^{1/2}$	$\delta = M_b^3\,\mathrm{Re}_\omega;\quad \left(M_b^2\,\mathrm{Re}_\omega\right)^{-1} \ll 1$
$\boldsymbol{\omega}_\zeta \sim \frac{1}{\delta}(1-i)e^{-n/\delta}\sin\zeta_1 e^{i(t-n/\delta)}\boldsymbol{\zeta}_2$	$\boldsymbol{\omega}_\zeta \sim \frac{1}{M_b}e^{-n/\delta}\sin\zeta_1 e^{i\left(t-(1/M_b)n\right)}\boldsymbol{\zeta}_2$
$\mathbf{A}_\zeta \sim \frac{1}{2}\delta(1+i)e^{-n/\delta}\sin\zeta_1 e^{i(t-n/\delta)}\boldsymbol{\zeta}_2$	$\mathbf{A}_\zeta \sim M_b e^{-n/\delta}\sin\zeta_1 e^{i\left(t-(1/M_b)n\right)}\boldsymbol{\zeta}_2$
$\mathbf{u}_{\omega\zeta} \sim ie^{-n/\delta}\sin\zeta_1 e^{i(t-n/\delta)}\boldsymbol{\zeta}_1$	$\mathbf{u}_{\omega\zeta} \sim ie^{-n/\delta}\sin\zeta_1 e^{i\left(t-(1/M_b)n\right)}\boldsymbol{\zeta}_1$
$u_{\omega n} \sim \frac{1}{2}\delta(1+i)e^{-n/\delta}\cos\zeta_1 e^{i(t-n/\delta)}$	$u_{\omega n} \sim M_b e^{-n/\delta}\cos\zeta_1 e^{i\left(t-(1/M_b)n\right)}$
$T_s \sim T_s(0)e^{-n\sqrt{\mathrm{Pr}}/\delta}\cos\zeta_1 e^{i\left(t-n\sqrt{\mathrm{Pr}}/\delta\right)}$	$T_s \sim T_s(0)e^{-n/(\mathrm{Pr}\,\delta)}\cos\zeta_1 e^{i\left(t-(1/M_b)n\right)}$
$u_{sn} \sim -\frac{\delta}{2\,\mathrm{Pr}^{1/2}}(1+i)T_s$	$u_{sn} \sim -i\left(M_b^2\,\mathrm{Re}_\omega\right)^{-1}\left(M_b/\mathrm{Pr}\right)T_s$

G. Calculations for Chapter 7

G.1 Terms indicating an interaction with the mean flow are scaled by the injection Mach number M_b and so the linear operators $\mathscr{L}_p(...)$ and $\mathscr{L}_\vartheta(...)$ can be written as

$$\mathscr{L}_p(...) = \mathscr{L}_{p0}(...) + M_b \mathscr{L}_{p\mu}(...) + ..., \quad \mathscr{L}_\vartheta(...) = \mathscr{L}_{\vartheta 0}(...) + M_b \mathscr{L}_{\vartheta\mu}(...) + ... \tag{G.1}$$

where

$$\begin{gathered} \mathscr{L}_{p0}(p,\vartheta) \equiv \vartheta \\ \mathscr{L}_{\vartheta 0}(p,\vartheta) \equiv \nabla^2 p \\ \mathscr{L}_{p\mu}(\mathbf{U},p,\mathbf{u}) = M_b \mathbf{U}\cdot\nabla p \\ \mathscr{L}_{\vartheta\mu}(\mathbf{U},p,\mathbf{u}) = \nabla\cdot\mathscr{L}_{u\mu}(\mathbf{U},p,\mathbf{u}) = M_b \nabla\cdot(\mathbf{u}\cdot\nabla\mathbf{U} + \mathbf{U}\cdot\nabla\mathbf{u}) \end{gathered} \tag{G.2}$$

Note that contributions owing to source terms have been omitted for simplicity.

G.2 To establish that

$$\begin{gathered} i(k_{m0}-k_{j0})\int\left(p_{j0}^{\dagger *}p_{m\mu} + \varphi_{j0}^{\dagger *}\vartheta_{m\mu}\right)dV + ik_{m\mu}2E_{m0}^2\delta_m^j = \\ = ik_{m0}\oint\varphi_{j0}^{\dagger *}\mathbf{n}\cdot\left(\mathbf{u}_{m\vartheta\mu} + M_b^{-1}\mathbf{u}_{m\omega 0}\right)dS - \int\mathscr{L}_{u\mu}(\mathbf{U},p_{m0},\mathbf{u}_{m0})\cdot\nabla\varphi_{j0}^{\dagger *}dV + \int\mathscr{L}_{p\mu}(\mathbf{U},p_{m0},\mathbf{u}_{m0})\,p_{j0}^{\dagger *}dV \end{gathered} \tag{G.3}$$

we begin by taking the inner product $\langle\mathbf{x},\mathbf{y}\rangle \equiv \int\mathbf{y}^{*T}\mathbf{x}dV$ of (7.5), i.e.,

$$\begin{bmatrix}\mathscr{L}_{p0}(p_{m\mu},\vartheta_{m\mu})\\ \mathscr{L}_{\vartheta 0}(p_{m\mu},\vartheta_{m\mu})\end{bmatrix} + \begin{bmatrix}\mathscr{L}_{p\mu}(\mathbf{U},p_{m0},\mathbf{u}_{m0})\\ \mathscr{L}_{\vartheta\mu}(\mathbf{U},p_{m0},\mathbf{u}_{m0})\end{bmatrix} = ik_{m0}\begin{bmatrix}p_{m\mu}\\ \vartheta_{m\mu}\end{bmatrix} + ik_{m\mu}\begin{bmatrix}p_{m0}\\ \vartheta_{m0}\end{bmatrix} \tag{G.4}$$

with $\mathbf{f}_{j0}^{\dagger} = \begin{bmatrix}p_{j0}^{\dagger} & \varphi_{j0}^{\dagger}\end{bmatrix}^T$ to obtain

$$\begin{gathered} ik_{m0}\int\left(p_{j0}^{\dagger *}p_{m\mu} + \varphi_{j0}^{\dagger *}\vartheta_{m\mu}\right)dV - \int\left(\mathscr{L}_{p0}(p_{m\mu},\vartheta_{m\mu})\,p_{j0}^{\dagger *} + \mathscr{L}_{\vartheta 0}(p_{m\mu},\vartheta_{m\mu})\varphi_{j0}^{\dagger *}\right)dV + ik_{m\mu}2E_{m0}^2\delta_m^j = \\ = \int\mathscr{L}_{\vartheta\mu}(\mathbf{U},p_{m0},\mathbf{u}_{m0})\varphi_{j0}^{\dagger *}dV + \int\mathscr{L}_{p\mu}(\mathbf{U},p_{m0},\mathbf{u}_{m0})\,p_{j0}^{\dagger *}dV \end{gathered} \tag{G.5}$$

where $E_{m0}^2 = \frac{1}{2}\int\left(p_{m0}^{\dagger *}p_{m0} + \varphi_{m0}^{\dagger *}\vartheta_{m0}\right)dV$ and δ_m^j is the discrete Dirac-delta function.

Now using the operator definitions (cf.§G.1), the identity $\alpha\nabla^2\beta - \beta\nabla^2\alpha = \nabla\cdot(\alpha\nabla\beta - \beta\nabla\alpha)$ and the leading order acoustic solution from §C.1 (i.e., $\varphi_{j0}^{\dagger} = ik_{j0}^{-1}p_{j0}^{\dagger},...$), some of the terms in (G.5) can be rewritten. In particular, we find

$$\begin{gathered} \int\mathscr{L}_{p0}(p_{m\mu},\vartheta_{m\mu})\,p_{j0}^{\dagger *}dV = \int p_{j0}^{\dagger *}\vartheta_{m\mu}dV = ik_{j0}\int\varphi_{j0}^{\dagger *}\vartheta_{m\mu}dV \\ \int\mathscr{L}_{\vartheta 0}(p_{m\mu},\vartheta_{m\mu})\varphi_{j0}^{\dagger *}dV = \int\varphi_{j0}^{\dagger *}\nabla^2 p_{m\mu}dV = ik_{j0}\int p_{j0}^{\dagger *}p_{m\mu}dV + \oint\varphi_{j0}^{\dagger *}\mathbf{n}\cdot\mathscr{L}_{u0}(p_{m\mu},\mathbf{u}_{m\mu})dS \\ \int\mathscr{L}_{\vartheta\mu}(\mathbf{U},p_{m0},\mathbf{u}_{m0})\varphi_{j0}^{\dagger *}dV = \oint\varphi_{j0}^{\dagger *}\mathbf{n}\cdot\mathscr{L}_{u\mu}(\mathbf{U},p_{m0},\mathbf{u}_{m0})dS - \int\nabla\varphi_{j0}^{\dagger *}\cdot\mathscr{L}_{u\mu}(\mathbf{U},p_{m0},\mathbf{u}_{m0})dV \end{gathered} \tag{G.6}$$

Substituting these results into (G.5) yields

$$i\left(k_{m0}-k_{j0}\right)\int\left(p_{j0}^{\dagger *}p_{m\mu}+\varphi_{j0}^{\dagger *}\vartheta_{m\mu}\right)dV+ik_{m\mu}2E_{m0}^{2}\delta_{m}^{j}=$$
$$=\oint\varphi_{j0}^{\dagger *}\mathbf{n}\cdot\left(\mathscr{L}_{u0}\left(p_{m\mu},\mathbf{u}_{m\mu}\right)+\mathscr{L}_{u\mu}\left(\mathbf{U},p_{m0},\mathbf{u}_{m0}\right)\right)dS-\int\mathscr{L}_{u\mu}\left(\mathbf{U},p_{m0},\mathbf{u}_{m0}\right)\cdot\nabla\varphi_{j0}^{\dagger *}dV+\int\mathscr{L}_{p\mu}\left(\mathbf{U},p_{m0},\mathbf{u}_{m0}\right)p_{j0}^{\dagger *}dV \tag{G.7}$$

It remains to consider the first term on the right-hand side of (G.7). Expanding the normal projection of the momentum equation on the boundary

$$\mathbf{n}\cdot\mathscr{L}_{u}\left(...\right)=ik_{m}\mathbf{n}\cdot\mathbf{u}_{m}=ik_{m}\mathbf{n}\cdot\left(\mathbf{u}_{m\vartheta}+\mathbf{u}_{m\omega}\right) \tag{G.8}$$

using (7.2), (7.3) and the multi-scale expansion for the vortical component of the flow (i.e., $\boldsymbol{\omega}_{\zeta}\sim\boldsymbol{\omega}_{\zeta 0}\left(\mathbf{x},\xi,t\right)+M_{b}\boldsymbol{\omega}_{\zeta\mu}\left(\mathbf{x},\xi,t\right)+...$), we have

$$\mathbf{n}\cdot\mathscr{L}_{u0}\left(p_{m0},\mathbf{u}_{m0}\right)+M_{b}\mathbf{n}\cdot\left(\mathscr{L}_{u0}\left(p_{m\mu},\mathbf{u}_{m\mu}\right)+\mathscr{L}_{u\mu}\left(\mathbf{U},p_{m0},\mathbf{u}_{m0}\right)\right)+...=ik_{m0}\mathbf{n}\cdot\left(M_{b}\mathbf{u}_{m\vartheta\mu}+\mathbf{u}_{m\omega 0}\right)+... \tag{G.9}$$

Note that unlike $\mathbf{n}\cdot\mathbf{u}_{m\vartheta 0}$, which is taken to satisfy the no-through condition, $\mathbf{n}\cdot\mathbf{u}_{m\omega 0}$ is non-zero but does scale as $O\left(M_{b}\right)$ (cf. (7.22)). Collecting terms of $O\left(M_{b}\right)$ in (G.9), we find

$$\mathbf{n}\cdot\left(\mathscr{L}_{u0}\left(p_{m\mu},\mathbf{u}_{m\mu}\right)+\mathscr{L}_{u\mu}\left(\mathbf{U},p_{m0},\mathbf{u}_{m0}\right)\right)=ik_{m0}\mathbf{n}\cdot\left(\mathbf{u}_{m\vartheta\mu}+M_{b}^{-1}\mathbf{u}_{m\omega 0}\right) \tag{G.10}$$

Now substituting this into (G.7), we obtain the desired result (G.3).

G.3 To solve for the $O\left(M_{b}\right)$ perturbations

$$\begin{bmatrix}\mathscr{L}_{p0}\left(p_{m\mu},\vartheta_{m\mu}\right)\\ \mathscr{L}_{\vartheta 0}\left(p_{m\mu},\vartheta_{m\mu}\right)\end{bmatrix}+\begin{bmatrix}\mathscr{L}_{p\mu}\left(\mathbf{U},p_{m0},\mathbf{u}_{m0}\right)\\ \mathscr{L}_{\vartheta\mu}\left(\mathbf{U},p_{m0},\mathbf{u}_{m0}\right)\end{bmatrix}=ik_{m0}\begin{bmatrix}p_{m\mu}\\ \vartheta_{m\mu}\end{bmatrix}+ik_{m\mu}\begin{bmatrix}p_{m0}\\ \vartheta_{m0}\end{bmatrix} \tag{G.11}$$

we multiply the first equation by $p_{j0}^{\dagger *}$, the second equation by $\varphi_{j0}^{\dagger *}$, and then integrate both over the domain. We then substitute in a series expansion in terms of the leading order mode shapes, i.e.,

$$p_{m\mu}=\sum_{\substack{k=1,\\ k\neq m}}^{\infty}\alpha_{mk\mu}^{p}p_{k0},\quad \vartheta_{m\mu}=\sum_{\substack{k=1,\\ k\neq m}}^{\infty}\alpha_{mk\mu}^{\vartheta}\vartheta_{k0} \tag{G.12}$$

and use the fact that $\varphi_{m0}^{\dagger}=ik_{m0}^{-1}p_{m0}^{\dagger}$, $\varphi_{m0}=-ik_{m0}^{-1}p_{m0}$ and $\varphi_{m0}^{\dagger *}\vartheta_{m0}=p_{m0}^{\dagger *}p_{m0}$, to obtain

$$\begin{aligned}k_{m0}\alpha_{m\,j\mu}^{p}-k_{j0}\alpha_{m\,j\mu}^{\vartheta}&=\tfrac{1}{iE_{j0}^{2}}\int\mathscr{L}_{p\mu}\left(\mathbf{U},p_{m0},\mathbf{u}_{m0}\right)p_{j0}^{\dagger *}dV\\ k_{m0}\alpha_{m\,j\mu}^{\vartheta}-k_{j0}\alpha_{m\,j\mu}^{p}&=\tfrac{1}{iE_{j0}^{2}}\left(ik_{m0}\oint\varphi_{j0}^{\dagger *}\mathbf{n}\cdot\left(\mathbf{u}_{m\vartheta\mu}+M_{b}^{-1}\mathbf{u}_{m\omega 0}\right)dS-\int\mathscr{L}_{u\mu}\left(\mathbf{U},p_{m0},\mathbf{u}_{m0}\right)\cdot\nabla\varphi_{j0}^{\dagger *}dV\right)\end{aligned} \tag{G.13}$$

when $j\neq m$. Expressions for the coefficients $\alpha_{mk\mu}^{p}$ and $\alpha_{mk\mu}^{\vartheta}$ follow by taking linear combinations of the above. We have

$$\alpha_{m\,j\mu}^{p}=\frac{k_{j0}}{i\left(k_{m0}^{2}-k_{j0}^{2}\right)E_{j0}^{2}}\begin{pmatrix}ik_{m0}\oint\varphi_{j0}^{\dagger *}\mathbf{n}\cdot\left(\mathbf{u}_{m\vartheta\mu}+M_{b}^{-1}\mathbf{u}_{m\omega 0}\right)dS-\int\mathscr{L}_{u\mu}\left(\mathbf{U},p_{m0},\mathbf{u}_{m0}\right)\cdot\nabla\varphi_{j0}^{\dagger *}dV+\\ +\frac{k_{m0}}{k_{j0}}\int\mathscr{L}_{p\mu}\left(\mathbf{U},p_{m0},\mathbf{u}_{m0}\right)p_{j0}^{\dagger *}dV\end{pmatrix} \tag{G.14}$$

and

$$\alpha^{\vartheta}_{m\,j\mu}=\frac{k_{m0}}{i\left(k_{m0}^2-k_{j0}^2\right)E_{j0}^2}\begin{pmatrix} ik_{m0}\oint\varphi^{\dagger *}_{j0}\mathbf{n}\cdot\left(\mathbf{u}_{m\vartheta\mu}+M_b^{-1}\mathbf{u}_{m\omega 0}\right)dS-\int\mathscr{L}_{u\mu}\left(\mathbf{U},p_{m0},\mathbf{u}_{m0}\right)\cdot\nabla\varphi^{\dagger *}_{j0}dV+\\ +\frac{k_{j0}}{k_{m0}}\int\mathscr{L}_{p\mu}\left(\mathbf{U},p_{m0},\mathbf{u}_{m0}\right)p^{\dagger *}_{j0}dV\end{pmatrix} \tag{G.15}$$

Adjoint Problem

A simple way to derive an expression for the perturbations to the adjoint mode shapes is to use the bi-orthogonality condition, i.e.,

$$\int\left(p^{\dagger *}_{j}p_m+\varphi^{\dagger *}_{j}\vartheta_m\right)dV=\begin{pmatrix}\int\left(p^{\dagger *}_{j0}p_{m0}+\varphi^{\dagger *}_{j0}\vartheta_{m0}\right)dV+\\ +M_b\int\left(p^{\dagger *}_{j0}p_{m\mu}+p^{\dagger *}_{j\mu}p_{m0}+\varphi^{\dagger *}_{j0}\vartheta_{m\mu}+\varphi^{\dagger *}_{j\mu}\vartheta_{m0}\right)dV\end{pmatrix}+\ldots=0 \tag{G.16}$$

when $j\neq m$. To ensure that this is satisfied, we set $\int p^{\dagger *}_{j0}p_{m\mu}dV=-\int p^{\dagger *}_{j\mu}p_{m0}dV$ and $\int\varphi^{\dagger *}_{j0}\vartheta_{m\mu}dV=-\int\varphi^{\dagger *}_{j\mu}\vartheta_{m0}dV$. It follows that

$$p^{\dagger}_{m\mu}=-\sum_{\substack{k=1,\\ k\neq m}}^{\infty}\frac{E_{m0}^2}{E_{k0}^2}\alpha^{p^*}_{k\,m\mu}\,p^{\dagger}_{k0},\quad \varphi^{\dagger}_{m\mu}=-\sum_{\substack{k=1,\\ k\neq m}}^{\infty}\frac{E_{m0}^2}{E_{k0}^2}\alpha^{\vartheta^*}_{k\,m\mu}\varphi^{\dagger}_{k0} \tag{G.17}$$

where $\alpha^{p}_{mk\mu}$ and $\alpha^{\vartheta}_{mk\mu}$ are given by (G.14) and (G.15), respectively.

G.4 *Steady Flow*

Following Berman (1953) and White (1962), we use here a similarity approach to solve for the steady incompressible flow within a cylindrical, uniformly porous tube—this is a commonly used model for the flow field inside a solid rocket motor with a cylindrical propellant grain[†]. That no new contributions are presently made should be emphasized.

We begin by considering the boundary conditions that constrain the flow:

$$\begin{gathered}U_r=0,\quad \partial U_z/\partial r=0\quad\text{at}\quad r=0\\ U_r=-1,\quad U_z=0\quad\text{at}\quad r=1\end{gathered} \tag{G.18}$$

If the endwall is taken to be non-burning, a global mass balance yields $\bar{U}_z(z)=2z$, where the overbar denotes a cross-sectional average, defined by

$$\bar{U}_z(z)=\frac{1}{A}\int_{r=0}^{1}2\pi rU_z\,dr=\frac{2}{\pi}\int_{\lambda=0}^{\pi/2}U_z\,d\lambda=2z \tag{G.19}$$

[†] Given the fine line between mathematical intractability and physical irrelevance, it is worth considering why this is a good description. First, even though the flame zone is characterized by complex chemistry and multiphase flow effects, the distance over which the propellant burns is on the order of millimeters—a scale that pales in comparison with other dimensions of the chamber. Thus, approximating the reacting surface by a transpiring one is a valid simplification of the description. Second, while gases generated by combustion processes are accelerated through the nozzle to supersonic speeds, compressibility effects only dominate in the aft end of a motor. Thus, the incompressible approximation is valid for the bulk of the chamber, especially when the slenderness ratio L/R is large compared with unity.

with $\lambda = \pi r^2/2$. This motivates the following ansatz $U_z = \pi z f'(\lambda)$, which satisfies (G.19) provided that $f(\pi/2) = 1$ and $f(0) = 0$. The equation of continuity $r^{-1}\partial(rU_r)/\partial r + \partial U_z/\partial z = 0$ then gives $rU_r = -f(\lambda)$, which allows us to solve for the stream function $\Psi = z f(\lambda)$ and the azimuthal component of the vorticity $\Omega_\theta/r = -\pi^2 z f''(\lambda)$.

Now substituting the above solution into the azimuthal component of the vorticity transport equation $\mathbf{e}_\theta \cdot \nabla \times (\mathbf{\Omega} \times \mathbf{U}) = \mathrm{Re}_\omega^{-1}\, \mathbf{e}_\theta \cdot \nabla^2 \mathbf{\Omega}$, derives a nonlinear ODE of the form

$$f' f'' - f f''' = \frac{2}{M_b \,\mathrm{Re}_\omega}\left(\lambda f^{iv} + 2 f'''\right) \tag{G.20}$$

for the unknown function f, subject to the following constraints:

$$\begin{gathered} \lim_{\lambda\to 0} f(\lambda)/\sqrt{\lambda} = 0, \quad \lim_{\lambda\to 0} \sqrt{\lambda} f'' = 0 \\ f = 1, \quad f' = 0 \quad \text{at} \quad \lambda = \pi/2 \end{gathered} \tag{G.21}$$

This constitutes an exact *self-similar* description of the steady incompressible flow field within a cylindrical, uniformly porous tube.

In solving (G.20), a small parameter multiplying the highest order derivative ordinarily implies the existence of some form of *boundary layer*. However, there is no mechanism to hold such a layer steadily in place against the convective effect of fluid injected through the boundary (Proudman 1960). Thus, the inviscid solution, which is governed by an equation of lower order

$$f' f'' - f f''' = 0 \tag{G.22}$$

must satisfy all the original boundary conditions; viscosity, in other words, has a negligible effect on the steady flow. The *laminar* analyses of Taylor (1956), Culick (1966) and others also recovered this same *inviscid rotational* result:

$$rU_r = -f(\lambda), \quad U_z = \pi z f'(\lambda), \quad \Psi = z f(\lambda), \quad \Omega_\theta/r = -\pi^2 z f''(\lambda) \tag{G.23}$$

where $f(\lambda) = \sin\lambda$.

Comparing (G.23) with his own experimental data, Taylor (1956) noted the *striking* agreement. More recently, Dunlap et al. (1974) have experimentally confirmed the adequacy of this flow description in the upstream region of a cylindrical chamber with porous wall. Numerical simulations (Vuillot and Avalon 1991)—both inviscid and viscous steady-state—with an exit Mach number of 0.10, are also in agreement.

Unsteady Flow

We now solve for the unsteady vorticity field that induces on the boundary a fluid motion equal and opposite that which accompanies the *leading order* acoustic field. Closed form solutions are generally too difficult to construct, except for simple geometries—here we consider the case of a cylindrical

propellant grain. Thus, we have that $p_0 = J_n\left(k_{ns} r\right)\cos\left(k_l z\right)e^{-i\left(k_{m0} t + \iota n\theta\right)}$, where $k_{m0} \equiv \sqrt{k_{ns}^2 + k_l^2}$ with $k_l = l\pi R/L$ proportional to the chamber radius-to-length ratio and k_{ns} the roots of the derivative of the Bessel function, i.e., $dJ_n\left(k_{ns} r\right)/dr\big|_{r=1} = 0$. Note that a traveling wave representation in the azimuthal direction is assumed; $\iota = \pm 1$ for right– and leftward traveling waves—the behavior for a standing wave follows from superposition.

Recall from §7.2 that a *two-scale* expansion for $\boldsymbol{\omega}_\varsigma \sim \boldsymbol{\omega}_{\varsigma 0}\left(\mathbf{x},\xi,t\right) + M_b \boldsymbol{\omega}_{\varsigma 1}\left(\mathbf{x},\xi,t\right) + \ldots$ is sought, where $\boldsymbol{\omega}_{\varsigma 0}\left(\mathbf{x},\xi,t\right) = \boldsymbol{\omega}_{\varsigma 0}^n\left(\mathbf{x}\right)e^{-ik_{m0}\left(t-\xi\right)}$. The objective here is to determine the unknown function $\boldsymbol{\omega}_{\varsigma 0}^n\left(\mathbf{x}\right)$ of the *original* spatial scales by suppressing secular terms at higher order. The correspondence between the normal-tangential coordinate framework used earlier and cylindrical polar coordinates is given by $\left(n,\boldsymbol{\varsigma}\right) = \left(r,\theta,z\right)$. Thus $\boldsymbol{\omega}_\varsigma = \omega_\theta \mathbf{e}_\theta + \omega_z \mathbf{e}_z$ with

$$\omega_{\theta 0}\left(\mathbf{x},\xi,t\right) = \omega_{\theta 0}^r\left(\mathbf{x}\right)e^{-ik_{m0}\left(t-\xi\right)}, \quad \omega_{z0}\left(\mathbf{x},\xi,t\right) = \omega_{z0}^r\left(\mathbf{x}\right)e^{-ik_{m0}\left(t-\xi\right)} \tag{G.24}$$

In terms of the behavior on the boundary, since the tangent gradient operator is now

$$\left(\mathbf{n}\times\nabla\right) f = -\frac{\partial f}{\partial z}\mathbf{u}_\theta + \frac{1}{r}\frac{\partial f}{\partial \theta}\mathbf{u}_z \tag{G.25}$$

it follows from (7.10) that

$$\omega_{\theta 0}\big|_{boundary} = -\frac{1}{M_b}\frac{\partial p_0}{\partial z} \sim O\left(k_l/M_b\right), \quad \omega_{z0}\big|_{boundary} = \frac{1}{M_b}\frac{\partial p_0}{\partial \theta} \sim O\left(1/M_b\right) \tag{G.26}$$

While Flandro (1995 a) derived the formula on the left, and offered the interpretation that when acoustic waves are parallel to the combustion zone a fluctuating pressure gradient acts across the incoming flow streamlines, the difference here—apart from the way in which the problem is formulated—is that the pressure is no longer assumed to be purely axial.

From (7.21), the tangent components of velocity are given by

$$u_{\omega\theta 0}\left(\mathbf{x},\xi,t\right) = \underbrace{-i\left(M_b/k_{m0}\right)U_r\,\omega_{z0}^r\left(\mathbf{x}\right)}_{u_{\omega\theta 0}^r\left(\mathbf{x}\right)}e^{-ik_{m0}\left(t-\xi\right)}, \quad u_{\omega z0}\left(\mathbf{x},\xi,t\right) = \underbrace{i\left(M_b/k_{m0}\right)U_r\,\omega_{\theta 0}^r\left(\mathbf{x}\right)}_{u_{\omega z0}^r\left(\mathbf{x}\right)}e^{-ik_{m0}\left(t-\xi\right)} \tag{G.27}$$

and from (7.22) the radial velocity is

$$u_{\omega r0}\left(\mathbf{x},\xi,t\right) = \underbrace{\left(M_b/k_{m0}\right)^2 U_r^2\left(r^{-1}\partial\omega_{z0}^r\left(\mathbf{x}\right)/\partial\theta - \partial\omega_{\theta 0}^r\left(\mathbf{x}\right)/\partial z\right)}_{u_{\omega r0}^r\left(\mathbf{x}\right)}e^{-ik_{m0}\left(t-\xi\right)} \tag{G.28}$$

Since only $\boldsymbol{\omega}^r_{\zeta 0}(\mathbf{x})$ needs to be determined, we begin with the tangent component of the vorticity transport equation (7.13)[†],

$$\frac{\partial \boldsymbol{\omega}_\zeta}{\partial t} + M_b \left(\begin{array}{c} \left(U_r \dfrac{\partial \boldsymbol{\omega}_\zeta}{\partial r} + U_z \dfrac{\partial \boldsymbol{\omega}_\zeta}{\partial z} \right) - \left(\omega_z \dfrac{\partial U_z}{\partial z} + \Omega_\theta \dfrac{\partial u_\theta}{\partial z} \right) \mathbf{e}_z + \\ + \left(- \dfrac{U_r \omega_\theta}{r} + u_r \dfrac{\partial \Omega_\theta}{\partial r} + u_z \dfrac{\partial \Omega_\theta}{\partial z} - \dfrac{u_r \Omega_\theta}{r} - \dfrac{\Omega_\theta}{r} \dfrac{\partial u_\theta}{\partial \theta} + \mathcal{G} \Omega_\theta \right) \mathbf{e}_\theta \end{array} \right) = \frac{1}{\mathrm{Re}_\omega} \left(\nabla^2 \boldsymbol{\omega} \right)_\zeta \qquad \text{(G.29)}$$

By introducing the multiple radial length scales $\partial/\partial r = \left(M_b U_r \right)^{-1} \partial/\partial \xi + \partial/\partial r$, we obtain

$$\frac{\partial \boldsymbol{\omega}_\zeta}{\partial t} + \frac{\partial \boldsymbol{\omega}_\zeta}{\partial \xi} = -M_b \left(\begin{array}{c} \left(U_r \dfrac{\partial \boldsymbol{\omega}_\zeta}{\partial r} + U_z \dfrac{\partial \boldsymbol{\omega}_\zeta}{\partial z} - \dfrac{1}{\delta k_{m0}^2} \dfrac{1}{U_r^2} \dfrac{\partial^2 \boldsymbol{\omega}_\zeta}{\partial \xi^2} \right) - \left(\omega_z \dfrac{\partial U_z}{\partial z} + \Omega_\theta \dfrac{\partial u_\theta}{\partial z} \right) \mathbf{e}_z + \\ + \left(- \dfrac{U_r \omega_\theta}{r} + u_r \dfrac{\partial \Omega_\theta}{\partial r} + u_z \dfrac{\partial \Omega_\theta}{\partial z} - \dfrac{u_r \Omega_\theta}{r} - \dfrac{\Omega_\theta}{r} \dfrac{\partial u_\theta}{\partial \theta} + \mathcal{G} \Omega_\theta \right) \mathbf{e}_\theta \end{array} \right) \qquad \text{(G.30)}$$

A few remarks are in order here. First, note that $\xi(r) = M_b^{-1} \int_1^r U_r^{-1} dr$; while this can be evaluated explicitly[‡], it should be emphasized that expressing the unsteady solution in terms of integrals of the steady flow is more general, since different representations of the latter can then be incorporated. Second, **U** has no functional dependence on ξ and thus is unaffected by the above transformation. Finally, only the dominant viscous term is retained, i.e., $\nabla^2 \sim \left(M_b^2 U_r^2 \right)^{-1} \partial^2/\partial \xi^2 + O\left(M_b^{-1} \right)$, with $\delta \equiv M_b^3 \, \mathrm{Re}_\omega / k_{m0}^2$ being a measure of the *damping*.

In solving (G.30), recall that a *two-scale* expansion for $\boldsymbol{\omega}_\zeta$ of the form $\boldsymbol{\omega}_\zeta \sim \boldsymbol{\omega}_{\zeta 0}(\mathbf{x}, \xi, t) + M_b \boldsymbol{\omega}_{\zeta 1}(\mathbf{x}, \xi, t) + \ldots$ is sought, where $\boldsymbol{\omega}_{\zeta 0}(\mathbf{x}, \xi, t) = \boldsymbol{\omega}^r_{\zeta 0}(\mathbf{x}) e^{-i k_{m0}(t - \xi)}$. The objective here is to determine the unknown function $\boldsymbol{\omega}^r_{\zeta 0}(\mathbf{x})$ of the *original* spatial scales by suppressing secular terms at higher order. Without substituting and carrying out the details, it should be apparent that the right-hand side of (G.30) represents the forcing of $\boldsymbol{\omega}_{\zeta 1}$; those effects that lead to secular behavior need to be identified.

With exception of the diffusive contribution, the $O(M_b)$ forcing terms in (G.30) are composed of the product of a steady with an unsteady flow component—only when this combination exhibits a dependence on ξ, does the *possibility* of secularity arise. By such arguments, acoustic/mean flow interactions clearly do not require suppression. The same does not hold true for thermal motions induced by entropy fluctuations, since such motions are also carried along by the steady flow; however, the magnitude of $\mathbf{u}_{s0}$ is negligible (cf. §7.3). Essentially then, it is the interaction between the unsteady

---

[†] Some terms have been recast. In particular, we set $\omega_r \left(\partial U_z / \partial r \right) + \left(\Omega_\theta / r \right) \left(\partial u_z / \partial \theta \right) = \Omega_\theta \left(\partial u_\theta / \partial z \right)$. This follows simply from the definition of vorticity, since $\omega_r = r^{-1} \partial u_{\omega z} / \partial \theta - \partial u_{\omega \theta} / \partial z$ and $\Omega_\theta = -\partial U_z / \partial r$ (recall that $U_r \neq U_r(z)$).

[‡] Using the steady flow model derived earlier, we have $\xi(\lambda) = -(\pi M_b)^{-1} \ln \tan(\lambda/2)$ with $\lambda = \pi r^2 / 2$.

vorticity field and the steady flow that leads to secular behavior; if not suppressed, $\boldsymbol{\omega}_{\zeta 1}$ would grow without bound—a reality not reflected by the physics of the problem.

Axial Component of Vorticity

Consider first the axial component of (G.30). Suppressing secular terms leads to an equation for $\omega^r_{z0}(r,\theta,z)$:

$$U_r\frac{\partial\omega^r_{z0}}{\partial r}+U_z\frac{\partial\omega^r_{z0}}{\partial z}+\frac{1}{\delta}\frac{1}{U_r^2}\omega^r_{z0}-\omega^r_{z0}\frac{\partial U_z}{\partial z}-\Omega_\theta\frac{\partial u^r_{\omega\theta 0}}{\partial z}=0 \tag{G.31}$$

Some simplifications are possible here. First, since $\mathbf{U}$ is divergence free, we can recast $\partial U_z/\partial z$ as $-r^{-1}\partial(rU_r)/\partial r$, and thus combine the first and fourth terms. Second, since $u^r_{\omega\theta 0}=-i(M_b/k_{m0})U_r\,\omega^r_{z0}$ the last term is at least an $O(M_b)$ smaller than the others and can therefore be omitted from further consideration—in other words, vorticity stretching and tilting effects do not significantly modify the axial vorticity distribution. After introducing these simplifications, we have

$$U_r\frac{\partial(rU_r\omega^r_{z0})}{\partial r}+U_z\frac{\partial(rU_r\omega^r_{z0})}{\partial z}+\frac{1}{\delta}\frac{1}{U_r^2}(rU_r\omega^r_{z0})\sim 0 \tag{G.32}$$

Now a simple way to solve (G.32) for $\omega^r_{z0}(r,\theta,z)$ is by introducing a Von Mises' like transformation. By changing dependent variables from (r,z) to (r,Ψ), where Ψ is the mean flow streamfunction,

$$\frac{\partial}{\partial r}=\frac{\partial}{\partial r}+rU_z\frac{\partial}{\partial\Psi},\quad \frac{\partial}{\partial z}=-rU_r\frac{\partial}{\partial\Psi} \tag{G.33}$$

the convective operator $U_r\partial/\partial r+U_z\partial/\partial z$ becomes $U_r\partial/\partial r$; ω^r_{z0} is then readily found from simple quadrature

$$\omega^r_{z0}(r,\theta,\Psi)=-\frac{1}{rU_r}e^{\phi(r)}\omega^r_{z0}(1,\theta,\Psi) \tag{G.34}$$

Note that the function $\phi(r)\equiv-\delta^{-1}\int_1^r U_r^{-3}dr$ represents the effects of viscous damping and is evaluated explicitly below†. Since U_r is directed inwards ($\phi(r)\ge 0$) and tends to zero as $r\to 0$, it follows that viscous effects become increasingly more important as the chamber axis of symmetry is approached.

---

† Using the steady flow model derived earlier, we have

$$\phi(\lambda)=-\frac{1}{\pi^2}\frac{1}{\delta}\left(\frac{\lambda\cos\lambda}{\sin\lambda}-\left(1-\frac{1}{\sin\lambda}\right)-\int_{\pi/2}^{\lambda}\frac{\sigma}{\sin\sigma}d\sigma\right)$$

where following Flandro (1995 b) the last integral can be approximated by a series expansion:

$$\int_{\pi/2}^{\lambda}\frac{\sigma}{\sin\sigma}d\sigma\sim -2\,\text{Catalan}+\lambda+\tfrac{1}{18}\lambda^3+\tfrac{7}{1800}\lambda^5+\tfrac{31}{105840}\lambda^7+\ldots,\quad \text{Catalan}\sim 0.915966$$

On the boundary, we have from (G.26) that

$$\omega_{z0}^{r}\left(1,\theta,\Psi\right)=-\frac{1}{M_b}in J_n\left(k_{ns}\right)\cos\left(k_l\Psi\right)e^{-in\theta} \tag{G.35}$$

Azimuthal Component of Vorticity

Having determined one component of $\boldsymbol{\omega}_{\zeta 0}^{r}\left(\mathbf{x}\right)$ it remains to determine the other. Suppressing secular terms in the azimuthal component of (G.30) leads to an equation for $\omega_{z0}^{r}\left(r,\theta,z\right)$:

$$U_r\frac{\partial\left(\omega_{\theta 0}^{r}/r\right)}{\partial r}+U_z\frac{\partial\left(\omega_{\theta 0}^{r}/r\right)}{\partial z}+\frac{1}{\delta}\frac{1}{U_r^2}\left(\omega_{\theta 0}^{r}/r\right)\sim\frac{\left(\Omega_\theta/r\right)}{r}\frac{\partial u_{\omega\theta 0}^{r}}{\partial\theta} \tag{G.36}$$

where only the significant terms have been retained†. Since $u_{\omega\theta 0}^{r}=-i\left(M_b/k_{m0}\right)U_r\,\omega_{z0}^{r}$ is known, it can be treated as a forcing. Solving (G.36) is not especially difficult; the procedure follows the earlier strategy, except a particular solution is now also needed. The result is

$$\omega_{\theta 0}^{r}\left(r,\theta,\Psi\right)=re^{\phi(r)}\left(\omega_{\theta 0}^{r}\left(1,\theta,\Psi\right)+i\left(M_b/k_{m0}\right)\left(\Omega_\theta/r\right)\chi\left(r\right)\frac{\partial\omega_{z0}^{r}\left(1,\theta,\Psi\right)}{\partial\theta}\right) \tag{G.37}$$

where $\chi\left(r\right)\equiv\int_1^r\left(r^2U_r\right)^{-1}dr$ and the behavior of $\omega_{\theta 0}^{r}\left(r,\theta,\Psi\right)$ on the boundary follows from (G.26),

$$\omega_{\theta 0}^{r}\left(1,\theta,\Psi\right)=\frac{k_l}{M_b}J_n\left(k_{ns}\right)\sin\left(k_l\Psi\right)e^{-in\theta} \tag{G.38}$$

Thus unlike ω_{z0}, *two* sources of azimuthal vorticity exist: acoustic coupling on the boundary, as evidenced by the first term, and stretching of the mean vorticity by the azimuthal component of the rotational velocity, as indicated by the second. To help assess the importance of the latter, we substitute into (G.37) the expressions for $\omega_{\theta 0}^{r}\left(1,\theta,\Psi\right)$ and $\omega_{z0}^{r}\left(1,\theta,\Psi\right)$ from (G.38) and (G.35) respectively,

$$\omega_{\theta 0}^{r}\left(r,\theta,\Psi\right)=\frac{k_l}{M_b}J_n\left(k_{ns}\right)re^{\phi(r)}\left(\sin\left(k_l\Psi\right)-iM_b\pi^2\left(k_{m0}/k_l\right)\left(n/k_{m0}\right)^2\chi\left(r\right)\Psi\cos\left(k_l\Psi\right)\right)e^{-in\theta} \tag{G.39}$$

† With all the terms retained, we have

$$U_r\frac{\partial\left(\omega_{\theta 0}^{r}/r\right)}{\partial r}+U_z\frac{\partial\left(\omega_{\theta 0}^{r}/r\right)}{\partial z}+\frac{1}{\delta}\frac{1}{U_r^2}\left(\omega_{\theta 0}^{r}/r\right)+u_{\omega r0}^{r}\frac{\partial\left(\Omega_\theta/r\right)}{\partial r}+u_{\omega z0}^{r}\frac{\partial\left(\Omega_\theta/r\right)}{\partial z}-\frac{\left(\Omega_\theta/r\right)}{r}\frac{\partial u_{\omega\theta 0}^{r}}{\partial\theta}=0$$

However, some terms can be omitted owing to their negligible contribution. For example, consider the fifth term; this describes the convection of the steady vorticity by the axial component of the unsteady vortical velocity. We can assess the order of magnitude of this effect, by first recalling that since Ω_θ is proportional to z, the axial derivative removes this dependence and thus the possibility of having to multiply by the chamber length-to-radius ratio. Then, because $u_{\omega z0}^{r}=i\left(M_b/k_{m0}\right)U_r\,\omega_{\theta 0}^{r}$ (cf. (G.27)) is $O\left(M_b\right)$ smaller than $\omega_{\theta 0}^{r}$, the effect is negligible in comparison with the complementary physics, i.e., the convection of the unsteady vorticity by the steady velocity. Similar arguments show that the fourth term contributes even less.

where we used the fact that $\Omega_\theta / r = \pi^2 \Psi$. Since, the steady flow stream function is proportional to the streamwise coordinate, i.e., $\Psi \propto (L/R)(z^*/L)$, with the superscript * used here to denote a dimensional quantity, vis-à-vis the first term in the parenthesis, whose maximum value is unity, the second term effectively scales as $O\left(M_b (L/R)^2\right)$.

Having solved for $\boldsymbol{\omega}^r_{\zeta 0}(\mathbf{x})$, the solution is complete. To help visualize the results, we consider two limiting cases. Absent any axial dependence for the acoustic wave, i.e., $(0, n, s)$, we have

$$\omega_{z0} = \frac{1}{M_b} i\, s\, n J_n(k_{ns}) \frac{1}{rU_r} e^{\phi(r)} e^{-i\left(k_{m0}(t-\xi)+\imath n\theta\right)} \tag{G.40}$$

$$u_{\omega\theta 0} = s \frac{n}{k_{m0}} J_n(k_{ns}) \frac{1}{r} e^{\phi(r)} e^{-i\left(k_{m0}(t-\xi)+\imath n\theta\right)}, \quad u_{\omega r 0} \sim M_b \frac{n^2}{k_{m0}^2} J_n(k_{ns}) \frac{1}{r^2} U_r e^{\phi(r)} e^{-i\left(k_{m0}(t-\xi)+\imath n\theta\right)} \tag{G.41}$$

Although $u_{\omega z 0}$ will also be non-zero in this instance—arising solely due to the stretching effect—it scales as $O(M_b)$. Figures G.1 and G.2 illustrate the time sequence for the azimuthal $u_{a\theta 0} + u_{\omega\theta 0}$ and radial $u_{ar0} + u_{\omega r0}$ velocity components when $(0,1,0)$.

The other limiting case is that of a purely axial acoustic wave $(l, 0, 0)$:

$$\omega_{\theta 0} = \frac{k_l}{M_b} r e^{\phi(r)} \sin(k_l \Psi) e^{-i k_{m0}(t-\xi)} \tag{G.42}$$

$$u_{\omega z 0} = i(rU_r) e^{\phi(r)} \sin(k_l \Psi) e^{-i k_{m0}(t-\xi)}, \quad u_{\omega r 0} = M_b \frac{1}{r} (rU_r)^3 e^{\phi(r)} \cos(k_l \Psi) e^{-i k_{m0}(t-\xi)} \tag{G.43}$$

This recovers Flandro's (1995 b) original viscous solution. The behavior of the axial $u_{az0} + u_{\omega z0}$ and radial $u_{\omega r0}$ velocity components when $l = 1$ is shown in Figures G.3 and G.4, respectively.

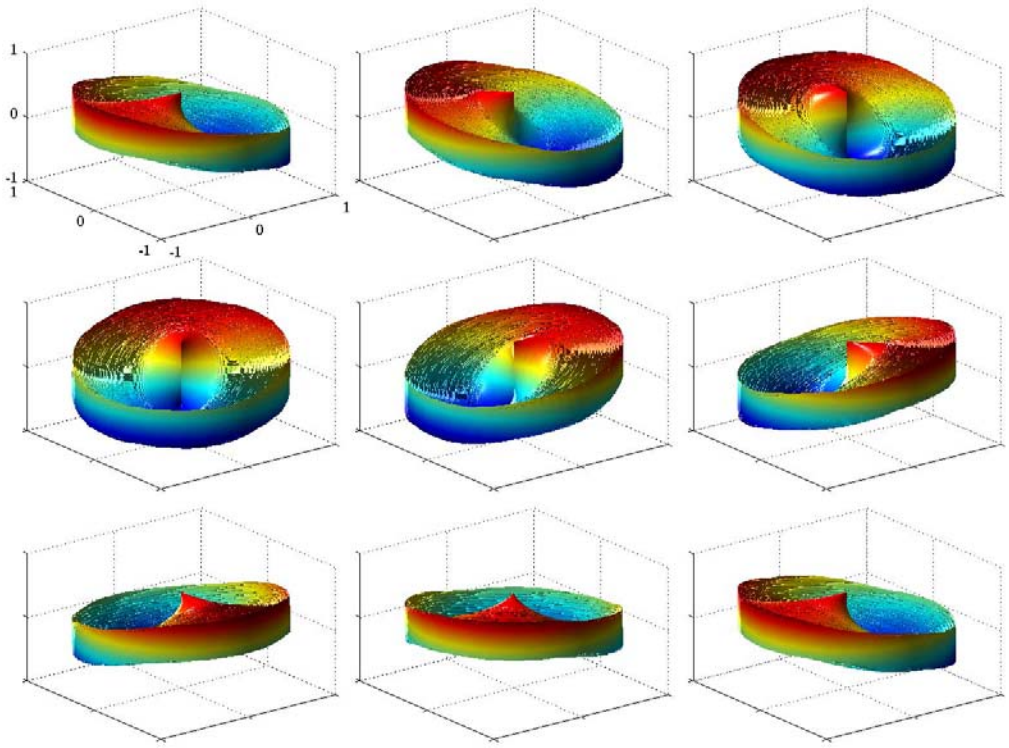

Figure G.1 Time sequence for the azimuthal velocity $u_{a\theta 0} + u_{\omega\theta 0}$ corresponding to the case $(0,1,0)$ for parameters typical of a Tactical Rocket

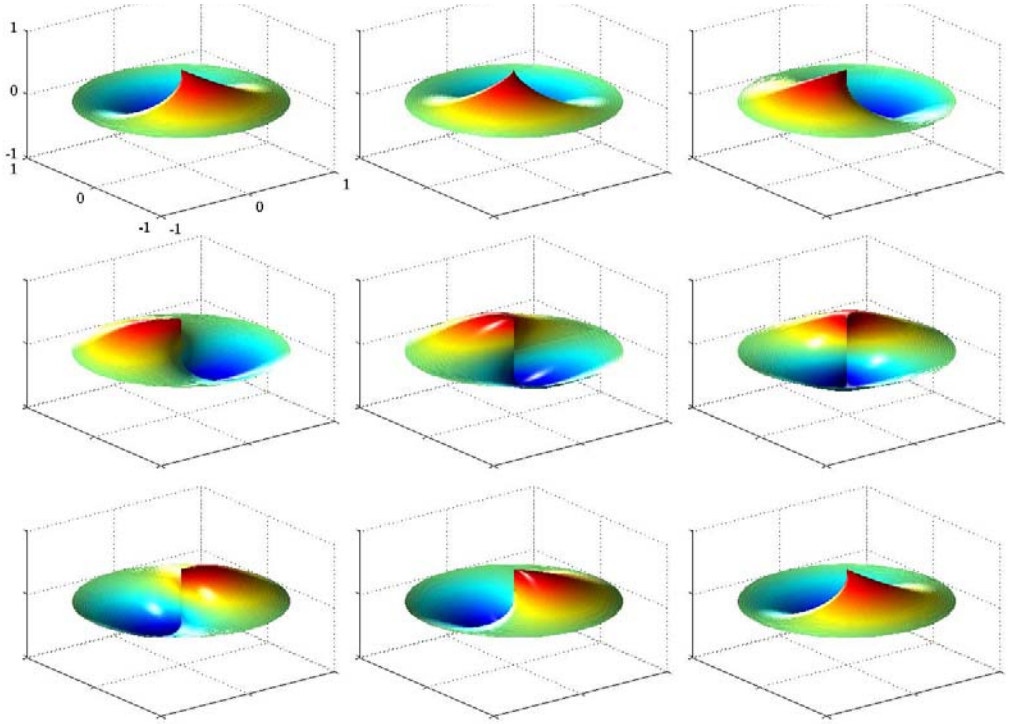

Figure G.2 Time sequence for the radial velocity $u_{ar0} + u_{\omega r0}$ corresponding to the case $(0,1,0)$ for parameters typical of a Tactical Rocket

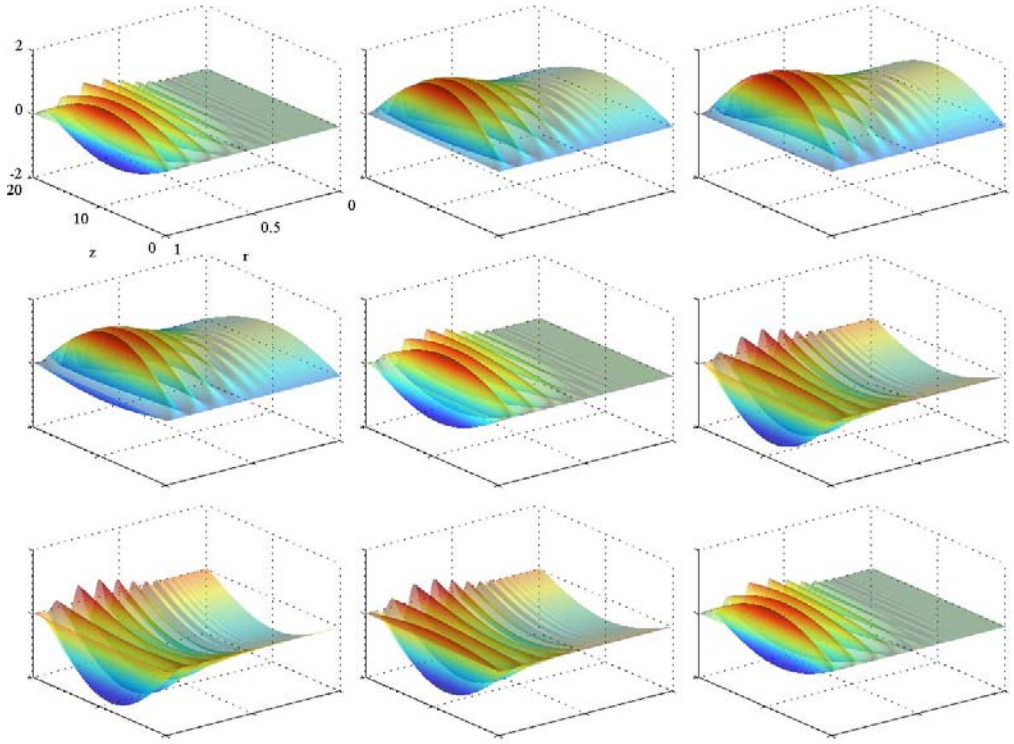

Figure G.3 Time sequence for the axial velocity $u_{az0} + u_{\omega z0}$ corresponding to the case $(1,0,0)$ for parameters typical of a Tactical Rocket

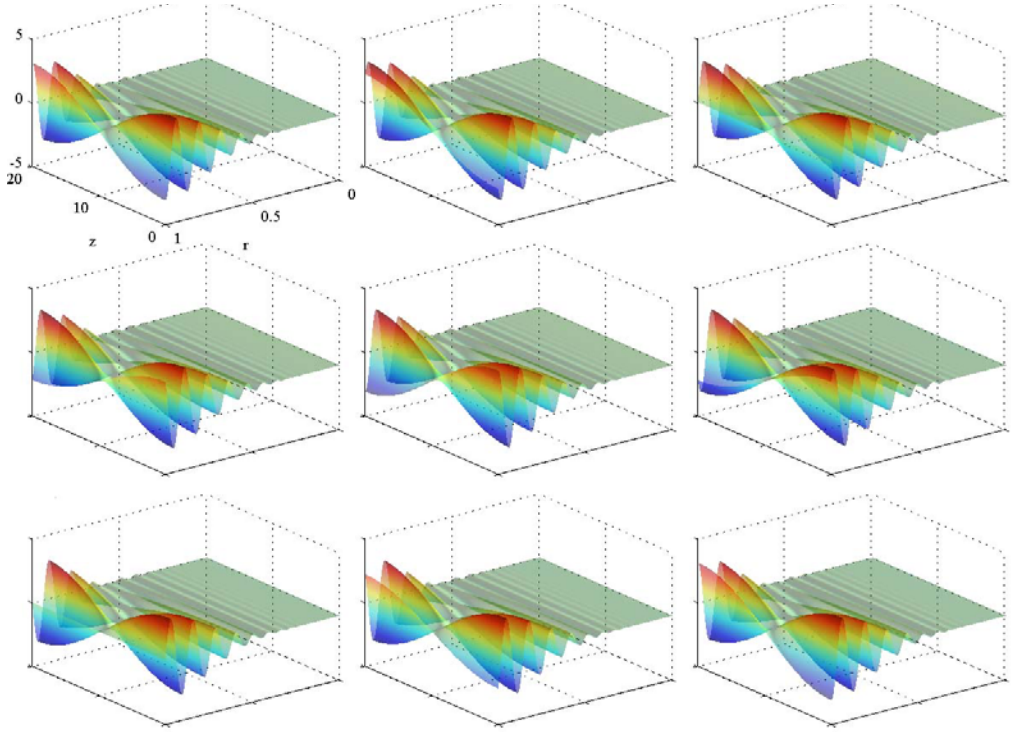

Figure G.4 Time sequence for the radial velocity $u_{\omega r0}$ corresponding to the case $(1,0,0)$ for parameters typical of a Tactical Rocket

H. Calculations for Chapter 8

H.1 We seek here to evaluate the formulas for $k_{m\mu}$, $\alpha^{p}_{m\,j\mu}$ and $\alpha^{\vartheta}_{m\,j\mu}$. Substituting in (7.7), (G.14) and (G.15) for $\mathscr{L}_{p\mu}\left(\mathbf{U}, p_{m0}, \mathbf{u}_{m0}\right)$ and $\mathscr{L}_{u\mu}\left(\mathbf{U}, p_{m0}, \mathbf{u}_{m0}\right)$ from (G.2), we have

$$ik_{m\mu} = -\alpha_{m\mu} - i\theta_{m\mu} = \tfrac{1}{2E^2_{m0}}\left(I^{\omega(m,m)} + I_1^{\vartheta(m,m)} + I^{\vartheta(m,m,1)}\right)$$

$$\alpha^{p}_{m\,j\mu} = \tfrac{k_{j0}}{i\left(k^2_{m0}-k^2_{j0}\right)E^2_{j0}}\left(I^{\omega(m,j)} + I^{\vartheta(m,j,1)}\right), \quad \alpha^{\vartheta}_{m\,j\mu} = \tfrac{k_{m0}}{i\left(k^2_{m0}-k^2_{j0}\right)E^2_{j0}}\left(I^{\omega(m,j)} + I^{\vartheta(m,j,-1)}\right) \tag{H.1}$$

where

$$I^{\omega(m,j)} = ik_{m0}\oint \varphi^{\dagger *}_{j0}\mathbf{n}\cdot M_b^{-1}\mathbf{u}_{m\omega 0}dS - \int\left(\mathbf{U}\cdot\nabla\mathbf{u}_{m\omega 0} + \mathbf{u}_{m\omega 0}\cdot\nabla\mathbf{U}\right)\cdot\nabla\varphi^{\dagger *}_{j0}dV \tag{H.2}$$

and

$$I^{\vartheta(m,j,t)} = ik_{m0}\oint \varphi^{\dagger *}_{j0}\mathbf{n}\cdot\mathbf{u}_{m\vartheta\mu}dS - \int\left(\mathbf{U}\cdot\nabla\mathbf{u}_{m\vartheta 0} + \mathbf{u}_{m\vartheta 0}\cdot\nabla\mathbf{U}\right)\cdot\nabla\varphi^{\dagger *}_{j0}dV + \left(\tfrac{k_{m0}}{k_{j0}}\right)^t\int p^{\dagger *}_{j0}\mathbf{U}\cdot\nabla p_{m0}dV \tag{H.3}$$

Consider those terms that arise owing to vortical flow effects first. To simply $I^{\omega(m,j)}$, we use some results from vector analysis. More specifically, we use $\oint\alpha\mathbf{n}\cdot\nabla\times\mathbf{a}dS = -\oint\mathbf{a}\cdot\left(\mathbf{n}\times\nabla\alpha\right)dS$ to rewrite the first term in (H.2) and[†]:

$$\int\left(\mathbf{U}\cdot\nabla\mathbf{u}_\omega + \mathbf{u}_\omega\cdot\nabla\mathbf{U}\right)\cdot\nabla\alpha\,dV = \oint\left(\mathbf{u}_{\omega\zeta}\cdot\nabla_\zeta\alpha\right)\mathbf{n}\cdot\mathbf{U}dS + \int\mathbf{u}_\omega\cdot\left(\nabla\mathbf{U}\cdot\nabla\alpha + \nabla\alpha\cdot\nabla\mathbf{U} - \boldsymbol{\Omega}\times\nabla\alpha\right)dV \tag{H.4}$$

to rewrite the second term; this gives

$$I^{\omega(m,j)} = \oint\nabla\varphi^{\dagger *}_{j0}\cdot\left(\mathbf{n}\times\tfrac{ik_{m0}}{M_b}\mathbf{A}_{m0} - U_n\mathbf{u}_{m\omega\zeta 0}\right)dS - \int\mathbf{u}_{m\omega 0}\cdot\left(\nabla\mathbf{U}\cdot\nabla\varphi^{\dagger *}_{j0} + \nabla\varphi^{\dagger *}_{j0}\cdot\nabla\mathbf{U} - \boldsymbol{\Omega}\times\nabla\varphi^{\dagger *}_{j0}\right)dV \tag{H.5}$$

Now applying the earlier asymptotic result (7.26), we find that when the flow is laminar, the volume integral in (H.5) scales as the injection Mach number and thus contributes negligibly. The surface integral vanishes as well owing to the behavior on the boundary, cf. (7.23). Therefore, to the order of approximation considered $I^{\omega(m,j)} \sim 0$, which indicates that no *net* contribution exists owing to the effects of vorticity.

[†] Note that

$$\begin{aligned}
&\left(\mathbf{U}\cdot\nabla\mathbf{u}_\omega + \mathbf{u}_\omega\cdot\nabla\mathbf{U}\right)\cdot\nabla\alpha = \\
&\quad = \left(\mathbf{U}\cdot\nabla\left(\mathbf{u}_\omega\cdot\nabla\alpha\right) + \mathbf{u}_\omega\cdot\left(\nabla\mathbf{U}\cdot\nabla\alpha - \mathbf{U}\cdot\nabla\left(\nabla\alpha\right)\right)\right) \\
&\quad = \mathbf{U}\cdot\nabla\left(\mathbf{u}_\omega\cdot\nabla\alpha\right) - \mathbf{u}_\omega\cdot\nabla\left(\mathbf{U}\cdot\nabla\alpha\right) + \mathbf{u}_\omega\cdot\left(\nabla\mathbf{U}\cdot\nabla\alpha + \nabla\alpha\cdot\nabla\mathbf{U} - \boldsymbol{\Omega}\times\nabla\alpha\right) \\
&\quad = \nabla\cdot\left(\left(\mathbf{u}_\omega\cdot\nabla\alpha\right)\mathbf{U} - \left(\mathbf{U}\cdot\nabla\alpha\right)\mathbf{u}_\omega\right) + \mathbf{u}_\omega\cdot\left(\nabla\mathbf{U}\cdot\nabla\alpha + \nabla\alpha\cdot\nabla\mathbf{U} - \boldsymbol{\Omega}\times\nabla\alpha\right)
\end{aligned}$$

where the first step follows from using $\nabla\mathbf{a}\cdot\mathbf{b} = \nabla\left(\mathbf{a}\cdot\mathbf{b}\right) - \nabla\mathbf{b}\cdot\mathbf{a}$ to rewrite some of the terms, the second step from substituting for $\mathbf{U}\cdot\nabla\left(\nabla\alpha\right)$ from $\mathbf{a}\cdot\nabla\mathbf{b} + \mathbf{b}\cdot\nabla\mathbf{a} = \nabla\left(\mathbf{a}\cdot\mathbf{b}\right) + \left(\nabla\times\mathbf{b}\right)\times\mathbf{a} + \left(\nabla\times\mathbf{a}\right)\times\mathbf{b}$ and the third step from using the divergence-free property of both $\mathbf{U}$ and $\mathbf{u}_\omega$. Integrating over the domain, and combing the two surface integrals that arise by using the fact that $\mathbf{U}_\zeta = 0$ on the boundary, gives (H.4).

Turning to $I^{\vartheta(m,j,\iota)}$, we first substitute $\mathbf{U}\cdot\nabla\mathbf{u}_{m\vartheta 0}+\mathbf{u}_{m\vartheta 0}\cdot\nabla\mathbf{U}=\nabla\left(\mathbf{U}\cdot\mathbf{u}_{m\vartheta 0}\right)+\boldsymbol{\Omega}\times\mathbf{u}_{m\vartheta 0}$; this gives

$$I^{\vartheta(m,j,\iota)}=ik_{m0}\oint\varphi_{j0}^{\dagger *}\mathbf{n}\cdot\mathbf{u}_{m\vartheta\mu}dS+\int\vartheta_{j0}^{\dagger *}\mathbf{U}\cdot\mathbf{u}_{m\vartheta 0}dV-\int\boldsymbol{\Omega}\cdot\left(\mathbf{u}_{m\vartheta 0}\times\nabla\varphi_{j0}^{\dagger *}\right)dV+\left(\tfrac{k_{m0}}{k_{j0}}\right)^{\iota}\int p_{j0}^{\dagger *}\mathbf{U}\cdot\nabla p_{m0}dV \quad \text{(H.6)}$$

Now introducing the leading order solution for the acoustic field from §C.1, we have

$$I^{\vartheta(m,j,\iota)}=\tfrac{k_{m0}}{k_{j0}}\oint p_{j0}\mathbf{n}\cdot\mathbf{u}_{m\vartheta\mu}dS+\left(\tfrac{k_{j0}}{k_{m0}}+\left(\tfrac{k_{m0}}{k_{j0}}\right)^{\iota}\right)\int p_{j0}\mathbf{U}\cdot\nabla p_{m0}dV+\tfrac{1}{k_{j0}k_{m0}}\int\boldsymbol{\Omega}\cdot\left(\nabla p_{m0}\times\nabla p_{j0}\right)dV \quad \text{(H.7)}$$

Note that when $j=m$ and $\iota=1$, this result simplifies to

$$I^{\vartheta(m,m,1)}=\oint p_{m0}\mathbf{n}\cdot\mathbf{u}_{m\vartheta\mu}dS+\oint p_{m0}^{2}\mathbf{n}\cdot\mathbf{U}dS \quad \text{(H.8)}$$

H.2 We seek here to establish that for the classic acoustic boundary layer,

$$\dot{\mathcal{K}}_{\vartheta}=\ldots-\dot{\mathcal{K}}_{\vartheta\to\omega}+\ldots \quad \text{(H.9)}$$

where $\dot{\mathcal{K}}_{\vartheta\to\omega}=-\oint\mathbf{A}\cdot\boldsymbol{\sigma}_{\zeta}dS\geq 0$.

We start by taking the inner product of (6.2), i.e., the irrotational projection of the momentum equation $\partial\mathbf{u}_{\vartheta}/\partial t=-\nabla\left(p-\mathrm{Re}_{\vartheta}^{-1}\vartheta\right)$, with $\mathbf{u}_{\vartheta}$ to obtain

$$\dot{\mathcal{K}}_{\vartheta}=\int p\vartheta dV-\mathrm{Re}_{\vartheta}^{-1}\int\vartheta^{2}dV-\oint\left(p-\mathrm{Re}_{\vartheta}^{-1}\vartheta\right)\mathbf{n}\cdot\mathbf{u}_{\vartheta}dS \quad \text{(H.10)}$$

Now by virtue of the no-through condition, it follows that on the boundary $\mathbf{n}\cdot\mathbf{u}_{\vartheta}=-\mathbf{n}\cdot\mathbf{u}_{\omega}$. Making this substitution in the last integral, using the identity $\oint\alpha\mathbf{n}\cdot\nabla\times\mathbf{a}dS=-\oint\mathbf{a}\cdot\left(\mathbf{n}\times\nabla\alpha\right)dS$ and introducing $\boldsymbol{\sigma}_{\zeta}=-\mathbf{n}\times\nabla\left(p-\mathrm{Re}_{\vartheta}^{-1}\vartheta\right)$ from (6.7), we have

$$\dot{\mathcal{K}}_{\vartheta}=\int p\vartheta dV-\mathrm{Re}_{\vartheta}^{-1}\int\vartheta^{2}dV-\dot{\mathcal{K}}_{\vartheta\to\omega} \quad \text{(H.11)}$$

That $\dot{\mathcal{K}}_{\vartheta\to\omega}\geq 0$ follows by substituting in the solution given in Table F.1.

H.3 To establish that $\dot{\mathcal{K}}_{\vartheta\leftrightarrow\mathbf{U}}=M_b\int\mathbf{u}_{\vartheta}\cdot\left(\nabla\left(\mathbf{U}\cdot\mathbf{u}\right)+\boldsymbol{\omega}\times\mathbf{U}+\boldsymbol{\Omega}\times\mathbf{u}\right)dV$ can be written as

$$\dot{\mathcal{K}}_{\vartheta\leftrightarrow\mathbf{U}}=M_b\left(\begin{array}{c}\oint\left(\tfrac{1}{2}\mathbf{u}_{\vartheta}\cdot\mathbf{u}_{\vartheta}\right)\mathbf{n}\cdot\mathbf{U}dS+\int\mathbf{u}_{\vartheta}\cdot\nabla\mathbf{U}\cdot\mathbf{u}_{\vartheta}dV+\oint\left(\mathbf{u}_{\vartheta\zeta}\cdot\mathbf{u}_{\omega\zeta}\right)\mathbf{n}\cdot\mathbf{U}dS\\+\int\mathbf{u}_{\omega}\cdot\left(\mathbf{u}_{\vartheta}\cdot\nabla\mathbf{U}+\nabla\mathbf{U}\cdot\mathbf{u}_{\vartheta}-\boldsymbol{\Omega}\times\mathbf{u}_{\vartheta}\right)dV\end{array}\right) \quad \text{(H.12)}$$

we start with the well-known identity $\mathbf{a}\cdot\nabla\mathbf{b}+\mathbf{b}\cdot\nabla\mathbf{a}=\nabla\left(\mathbf{a}\cdot\mathbf{b}\right)+\left(\nabla\times\mathbf{b}\right)\times\mathbf{a}+\left(\nabla\times\mathbf{a}\right)\times\mathbf{b}$, set $\mathbf{a}=\mathbf{U}$, $\mathbf{b}=\mathbf{u}$ and take the inner product of both sides with $\mathbf{u}_{\vartheta}$, to obtain

$$\begin{aligned}\mathbf{u}_{\vartheta}\cdot\left(\nabla\left(\mathbf{U}\cdot\mathbf{u}\right)+\boldsymbol{\omega}\times\mathbf{U}+\boldsymbol{\Omega}\times\mathbf{u}\right)&=\mathbf{u}_{\vartheta}\cdot\left(\mathbf{U}\cdot\nabla\mathbf{u}+\mathbf{u}\cdot\nabla\mathbf{U}\right)\\&=\mathbf{u}_{\vartheta}\cdot\left(\mathbf{U}\cdot\nabla\mathbf{u}_{\vartheta}+\mathbf{u}_{\vartheta}\cdot\nabla\mathbf{U}\right)+\mathbf{u}_{\vartheta}\cdot\left(\mathbf{U}\cdot\nabla\mathbf{u}_{\omega}+\mathbf{u}_{\omega}\cdot\nabla\mathbf{U}\right)\\&=\left(\mathbf{U}\cdot\nabla\left(\tfrac{1}{2}\mathbf{u}_{\vartheta}\cdot\mathbf{u}_{\vartheta}\right)+\mathbf{u}_{\vartheta}\cdot\nabla\mathbf{U}\cdot\mathbf{u}_{\vartheta}\right)+\mathbf{u}_{\vartheta}\cdot\left(\mathbf{U}\cdot\nabla\mathbf{u}_{\omega}+\mathbf{u}_{\omega}\cdot\nabla\mathbf{U}\right)\end{aligned} \quad \text{(H.13)}$$

It follows that

$$\dot{\mathcal{K}}_{\vartheta\leftrightarrow\mathbf{U}}=M_b\left(\oint\left(\tfrac{1}{2}\mathbf{u}_{\vartheta}\cdot\mathbf{u}_{\vartheta}\right)\mathbf{n}\cdot\mathbf{U}dS+\int\mathbf{u}_{\vartheta}\cdot\nabla\mathbf{U}\cdot\mathbf{u}_{\vartheta}dV+\int\mathbf{u}_{\vartheta}\cdot\left(\mathbf{U}\cdot\nabla\mathbf{u}_{\omega}+\mathbf{u}_{\omega}\cdot\nabla\mathbf{U}\right)dV\right) \quad \text{(H.14)}$$

Now using (H.4) to rewrite the last group of integrals yields the desired result (H.12).

H.4 Using the leading order solution for the acoustic field, we seek here to establish that

$$\left\langle \oint \left(\tfrac{1}{2}\mathbf{u}_\vartheta \cdot \mathbf{u}_\vartheta\right)\mathbf{n}\cdot\mathbf{U}dS + \int \mathbf{u}_\vartheta \cdot \nabla\mathbf{U}\cdot\mathbf{u}_\vartheta dV \right\rangle \sim \left\langle \oint \tfrac{1}{2}p^2\mathbf{n}\cdot\mathbf{U}dS \right\rangle \tag{H.15}$$

To do so, we first use the following easily verified identity[†]:

$$\oint \left(\tfrac{1}{2}\mathbf{u}_\vartheta \cdot \mathbf{u}_\vartheta\right)\mathbf{n}\cdot\mathbf{U}dS + \int \mathbf{u}_\vartheta \cdot \nabla\mathbf{U}\cdot\mathbf{u}_\vartheta dV = \oint \left(\mathbf{U}\cdot\mathbf{u}_\vartheta\right)\mathbf{n}\cdot\mathbf{u}_\vartheta dS - \int \vartheta\mathbf{U}\cdot\mathbf{u}_\vartheta dV \tag{H.16}$$

Note that the surface integral on the right-hand side scales as $O\left(M_b^2\right)$ since $u_{\vartheta n} \sim O\left(M_b\right)$ on the boundary. To compute the volume integral on the right-hand side, we substitute the leading order acoustic solution from §C.1, i.e., $\vartheta \sim ik_{m0}\,p$ and $\mathbf{u}_\vartheta \sim -\left(i/k_{m0}\right)\nabla p$; because quadratic combinations of the variables appear however, it is first necessary to take the real parts of the variables involved,

$$\left\langle \int \vartheta\mathbf{U}\cdot\mathbf{u}_\vartheta dV \right\rangle \sim -\left\langle \int p\mathbf{U}\cdot\nabla p dV \right\rangle \sim -\left\langle \oint \tfrac{1}{2}p^2\mathbf{n}\cdot\mathbf{U}dS \right\rangle \tag{H.17}$$

Introducing (H.17) in (H.16) yields the desired result.

H.5 To place *flow turning* $\dot{\mathcal{K}}_{\vartheta\to\mathbf{U}} \equiv M_b \oint \left(\mathbf{u}_{\vartheta\zeta}\cdot\mathbf{u}_{\omega\zeta}\right)\mathbf{n}\cdot\mathbf{U}dS$ correctly in the larger context of energy pathways between the longitudinal and transverse fields, we seek here to establish that

$$\left\langle \dot{\mathcal{K}}_{\vartheta\to\mathbf{U}} \right\rangle \sim -\oint \left\langle \mathbf{A}\cdot\boldsymbol{\sigma}_\zeta \right\rangle dS \tag{H.18}$$

Using the identity $\mathbf{b}\cdot\nabla\times\mathbf{a} = \nabla\cdot\left(\mathbf{a}\times\mathbf{b}\right) + \mathbf{a}\cdot\nabla\times\mathbf{b}$, with $\mathbf{a}=\mathbf{A}$ (i.e., the vector potential) and $\mathbf{b}=\mathbf{u}_\omega = \nabla\times\mathbf{A}$, and the no-slip condition $\mathbf{u}_{\omega\zeta} = -\mathbf{u}_{\vartheta\zeta}$, we have

$$\mathbf{u}_{\vartheta\zeta}\cdot\mathbf{u}_{\omega\zeta} = -\nabla\cdot\left(\mathbf{A}\times\mathbf{u}_\omega\right) - \mathbf{A}\cdot\boldsymbol{\omega} + u_{\omega n}^2 \sim -\nabla\cdot\left(\mathbf{A}\times\mathbf{u}_\omega\right) - \mathbf{A}\cdot\boldsymbol{\omega} + O\left(M_b^2\right) \tag{H.19}$$

Note that the simplification on the far right follows since $u_{\omega n} \sim O\left(M_b\right)$.

We now consider the divergence term in (H.19), the dominant contribution of which is[‡]

$$\nabla\cdot\left(\mathbf{A}\times\mathbf{u}_\omega\right) \sim \frac{\partial}{\partial n}\left(\mathbf{u}_{\omega\zeta}\cdot\left(\mathbf{n}\times\mathbf{A}_\zeta\right)\right) + O\left(M_b\right) \tag{H.20}$$

and introduce some details of our solution for the vorticity field on the boundary. Specifically, since $\mathbf{A}_\zeta \sim \left(\mathbf{n}\cdot M_b\mathbf{U}/k_{m0}^2\right)\mathbf{n}\times\nabla_\zeta p$ and $\mathbf{u}_{\omega\zeta} \sim \left(i/k_{m0}\right)\nabla_\zeta p$ are $\pi/2$ out of phase on the boundary (cf. (7.20) and

---

[†] Taking the inner product of $\mathbf{u}_\vartheta\cdot\nabla\mathbf{u}_\vartheta = \nabla\left(\tfrac{1}{2}\mathbf{u}_\vartheta\cdot\mathbf{u}_\vartheta\right)$ with $\mathbf{U}$, we have $\mathbf{u}_\vartheta\cdot\nabla\mathbf{u}_\vartheta\cdot\mathbf{U} = \nabla\left(\tfrac{1}{2}\mathbf{u}_\vartheta\cdot\mathbf{u}_\vartheta\right)\cdot\mathbf{U}$. The left-hand side can be re-expressed by noting that $\nabla\mathbf{u}_\vartheta\cdot\mathbf{U} = \nabla\left(\mathbf{U}\cdot\mathbf{u}_\vartheta\right) - \nabla\mathbf{U}\cdot\mathbf{u}_\vartheta$; this follows from the identity $\nabla\left(\mathbf{a}\cdot\mathbf{b}\right) = \nabla\mathbf{a}\cdot\mathbf{b} + \nabla\mathbf{b}\cdot\mathbf{a}$. We also use $\nabla\cdot\left(\alpha\mathbf{a}\right) = \nabla\alpha\cdot\mathbf{a} + \alpha\nabla\cdot\mathbf{a}$ to re-express the right-hand side, taking note of the fact that $\nabla\cdot\mathbf{U} = 0$. Thus,

$$\mathbf{u}_\vartheta\cdot\nabla\left(\mathbf{U}\cdot\mathbf{u}_\vartheta\right) - \mathbf{u}_\vartheta\cdot\nabla\mathbf{U}\cdot\mathbf{u}_\vartheta = \nabla\cdot\left(\left(\tfrac{1}{2}\mathbf{u}_\vartheta\cdot\mathbf{u}_\vartheta\right)\mathbf{U}\right)$$

Re-expressing the first term using $\mathbf{u}_\vartheta\cdot\nabla\left(\mathbf{U}\cdot\mathbf{u}_\vartheta\right) = \nabla\cdot\left(\left(\mathbf{U}\cdot\mathbf{u}_\vartheta\right)\mathbf{u}_\vartheta\right) - \left(\mathbf{U}\cdot\mathbf{u}_\vartheta\right)\vartheta$, we have the desired result after rearranging slightly

$$\nabla\cdot\left(\left(\tfrac{1}{2}\mathbf{u}_\vartheta\cdot\mathbf{u}_\vartheta\right)\mathbf{U}\right) + \mathbf{u}_\vartheta\cdot\nabla\mathbf{U}\cdot\mathbf{u}_\vartheta = \nabla\cdot\left(\left(\mathbf{U}\cdot\mathbf{u}_\vartheta\right)\mathbf{u}_\vartheta\right) - \left(\mathbf{U}\cdot\mathbf{u}_\vartheta\right)\vartheta$$

[‡] The exact result is $\nabla\cdot\left(\mathbf{A}\times\mathbf{u}_\omega\right) = \left(\partial/\partial n - \kappa\right)\left(\mathbf{u}_{\omega\zeta}\cdot\left(\mathbf{n}\times\mathbf{A}_\zeta\right)\right) + \nabla_\zeta\cdot\left(A_n\,\mathbf{n}\times\mathbf{u}_{\omega\zeta} - u_{\omega n}\,\mathbf{n}\times\mathbf{A}_\zeta\right)$.

(7.21), respectively)), it follows that $\left\langle \mathbf{u}_{\omega\zeta} \cdot \left(\mathbf{n} \times \mathbf{A}_{\zeta} \right) \right\rangle \sim 0$, where $\langle ... \rangle$ denotes the time average. Therefore $\nabla \cdot \left\langle \mathbf{A} \times \mathbf{u}_{\omega} \right\rangle \sim 0$; using (H.19) this implies that $\left\langle \mathbf{u}_{\vartheta\zeta} \cdot \mathbf{u}_{\omega\zeta} \right\rangle \sim -\left\langle \mathbf{A} \cdot \boldsymbol{\omega} \right\rangle$. Substituting into our definition of $\dot{\mathcal{K}}_{\vartheta \to \mathbf{U}}$, we have $\left\langle \dot{\mathcal{K}}_{\vartheta \to \mathbf{U}} \right\rangle \sim -\oint \left\langle \mathbf{A} \cdot \left(\mathbf{n} \cdot M_b \mathbf{U} \right) \boldsymbol{\omega}_{\zeta} \right\rangle dS$.

It remains to recall that for the problems of interest here $\boldsymbol{\sigma}_{\zeta} \sim \left(\mathbf{n} \cdot M_b \mathbf{U} \right) \boldsymbol{\omega}_{\zeta}$ since the transport of boundary vorticity is controlled by convective rather than diffusive mechanisms (cf. §7.2.2). Combining this expression with the result from the previous paragraph derives (H.18).

I. Calculations for Chapter 9

I.1 *Sound-Sound Interactions*

The expressions are already given in §C.2.

I.2 *Sound-Vortical Interactions*

Recall that

$$I_1^{\vartheta\omega(m,j,k)} \equiv \frac{1}{k_{j0}k_{k0}} \oint U_n c_{m0} \nabla_\zeta c_{j0} \cdot \nabla_\zeta c_{k0}\, dS$$

$$I_2^{\vartheta\omega(m,j,k)} \equiv \frac{1}{k_{j0}k_{k0}^2 k_{m0}^2} \oint U_n \nabla_\zeta c_{j0} \cdot \nabla \times \left(\nabla c_{k0} \times \nabla c_{m0}\right) dS \tag{I.1}$$

$$I_3^{\vartheta\omega(m,j,k)} \equiv \frac{1}{k_{j0}k_{m0}} \oint \left(\nabla_\zeta c_{m0} \cdot \nabla_\zeta c_{j0}\right) \mathbf{n} \cdot \nabla \varphi_{k\mu}\, dS$$

Axial Modes

$$I_1^{\vartheta\omega(m,j,k)} = -E_1^2 \left(\delta_{|m|}^{|j-k|} - \delta_{|m|}^{|j+k|}\right), \quad I_2^{\vartheta\omega(m,j,k)} = 0 \tag{I.2}$$

Tangential Modes

It is a simply matter to show that on the surface,

$$\nabla_\zeta c_{j0} \cdot \nabla \times \left(\nabla c_{k0} \times \nabla c_{m0}\right) = \frac{1}{r}\frac{\partial c_{j0}}{\partial \theta}\left(\frac{1}{r}\frac{\partial c_{k0}}{\partial \theta}\frac{\partial^2 c_{m0}}{\partial r^2} - \frac{1}{r}\frac{\partial c_{m0}}{\partial \theta}\frac{\partial^2 c_{k0}}{\partial r^2}\right) \tag{I.3}$$

Therefore, we have

$$\begin{aligned} I_1^{\vartheta\omega(m,j,k)} &= -\tfrac{\pi}{2}\tfrac{j}{k_{j0}}\tfrac{k}{k_{k0}} J_m\left(k_{m0}\right) J_j\left(k_{j0}\right) J_k\left(k_{k0}\right)\left(\delta_{|m|}^{|j-k|} - \delta_{|m|}^{|j+k|}\right) \\ I_2^{\vartheta\omega(m,j,k)} &= \tfrac{\pi}{2}\tfrac{j}{k_{j0}} J_j\left(k_{j0}\right)\begin{pmatrix} \tfrac{m}{k_{m0}}\tfrac{1}{k_{m0}} J_m\left(k_{m0}\right) J_k''\left(k_{k0}\right)\left(\delta_{|k|}^{|j-m|} - \delta_{|k|}^{|j+m|}\right) - \\ -\tfrac{k}{k_{k0}}\tfrac{1}{k_{k0}} J_k\left(k_{k0}\right) J_m''\left(k_{m0}\right)\left(\delta_{|m|}^{|j-k|} - \delta_{|m|}^{|j+k|}\right) \end{pmatrix} \end{aligned} \tag{I.4}$$

I.3 *Vortical-Vortical Interactions*

Evaluating the surface integral (9.18) is straightforward, and leads to

$$I_1^{\omega\omega(m,j,k)} \equiv \frac{1}{k_{j0}k_{k0}^2 k_{m0}^2} \oint U_n \nabla_\zeta c_{j0} \cdot \nabla \left(\nabla_\zeta c_{k0} \cdot \nabla_\zeta c_{m0}\right) dS \tag{I.5}$$

How we evaluate $\int \mathbf{u}_{\omega\zeta} \cdot \nabla_\zeta \left(\nabla_\zeta \varphi_m^{+*}\right) \cdot \mathbf{u}_{\omega\zeta}\, dV$ requires some elaboration. Of course, the basic idea is the same. We expand $\mathbf{u}_{\omega\zeta}$ in a basis of eigenfunctions (cf. (7.21)),

$$\mathbf{u}_{\omega\zeta}\left(\mathbf{x},t\right) = \tfrac{1}{2}\sum_{j=-\infty}^{\infty} \mathbf{u}_{j\omega\zeta}\left(\mathbf{x}\right)\eta_j\left(t\right) \sim \tfrac{1}{2}\sum_{j=-\infty}^{\infty} i\left(M_b U_n / k_{j0}\right)\mathbf{n} \times \boldsymbol{\omega}_{j\zeta}^n\left(\mathbf{x}\right)\exp\left(ik_{j0}\xi\right)\eta_j\left(t\right) \tag{I.6}$$

It follows that the integrand assumes the form

$$\mathbf{u}_{\omega\zeta}\cdot\nabla_\zeta\left(\nabla_\zeta\varphi_m^{\dagger *}\right)\cdot\mathbf{u}_{\omega\zeta}\sim\sum_{j,k}f^{(j,k)}(\mathbf{x})\exp\left(i\left(k_{j0}+k_{k0}\right)\xi\right)\eta_j\eta_k \tag{I.7}$$

were $f^{(j,k)}(\mathbf{x})$ is a function of the original spatial coordinates.

When $j\neq -k$, the integrand has a dependence on ξ, and so we can apply the earlier asymptotic result (7.26). This collapses volume integrations to integration over burning surfaces. After some work, this leads to

$$\int\mathbf{u}_{\omega\zeta}\cdot\nabla_\zeta\left(\nabla_\zeta\varphi_m^{\dagger *}\right)\cdot\mathbf{u}_{\omega\zeta}\,dV\sim\tfrac{1}{8(\Gamma-1)}M_b\sum_{\substack{j,k\\ j\neq -k}}\left(\tfrac{2k_{m0}}{k_{j0}+k_{k0}}I_2^{\omega\omega(m,j,k)}\right)\eta_j\eta_k \tag{I.8}$$

where

$$I_2^{\omega\omega(m,j,k)}\equiv\frac{1}{k_{j0}k_{k0}k_{m0}^2}\oint U_n\nabla_\zeta c_{j0}\cdot\nabla_\zeta\left(\nabla_\zeta c_{m0}\right)\cdot\nabla_\zeta c_{k0}\,dS \tag{I.9}$$

When $j=-k$, the exponential term in (I.7) vanishes, and so (7.26) is no longer applicable. This is not cause for concern however, since no resonant triad conditions can be satisfied when $j=-k$ (cf. Chapter 4). Thus, this value of the coefficient does not play an important role in determining the dynamics of the system and can therefore be safely omitted.

Axial Modes

$$\begin{aligned}I_1^{\omega\omega(m,j,k)}&=E_1^2\left(\tfrac{1}{k_{m0}}\left(\delta_{|k|}^{|j-m|}-\delta_{|k|}^{|j+m|}\right)+\tfrac{1}{k_{k0}}\left(\delta_{|m|}^{|j-k|}-\delta_{|m|}^{|j+k|}\right)\right)\\ I_2^{\omega\omega(m,j,k)}&=E_1^2\left(\delta_{|m|}^{|j-k|}-\delta_{|m|}^{|j+k|}\right)\end{aligned} \tag{I.10}$$

Tangential Modes

$$\begin{aligned}I_1^{\omega\omega(m,j,k)}&=\tfrac{\pi}{2}J_j\left(k_{j0}\right)J_k\left(k_{k0}\right)J_m\left(k_{m0}\right)\tfrac{j}{k_{j0}}\tfrac{k}{k_{k0}}\tfrac{m}{k_{m0}}\left(\begin{array}{l}\tfrac{k}{k_{k0}}\tfrac{1}{k_{m0}}\left(\delta_{|k|}^{|j-m|}-\delta_{|k|}^{|j+m|}\right)+\\ +\tfrac{m}{k_{m0}}\tfrac{1}{k_{k0}}\left(\delta_{|m|}^{|j-k|}-\delta_{|m|}^{|j+k|}\right)\end{array}\right)\\ I_2^{\omega\omega(m,j,k)}&=\tfrac{\pi}{2}\tfrac{j}{k_{j0}}\tfrac{k}{k_{k0}}\tfrac{m^2}{k_{m0}^2}J_j\left(k_{j0}\right)J_k\left(k_{k0}\right)J_m\left(k_{m0}\right)\left(\delta_{|m|}^{|j-k|}-\delta_{|m|}^{|j+k|}\right)\end{aligned} \tag{I.11}$$

I.4 *Boundary Terms*

$$\begin{aligned}I_1^{\mathcal{B}(m,j,k)}&\equiv\frac{1}{k_{j0}k_{k0}k_{m0}}\oint U_n\nabla_\zeta c_{j0}\cdot\nabla_\zeta\left(c_{k0}c_{m0}\right)dS\\ I_2^{\mathcal{B}(m,j,k)}&\equiv\oint U_n c_{m0}c_{j0}c_{k0}\,dS,\quad I_3^{\mathcal{B}(m,j,k)}\equiv\oint c_{m0}c_{j0}\mathbf{n}\cdot\nabla\varphi_{k\mu}dS\end{aligned} \tag{I.12}$$

Axial Modes

$$I_1^{\mathcal{B}(m,j,k)} = -E_1^2\left(\frac{1}{k_{m0}}\left(\delta_{|m|}^{|j-k|} - \delta_{|m|}^{|j+k|}\right) + \frac{1}{k_{k0}}\left(\delta_{|k|}^{|j-m|} - \delta_{|k|}^{|j+m|}\right)\right)$$

$$I_2^{\mathcal{B}(m,j,k)} = -E_1^2\left(\delta_{|m|}^{|j-k|} + \delta_{|m|}^{|j+k|}\right) \tag{I.13}$$

Tangential Modes

$$I_1^{\mathcal{B}(m,j,k)} = -\frac{\pi}{2}\frac{j}{k_{j0}}J_j\left(k_{j0}\right)J_k\left(k_{k0}\right)J_m\left(k_{m0}\right)\left(\frac{k}{k_{k0}}\frac{1}{k_{m0}}\left(\delta_{|m|}^{|j-k|} - \delta_{|m|}^{|j+k|}\right) + \frac{m}{k_{m0}}\frac{1}{k_{k0}}\left(\delta_{|k|}^{|j-m|} - \delta_{|k|}^{|j+m|}\right)\right)$$

$$I_2^{\mathcal{B}(m,j,k)} = -\frac{\pi}{2}J_m\left(k_{m0}\right)J_j\left(k_{j0}\right)J_k\left(k_{k0}\right)\left(\delta_{|m|}^{|j-k|} + \delta_{|m|}^{|j+k|}\right) \tag{I.14}$$

References

Ananthkrishnan, N. and Culick, F.E.C. (2002) "Modeling and Dynamics of Nonlinear Acoustic Waves in a Combustion Chamber," 38th AIAA/ASME/SAE/ASEE Joint Propulsion Conference & Exhibit, AIAA Paper No. 2002-3592.

Apte, S.V. and Yang, V. (2001) "Unsteady flow evolution in a porous chamber with surface mass injection, I: free oscillations," *AIAA Journal*, Vol. 39, No. 8, pp. 1577-1586.

Apte, S.V. and Yang, V. (2002) "Unsteady flow evolution in a porous chamber with surface mass injection, II: acoustic excitations," *AIAA Journal*, Vol. 40, No. 2, pp. 244-253.

Awad, E. and Culick, F.E.C. (1986) "On the Existence and Stability of Limit Cycles for Longitudinal Acoustic Modes in a Combustion Chamber," *Combustion Science and Technology*, Vol. 46, No. 6, pp. 195-222.

Beddini, R.A. (1998) "The Role of Turbulence Interactions in Solid Propellant Combustion Instability," 34th AIAA/ASME/SAE/ASEE Joint Propulsion Conference & Exhibit, AIAA Paper No. 98-3703.

Berman, A. (1953) "Laminar Flow in Channels with Porous Wall," *Journal of Applied Physics*, Vol. 24, No. 9, pp. 1232-1235.

Bleistein, N. and Handelsman, R.A. (1975) *Asymptotic Expansion of Integrals*, Holt, Rinehart and Winston, New York.

Bloomshield, F. (2000) "Summary of Multidisciplinary University Research Initiative in Solid Propellant Combustion Instability," 36th AIAA/ASME/SAE/ASEE Joint Propulsion Conference & Exhibit, AIAA Paper No. 2000-3172.

Boys, S.F. and Schofield, A. (1943) "Investigations of Secondary Peaks," Propulsion Development Establishment, Report 1943/5, Abesporth , England, UK.

Brown, R. S., Blackner, A. M., Willoughby, P. G. and Dunlap, R. (1986) "Coupling between Velocity Oscillations and Solid Propellant Combustion," 24th Aerospace Sciences Meeting, AIAA Paper No. 86-0531.

Brownlee, W.G. (1959) "An Experimental Investigation of Unstable Combustion in Solid Propellant Rocket Motors," Ph.D. Thesis, Aeronautics, California Institute of Technology.

Brownlee, W.G. (1964) "Nonlinear Axial Combustion Instability in Solid Rocket Propellant Rocket Motors," *AIAA Journal*, Vol. 2, No. 2, pp. 275-284.

Burnley, V. (1996) "Nonlinear Combustion Instabilities and Stochastic Sources," Ph.D. Thesis, Aeronautics, California Institute of Technology.

Cantrell, R.H. and Hart, R.W. (1964) "Interaction Between Sound and Flow in Acoustic Cavities: Mass, Momentum and Energy Considerations," *Journal of the Acoustical Society of America*, Vol. 36, No. 4, pp. 697-706.

Casalis, G., Avalon, G. and Pineau, J.-P (1998) "Spatial Instability of Planar Channel Flow with Fluid Injection through Porous Walls," *Physics of Fluids*, Vol. 10, No. 10, pp. 2558-2568.

Chu, B.-T. and Kovasznay, L.S.G. (1958) "Non-linear Interactions in a Viscous Heat Conducting Compressible Gas," *Journal of Fluid Mechanics*, Vol. 3, No. 5, pp. 494-512.

Culick, F.E.C. (1966) "Rotational Axisymmetric Mean Flow and Damping of Acoustic Waves in a Solid Propellant Rocket," *AIAA Journal*, Vol. 4, No. 8, pp. 1462-1464.

Culick, F.E.C. (1970) "Stability of Longitudinal Oscillations with Pressure and Velocity Coupling in a Solid Propellant Rocket," *Combustion Science and Technology*, Vol. 2, No. 4, pp. 179-201.

Culick, F.E.C. (1973) "The Stability of One-Dimensional Motions in a Rocket Motor," *Combustion Science and Technology*, Vol. 7, No. 4, pp. 165-175.

Culick, F.E.C. (1975) "Stability of Three-Dimensional Motions in a Combustion Chamber," *Combustion Science and Technology*, Vol. 10, No.3, pp. 109-124.

Culick, F.E.C. (1976) "Nonlinear Behavior of Acoustic Waves in Combustion Chambers," Parts I and II, *Acta Astronautica*, Vol. 3, pp. 714-757.

Culick, F.E.C. (1994) "Some Recent Results for Nonlinear Acoustics in Combustion Chambers," *AIAA Journal*, Vol. 32, No. 1, pp. 146-169.

Culick, F.E.C. (1997) "A Note on Ordering Perturbations and the Insignificance of Linear Coupling in Combustion Instabilities," *Combustion Science and Technology*, Vol. 126, pp. 359-379.

Culick, F.E.C. (2000) "Combustion Instabilities: Mating Dance of Chemical, Combustion, and Combustor Dynamics," 36th AIAA/ASME/SAE/ASEE Joint Propulsion Conference & Exhibit, AIAA Paper No. 2000-3178.

Culick, F.E.C. and Yang, V. (1992) "Prediction of the Stability of Unsteady Motions in Solid Propellant Rocket Motors," *Nonsteady Burning and Combustion Stability of Solid Propellants*, edited by L. DeLuca, E.W. Price and M. Summerfield, Vol. 143, *Progress in Astronautics and Aeronautics*, AIAA, Washington DC, Chapter 18, pp. 719-779.

Doedel, E.J., Champneys, A.R., Fairgrieve, T.F., Kuznetsov, Y.A., Sandstede, B. and Wang, X. (1997) "AUTO 97: Continuation and Bifurcation Software for Ordinary Differential Equations," Concordia University, Montreal, Canada.

Doedel, E.J., Keller, H.B. and Kernevez, J.P. (1991a) "Numerical Analysis and Control of Bifurcation Problems, (I) Bifurcation in Finite Dimensions," *International Journal of Bifurcation and Chaos*, Vol. 1, No. 3, pp. 493-520.

Doedel, E.J., Keller, H.B. and Kernevez, J.P. (1991b) "Numerical Analysis and Control of Bifurcation Problems, (II) Bifurcation in Infinite Dimensions," *International Journal of Bifurcation and Chaos*, Vol. 1, No. 4, pp. 745-772.

Doedel, E.J., Paffenroth, R.C., Champneys, A.R., Fairgrieve, T.F., Kuznetsov, Y.A., Oldeman, B.E., Sandstede, B. and Wang, X. (2000) "Auto 2000: Continuation and Bifurcation Software for Ordinary Differential Equations (with HomCont)," California Institute of Technology.

Dunlap, R., Willoughby, P. G. and Hermsen, R. W. (1974) "Flowfield in the Combustion Chamber of a Solid Propellant Rocket Motor," *AIAA Journal*, Vol. 12, No.10, pp. 1440-1442.

Flandro, G.A. (1985) "Energy Balance Analysis of Nonlinear Combustion Instability," *Journal of Propulsion and Power*, Vol. 1, No. 3, pp. 210-221.

Flandro, G.A. (1986) "Vortex Driving Mechanism in Oscillatory Rocket Flows," *Journal of Propulsion and Power*, Vol. 2, No. 3, pp. 206-214.

Flandro, G.A. (1995a) "Effects of Vorticity on Rocket Combustion Instability," *Journal of Propulsion and Power*, Vol. 11, No. 4, pp. 607-625.

Flandro, G.A. (1995b) "On Flow Turning," 31st AIAA/ASME/SAE/ASEE Joint Propulsion Conference & Exhibit, AIAA Paper No. 95-2530.

Flandro, G.A. and Jacobs, H.R. (1974) "Vortex-Generated Sound in Cavities," AIAA Paper No. 73-1014, published in *Aeroacoustics: Jet and Combustion Noise*, AIAA Series *Progress in Astronautics and Aeronautics*. Vol. 37, pp. 521-533.

Fox, P.A (1955) "Perturbation Theory of Wave Propagation Based on the Method of Characteristics," *Journal of Mathematics and Physics*, Vol. 34, pp. 133-151.

French, J.C., Flanagan, S.N. and Flandro, G.A. (1996) "A New Method for Combustion Instability Mode Shape and Frequency Computation," Proceedings of the 33rd JANNAF Combustion Meeting, Monterey, CA.

Garcia-Schafer, J.E. and Linan, A. (2001) "Longitudinal Acoustic Instabilities in Slender Solid Propellant Rockets: Linear Analysis," *Journal of Fluid Mechanics*, Vol. 437, pp. 229-254.

Grad, H. (1949) "Resonance Burning in Rocket Motors," *Communications on Pure and Applied Mathematics*, Vol. 2, pp. 79-102.

Griffond, J. and Casalis, G. (2000) "On the Dependence on the Formulation of Some Nonparallel Stability Approaches Applied to the Taylor Flow," *Physics of Fluids*, Vol. 12, No. 2, pp. 466-468.

Griffond, J. and Casalis, G. (2001) “On the Nonparallel Stability of the Injection Induced Two-Dimensional Taylor Flow,” *Physics of Fluids*, Vol. 13, No. 6, pp. 1635-1644.

Hart, R.W. and McClure, F.T. (1965) “Theory of Acoustic Instability in Solid Propellant Rocket Combustion,” *Tenth Symposium (International) on Combustion*, The Combustion Institute, Pittsburgh, PA, pp. 1047-1065.

Isella, G.C. (2001) “Modeling and Simulation of Combustion Chambers and Propellant Dynamics and Issues in Active Control of Combustion Instabilities,” Ph.D. Thesis, Aeronautics, California Institute of Technology.

Jahnke, C. and Culick, F.E.C. (1994) “An Application of Dynamical Systems Theory to Nonlinear Combustion Instabilities,” *Journal of Propulsion and Power*, Vol. 10, No. 4, pp. 508-517.

Kevorkian, J. and Cole, J.D. (1996) *Multiple Scale and Singular Perturbation Methods*, Springer, New York.

Krylov, N. and Bogoliubov, N. (1947) *Introduction to Nonlinear Mechanics*, Princeton University Press, Princeton, New Jersey.

Lagerstrom, P.A. (1964) *Laminar Flow Theory*, Princeton University Press, Princeton, New Jersey.

Lagerstrom, P.A. (1988) *Matched Asymptotic Expansions*, Springer-Verlag, New York.

Lee, Y. and Beddini, R.A. (2000) “Effect of Solid Rocket Chamber Pressure on Acoustically-Induced Turbulent Transition,” AIAA Paper No. 2000-3802.

Lighthill, M.J. (1949) “A Technique for Rendering Approximate Solutions to Physical Problems Uniformly Valid,” *The Philosophical Magazine*, Vol. 40, pp. 1179-1201.

Lighthill, M.J. (1952) “On Sound Generated Aerodynamically,” *Proceedings of the Royal Society of London Series A*, Vol. 211, pp. 564-587.

Lighthill, M.J. (1963) “Introduction: Boundary Layer Theory,” *Laminar Boundary Layer*, edited by L. Rosenhead, Vol. 90, Oxford University Press, Oxford, pp. 46-113.

Lovine, R.L., Dudley, D.P. and Waugh, R.D. (1976) “Standardized Stability Prediction Method for Solid Rocket Motors,” Vols. I, II and III, Aerojet Solid Propulsion Co., Report AFRPL TR 76-32.

Lupoglazoff, N. and Vuillot, F. (1992) “Numerical Simulation of Vortex Shedding Phenomenon in 2D Test Case Solid Rocket Motors,” AIAA Paper No. 92-0776.

Lupoglazoff, N. and Vuillot, F. (1996) “Parietal Vortex-Shedding as a Cause of Instability for Long Solid Propellant Motors,” AIAA Paper No. 96-0761.

Lupoglazoff, N. and Vuillot, F. (1998) “Numerical Simulations of Parietal Vortex Shedding Phenomena in a Cold Flow Set-Up,” AIAA Paper No. 98-3220.

Magiawala, K. and Culick, F.E.C. (1979) “Measurements of Energy Exchange Between Acoustic Fields and Non-Uniform Steady Fields,” *Journal of Sound and Vibration*, Vol. 75, pp. 503-512.

Majdalani, J. and Roh, T.S. (2000) “The Oscillatory Channel Flow with Large Wall Injection,” *Proceedings of the Royal Society, Series A*, Vol. 456, No. 1999, pp. 1625-1657.

Majdalani, J. and Van Moorhen, W.K. (1998) “Improved Time-Dependent Flowfield Solution for Solid Rocket Motors,” *AIAA Journal*, Vol. 36, No. 2, pp. 241-248.

Margolis, S.B. (1993) “Nonlinear Stability of Combustion-Drive Acoustic-Oscillations in Resonance Tubes," *Journal of Fluid Mechanics*, Vol. 253, pp. 67-103.

Maslen, S.H. and Moore, F.K. (1956) “On Strong Transverse Waves Without Shocks in a Circular Cylinder,” *Journal of the Aeronautical Sciences*, Vol. 23, No. 6, pp. 583-593.

McClure, F.T., Hart, R.W. and Bird, J.F. (1960) “Acoustic Resonance in Solid Propellant Rockets,” *Journal of Applied Physics*, Vol. 31, pp. 884-896.

Mitchell, C.E., Crocco, L. and Sirignano, W.A. (1969) “Nonlinear Longitudinal Instability in Rocket Motors with Concentrated Combustion,” *Combustion Science and Technology*, Vol. 1, No. 4, pp. 269-274.

Morse, P. and Ingard, L. (1968) *Theoretical Acoustics*, McGraw-Hill Book Co., New York.

Nickerson, G. R., Culick, F. E. C. and Dang, L. G. (1983) “Standardized Stability Prediction Method for Solid Rocket Motors Axial Mode Computer Program,” Software and Engineering Associates, Inc., Report AFRPL TR 83-017.

Price, E.W. (1992) “Solid Rocket Combustion Instability—An American Historical Account,” *Nonsteady Burning and Combustion Stability of Solid Propellants*, edited by L. DeLuca, E.W. Price and M. Summerfield, Vol. 143, *Progress in Astronautics and Aeronautics*, AIAA, Washington DC, Chapter 1, pp. 1-16.

Proudman, I. (1960) “An Example of Steady Laminar Flow at Large Reynolds Number,” *Journal of Fluid Mechanics*, Vol. 9, No. 4, pp. 593-602.

Seywert, C. (2001) “Combustion Instabilities: Issues in Modeling and Control,” Ph.D. Thesis, Aeronautics, California Institute of Technology.

Shaeffer, C.W. and Brown, R.S. (1992) “Oscillatory Internal Flow Studies”, United Technologies, Chemical Systems Division Report No. 2060 FR.

Sirignano, W.A. (1964) “A Theoretical Study of Nonlinear Combustion Instability: Longitudinal Mode,” Ph.D. Thesis, Princeton University.

Sirignano, W.A. and Crocco, L. (1964) “A Shock Wave Model of Unstable Rocket Combustors,” *AIAA Journal*, Vol. 2, No. 7, pp. 1285-1296.

Smith, R.P. and Sprenger, D.F. (1953) “Combustion Instability in Solid Propellant Rockets,” *Proceedings of the Fourth Symposium (International) on Combustion*, Williams and Wilkins, Baltimore MD, p. 893.

Stakgold, I. (1967) *Boundary Value Problems of Mathematical Physics*, Vols. I and II, MacMillan, New York.

Swanson, C.D. (1951) “Resonance Burning in Rocket Grains,” U.S. Naval Ordinance Test Station, NOTS TM 439.

Tai, C.-T. (1992) *Generalized Vector and Dyadic Analysis*, University of Michigan, IEEE.

Taylor, G.I. (1956) “Fluid Flow in Regions Bounded by Porous Surfaces,” *Proceedings of the Royal Society of London Series A*, Vol. 234, pp. 456-475.

Varapev, V.N. and Yagodkin, V.I. (1969) “Flow Stability in a Channel with Porous Walls,” *Fluid Dynamics (Izvestiya Akademii Nauk SSSR, Meckanika Zhidkosti i Gaza)*, Vol. 4, No. 5, pp. 91-95.

Vuillot, F. and Avalon, G. (1991) “Acoustic Boundary Layer in Large Solid Propellant Rocket Motors Using Navier-Stokes Equations,” *Journal of Propulsion and Power*, Vol. 7, No. 2, pp. 231-239.

White, F.M. (1962) “Laminar Flow in a Uniformly Porous Tube,” *Journal of Applied Mechanics*, vol. 29, pp. 201-204.

Whitham, G.B. (1952) “The Flow Pattern of a Supersonic Projectile,” *Communications on Pure and Applied Mathematics*, Vol. 5, pp. 301-349.

Wu, J.Z. and Wu, J.M. (1996) “Vorticity Dynamics on Boundaries,” *Advances in Applied Mechanics*, Vol. 32, pp. 119-275.

Yang, V. and Culick, F.E.C. (1990) “On the Existence and Stability of Limit Cycles for Transverse Acoustic Oscillations in a Cylindrical Combustion Chamber, I. Standing Modes” *Combustion Science and Technology*, Vol. 72, No. 1, pp. 37-65.

Yang, V., Kim, S.I. and Culick, F.E.C. (1987) “Third Order Nonlinear Acoustic Instabilities in Combustion Chambers, Part I: Longitudinal Modes,” AIAA Paper No. 87-1873.

Yang, V., Kim, S.I. and Culick, F.E.C. (1988) “Third Order Nonlinear Acoustic Instabilities in Combustion Chambers, Part II: Transverse Modes,” AIAA Paper No. 88-0152.

Zhao, Q., Staab, P.L., Kassoy, D.R. and Kirkkopru, K. (2000) “Acoustically Generated Vorticity in an Internal Flow,” *Journal of Fluid Mechanics*, Vol. 413, pp. 247-285.